DEVELOPMENT OF BIONANOCOMPOSITES BASED ON PCL/PBS DOUBLE CRYSTALLINE BLENDS AND CARBON NANOTUBES

by

THANDI PATRICIA GUMEDE (M.Sc.)

Submitted in accordance with the requirements for the degree

PHILOSOPHY DOCTOR (Ph.D.) in Polymer Science

Department of Chemistry

Faculty of Natural and Agricultural Sciences

at the

UNIVERSITY OF THE FREE STATE (QWAQWA CAMPUS)

SUPERVISOR: PROF A.S. LUYT

CO-SUPERVISOR: PROF A.J. MÜLLER

August 2018

DECLARATION

I, the undersigned, hereby declare that the research in this thesis is the product of my own independent work. All content and ideas drawn directly or indirectly from external sources are indicated as such. The thesis has not been submitted by me to any other examining body. I furthermore cede copyright of the thesis in favour of the University of the Free State.

_____

Gumede T.P. (Miss)

DEDICATION

To my mom and dad (Busisiwe Minah Gumede and Mvulani Alfred Gumede):

Throughout my life, you have always been the strength that holds me up in the storm of life. Thank you for giving me a chance to prove and improve myself through all walks of life. Thank you once again for your unconditional support throughout my studies, and for always believing in me. I am really blessed to have you in my life. I love you mom and dad ☺

To my granny (Nomadlozi Lephinah Mofokeng):

Words cannot express the true appreciation I have for you gogo. You always opened your arms for me. When people shut their ears for me, you always opened your heart for me. Thank you for always being there for me in good and bad times. You are highly appreciated. As we celebrate your 70th birthday, may the Almighty God grant you with many more years so that you can see your great grandchildren.

To my brothers (Sibusiso Edward Gumede & Kabelo Mofokeng):

Never forget the powerful resources you always have available to you which is: love, prayer, appreciation, responsibility and forgiveness. I hope that with this research I have proven to you that you don't have to be great to start, but you have to start to be great. I hope that you will walk again and be able to fulfil your dreams.

To my son (Bokang Siphosethu Gumede):

I dedicate this entire thesis to you. You are truly a blessing and the greatest gift God has ever given me. I will always be there for you in good and bad times, when we are not together, God will be your guide. God bless you, I love you my son ☺

To Bokang's twin (Pakiso Mofokeng):

You are like my son ☺, I love you more than the world. Take care of each other.

ABSTRACT

The main purpose of this research was to use commercially available crystalline biobased polymers, namely poly(ε-caprolactone) (PCL) and poly(butylene succinate) (PBS), and introduce polycarbonate (PC)/multi-walled carbon nanotubes (MWCNTs) masterbatch into these polymers in order to provide additional functionalities, especially those associated with electronic applications. All the samples were prepared through melt-mixing in a twin-screw extruder.

According to our results, the PCL/PBS blends showed a sea-island morphology with discrete droplets of the minor phase within the matrix of the major phase, indicating immiscibility. The introduction of the PC/MWCNTs masterbatch to PCL, PBS and the PCL/PBS blends showed partial miscibility, where PC-rich, PCL-rich and PBS-rich phases were formed. A number of MWCNTs diffused from the PC-rich phase to the PCL-rich and the PBS-rich phases, although the MWCNTs were mostly agglomerated in the PC-rich phases. However, the extent of partial miscibility was different for each system. The polar component surface energy, interfacial tension and isothermal crystallization results suggested that the MWCNTs would preferably diffuse into the PBS-rich phase, rather than the PCL-rich phase.

Standard DSC measurements for the PCL/PBS blends, PCL/(PC/MWCNTs) and PBS/(PC/MWCNTs) nanocomposites demonstrated nucleation effects. In the PCL/PBS blends, nucleation was ascribed to (1) transference of the impurities from the PCL phase to the PBS phase, and (2) since the PBS crystallizes first, the PCL droplets may have crystallized by surface induced nucleation on the interface with the PBS crystallized matrix and nucleate at the interphase. In the case of the nanocomposites, the nucleation effect was attributed to the MWCNTs that diffused from the PC-rich to the PCL-rich and PBS-rich phases, even though the nucleating efficiency was lower than reported in the literature, which probably was due to the limited phase mixing between the PC-rich, the PCL-rich and PBS-rich phases. For the PCL/PBS/(PC/MWCNTs) nanocomposites, there was a decrease in the T_c values. This was due to the competition between two effects: (1) the partial miscibility of the PC-rich with the PCL-rich and PBS-rich phases, and (2) the nucleation effect of the MWCNTs. The decrease in the T_c values indicated that miscibility was the dominating effect.

Isothermal crystallization experiments performed by DSC showed an increase in the overall crystallization rate of PCL with increases in MWCNTs contents, which was

the result of their nucleating effect. However, for the PBS/(PC/MWCNTs) nanocomposites, the crystallization rate increased up to 0.5 wt% MWCNTs, while further increases in MWCNTs loading (and also in PC content) resulted in progressive decreases in crystallization rate. The results were explained through increased MWCNTs aggregation and reduced diffusion rates of PBS chains, as the masterbatch content in the blends increased. In the case of the PCL/PBS/(PC/MWCNTs) nanocomposites, the overall crystallization rates decreased as a result of the competition between the nucleating effect and miscibility. Since the PC-rich phase is partially miscible with the PCL-rich and PBS-rich phases, the PC probably immobilized the PCL and PBS chains and inhibited the rate of crystallization.

The thermal conductivities and mechanical strengths of the nanocomposites were generally enhanced compared to those of the neat material. The nanocomposites prepared in this work could be used in applications where electrical conductivity, as well as low weight and tailored mechanical properties, are required.

LIST OF SYMBOLS AND ABBREVIATIONS

2θ	scattering vector
a	amorphous component
a_0b_0	cross-sectional area of the chain
AC	alternating current
AFM	atomic force microscopy
b_0	width of the chain
BCB-EO	2-hydroxyethyl benzocyclobutene
c	crystalline component
CB	carbon black
CNF	carbon nanofibres
CNTs	carbon nanotubes
CO	carbon monoxide
CO_2	carbon dioxide
C-PCL	cyclic poly(ε-caprolactone)
D	particle size polydispersity
d	dispersive component
d^*	long period
d_n	number average diameter
d_v	volume average diameter
DC	direct current
DCC	N,N'-dicyclohexylcarbodiimide
DEA	dielectric analysis
λ	X-ray wavelength
$\Delta\gamma_2V_2$	the difference between the volume expansion coefficients in the glassy and liquid states of component 2
$\Delta\gamma_i$	change in the volumetric expansion coefficient
ΔH_m^o	molar heat of fusion
Δh_f	heat of fusion of a perfect crystal
ΔH_m	melting enthalpy
$\Delta H_{m,100}$	melting enthalpy for 100% crystalline polymer
ΔT	supercooling (T_m^o - T_c)
DMA	dynamic mechanical analysis

DSC	differential scanning calorimetry
ε’	dielectric permittivity storage
ε’’	dielectric loss factor
ε_b	strain at break
η*	complex viscosity
E	Young’s modulus
E’	storage modulus
E”	loss modulus
EASTAR	copolyester of adipic acid, terephthalic acid, and 1,4-butanediol
EMI	electromagnetic interference
f	correction factor, frequency
F	fullerene
f_{g2}	free volume fraction of polymer 2 at T_{g2}
f-MWCNTs	functionalized multi-walled carbon nanotubes
g	interaction term
γ	surface energy
$\gamma_{polymerA\text{-}Filler}$	interfacial tension between polymer A and the filler
$\gamma_{polymerA\text{-}polymerB}$	interfacial tension between polymers A and B
$\gamma_{polymerB\text{-}Filler}$	interfacial tension between polymer B and the filler
GO	graphene oxide
GPC	gel permeation chromatography
k	Boltzmann constant
K	dimensionless binary constant, overall crystallization rate constant
K_g^{τ}	constant related to the energy barrier for crystallization and growth
l	liquid
LH	Lauritzen and Hoffman
L-PCL	linear poly(ε-caprolactone)
M_n	number-average molecular weight
M_w	weight-average molecular weight
MWCNTs	multi-walled carbon nanotubes

MWS	Maxwell–Wagner–Sillars
n	Avrami index
NA	nucleating agent
p	polar component
P(BS-*co*-CL)	poly(butylene succinate-*co*-ε-caprolactone)
PBS	poly(butylene succinate)
PC	polycarbonate
PCL	poly(ε-caprolactone)
PE	polyethylene
PEO-PPO-PEO	poly(ethylene oxide)-block-poly(propylene oxide)-block-poly(ethylene oxide)
PET	polyethylene terephthalate
PHA	polyhydroxyalkanoates
PHB	polyhydroxybutyrate
PHBV	poly(3-hydroxybutyrate-co-3-hydroxyvalerate)
PLA	poly(lactic acid)
PLLA	poly(L-lactic acid)
PLOM	polarized light optical microscopy
PP	polypropylene
PS	polystyrene
PSS	poly(sodium 4-styrenesulfonate)
PVC	polyvinyl chloride
q	work needed for the chains to fold
R	universal gas constant
s	solid
SAXS	Small angle X-ray scattering
SEM	scanning electron microscopy
σ	lateral surface free energy
σ_b	stress at break
σ_e	fold surface free energy
σ_y	yield strength
SN	self-nucleation
SWCNTs	single-walled carbon nanotubes
t_0	induction time

T_{mb}^{o}	equilibrium melting points of the blend
T_{m}^{o}	equilibrium melting temperature
t	experimental time
T_{∞}	temperature at which chain mobility ceases
t_c	crystallization time
T_c	isothermal crystallization temperature
$T_{c,max}$	maximum peak crystallization temperature
$T_{c,NA}$	peak T_c-value determined from non-isothermal DSC
$T_{c,PCL}$	peak T_c value for neat PCL
T_g	glass transition temperature
$T_{m(obs)}$	observed melting temperature
T_s	self-nucleation temperature
$T_{s,ideal}$	ideal self-nucleation temperature
$\tau_{50\%}$	half-crystallization time
$1/\tau_0$	pre-exponential factor that includes nucleation and growth
$1/\tau_{50\%}$	overall crystallization rate
TEM	transmission electron microscopy
θ	contact angle
TSM	thermoplastic soy meal
U^*	activation energy for the transport of the chains to the growing front
V	molar volume, volume of the blend
V_c	relative volumetric transformed fraction
V_e	excess volume
V_i	specific volumes
W_f	weight fraction
w_α	wetting coefficient
WAXS	wide angle X-ray scattering
X_c	degree of crystallinity

TABLE OF CONTENTS

LIST OF TABLES

LIST OF FIGURES

CHAPTER 1

General introduction

1.1 Overview

Plastic waste is a growing problem in the whole world. The governments and many organizations are working to save the environment by utilizing biodegradable materials. Biodegradable polymers are materials that can fully decompose to carbon dioxide, methane, water, biomass and inorganic compounds under aerobic or anaerobic conditions. They should reduce waste and address the problem of a shortage in landfill availability [1-4].

Biodegradable polymers consist of a family of polyesters made up of two major groups; aliphatic (linear) polyesters, and aromatic (ring) polyesters. Aliphatic polyesters include poly(ε-caprolactone) (PCL) and poly(butylene succinate) (PBS), while aromatic polyesters include poly(butylene adipate-co-terephthalate) (PBAT) [5-7]. Amongst the polyesters, PCL received the most attention due to its elasticity, biocompatibility, and good ductility caused by its low T_g of -60 °C. PCL is a linear semicrystalline polyester with a moderate degree of crystallinity, and a low glass transition temperature. It is produced by ring opening polymerization of ε-caprolactone (see Figure 1.1) [8]. Its chains undergo degradation through hydrolytic or enzymatic reactions. It is used in medical applications as controlled drug release carriers, and lately it has been examined as potential biodegradable material for packaging applications. However, it has a relatively low mechanical strength, which limits its practical applications [9,10]. In order to improve the properties of PCL and maintain its biodegradability, several authors blended it with polymers such as poly(butylene succinate) (PBS), poly(lactic acid) (PLA) and poly(alkanoates) (PHA, PHB, PHBV) [11-18].

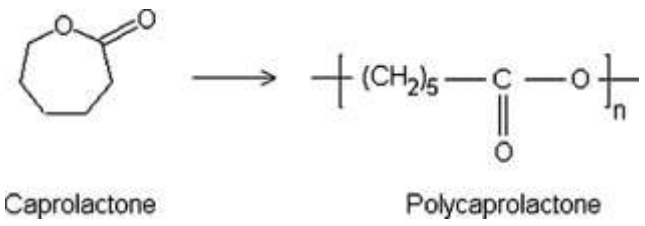

Figure 1.1 Ring-opening polymerization of ε-caprolactone to polycaprolactone [8].

Polymer blending offers advantages such as cost effectiveness and less time-consumption compared to the development of new monomers as a basis for new polymeric materials [19]. Blending of PCL with PBS was found to be interesting because of the mutual improvement in the properties of the individual polymers [11-16]. PBS is an aliphatic polyester synthesized through the polycondensation reaction of glycols, such as ethylene glycol and 1,4-butanediol, and aliphatic dicarboxylic acids, such as succinic acid and adipic acid. The chemical structure of PBS is shown in Figure 1.2 [8]. It has excellent mechanical properties that are closely comparable to those of the widely used polyethylene (PE) and polypropylene (PP).

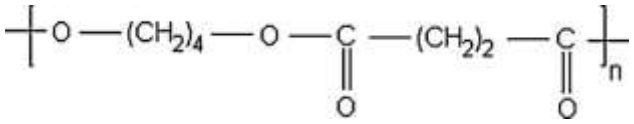

Figure 1.2 Chemical structure of poly(butylene succinate) (PBS) [8].

Although polymer blending is a good method for improving the properties of the individual polymers, some of the engineering applications cannot be met by merely blending polymers. For instance, many polymeric materials are transparent to electromagnetic radiation; thus no shielding is provided against electromagnetic interference (EMI). Recent reports revealed that the introduction of conductive carbon based nanofillers such as carbon nanotubes (CNTs), carbon black (CB), carbon nanofibres (CNF), and graphite into polymers gave rise to a number of new technological achievements, especially those associated with electronic applications. This is due to their low density, inertness and better compatibility than metal powders with most polymers [20-22]. In household electronic applications, polymer based nanocomposites are popular due to their light weight, easy processing and high strength. A major portion of polymer based nanocomposites are utilised in electrical circuits and insulation against atmospheric agents. The polymer adhesives industry is recently placing importance on structural applications and reparability as a part of the integration of such materials in petroleum and aerospace production systems [11,23].

One of the extraordinary materials for such applications is carbon nanotubes (CNTs). Carbon nanotubes are extremely strong and stiff nanostructures of carbon atoms arranged in a cylindrical hexagonal network, and are often categorized in two different groups: single walled carbon nanotubes (SWCNTs) and multi-walled carbon nanotubes

(MWCNTs). SWCNTs consist of a single graphene layer rolled up into a seamless cylinder, whereas MWCNTs consist of two or more concentric shells of grapheme sheets coaxially arranged around a central hollow core with van der Waals forces between adjacent layers (see Figure 1.3) [24]. MWCNTs are the ideal choice for high-volume industrial applications due to their bulk availability and better dispersion compared to SWCNTs.

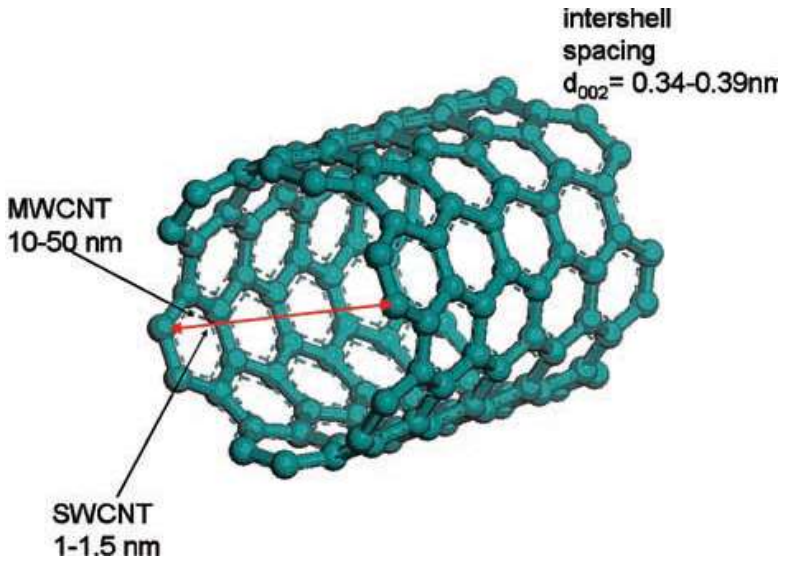

Figure 1.3 Model of carbon nanotubes with specific dimensions [24].

The introduction of MWCNTs into polymers did not only improve the thermal/mechanical performance of the nanocomposites, but also provided additional functionalities such as fire retardance, moisture resistance, electromagnetic shielding and barrier performances [22,25-27]. As a result, in this research project, MWCNTs were added to biodegradable polymers to form conductive materials for various applications.

1.2 Research objectives

In this work, nanocomposites were prepared by melt blending poly(ε-caprolactone) (PCL), poly(butylene succinate) (PBS) and PCL/PBS blends with a polycarbonate (PC)/MWCNTs masterbatch in a twin-screw extruder. The structure and properties of the nanocomposites were correlated with the dispersion, morphology, and nucleating effect of the MWCNTs on the PCL and PBS matrices. Additionally, the efficiency of the nucleation and the overall crystallization kinetics were determined by self-nucleation and isothermal crystallization studies.

1.3 Thesis organization

This thesis contains six chapters. Between this chapter and the 'Conclusions' chapter, there are four chapters in publication format, because this work has already been published in or submitted to international journals. Furthermore, the thesis does not have an experimental chapter, because the materials and methods details are included in Chapters 2 to 5 that are in scientific journal paper format.

1.4 References

[1] J.H. Song, R.J. Murphy, R. Narayan, G.B.H. Davies. Biodegradable and compostable alternatives to conventional plastics. Philosophical Transactions of the Royal Society B 2009; 364:2127-2139.
DOI: 10.1098/rstb.2008.0289

[2] T.S. Mdletshe, S.B. Mishra, A.K. Mishra. Studies on the effect of silicon carbide nanoparticles on the thermal, mechanical, and biodegradation properties of poly(caprolactone). Journal of Applied Polymer Science 2015; 132:42145.
DOI: 10.1002/app.42145

[3] A. Bhatia, R.K. Gupta, S.N. Bhattacharya, H.J. Choi. Compatibility of biodegradable poly(lactic acid) (PLA) and poly(butylene succinate) (PBS) blends for packaging application. Korea-Australia Rheology Journal 2007; 19:125-131.

[4] M. Gigli, A. Negroni, G. Zanaroli, N. Lotti, F. Fava, A. Munari. Environmentally friendly PBS-copolyesters containing PEG-like subunit: Effect of block length on solid-state properties and enzymatic degradation. Reactive & Functional Polymers 2013; 73:764-771.
DOI: 10.1016/j.reactfunctpolym.2013.03.007

[5] M.D. Sanchez-Garcia, E. Gimenez, J.M. Lagaron. Morphology and barrier properties of nanobiocomposites of poly(3-hydroxybutyrate) and layered silicates. Journal of Applied Polymer Science 2008; 108:2787-2801.
DOI: 10.1002/app.27622

[6] M.D. Sanchez-Garcia, A. Lopez-Rubio, J.M. Lagaron. Natural micro and nanobiocomposites with enhanced barrier properties and novel functionalities for

food biopackaging applications. Trends in Food Science & Technology 2010; 21:528-536.
DOI: 10.1016/j.tifs.2010.07.008

[7] J. Li, Y. He, Y. Inoue. Thermal and mechanical properties of biodegradable blends of poly(L-lactic acid) and lignin. Polymer International 2003; 52:949-955.
DOI: 10.1002/pi.1137

[8] R. Morent, N. De Geyter, T. Desmet, P. Dubruel, C. Leys. Plasma surface modification of biodegradable polymers: A Review. Plasma Process and Polymers 2011; 8:171-190.
DOI: 10.1002/ppap.201000153

[9] J. Peña, T. Corrales, I, Izquierdo-Barba, A.L. Doadrio, M. Vallet-Regí. Long term degradation of poly(ε-caprolactone) films in biologically related fluids. Polymer Degradation and Stability 2006; 91:1424-1432.
DOI: 10.1016/j.polymdegradstab.2005.10.016

[10] Y. Xu, C. Wang, N.M. Stark, Z. Cai, F. Chu. Miscibility and thermal behavior of poly(ε-caprolactone)/long-chain ester of cellulose blends. Carbohydrate Polymers 2012; 88:422-427.
DOI: 10.1016/j.carbpol.2011.11.079

[11] M.M. Reddy, A.K. Mohanty, M. Misra. Biodegradable blends from plasticized soy meal, polycaprolactone, and poly(butylene succinate). Macromolecular Materials and Engineering 2012; 297:455-463.
DOI: 10.1002/mame.201100203

[12] P. Nugroho, H. Mitomo, F. Yoshii, T. Kume, K. Nishimura. Improvement of processability of PCL and PBS blend by irradiation and its biodegradability. Macromolecular Materials and Engineering 2001; 286:316-323.
DOI: 10.1002/1439-2054(20010501)286:5<316::AID-MAME316>3.0.CO;2-N

[13] Z. Qiu, M. Komura, T. Ikehara, T. Nishi. Miscibility and crystallization behavior of biodegradable blends of two aliphatic polyesters. Poly(butylene succinate) and poly(ε-caprolactone). Polymer 2003; 44:7749-7756.
DOI: 10.1016/j.polymer.2003.10.013

[14] E. Can, S. Bucak, E. Kinaci, A.C. Çalikoğlu, G.T. Köse. Polybutylene succinate (PBS)-polycaprolactone (PCL) blends compatibilized with poly(ethylene oxide)-block poly(propylene oxide)-blockpoly(ethylene oxide) (PEO-PPO-PEO)

copolymer for biomaterial applications. Polymer-Plastics Technology and Engineering 2014; 53:1178-1193.
DOI: 10.1080/03602559.2014.886119

[15] Q. Liu, X.M. Zhou. Preparation of poly(butylene succinate)/poly(ε-caprolactone) blends compatibilized with poly(butylene succinate-co-ε-caprolactone) copolymer. Journal of Macromolecular Science, Part A: Pure and Applied Chemistry 2015; 52:625-629.
DOI: 10.1080/10601325.2015.1050634

[16] J. John, R. Mani, M. Bhattacharya. Evaluation of compatibility and properties of biodegradable polyester blends. Journal of Polymer Science: Part A: Polymer Chemistry 2002; 40:2003-2014.
DOI: 10.1002/pola.10297

[17] J.P. Mofokeng, A.S. Luyt. Morphology and thermal degradation studies of melt-mixed poly(lactic acid) (PLA)/poly(ε-caprolactone) (PCL) biodegradable polymer blend nanocomposites with TiO_2 as filler. Polymer Testing 2015; 45:93-100.
DOI: 10.1016/j.polymertesting.2015.05.007

[18] J.P. Mofokeng, A.S. Luyt. Morphology and thermal degradation studies of melt-mixed poly(hydroxybutyrate-co-valerate) (PHBV)/poly(ε-caprolactone) (PCL) biodegradable polymer blend nanocomposites with TiO_2 as filler. Journal of Materials Science 2015; 50:3812-3824.
DOI: 10.1007/s10853-015-8950-z

[19] L.M. Robeson. Polymer blends. A Comprehensive Review. Carl Hanser Verlag: München (2007).

[20] L. Wang, J. Qiu, E. Sakai, X. Wei. The relationship between microstructure and mechanical properties of carbon nanotubes/polylactic acid nanocomposites prepared by twin-screw extrusion. Composites Part A: Applied Science and Manufacturing 2016; 89:18-25.
DOI: 10.1016/j.compositesa.2015.12.016

[21] J.J. George, S. Bhadra, A.K. Bhowmick. Influence of carbon-based nanofillers on the electrical and dielectric properties of ethylene vinyl acetate nanocomposites. Polymer Composites 2010; 31:218-225.
DOI: 10.1002/pc.20788

[22] M. Bhattacharya. Review: Polymer nanocomposites – A comparison between carbon nanotubes, graphene, and clay as nanofillers. Materials 2016; 9:1-35. DOI: 10.3390/ma9040262

[23] Z. Han, A. Fina. Thermal conductivity of carbon nanotubes and their polymer nanocomposites: A review. Progress in Polymer Science 2011; 36:914-944. DOI: 10.1016/j.progpolymsci.2010.11.004

[24] M. Šupová, Gražyna S. Martynková, K. Barabaszová. Effect of nanofillers dispersion in polymer matrices: A Review. Science of Advanced Materials 2011; 3:1–25. DOI: 10.1166/sam.2011.1136

[25] P.C. Ma, N.A. Siddiqui, G. Marom, J.K. Kim. Dispersion and functionalization of carbon nanotubes for polymer-based nanocomposites: A review. Composites: Part A 2010; 41:1345-1367. DOI: 1016/j.compositesa.2010.07.003

[26] T.P. Gumede, A.S. Luyt, A.J. Müller. Review on PCL, PBS, and PCL/PBS blends containing carbon nanotubes. eXPRESS Polymer Letters 2018; 12:505-529. DOI: 10.3144/expresspolymlett.2018.43

[27] M.M. Reddy, S. Vivekanandhan, M. Misra, S.K. Bhatia, A.K. Mohanty. Biobased plastics and bionanocomposites: Current status and future opportunities. Progress in Polymer Science 2013; 38:1653– 1689. DOI: 10.1016/j.progpolymsci.2013.05.006

CHAPTER 2

Review on PCL, PBS, and PCL/PBS blends containing carbon nanotubes

This chapter has been published as:

T.P. Gumede, A.S. Luyt, A.J. Müller. Review on PCL, PBS, and PCL/PBS blends containing carbon nanotubes. eXPRESS Polymer Letters 2018; 12:505-529.*
(DOI: 10.3144/expresspolymlett.2018.43)

Author contributions: *Luyt and Müller conceived the project and guided the student, Gumede wrote this review.*

Abstract

Biodegradable polymers received considerable attention due to their contribution in the reduction of environmental concerns and the realization that global petroleum resources are finite. The development of double crystalline biobased blends such as poly(ε-caprolactone) (PCL) and poly(butylene succinate) (PBS) are particularly interesting because each component has an influence on the crystallization behaviour of the other component, and thus influences the strength and mechanical properties of a polymer blend. The lack of miscibility between PCL and PBS constitutes a bottleneck, and efforts have been made to improve the miscibility through the inclusion of copolymers. Having realized that incorporating conductive nanofillers such as carbon nanotubes (CNTs), (especially when the CNTs are functionalized or used as a masterbatch i.e., polycarbonate/MWCNTs masterbatch), into biopolymer matrices, can enhance the thermal and mechanical properties, as well as electrical and thermal conductivity, a lot of research was aimed at the production of bionanocomposites. This review paper discusses the properties of PCL, PBS, their blends, and their CNTs containing nanocomposites.

Keywords: nanocomposites, poly(ε-caprolactone); poly(butylene succinate); polycarbonate; carbon nanotubes

2.1 Introduction

Most plastic products that are used in our everyday lives such as polypropylene (PP), polyethylene (PE), polystyrene (PS), polyvinyl chloride (PVC) and polyethylene terephthalate (PET) are derived from petrochemical resources [1]. Fossil fuel and natural gases are the basic raw materials for the synthesis of petroleum based polymers. These polymers have excellent mechanical properties, good thermal stability, and chemical and biological inertness, and they have wide applications in the packaging industry (bottles, plastic bags, etc). They are, however, resistant to biodegradation and they survive in the environment for a long time, forming a significant part of municipal solid waste, due to the difficulty of recycling or reuse caused by various levels of contamination [2]. Packaging industries use up to 40% of produced plastics for short service life applications, and most of these plastics end up in landfills. Some of these polymers end up in the aquatic environment, and they pollute water. During incineration of these petroleum based plastics, harmful gases like carbon dioxide (CO_2), carbon monoxide (CO), dioxins and furans are released, and these are the major causes of atmospheric pollution, which leads to the deterioration of the ozone layer, resulting in climate change. There is thus a need to develop biodegradable polymers with similar functionality as petrochemical polymers, but that are readily susceptible to microbial action. This will contribute to a reduction in the environmental pollution caused by plastic waste, and also conserve petrochemical resources [2-5].

Biodegradable polymers are mainly synthesized from renewable natural resources and they degrade over a period of time through enzymolysis of microorganisms when exposed to a natural environment [2]. Different types of biodegradable polymers such as poly(ε-caprolactone) (PCL), poly(butylene succinate) (PBS), poly(lactic acid) (PLA), and poly(alkanoates) (PHA, PHB, PHBV) have been studied as potential biomaterials for a variety of applications such as biomedical devices, biodegradable packaging, adhesives, agricultural areas, auto-motion and construction [6-10]. However, some of these applications are limited due to the polymers' poor thermal and mechanical properties such as brittleness, low toughness and slow crystallization rates. Amongst the commercial biodegradable polymers, PCL received the most attention due to its elasticity, biocompatibility and good ductility caused by its low glass transition temperature (T_g) of -60 °C. It is easy to be melt processed by extrusion, melt-spinning, film blowing and

injection moulding, but it has relatively low mechanical strength which limits some practical applications.

Polymer blending is a useful method for achieving a desirable combination of properties, that are often absent in the neat polymers. It offers advantages such as cost effectiveness and less time-consumption compared to the development of new monomers as a basis for new polymeric materials. Additionally, a wide range of material properties is within reach by merely changing the blend composition [11]. PCL was blended with various other biodegradable polymers in a number of studies [12-22]. Amongst various biodegradable polymers, PBS was the most interesting aliphatic polyester due to its relatively good melt processability, thermal and chemical resistance, biodegradability, and excellent mechanical properties, closely comparable to those of the widely-used polyethylene (PE) and polypropylene (PP) [4,5,15-21,23-36]. Double crystalline PCL/PBS blends are particularly interesting because each component has an influence on the crystallization behaviour of the other component. Crystallinity and crystalline morphology have an influence on the strength and mechanical properties of a polymer blend, and it is therefore important to understand the influence of the other component in a blend on the crystallization behaviour of a particular component. Although blending is a good method for improving the properties of the individual polymers, the PCL/PBS blends are immiscible as evidenced by composition independent T_gs and a biphasic melt, which leads to poor interfacial adhesion and macrophase separation. Several methods, such as the addition of the copolymers (poly(ethylene oxide)-block-poly(propylene oxide)-block-poly(ethylene oxide) (PEO-PPO-PEO) and poly(butylene succinate-*co*-ε-caprolactone) (P(BS-*co*-CL)) and thermoplastic soy meal (TSM), have been applied to improve miscibility, interfacial adhesion and the resultant mechanical properties of PCL/PBS blends [16,20,21].

Recent reports [37-39] revealed that adding conductive carbon-based nano-fillers such as carbon nanotubes (CNTs) into PCL and PBS matrices can enhance some of the matrix properties to better levels than those of the copolymers or polymers filled with metal powders, as well as produce electrically conductive materials with better mechanical properties. This is due to their low density, inertness and better compatibility than metal powders with most polymers. CNTs have shown to have greater potential than any other carbon-based nano-fillers (i.e., carbon black (CB), carbon nanofibres (CNF), and graphite) because of their unique one-dimensional structure with good electrical conductivity, as well as excellent mechanical and thermal properties [40-42]. These

improved properties depend not only on the unique mechanical strength, large aspect ratio, and excellent thermal and electrical conductivities, but also on the alignment, adhesion, and dispersion in the polymer matrix. The enhanced mechanical properties, thermal properties and conductivity enable the PBS/CNTs nanocomposites to be used in industry fields, as well as in tissue engineering scaffolds or drug delivery systems. The potential applications for PCL/CNTs nanocomposites include vapour sensors, electromagnetic interference shielding and structural biomaterials for tissue engineering when electro-spun into membranes. PCL/PBS/CNTs nanocomposites can be used as biomaterials in applications such as tissue engineering, stent materials or drug delivery systems where their crystallinities, thermomechanical properties and biodegradation rates can be tailored according to the intended use. CNTs are extremely strong and stiff nanostructures of carbon atoms arranged in a cylindrical hexagonal network, and are often categorized in two different groups: single-walled carbon nanotubes (SWCNTs) and multi-walled carbon nanotubes (MWCNTs). SWCNTs consist of a single graphene layer rolled up into a seamless cylinder, whereas MWCNTs consist of two or more concentric cylindrical shells of graphene sheets coaxially arranged around a central hollow core with van der Waals forces between adjacent layers. MWCNTs are the ideal choice for high-volume industrial applications due to their bulk availability and better dispersion compared to SWCNTs [39,43].

Despite the advantages of carbon nanotubes, they have a tendency to form aggregates during mixing with polymers. This is due to the van der Waals attraction between the nanotubes, which makes it difficult for them to be dispersed into polymers. This has been a major drawback in the development of CNT-based polymeric nanocomposites. Several methods have been employed to enhance the dispersion of MWCNTs into polymer matrices, such as (i) treatment of CNTs with inorganic solvents (nitric acid (HNO_3), sulphuric acid (H_2SO_4) and phosphoric acid (H_3PO_4)) in order to attach hydroxyl and carboxylic acid functional groups to the nanotubes, and (ii) the masterbatch approach, which is a direct encapsulation of the CNTs into a polymer matrix, and the subsequent release of the carbon nanotubes into the polymer matrix during mixing in the melt. The masterbatch method has received great interest from an industrial point of view, because it does not involve solvents that are harmful to the environment [43-45].

The ultimate properties of the nanocomposites are dependent on the processing methods and processing conditions. Most CNTs/polymer nanocomposites were processed using the following methods: melt blending, solution mixing and *in situ* polymerization

[43,46,47]. Melt blending is one of the most economical and environmentally friendly methods of fabricating composites. The compounding is generally achieved in a single or twin-screw extruder where the polymer and the nanoparticle mixture are heated to form a melt. The mixer imparts shear and elongational stress to the process, helping to break apart the filler agglomerates and uniformly dispersing them in the polymer matrix. Another advantage of melt processing is that it does not require the use of organic solvents during processing. The compounded nanoparticle-polymer composite can be further processed using other polymer-processing techniques such as injection moulding, profile extrusion, blow moulding and hydraulic melt pressing. This is the processing method of choice for most industries [39]. Solution mixing is the most common method used for small-scale processing, while *in situ* polymerization has also been used. These two techniques are, however, not commercially viable and they are environmentally unfriendly, due to the use of toxic and/or volatile solvents. This review will explore the morphology and physical properties of PCL, PBS, their blends and their CNTs containing nanocomposites.

2.2 PCL/PBS blends

2.2.1 Morphology

Polymers are often blended together to improve the thermal and mechanical properties of the final product. The morphology of the polymer blend plays a critical role in understanding the structure-property relationships between the blend components, and hence there has been much research on structure development in such blends. Several studies were conducted on evaluating the morphology of PCL/PBS blends by employing scanning electron microscopy (SEM) and polarized light optical microscopy (PLOM) [16,17,19-21,27]. These blends were mostly prepared through melt blending and solution mixing methods. Regardless of the preparation method used, the morphologies of the blends were found to depend on the ratios of the components in the blend, their viscosities, and the interfacial tension between the component phases [27,48]. Depending on the PCL/PBS blend ratios, the minor component generally formed discrete spherical domains in a matrix of the major component, which indicates poor interfacial interactions between the components. This implied that PCL/PBS blends are immiscible because of the biphasic separation between the components in the blend. The non-uniform distribution

of the spherical domains is a result of the difference between the melt viscosities of PCL and PBS [27].

Immiscible polymer blends need to be compatibilized in order to achieve better interfacial interaction between the blend components. The compatibilization can be achieved through (i) optimization of the interfacial tension, (ii) stabilizing the morphology against high stresses, and (iii) enhancing the adhesion between the component phases. A number of studies investigated the effect of adding a compatibilizer on the morphologies of PCL/PBS blends [16,20,21]. In these studies, copolymers (PEO-PPO-PEO and P(BS-*co*-CL)) and thermoplastic soy meal (TSM) were used as compatibilizers. The compatibilizer was generally found to encapsulate itself between the polymer phases, reducing the spherical particle sizes and increasing the surface contact area between the blend components. In some cases, the addition of the compatibilizer resulted in the disappearance of the spherical domains, exhibiting a rougher fracture surface than the blend without the compatibilizer. This apparently confirmed the effective reduction of interfacial tension and a significant improvement in compatibility and interfacial adhesion [20]. Some researchers studied ternary blends of PCL and PBS with PLA or a copolyester of adipic acid, terephthalic acid, and 1,4-butanediol (EASTAR) as a third component [27]. The third component was also located at the interface of the PCL/PBS blends, demonstrating a three-phase line of contact at the interface, with improved intermolecular interactions.

2.2.2 Mechanical properties

The mechanical properties of immiscible polymer blends depend on the intermolecular forces, chain stiffness and the crystalline nature of the individual components in the blend [27]. Very few studies reported the mechanical properties of PCL/PBS blends, with the available reports showing tensile testing and dynamic mechanical analysis results [16,20,21,27]. The tensile strength was found to decrease as the PCL content increased in the blends, while the elongation at break and impact strength increased with increasing PCL content. The decreased tensile strength indicated poor interfacial interactions between the blend phases. The higher elongation values showed improved ductility and toughness in the blends, due to the plasticization by PCL, which led to improved chain mobility and energy absorbed by the material before fracturing.

When a P(BS-*co*-CL) compatibilizer was added in amounts up to 5 wt% in a 80/20 *w/w* PBS/PCL blend system, the modulus of elasticity, yield stress and fracture strain dramatically increased with increasing compatibilizer content [21]. This behaviour was attributed to the improved interfacial compatibility in the presence of the compatibilizer. However, the properties declined significantly with further increases in the compatibilizer content, but no explanation was offered for this observation. It is well known that the effectiveness of a compatibilizer depends on the content added in the blend, and in this case saturation was probably reached at 5 wt% content.

Since immiscibility of polymer blends strongly affect its mechanical properties, the effect of a compatibilizer on the thermo-mechanical properties of PCL/PBS blends was investigated by dynamic mechanical analysis (DMA) [20]. When PEO-PPO-PEO was used as a compatibilizer in PCL/PBS blends with different ratios, the storage modulus (E') values decreased with increasing PCL content. This result was attributed to the plasticizing effect of the copolymer backbone of the compatibilizer, that caused homogeneity in the sequence lengths. In the loss modulus (E") curves, both the PBS and PCL glass transition peaks were present, especially for the 20-40% PCL blends. This indicated that there was limited phase mixing of PCL and PBS. However, in the presence of the compatibilizer, the E" value for PBS shifted to lower temperatures with increasing PCL content, while the E" value for PCL slightly increased compared to that of neat PCL. This indicated interaction and compatibility between the two polymers in the presence of the compatibilizer.

2.2.3 Melting and crystallization behaviour

The immiscible nature of the two phases in the blends influence the thermal behaviour of the PCL/PBS blends. Several authors investigated the effect of blend composition, cooling and heating rates on the melting and crystallization behaviour of PCL/PBS blends [16,19-21,27]. The non-isothermal crystallization behaviour of PCL/PBS blends was studied using differential scanning calorimetry (DSC). Generally, the blends were cooled from the melt at various cooling rates of 2, 5 and 10 °C min^{-1}, and the subsequent melting behaviour was investigated at a heating rate of 20 °C min^{-1}. Two crystallization peaks were reported for the non-isothermal crystallization of these blends, corresponding to the crystallization of PBS and PCL, respectively. The crystallization peak temperature of PBS was higher than that of PCL, and the crystallization peak temperatures for PCL and

PBS in the blends remained almost the same as those of the neat materials, which confirmed the blend immiscibility. However, the crystallization exotherm of PCL in a 40/60 *w/w* PCL/PBS blend split into two peaks, although no explanation was given for this observation [19]. One possible explanation could be fractional crystallization, indicating better dispersion and a significant improvement in the interfacial adhesion compared to the PCL rich blends. For a given blend composition, the crystallization peak temperatures of PCL and PBS shifted to lower temperatures with increasing cooling rate due to supercooling.

The melting behaviour of the PCL/PBS blends, after the completion of the non-isothermal crystallization at various cooling rates, was also studied by DSC. Generally, two separate melting endotherms were reported for all the blends independent of the cooling rate used, corresponding to the melting of PCL at the lower temperature and PBS at the higher temperature. Double melting endotherms, or one main melting endotherm with a shoulder on the left side of the main melting peak, were found for PBS, and the ratio of the areas of the two melting peaks was influenced by the cooling rate used and the blend composition. The lower temperature melting peak was ascribed to the melting of the PBS crystals formed during the cooling process from the melt, while the higher temperature melting peak was attributed to the recrystallization-melting of the material which melted at the lower temperature. At a given cooling rate, and for a given blend composition, the ratio of the area of the lower melting peak to that of the higher melting peak decreased with increasing PCL content, indicating that the crystallization of PBS from the melt was hindered by the presence of PCL, especially during fast cooling, because less time was available for the crystallization of PBS.

In the case of the melting of PCL, only one well-defined melting peak was reported for the PCL-rich blends (100/0, 80/20, 60/40 *w/w*) at cooling rates of 2 and 5 °C min^{-1}, while a main melting peak with a small shoulder on the right side of the main melting peak was reported at a faster cooling rate of 10 °C min^{-1} [19]. For the PBS-rich blends (40/60 and 20/80 *w/w*), two melting peaks were reported for PCL independent of the cooling rate used. This double melting behaviour was ascribed to a melting–recrystallization mechanism. However, the blend composition also played an important role in the melting behaviour of the two components. When the content of the other component was higher in the blends, the appearance of a double melting peak due to melting-recrystallization was more pronounced. The degree of crystallinity (X_c) of the components in the blends was calculated using Equation 2.1.

$$X_c(\%) = \frac{\Delta Hm}{\Delta Hm,100\ x\ Wf}\ x\ 100 \qquad (2.1)$$

where ΔH_m was the melting enthalpy, W_f the weight fraction of PCL or PBS in the blends, and $\Delta H_{m,100}$ was the melting enthalpy for 100% crystalline polymer. For PBS, $\Delta H_{m,100}$ was taken as 110 J g^{-1}, which was calculated through extrapolation. For PCL, $\Delta H_{m,100}$ was taken as 136 J g^{-1}. The degree of crystallinity of PBS in the blend remained almost the same and was independent of the blend composition, while the degree of crystallinity of PCL in the blends decreased sharply, especially for the 60/40 *w/w* PBS/PCL blend, indicating that the presence of a high PBS content had a significant negative influence on the crystallization of PCL. PBS also showed a cold crystallization peak, which was enhanced by the addition of PCL. It was probably the larger free volume created by the molten PCL, which improved the mobility of the PBS chains and gave rise to its crystallization during heating.

The melting and crystallization behaviour of the PCL/PBS blends compatibilized with PEO-PPO-PEO and P(BS-*co*-CL) copolymers was reported in some studies [20,21]. The melting and crystallization temperature of PBS generally decreased in the presence of a PEO-PPO-PEO compatibilizer, which was attributed to the plasticizing effect of the copolymer backbone of the compatibilizer that caused homogeneity in the sequence lengths. However, there was no significant change in the melting temperature of PCL in the blends. It was further observed that the percentage crystallinity of PBS was influenced differently by the presence and amount of PCL in the blends, depending on whether the blends were compatibilized or non-compatibilized. This value increased with increasing PCL content throughout the composition range for the compatibilized blends, but for the non-compatibilized blends it increased with increasing PCL content up to 30 wt%, after which it declined. This indicates a saturation point due to limited phase mixing [20]. The addition of 5 wt% P(BS-*co*-CL) compatibilizer to a blend composition of 20/80 *w/w* PCL/PBS was found to result in a stronger interaction between the two components compared to 2 and 8 wt% compatibilizer contents. The latter two compatibilizer contents seemed to have retarded the crystallization of PBS and enhanced that of PCL in the blend [21].

2.3 PCL/PC blends

This section describes previous research on polycarbonate (PC)/PCL blends, because of the effective use of PC as matrix polymer in the preparation of CNTs masterbatches [49,50]. The PC/CNTs masterbatch can be added to PCL to improve the dispersion of CNTs in the PCL matrix.

2.3.1 Miscibility assessment

The most widely used method to evaluate whether miscibility was achieved, is by measuring the glass transition temperature. The PCL/PC blend system is an example in which homogeneous mixing of the components in the melt and in the amorphous phase, over the whole composition range, is envisaged [51-57]. PCL/PC blends were found to be miscible, because a single T_g, that varied with composition between those of the neat components, was observed (Figure 2.1). This is because, upon cooling, the amorphous phase remained a homogeneous mixture of the two polymers. Since the T_g of PCL is much lower than that of PC, the T_g of the blends decreased upon the addition of PCL to PC. The low T_g of PCL enabled the PC to crystallize at a rate that was much higher than that for neat PC, indicating that the PCL acted as a very effective macromolecular plasticizer [51,53]. Even though PCL and PC have been reported to be miscible, some authors [50] reported partial miscibility, where two phases were formed (PC-rich and PCL-rich phases). In the PC-rich phase, the small amount of PCL chains included within this phase plasticized the PC component and the PC-rich phase was therefore able to crystallize. In contrast, in the PCL-rich phase, the presence of PC chains caused changes in the glass transition temperature of the PCL phase that were much smaller than those predicted by the Fox equation.

Several equations were proposed to predict the values of the glass transition temperature for miscible polymer blends [51-53,58]. The earliest of these equations was the Fox equation (Equation 2.2):

$$\frac{1}{T_g} = \frac{w_1}{T_{g1}} + \frac{w_2}{T_{g2}} \qquad (2.2)$$

where T_g is the glass transition of the blend, and T_{gi} and w_i are the respective glass transitions and weight fractions of the components in the blend. For most blends, positive or negative deviations were observed from the Fox equation, because this equation does not take into account the interaction between the components. Another equation, which does factor in this interaction, is the Gordon-Taylor equation (Equation 2.3).

$$T_g = \frac{w_1 T_{g1} + K w_2 T_{g2}}{w_1 + k w_2} \tag{2.3}$$

where K is a dimensionless binary constant described by Equation 2.4.

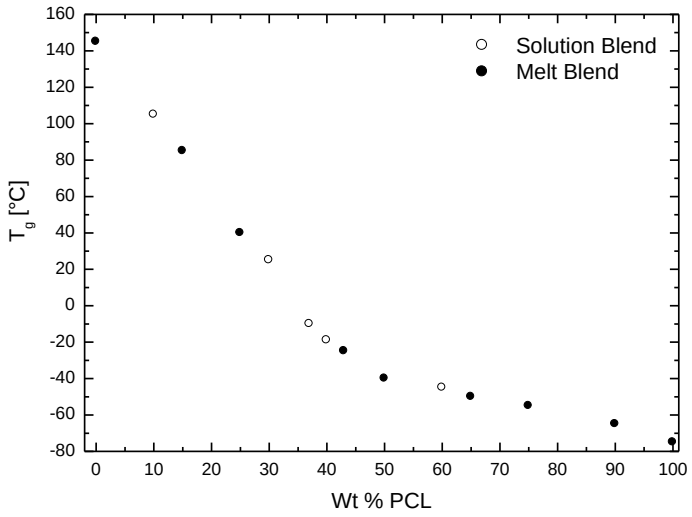

Figure 2.1 Effect of overall blend composition on the T_g observed by differential thermal analysis (DTA) on melt- and solution mixed blends [54].

$$K = \frac{\Delta\gamma_2 V_2}{\Delta\gamma_1 V_1} \tag{2.4}$$

where $\Delta\gamma_i$ is the change in the volumetric expansion coefficient at the glass transition temperature of each component, and V_i are their specific volumes. This equation was originally derived for random copolymers, and can be used to describe the composition dependence of miscible polymer blends exhibiting negative or positive deviations if K is treated as an adjustable parameter. However, it should only be applied to blends and mixtures with relatively weak specific intermolecular interactions. These classical equations predict that T_g increases continuously (smoothly) and monotonically with

composition. However, it has been reported that the T_g-composition variation of several polymer blend systems is not monotonic and exhibited a cusp at a certain critical composition. This phenomenon became very prominent when the T_g difference between the two homopolymers exceeded 50 °C. The classical equations became invalid below a critical temperature, T_c, as the free volume of the high T_g component became zero. The relationship between the critical temperature and the composition is given by the Kovacs expression (Equation 2.5):

$$T_c = T_{g2} - \frac{f_{g2}}{\Delta\gamma_2 V_2} \quad \text{if } T_{g2} > T_{g1} \tag{2.5}$$

where $\Delta\gamma_2 V_2$ is the difference between the volume expansion coefficients in the glassy and liquid states of component 2, and f_{g2} is the free volume fraction of polymer 2 at T_{g2}. Below T_c, the T_g is described by Equation 2.6:

$$T_g = T_{g1} + \left(\frac{f_{g1}}{\Delta\gamma_1 V_1}\right)\left(\frac{\phi_2}{\phi_1}\right) \tag{2.6}$$

According to this equation, the T_g of the blend is uniquely determined by the properties of the low T_g polymer at temperatures below T_c or at compositions below ϕ_c. For excess volume between the two polymers upon mixing, Braun and Kovacs derived Equation 2.7:

$$T_g = T_{g1} + \frac{\phi_2 f_{g2} + g\phi_1 \phi_2}{\phi_1 \Delta\gamma_1 V_1} \tag{2.7}$$

where g is an interaction term defined by Equation 2.8:

$$g = \frac{(Ve / V)}{\phi_1 \phi_2} \tag{2.8}$$

where V_e is the excess volume and V the volume of the blend. The excess volume of g is positive if blend interactions are stronger than those between the homopolymers. g is obtained by fitting the T_g-composition data to the Braun-Kovacs equation. Even though the literature conflicts in some aspects such as different methods used for preparing the blends, solution- or melt mixing, and the compositional variation of the glass transition, Cheung and co-workers [52] concluded that the Fox equation can only accurately predict

the glass transition temperature for compositions above 70% PC and that the Braun-Kovacs expression should be used in the other range. In contrast, Balsamo *et al*. [53] and Ketelaars *et al*. [51] accurately described the compositional variation with the Fox equation over the entire composition range.

2.3.2 Melting behaviour

The melting behaviour of the components in the blend was investigated in several studies [53,54,56]. In order to evaluate the miscibility in polymer blends, the equilibrium melting temperature (T_m^o) was determined [53,54]. Two different approaches are often used to obtain the equilibrium melting point. In the Gibbs-Thompson approach, T_m^o is obtained from the intercept of a plot of the reciprocal of lamellar thickness versus T_m. The most popular approach is the Hoffman-Weeks extrapolation, in which T_m^o is derived from a plot of apparent T_m versus T_c, the values of which are obtained after isothermal crystallization. The temperature at which the experimental T_m versus T_c line intercepts the $T_m = T_c$ line gives the equilibrium melting point. There are conflicting reports in the literature on certain aspects, such as the depression of the equilibrium melting temperature of one or more components in compositions where crystallization is possible, for example in PCL/PC blends where PCL was the major component. In [53,54], an equilibrium melting temperature depression was reported for both the PCL and PC components as the content of the other component increased. This decrease was attributed to (i) the reduction in the chemical potential of the component in the amorphous phase caused by the diluent polymer, (ii) polymer-polymer interactions, and (iii) lack of influence of morphological effects such as lamellar thickening and crystal perfection. However, in [56] no melting temperature depression was reported for either PCL or PC, and the authors concluded that the Flory interaction parameter, χ, for this PCL/PC blend system was possibly zero or slightly positive. Other authors were not able to perform the calculation of the Flory-Huggins interaction parameter, χ from Equation 2.9. This was due to a nonlinear dependence of the curves in a plot of $(1/T_{mb}^o)$-$(1/T_m^o)$ versus ϕ_a^2, suggesting that the interaction parameter could be composition dependent [53]:

$$\frac{1}{T_{mb}^o} - \frac{1}{T_m^o} = -\frac{R\bar{v}_c}{\Delta H_{mf}^o \bar{v}_\alpha} \chi \phi_\alpha^2 \qquad (2.9)$$

where T_m^o and T_{mb}^o are the equilibrium melting points of the neat crystalline component (PCL) and the PCL/PC blend, respectively. The subscripts *a* and *c* denote the amorphous and crystalline components. *R* is the universal gas constant, $\Delta H_m^o$is the molar heat of fusion for PCL (3880 cal mol^{-1}) and *V* is the molar volume (V_c for PCL = 105 cm^3 mol^{-1}, V_a for PC = 193.4 cm^3 mol^{-1}).

2.3.3 Crystallization behaviour

To be certain that the PCL/PC blends are not phase-separated upon preparation, the isothermal crystallization kinetics were investigated by employing DSC and synchrotron SAXS [52,53,56,57]. For neat PCL, the Avrami index *n* was found to be between 3 and 3.7 and for the blends it varied between 3 and 4, depending on the crystallization temperature used. This indicated that the nucleation mechanism changed from instantaneous (n = 3) to sporadic (n = 4) if spherulitic growth was assumed. When analyzing the variation of *n* with composition and the variation of *n* with increasing T_c, the *n* values in both cases exhibited an increase. This indicated a change in nucleation from instantaneous to sporadic. However, there was a general reduction in the values of *K* both with increasing T_c and increasing PC content. This is due to the higher rigidity of PC in comparison with PCL, which disturbed PCL's nucleation and molecular diffusion to the crystallizing front [53].

From the *n* and *K* values, the half-crystallization time (the time required to achieve 50% relative crystallinity or the time that the sample needs to develop half the amount of crystals it will eventually produce) was calculated according to Equation 2.10:

$$\tau_{50\%} = \left(\frac{\ln 2}{k}\right)^{1/n} \qquad (2.10)$$

The inverse of the experimentally determined half-crystallization time ($1/\tau_{50\%}$), is a quantity proportional to the overall crystallization rate (which includes both nucleation and growth). When the DSC results are coupled with the synchrotron findings, there existed a very strong parallel relationship between the overall rate of crystallization and the lamellar growth. The overall crystallization rate, $1/\tau_{50\%}$, as measured by DSC, and the lamellar growth, as monitored by synchrotron SAXS, decreased with increasing crystallization temperature and PC content [53,56]. This was due to the presence of PC,

that retarded both the overall crystallization rate and the lamellar growth of PCL, as well as the lower supercooling that slowed the crystallization process for all the composites [52].

2.4 PCL/CNTs nanocomposites

2.4.1 Morphology

Morphology characterization can answer many important questions about the distribution of nanotubes in a polymer matrix, the dispersion/agglomeration of the particles, and the interfacial interaction between the nanofiller and the polymer matrix [11]. Therefore, the visual aspects of morphology determination allow the investigator to hypothesize explanations concerning the observed property behaviour.

Extensive work has been conducted on PCL/MWCNTs nanocomposites [40-43,46,59-68]. The samples were mostly prepared by melt blending, solution mixing and *in situ* polymerization. The melt blending method is generally considered less effective to disperse MWCNTs in PCL than the other techniques, due to primary MWCNT aggregates that could not be fully detached during melt processing. Solution mixing is a two-step sonication method in which the polymer is first dispersed in a solvent and then the MWCNTs are dispersed in the polymer solution, while *in situ* polymerization involves the polymerization of the monomer using a radical initiator, with the MWCNTs dispersed in the prepolymer through ultrasonication. The nanocomposites prepared through solution mixing and *in situ* polymerization showed a uniform dispersion of the MWCNTs in the polymer matrix, because the agglomerates could be broken down giving rise to better contact and interfacial interactions between PCL and the MWCNTs [43,63]. However, the dispersed MWCNTs sometimes tended to reaggregate due to the van der Waals interactions among the MWCNTs, if the space between the dispersed MWCNTs was close enough. This tendency of reaggregation was more pronounced after stopping the ultrasonication and mechanical stirring. Several methods have been used to enhance the dispersion of MWCNTs into polymer matrices [43-45]. The methods commonly employed to improve dispersion include: (i) treatment of CNTs with inorganic solvents such as nitric acid (HNO_3), sulphuric acid (H_2SO_4) and phosphoric acid (H_3PO_4), in order to attach hydroxyl and carboxyl acid functional groups to the nanotubes, and (ii) the masterbatch approach, which is a direct encapsulation of the MWCNTs into a polymer

matrix, and the subsequent release of the carbon nanotubes into the matrix polymer during mixing in the melt. The masterbatch method has received great interest from an industrial point of view, because it does not involve solvents that are harmful to the environment [44,45,50]. During the functionalization process, the use of strong acids could damage the nanotubes by shortening of the length or unzipping the MWCNTs [43].

In investigations of the effect of pristine and functionalized MWCNTs on the morphologies of PCL/MWCNTs nanocomposites, the functionalized MWCNTs were found to be embedded in the PCL matrix and uniformly dispersed without apparent aggregation (Figure 2.2(b)). This was due to the formation of chemical bonds between the ester groups through a reaction between the carboxylic acid groups of PCL and the hydroxyl groups of functionalized MWCNTs. Some of the MWCNTs were emerging from the surface, but they were still surrounded by PCL, indicating good compatibility between the MWCNTs and the PCL matrix. On the other hand, the pristine MWCNTs (Figure 2.2(a)) were dispersed in the PCL matrix along with minor agglomerates due to the van der Waals interaction between the entangled carbon nanotubes [64].

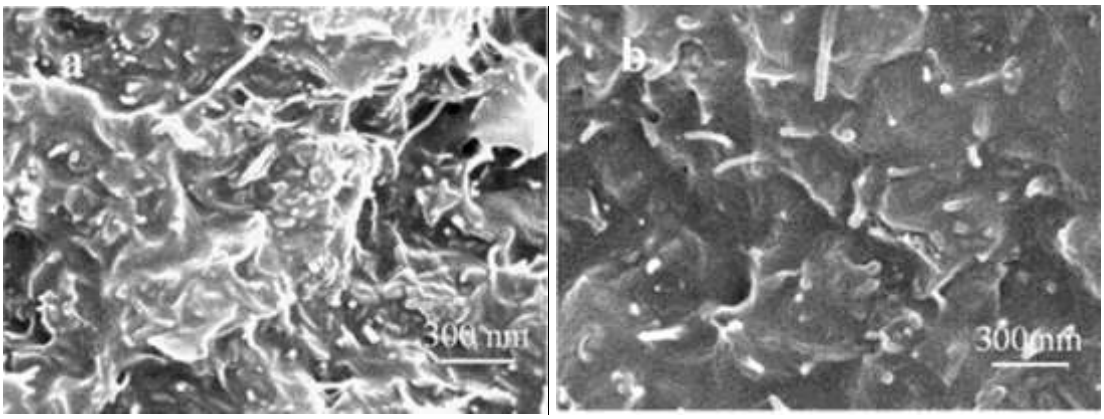

Figure 2.2 SEM images of the fractured surfaces (a) *p*-MWNT (5 wt%)/PCL and (b) *f*-MWNT (5 wt%)/PCL [64].

Elsewhere in the literature [50], the authors prepared nanocomposites by melt blending PCL with a polycarbonate (PC)/multi-wall carbon nanotubes (MWCNTs) masterbatch in a twin screw extruder. Their results indicated the presence of two phases (PC-rich and PCL-rich phases), where a small amount of PCL chains were present in the PC-rich phase, and can plasticize the PC component, such that it can crystallize. The PCL-rich phase contained only a small amount of PC chains, such that changes in the T_g of the PCL phase were much smaller than those predicted by the Fox equation. Due to the partial miscibility and the establishment of PC-rich and PCL-rich phases, a fair number of

MWCNTs diffused from the PC-rich phase to the PCL-rich phase, but their diffusion depended on the masterbatch content in the blend.

2.4.2 Mechanical and thermo-mechanical properties

Mechanical performance of polymer nanocomposites is dependent upon the interfacial interaction between the nanofiller and the polymer matrix, chain stiffness, and the crystallinity of the polymer in the nanocomposite. This implies that to utilize the reinforcing capability of carbon nanotubes and to maximize the mechanical properties of the nanocomposites, strong interfacial bonding is necessary. The extent of interaction depends on how well the filler is dispersed in the matrix [27]. Several authors evaluated the mechanical and thermo-mechanical performance of pristine and functionalized MWCNTs (*f*-MWCNTs) in PCL nanocomposites [39,59,60,62,68]. Generally, non-functionalized MWCNTs existed as agglomerates, because of the van der Waals forces and electrostatic interactions between the carbon nanotubes. The carbon nanotube agglomerates act as stress concentration points in the polymer matrix and can, in some cases, reduce the mechanical properties of the original polymer [39]. Functionalized MWCNTs nanocomposites gave much better mechanical properties than non-functionalized MWCNTs nanocomposites, which was ascribed to a better dispersion of the functionalized MWCNTs in the PCL matrix compared to the non-functionalized MWCNTs [59,60,68]. The mechanical properties such as tensile modulus, compressive modulus, tensile strength, storage modulus and elastic modulus increased with increasing MWCNTs content up to 0.5 wt%. However, the properties were more improved for the *f*-MWCNTs than for the pristine MWCNTs nanocomposites [41,62,68]. The improvement of these properties was related to the better dispersion of the *f*-MWCNTs in the polymer matrix that provided more uniform stress distribution, minimized the presence of stress-concentration centres, and increased the interfacial area for stress transfer from the polymer matrix to the MWCNTs [39,59,60,62,68]. Increasing the MWCNTs content above 0.5 wt% (especially for pristine MWCNTs) resulted in a decline in the mechanical properties of the nanocomposites. This was due to the formation of MWCNTs aggregates, which led to poor dispersion in the polymer matrix [41].

2.4.3 Nucleation and crystallization behaviour

The nucleation and crystallization behaviour of polymer nanocomposites is very important, because it affects not only the crystalline structure and morphology of semi-crystalline polymers, but also the final physical properties of the material. In previous research [46,60,64,67-69], different functional groups such as N-methylpyrrolidine, carboxyl and hydroxyl, urethane, phenylmethanol, primary amine groups and 2-hydroxyethylbenzocyclobutene were used to functionalize MWCNTs. In some cases, the MWCNTs were not modified [40,50,66,69]. In order to evaluate the efficiency of the MWCNTs as nucleating agents, it is necessary to compare their effect with that of the PCL self-nuclei or self-seeds. Self-nucleation (SN) experiments deal with the dependence of the melting temperature or self-nucleation temperature (T_s) on the subsequent crystallization process. According to Fillon *et al.* [70], three different domains can be identified. *Domain I* is when the T_s temperature is high enough to melt all the crystals and destroy the crystalline memory. *Domain II* is when lower T_s values will partially melt the crystals or leave some residual crystalline memory that can self-nucleate the material during cooling from T_s. *Domain III* is when lower T_s temperatures can only partially melt the material, and unmolten crystals can anneal during the time the sample stays at T_s (usually 5 min), while the molten material can self-nucleate during cooling from T_s. The self-nucleation temperature that originates the largest amount of self-nuclei is the lowest temperature belonging to *Domain II*. This temperature is called the ideal T_s ($T_{s,ideal}$). It is expected that the T_c values after SN at $T_{s,ideal}$ are the highest temperatures for the crystallization under non-isothermal conditions for a polymer. In fact, Fillon *et al.* [70] used such values as a reference to calculate the efficiency of a nucleating agent. The efficiency of the MWCNTs as nucleating agents for PCL was calculated according to Equation 2.11, which was proposed by Fillon *et al.* [71]:

$$NE = \frac{T_{c,NA} - T_{c,PCL}}{T_{c,max} - T_{c,PCL}} \text{ x } 100 \qquad (2.11)$$

where $T_{c,NA}$ is the peak T_c value determined from a non-isothermal DSC cooling run for a sample of the polymer with the nucleating agent (NA), $T_{c,PCL}$ is the peak T_c value for neat PCL after its crystalline history has been erased (also determined from a non-isothermal DSC cooling scan), and $T_{c,max}$ is the maximum peak crystallization temperature

determined after neat PCL has been self-nucleated at the ideal self-nucleation temperature or $T_{s,ideal}$ (i.e., the self-nucleation temperature that produces maximum self-nucleation without any annealing) [71,72].

Müller *et al*. first described supernucleation effects for PCL/CNT nanocomposites [66,69]. Supernucleation refers to the nucleation action that is better than that provided by the polymer's own crystals. A characteristic of this behaviour is a large increase in T_c. Some authors did, however, encounter antinucleation effects when the interaction between the CNTs' surfaces and the polymer was very poor [46]. Figure 2.3 summarizes the shifts in non-isothermal crystallization temperatures from that of neat PCL after introduction of CNTs, and the reasons for the differences observed in this figure are discussed in the next paragraphs.

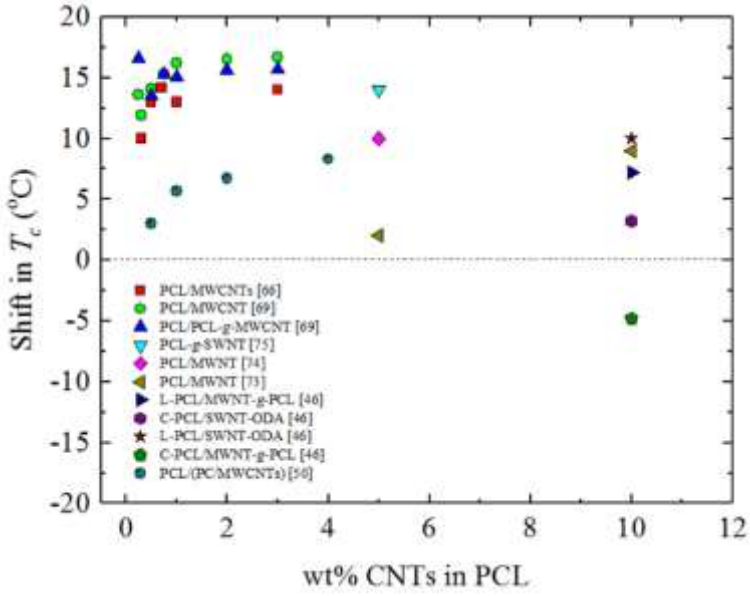

Figure 2.3 Crystallization temperature (T_c) shift (difference between the T_c value of neat PCL and the T_c value of the PCL with CNTs) for different PCL/CNT systems reported in the literature.

Trujillo *et al*. [66] investigated the nucleation behaviour of simple melt mixed, untreated PCL/MWCNTs nanocomposites, and reported for the first time a supernucleation effect in a well dispersed melt mixed system. This result indicated that the CNTs supernucleation could be dominated by (i) the strong interaction between the polymer and the MWCNTs and (ii) the dispersion quality of the blend. A similar or better supernucleation effect was reported when PCL was blended with PCL grafted MWCNTs (MWCNTs-*g*-PCL) [69]. The supernucleation effect of the MWCNTs was the result of

an excellent dispersion of the MWCNTs in the polymer matrix. However, the improvement in the dispersion with the modification of MWCNTs approach led to a decrease of its nucleation capacity, as a result of the agents introduced. Sanchez-Garcia *et al*. [73] prepared PCL/MWCNT nanocomposites by solution blending and obtained an increase in T_c of the PCL of only 2 °C for 5 wt% CNT content. When they increased the MWNT content to 10 wt%, they observed a maximum increase in T_c of 9 °C. Wu *et al*. [74] obtained T_c shifts of up to 10 °C in nanocomposites of PCL with 5 wt% functionalized MWNTs (the nanocomposites were prepared by a 'grafting to' technique during melt blending). On the other hand, Mitchell and co-workers [75] prepared PCL-*g*-SWNT nanocomposites with a 'grafting from' method and were able to observe a maximum increase in T_c of 14 °C with a 5 wt% MWNT content. Gumede *et al.* [50] prepared PCL/(PC/MWCNTs) nanocomposites by melt blending and obtained an increase in T_c of the PCL up to 1 wt% MWCNTs content. At MWCNT concentrations above 1 wt%, the increase was slow due to (i) limited phase mixing between the PC-rich and the PCL-rich phases, and (ii) an agglomeration of MWCNTs and PC crystallization.

Not all the literature reported increases in T_c for the PCL/CNT nanocomposites, because the efficiency of a nucleating agent depends on, among other factors, the interaction between the polymer and the CNT surface, and the quality of the dispersion and distribution of the particles. Pérez and co-workers [46] reported that MWCNTs, functionalized with 2-hydroxyethyl benzocyclobutene (BCB-EO) through a Diels-Alder cycloaddition reaction, nucleated linear PCL (L-PCL), but showed an antinucleation effect in cyclic PCL (C-PCL). This was due to the reduced diffusion of C-PCL induced by the threading effect induced by the L-PCL molecules grafted to the MWCNTs, which opposed the nucleating effect of the MWCNTs.

Crystallinity and crystalline morphology have an influence on the strength and mechanical properties of a polymer nanocomposite, and it is therefore important to understand the influence of the other component in the nanocomposite on the crystallization behaviour of a particular component. To describe the crystallization kinetics, the overall crystallization rate, $1/\tau_{50\%}$ (which includes both primary nucleation and growth kinetics components) is expressed as the inverse of the experimentally determined half-crystallization time and depends on isothermal crystallization temperatures. Table 2.1 shows crystallization temperature ranges for neat PCL and different PCL/CNT systems reported in the literature. In most of the kinetic studies

[50,66,69] on the crystallization of PCL/CNTs nanocomposites there were three general observations: (i) The crystallization temperature range for neat PCL was lower than those for the nanocomposites. This was an indication that the supercooling needed for the development of isothermal crystallization in the nanocomposites is much lower than that for neat PCL in view of the nucleation effect that they cause on the PCL matrix; (ii) The overall crystallization rate increased with MWCNTs loading for the systems explored, which was probably due to the nucleation effect that accelerated the primary nucleation and contributed to increasing the overall crystallization kinetics; (iii) The temperature dependence of the overall crystallization rate was not the same [46,50,66,69]. However, in study [46] the crystallization temperature range for C-PCL was higher than that of the C-PCL/MWNT-g-PCL nanocomposite, and the nanocomposite exhibited a decrease in overall crystallization rate compared to C-PCL. This was because of the antinucleation effect caused by the MWNT-*g*-PCL on C-PCL (caused by the threading effects of the grafted linear PCL chains and the C-PCL chains).

Table 2.1 Crystallization temperature range for neat PCL and different PCL/CNT systems reported in the literature.

Sample	**T_c range (°C)**			
Neat PCL	*33.0 - 40.5 [46] **43.0 - 46.5 [46]	45.0 - 49.5 [66]	35.0 - 44.0 [69]	41.0 - 50.0 [50]
Nanocomposites	*36.5 - 40.5 [46] **39.0 - 46.5 [46]	49.0 - 54.5 [66]	48.0 - 53.0 [69]	42.0 - 54.0 [50]

*L-PCL, **C-PCL

The influence of MWCNTs on the crystallinity of a polymeric matrix can vary, depending on the polymer/MWCNTs interaction and the nanofiller dispersion achieved. Different trends were reported in terms of evaluating the percentage crystallinity of PCL/MWCNTs nanocomposites, amongst others an increase [66], a decrease [50,60] and no change [46] after the addition of MWCNTs. The increase in crystallinity was attributed to the excellent dispersion and nucleating power of the MWCNTs, and the decrease to steric restrictions between the polymer chains and the MWCNTs that limited chain diffusion during crystallization.

The data obtained during the isothermal crystallization experiments were analyzed employing the Avrami equation, which is expressed in Equation 2.12 [76]:

$$1 - V_c(t - t_0) = \exp(-K(t - t_0)^n) \qquad (2.12)$$

where t is the experimental time, t_0 is the induction time, V_c is the relative volumetric transformed fraction, n is the Avrami index, and K is the overall crystallization rate constant. The Avrami index n, which is obtained from the slope of the linear fit in Equation 2.12, represents the order of the crystallization kinetics and depends on the dimensionality of the crystalline superstructure and on their nucleation kinetics [76,77]. Generally, neat PCL revealed Avrami index values of approximately $n = 3$. This indicates that (i) the crystal geometry is spherulitic and follows an athermal nucleation which leads to spherulites of roughly the same size during isothermal crystallization, and that (ii) the nucleation is very fast (instantaneous), and the nucleation starts almost immediately after the isothermal crystallization temperature was reached [47,66,69]. Trujillo *et al*. [66] reported lower Avrami index values (approximately $n = 2$) for PCL/CNT nanocomposite systems compared to the $n = 3$ for neat PCL, corresponding to the formation of axialites. This indicates that the growth of the polymer crystals was affected by the dense nucleation on the MWCNTs surfaces, thereby decreasing the dimensions of the polymer crystals. Gumede and co-workers [50] reported values higher than 3 for the PCL/(PC/MWCNTs) nanocomposites, which was unexpected because it was reported that MWCNTs are effective in nucleating PCL. In some cases, the Avrami index values showed slight variations for both neat PCL and the nanocomposites in the range of 1.4 to 1.8. The slight variation of n indicates that the crystallization mechanism may not change within the investigated crystallization temperature range, irrespective of the content of the MWCNTs [68]. An increase in n values was also reported [46], as nucleation tends to be more sporadic with increasing temperature. The Avrami index values were within 2.5-3, indicating instantaneous spherullites were formed. At low T_c values, the Avrami index approached 2 (corresponding to axialites) indicating that nucleation densities are too high and early impingement prevented superstructures from developing full tridimensional spherulites. However, in the case of C-PCL/MWNT-*g*-PCL, the effect caused a relatively more sporadic nucleation as Avrami indices were between 3.5 and 4 at high T_c temperatures. Since the unit of K (intercept of the linear fit in Equation 2.12) is min^{-n} and n is not constant, it is difficult to compare the crystallization rate directly from the values of K. However, the values of $K^{1/n}$ display a similar trend to $1/\tau_{50\%}$, since $K^{1/n}$ is also related to the overall crystallization kinetics.

In addition to the use of the Avrami equation, many researchers employed nucleation and growth theories to fit the crystallization kinetics data. The most widely employed approach is the Lauritzen and Hoffman (LH) theory, originally derived for secondary nucleation, and extended to nucleation and growth DSC data, in the expression given by Equation 2.13 [78]:

$$\frac{1}{\tau_{50\%}}(T) = \frac{1}{\tau_0}\exp\left(\frac{-U^*}{R(T_c - T_\infty)}\right)\exp\left(\frac{-K_g^\tau}{T_c \Delta T_f}\right), \qquad (2.13)$$

where $1/\tau_{50\%}$ is the inverse of the experimental half-crystallization time (obtained by DSC isothermal experiments), $1/\tau_0$ is a pre-exponential factor that includes nucleation and growth, U^* is the activation energy for the transport of the chains to the growing front (a value of 1500 cal.mol^{-1} is usually employed), R is the gas constant, T_c is the isothermal crystallization temperature (K), T_∞ is the temperature at which chain mobility ceases (usually taken as T_g – 30 K), and ΔT is the supercooling (T_m^o - T_c), with T_m^o as the equilibrium melting temperature. The correction factor f is a temperature correction term equal to $2T_c/(T_c + T_m^o)$, and K_g^τ is a constant related to the energy barrier for crystallization and growth. If the crystallization rate is approximated to experimentally determined values of the inverse of half crystallization times ($1/\tau_{50\%}$), then K_g^τ values are proportional to the energy barrier for overall crystallization. The value of K_g^τ is given by Equation 2.14 according to the Lauritzen and Hoffman theory.

$$K_g^\tau = \frac{j b_0 \sigma \sigma_e T_m^0}{k \Delta h_f}, \qquad (2.14)$$

where b_0 is the width of the chain, σ is the lateral surface free energy, σ_e is the fold surface free energy, T_m^0 is the equilibrium melting temperature (K), k is the Boltzmann constant and Δh_f is the heat of fusion of a perfect crystal. The parameter j is determined by the crystallization regime and is equal to 4 for regime I and III, and equal to 2 for regime II. The Lauritzen-Hoffman theory analyzes the growth data according to competition between the rate of deposition of secondary nuclei (i) and the rate of lateral surface spreading (g), resulting in three different regimes. Regime I occurs when $i << g$ and may be found at very low supercoolings; in regime II, i is of the order of g and occurs at

moderate supercoolings; in regime III, $i > g$ and is found at very high supercoolings. From the values of K_g^{τ}, the product $\sigma\sigma_e$ is obtained from Equation 2.14. Equations 2.15 and 2.16 allow the calculation of σ (and therefore σ_e) and q, the work done by the chain to form a fold.

$$\sigma = 0.1\Delta h_f\sqrt{a_0 b_0} \quad (2.15)$$

$$q = 2a_0 b_0 \sigma_e \quad (2.16)$$

where $a_0 b_0$ is the cross-sectional area of the chain. To obtain the parameters of the LH theory, the following values were used: T_g = 213 K, T_g – 30 K, ΔH = 163 J g^{-1}, a_0 = 4.52 Å, b_0 = 4.12 Å, p_c = 1.1 g cm^{-3}, U^* =1500 cal mol^{-1}. According to the literature [78], the K_g^{τ} values are lower for the nanocomposites than for neat PCL. This result was interpreted by considering that a supernucleation effect contributed to decreasing the energy barrier for overall crystallization (which includes both nucleation and growth) and decreased the fold surface free energy (σ_e) and the work needed for the chains to fold (q). It was found that above 0.5 wt% MWCNTs loading [66], the supernucleation effect was so large that a transition to Regime III occurred, since nucleation was much faster than the spreading rate. However, some studies reported only Regime II for the nanocomposites, indicating that the nucleation was not so fast due to the moderate supercoolings and interaction between the polymer and the MWCNTs [79,80].

2.4.4 Conductivity

Heat dissipation in modern electronic devices require interface materials with high electrical and thermal conductivities. Nanocomposites made up of polymer matrices and carbon nanotubes have been investigated with the aim of utilizing the good thermal and electrical properties of carbon nanotubes. Currently, the proposed applications for PCL/CNTs nanocomposites include vapour sensors, electromagnetic interference shielding and structural biomaterials for tissue engineering when electro-spun into membranes. A low electrical percolation threshold and good electrical conductivity are the critical properties required. It is important to note that electrical and thermal conductivities occur according to different mechanisms. The mechanism of thermal

energy transport in CNTs is perceived to take place through phonon conductivity, and it preferably occurs in the crystalline parts in the bulk of the polymer, and to a smaller extent at the points of contact with the CNTs. Phonons transfer heat energy through interactions with each other and with subatomic particles. On the other hand, the mechanism of electrical energy transport in CNTs is dominated by the tunneling distances at the nanotube-nanotube contacts [40-42,49,64]. The type of processing method, dispersion and concentration of the CNTs play a significant role in their electrical conductivities.

Table 2.2 A comparative study of PCL/MWCNTs nanocomposites.

Functionalization technique	Dispersion technique	MWCNTs content	Percolation threshold
No MWCNTs modification [40]	Melt-mixing	0.2 - 0.5 wt%	0.2 wt%
No MWCNTs modification [41]	Melt-mixing	0.05 – 5.0 wt%	0.3 wt%
No MWCNTs modification [42]	Melt-mixing	0.5 wt%	2.0 wt%
Nitric acid treatment [64]	*In situ* polymerization	0.5 – 5.0 wt%	-
No MWCNTs Modification [49]	Melt blending	0.35 – 7.0 wt%	0.14 wt%
PC/MWCNTs Masterbatch [50]	Melt blending	0.5 – 4.0 wt%	0.5 - 1.0 wt%

Several studies investigated (i) the electrical conductivities of pristine and functionalized MWCNTs, (ii) the percolation threshold in PCL nanocomposites, and (iii) the dependence of electrical and thermal conductivities on the degree of crystallinity of PCL [40-42,50,64,49,81,82]. In general, irrespective of the reported methods of PCL/MWCNTs nanocomposites preparation, the percolation threshold of the nanocomposites was less than 1.0 wt% in most cases (Table 2.2). This indicated that the MWCNTs were fairly well dispersed in the polymer matrix and could connect with each other, and subsequently form an interconnecting conductive pathway. The electrical conductivity values increased by more than one order of magnitude. The increase in the electrical conductivity with increasing crystallinity can be explained by the reduction of the nanotube-nanotube distances in their contact regions, which suggested an

enhancement in the electron transport and a reduction in ion mobility in the crystalline phase [40]. Both the pristine and functionalized nanocomposites showed good electrical conductivity at low MWCNTs contents, which is related to the formation of a conductive nanotube network. However, the electrical conductivity values of the nanocomposites with pristine MWCNTs was higher than those of the nanocomposites with functionalized MWCNTs. This is due to the acid treatment in the functionalized MWCNTs, which usually destroys the π-network in the carbon nanotubes [64]. The thermal conductivities of the PCL/(PC/MWCNTs) nanocomposites (with 4 wt% MWCNTs content) increased by 20% in comparison to that of the neat material [50]. This is because the thermal conductivity of carbon nanotubes ranges between 650 and 10,000 W m K^{-1}, and the thermal conductivity of a typical polymer ranges between 0.1 and 0.3 W m K^{-1} [39], and therefore the improvement in the thermal conductivity is most probably caused by the increasing numbers of high thermal conductive MWCNTs in the nanocomposites. Since the MWCNTs were fairly well dispersed in the PCL/PC blend (although there were pockets where the MWCNTs were concentrated), the MWCNTs were positioned closer to each other as the MWCNTs content increased, which gave rise to more effective transport of the phonons through the nanocomposite, and which improved the transportation of heat by high frequency phonon vibration, leading to higher thermal conductivities.

2.4.5 Rheological properties

Rheology is the study of the flow behaviour of a material under conditions in which they flow rather than deform. The study of the rheological response of CNT/polymer nanocomposites has both practical importance related to composite processing and scientific importance as a probe of the composite dynamics and microstructure. The rheological properties of CNT/polymer nanocomposites depend on factors such as aspect ratio, dispersion, polymer molecular weight, the interfacial interaction between the polymer and filler, and the characteristics of the filler loading [83]. The variations of viscosity and storage modulus of composites as a function of frequency are two commonly used techniques to characterize the rheological properties of CNT/polymer nanocomposites.

The complex viscosity (η*) at low frequencies increased as the MWNT content increased for P-MWNT/PCL and A-MWNT/PCL. The η* of P-MWNT/PCL and A-

MWNT/PCL showed Newtonian behaviour for MWCNT contents less than 2 wt%, while those of higher than 2 wt% MWCNTs showed profound shear-thinning behaviour. This viscosity behaviour indicated that a percolation threshold, which represents a starting MWCNT content for a three-dimensional network, was 2 wt% for both the P-MWNT/PCL and A-MWNT/PCL [64].

Pötschke *et al.* [42] prepared composites of PCL and 0.5 wt% MWCNTs at different rotation speeds by melt-mixing in a conical twin-screw micro-compounder. The results for the composite produced at the lowest mixing speed (25 rpm) and having the highest agglomerate ratio were similar to those of neat PCL, but at low frequencies there was already a deviation towards higher values. The two composites produced at 50 and 75 rpm (showing decreased agglomerate area ratios) showed a pronounced increase in complex viscosity and storage modulus at all frequencies, but especially at low frequencies. These changes implied the better development of a combined filler-polymer network. However, at higher rotation speeds (above 75 rpm), a decrease in the complex viscosity and storage modulus at low frequencies was reported, which was explained through an overlapping influence of nanotube shortening during the mixing process at the corresponding higher shear stresses. The effects were also related to the dispersion and nanotube shortening, but a third possible influence, namely PCL degradation at higher mixing speeds, could be excluded.

2.5 PBS/CNTs nanocomposites

2.5.1 Morphology

In the reported research, multi-walled carbon nanotubes (MWCNTs)/polybutylene succinate (PBS) nanocomposites were prepared by two frequently used methods, melt and solution mixing. The state of dispersion of MWCNTs depended on the mixing method, modification and concentration of MWCNTs in the nanocomposites.

Nanocomposites prepared by melt blending resulted in MWCNTs aggregation, which is inefficient in dispersing the aggregates into individual MWCNTs, despite the large shear forces applied during mixing [83-87]. In the case of nanocomposites prepared through solution mixing, no apparent aggregation was reported. This is due to the use of ultrasonication that is able to disrupt nanotube aggregation, giving rise to better contact between PBS and the MWCNTs [88]. Several chemical methods have been reported for

the functionalization of MWCNTs, such as (i) the use of N,N'-dicyclohexylcarbodiimide (DCC) to introduce a long alkyl chain onto the MWCNTs, and (ii) surface wrapping of poly(sodium 4-styrenesulfonate) (PSS) with the aid of ultrasound [47,88]. In these studies, the MWCNTs were well dispersed in the PBS matrix and showed better interfacial adhesion with the PBS phase than with each other. This is due to π–π interactions between the benzene rings, and between the long alkyl chain groups and the graphite rings of the MWCNTs.

The concentration of the MWCNTs was found to have an influence on the state of dispersion and distribution in the polymer matrix. Some authors studied the effect of melt-mixed MWCNTs on the morphology of the PBS/MWCNTs nanocomposites [83-85]. Their results indicated that at low MWCNTs content (i.e., 1 wt%), the carbon nanotubes were well dispersed and embedded in the PBS matrix. However, at high MWCNTs loadings (i.e., 3 wt%), the carbon nanotubes were poorly dispersed as aggregates. It is well known that agglomeration of filler nanoparticles increases with increasing filler content. This is because the nanotubes are closer to each other as the content of the nanotubes increases, and agglomeration occurs due to the Van der Waals interactions between the MWCNTs. It is difficult separating these MWCNTs during melt processing, even when the MWCNTs are modified. MWCNTs were also functionalized by surface wrapping of PSS with the aid of ultrasound, and the nanocomposites were prepared by solution mixing [88]. In this case, the carbon nanotubes were uniformly dispersed in the PBS matrix. No obvious aggregation was reported for all the nanocomposites.

2.5.2 Mechanical and thermo-mechanical properties

Several factors, such as dispersion, distribution and matrix-CNTs interfacial adhesion, influence the mechanical and thermo-mechanical properties of polymer nanocomposites [83,86]. Tensile testing and dynamic mechanical analysis (DMA) were employed to study the mechanical and thermo-mechanical properties of the nanocomposites. The nanocomposite preparation methods, in most cases either melt-mixing or solution-blending, led to different properties of the materials. For instance, PBS/MWCNTs nanocomposites prepared by solution mixing exhibited better mechanical properties, such as higher tensile strength and storage modulus, than the melt-mixed nanocomposites. This was due to the better dispersion of the MWCNTs in the PBS matrix for the solution mixed samples [88].

The effect of pristine and functionalized MWCNTs on the mechanical and thermo-mechanical properties of the PBS/CNTs nanocomposites were investigated in a number of studies [33,47,83,84,86,88,89]. The carbon nanotubes were mostly functionalized using (i) acid solution followed by grafting MWCNTs with polyetheramines, (ii) N,N'-dicyclohexylcarbodiimide (DCC) dehydrating agents, (iii) nitric acid, and (iv) surface wrapping of MWCNTs with PSS with the aid of ultrasound. The nanocomposites containing functionalized MWCNTs exhibited an increase in the storage modulus and Young's modulus with increasing MWCNTs content, while the elongation at break for the nanocomposite samples was smaller than that of neat PBS. This was attributed to the well dispersed carbon nanotubes in the PBS matrix and the good interaction between the components in the nanocomposites, that resulted in more uniform stress distribution and minimization of the presence of stress-concentration centres. This further implied that the nanotubes could enhance the rigidity of the nanocomposites, because reinforcement by incorporation of MWCNTs causes a loss in flexibility [33,47,83,88]. For nanocomposites containing pristine MWCNTs, the storage modulus, loss modulus, and tensile strength initially increased with increasing MWCNTs contents, but then decreased for MWCNTs contents above 3 wt%. This was attributed to the significant aggregation of the pristine MWCNTs that prevented efficient load transfer to the polymer matrix. The significant improvement in mechanical properties at lower MWCNT contents was attributed to the incorporation of rigid MWCNTs into the relatively soft PBS matrix that caused a reinforcement effect [86]. Elsewhere in the literature [88], the authors investigated the effects of different carbonaceous nanoparticle types such as carbon nanotubes (CNT), carbon black (CB), and fullerene (F) on the dynamic mechanical properties of PBS. Their results indicated that all the nanocomposites exhibited higher storage modulus with respect to neat PBS below the glass transition temperature. This was attributed to the reinforcement effect of the presence of rigid carbon nanoparticles and the good interaction between PBS and nanofillers, leading to a prominent improvement in the stiffness of the PBS matrix. The modulus of PBS/1 wt% CNT nanocomposite was the highest, because of the higher interfacial area between CNT and the PBS. However, the storage modulus leveled off at temperatures above 50 °C for both neat PBS and its nanocomposites, indicating that the effect of the nanofiller incorporation became negligible, and the rigidity of the nanocomposites was matrix-dependent. The glass transition temperature of the nanocomposites did not change with respect to PBS by the addition of different carbonaceous nanoparticles. The results indicated that the molecular movements or

segmental motions of the PBS matrix were not significantly affected by the incorporation of the nanofillers.

2.5.3 Melting and crystallization behaviour

The melting and crystallization behaviour of polymer nanocomposites has an influence on the strength and mechanical properties of the final product. It is therefore important to understand the influence of the nanofiller in the nanocomposite on the crystallization behaviour of the polymer. A number of studies investigated the melting, nucleation, and crystallization behaviour of PBS/MWCNTs nanocomposites by DSC and polarized light optical microscopy (PLOM) [47,84-86,88-91]. Generally, double melting peaks were reported for all the PBS/MWCNTs nanocomposites, associated with the partial melting, recrystallization, and re-melting of the PBS crystallites. The main peak remained at the same temperature as the melting of neat PBS, but the small peak shifted towards a lower temperature with increasing MWCNTs content. The main peak was attributed to the melting of larger, more perfect crystals that was not affected by the presence of MWCNTs, while the small peak was ascribed to the melting of unstable crystals formed at a higher temperature. This was due to the nucleating effect of the MWCNTs that reduced the ability of the PBS chains to be fully incorporated into the growing crystalline lamellae.

In most cases, the crystallization temperature, T_c, of all the PBS/MWCNTs nanocomposites was higher than that of neat PBS, and increased with increasing MWCNTs content. This was attributed to the nucleating effect of the MWCNTs on PBS crystallization that improved the crystallizability of the PBS. However, with an increase in MWCNTs content above 0.5 wt%, the T_c increased only slowly, indicating a saturation in the nucleation effect at higher MWCNTs contents [47,84,86,88-90]. In order to visualize the nucleating ability of MWCNTs on the crystallization of PBS, the spherulitic morphology of neat PBS and its nanocomposites was investigated (Figure 2.4). Neat PBS showed well-developed, large Maltese-cross pattern spherulites with clear boundaries. However, with increasing MWCNTs content, the sizes of the spherulites decreased while the number of spherulites gradually increased. This was an indication of the nucleating effect of the MWCNTs on the PBS crystallization that hindered the growth of the PBS crystals through obstruction of the folding of the PBS chains during the crystallization process. At high MWCNTs content the spherulites were not well-developed, imperfect

and grew rapidly. The presence of MWCNTs caused impingement and restricted further growth of the spherulites. This was due to the formation of large numbers of nucleation sites at high MWCNTs contents [84,85,88,90,91].

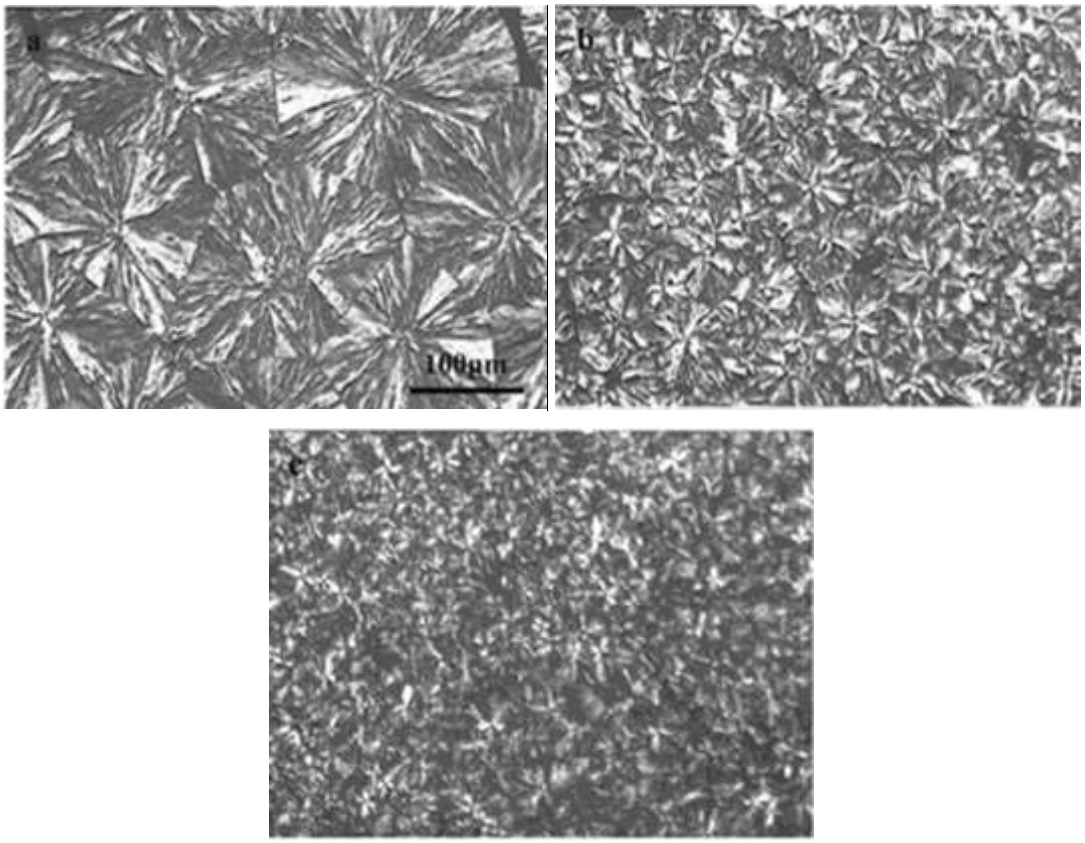

Figure 2.4 Polarized optical micrographs for neat PBS and its nanocomposites. These samples were all melt crystallized at 95 °C [84].

Since the presence of CNTs had a large influence on the crystallization behaviour of PBS, it was necessary to further explore the crystallization kinetics of the PBS/CNTs nanocomposites. Both the isothermal [85,90] and non-isothermal [87,91] crystallization kinetics of neat PBS and the nanocomposites were explored. For non-isothermal crystallization kinetics, several different kinetic models were employed [87,91]. The Avrami equation (as described in section 2.3.3) was used to describe the isothermal crystallization. Irrespective of the nanocomposite preparation method, the type of CNTs (single or multi walled), or the crystallization temperature range used, the Avrami index values for both neat PBS and the PBS/CNTs nanocomposites were approximately 3. This indicated that although the CNTs provided additional nucleation sites and enhanced the nuclei density, the mechanism of crystal growth for PBS did not change with the addition of MWCNTs. In contrast, the Avrami index values for the PCL/MWCNTs

nanocomposites (n = 2) were lower than that of neat PCL (n = 3). This indicated that for the PCL/MWCNT nanocomposites the dimensionality of growth switched from 3D to 2D due to the nucleation density that was greatly enhanced.

The overall isothermal crystallization rate decreased with an increase in T_c (in the crystallization temperature range of 82-101 ºC) due to the low supercooling. However, the overall crystallization rate of the nanocomposites was higher than that of neat PBS in this temperature range, and increased with increasing CNTs content. This was due to the nucleation effect of the CNTs in the PBS matrix [85,90].

2.5.4 Conductivity

The incorporation of electrically conductive particles into a polymer can impart electrical conductivity to the nanocomposite. The level of conductivity strongly depends on the dispersion of the filler. When the filler disperses as well separated particles in the polymer, the improvement in the electrical conductivity is limited, since a conductive path cannot be formed because of the insulating nature of the polymer matrix. The electrical conductivity can be enhanced by several orders of magnitude if a filler network is formed. In the reported literature, the MWCNTs were either used as received [89] or modified by (i) polyetheramines, (ii) N,N'-dicyclohexyl carbodiimide (DCC) dehydrating agents, and (iii) nitric acid [33,47,83]. The effect of modified and unmodified MWCNTs on the surface resistivity of PBS/MWCNTs nanocomposites was reported [33,47,83,89]. The surface resistivity decreased from $>10^{16}$ Ω (pristine PBS) to $>10^{9}$ Ω with the addition of 3 wt% unmodified MWCNTs, a decrease of about 10^{7} fold in value of the electrical resistivity [47]. Elsewhere in the literature, the surface resistivity of the PBS/MWCNTs nanocomposites decreased from $>10^{14}$ Ω (pristine PBS) to $>10^{3}$ Ω (for modified MWCNTs/PBS), a decrease of about 10^{11} fold in the value of the electrical resistivity [33]. Ray and co-workers [83] prepared unmodified MWCNTs/PBS nanocomposites by melt blending in a batch mixer. The electrical conductivity of the nanocomposites dramatically increased compared to that of the pristine PBS sample. The in-plane conductivity increased from 5.8 x 10^{-9} S cm^{-1} for neat PBS to 4.4 x 10^{-3} S cm^{-1} for a 3 wt% MWCNTs-containing nanocomposite, an increase of 10^{6} fold in the value of the electrical conductivity. The surface resistivity of the PBS/MWCNTs nanocomposites decreased from $>10^{16}$ Ω (pristine PBS) to $>10^{6}$ Ω for 3 wt% modified MWCNTs nanocomposites, a decrease of over 10^{9} fold. The decrease in surface resistivity of

modified MWCNTs/PBS nanocomposites was larger than that of the unmodified MWCNTs/PBS, indicating the better dispersion of the modified MWCNTs in the polymer matrix compared to the unmodified MWCNTs. This implies that the percolation threshold of electrical conductivity was depressed. For this reason, the well dispersed MWCNTs in the PBS matrix could easily connect with each other, and subsequently form an interconnecting conductive pathway. Therefore, the amount of MWCNTs needed to construct a conductive pathway was relatively small [33,47,89].

2.6 PBS/PCL/CNTs nanocomposites

2.6.1 Morphology

There is currently only one research paper available on PBS/PCL/CNTs nanocomposites [92]. The authors introduced MWCNTs into double-crystalline multiblock PBS/PCL copolymers using solution mixing and solvent casting processes. The morphologies of the resulting PBS/PCL/MWCNTs nanocomposites of different compositions are shown in a series of TEM images (Figure 2.5). The MWCNTs exhibited a much finer dispersion morphology in the PBS/MWCNT nanocomposite (Figure 2.5(b)) than in the PCL/MWCNT nanocomposite (Figure 2.5(a)). This was attributed to the wetting coefficient data for MWCNTs introduced into the binary copolymer which was calculated as 1.74 (harmonic-mean equation) or -3.43 (geometric-mean equation). According to the authors, this meant that the MWCNTs were selectively distributed in the PBS phase. Similar results were reported by Fenni *et al.* [93] who added graphene oxide (GO) to a 70/30 *w/w* poly(L-lactic acid) (PLLA)/poly(butylene succinate) (PBS) blend. Their morphology results indicated microsize droplets of PBS dispersed in the PLLA phase, with most of the GO nanoparticles located in the PBS phase, although some GO stacks were also observed in the PLLA matrix. This was probably, during the preparation of the nanocomposites, the GO nanoparticles were first added to the PBS matrix via solution dispersion, and this was followed by melt blending with PLLA. The GO nanoparticles therefore had a good interaction with each other and with the PBS, but not so much with the PLLA.

In the ternary PBS/PCL/MWCNT system, a selective dispersion morphology was formed. It was assumed that the blank area in light color is the PCL-enriched domain while the MWCNT located area is the PBS-enriched domain (Figure 2.5(c)). When 1 wt% MWCNT was loaded, varying the PBS content resulted in different dispersion states. When the PBS

content was 20 wt% (Figure 2.5(d)), the blank area in light color was dominant and the MWCNTs were sporadically distributed in the PBS phase. This indicated that the MWCNTs containing PBS was dispersed in the PCL continuous phase. Upon increasing the PBS content to 30 wt% (Figure 2.5(e)), it was found that the area occupied by the MWCNTs increased, while the PCL phase was reduced. This was attributed to a co-continuous phase between PCL and PBS at 40 wt% PBS, as well as the formation of a conductive MWCNTs network at this content (Figure 2.5(f)). When the loading capacity of MWCNTs increased to 3 wt% (Figure 2.5(g–i)), the advantage of the selective dispersion was weakened because part of the MWCNTs spread to the PCL-enriched domain when the PBS-enriched domain was saturated, especially in the $PBS_{4.2}{}^{4}PCL_{6.3}{}^{6}/CNTs_{3.0}$ sample (Figure 2.5(i)).

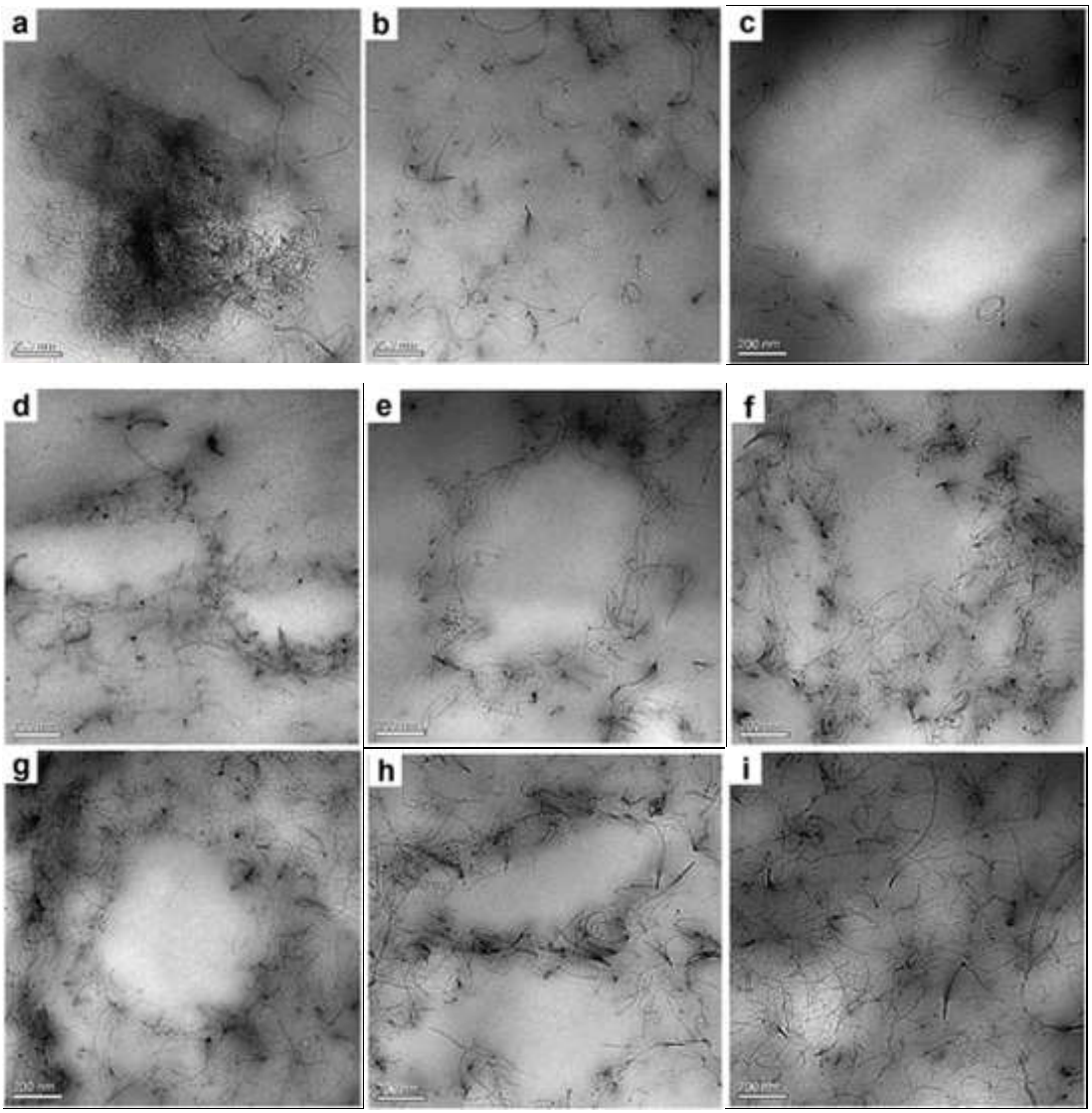

Figure 2.5 TEM images of (a) $PCL_{6.3}/MWCNTs_{1.0}$, (b) $PBS_{4.2}/MWCNTs_{1.0}$, (c) $PBS_{4.2}{}^{2}/PCL_{6.3}{}^{8}/MWCNTs_{1.0}$, (d) $PBS_{4.2}{}^{2}PCL_{6.3}{}^{8}/MWCNTs_{1.0}$, (e) $PBS_{4.2}{}^{3}PCL_{6.3}{}^{7}/MWCNTs_{1.0}$, (f) $PBS_{4.2}{}^{4}PCL_{6.3}{}^{6}/MWCNTs_{1.0}$, (g) $PBS_{4.2}{}^{2}PCL_{6.3}{}^{8}/MWCNTs_{3.0}$, (h) $PBS_{4.2}{}^{3}PCL_{6.3}{}^{7}/MWCNTs_{3.0}$, and (i) $PBS_{4.2}{}^{4}PCL_{6.3}{}^{6}/MWCNTs_{3.0}$ [92].

2.6.2 Mechanical properties

Generally, carbon nanotubes improve selective mechanical properties, depending on the system employed. It is well known that a flexible polymer has a high elongation at break, as a result of its high ductility. The addition of rigid materials such as carbon nanotubes normally improves the modulus of flexible polymers at the expense of its ductility. He *et al*. [92] reported on the tensile properties of multiblock PBS/PCL copolymers and their nanocomposites, and found a good compromise between strength and flexibility. The authors reported an increase in the elongation at break for the multiblock PBS/PCL copolymers with an increase in PCL content, which resulted in a high ductility. However, the addition of MWCNTs resulted in a decrease in elongation at break but an increase in stiffness (Table 2.3). The decrease in elongation at break is due to an increase in the amount of rigid areas in the blend caused by the increasing MWCNTs content, giving rise to a reduction in the deformable polymer portion in the nanocomposites.

Table 2.3 Mechanical properties of multiblock copolymers and nanocomposites [92].

Samples	σ_y (MPa)	σ_b (MPa)	ε (%)	E (MPa)
$PBS_{4.2}^{2}PCL_{6.3}^{8}$	8.12 ± 0.80	18.57 ± 2.12	1294 ± 38	221 ± 7
$PBS_{4.2}^{3}PCL_{6.3}^{7}$	11.52 ± 1.96	19.47 ± 0.76	1004 ± 94	234 ± 5
$PBS_{4.2}^{4}PCL_{6.3}^{6}$	13.58 ± 3.87	23.73 ± 1.23	892 ± 95	237 ± 18
$PBS_{4.2}^{5}PCL_{6.3}^{5}$	14.89 ± 2.49	27.41 ± 3.54	746 ± 67	376 ± 15
$PBS_{4.2}^{6}PCL_{6.3}^{4}$	16.32 ± 1.39	36.51 ± 5.26	647 ± 56	406 ± 37
$PBS_{4.2}^{2}PCL_{6.3}^{8}/MWCNTs_{1.0}$	13.28 ± 1.02	18.90 ± 1.08	1158 ± 22	256 ± 22
$PBS_{4.2}^{3}PCL_{6.3}^{7}/MWCNTs_{1.0}$	13.37 ± 4.03	19.54 ± 2.64	945 ± 125	285 ± 13
$PBS_{4.2}^{4}PCL_{6.3}^{6}/MWCNTs_{1.0}$	14.70 ± 2.93	20.80 ± 2.49	733 ± 59	380 ± 20
$PBS_{4.2}^{5}PCL_{6.3}^{5}/MWCNTs_{1.0}$	17.52 ± 1.24	24.14 ± 1.33	723 ± 94	417 ± 11
$PBS_{4.2}^{6}PCL_{6.3}^{4}/MWCNTs_{1.0}$	20.84 ± 1.20	26.88 ± 2.27	708 ± 39	424 ± 24

2.6.3 Melting and crystallization behaviour

For a double-crystalline PBS/PCL system, all the samples exhibited two crystallization peaks and two melting peaks. The variation of the composition had no obvious effect on

the melting temperature, but increasing the content of one segment increased its crystallinity (especially for the PBS segment). The addition of 1 wt% MWCNTs to the PBS/PCL copolymer had no obvious effect on the melting temperature of both segments, but the crystallinity significantly increased when compared to the pristine PBS/PCL copolymers. For the PBS/PCL/MWCNTs nanocomposite with the lowest PBS content, the crystallinity of the PBS segment was enhanced, while a slight change was reported in the PCL segment. This was attributed to the nucleating effect of a large concentration of MWCNTs in the PBS domain. It is worth noting that the nucleating effect became less significant when the PBS content decreased. For the PLLA/PBS/GO system [94], the GO nanoparticles also acted as nucleating agents for both semicrystalline polymers. A nucleating value of about 80% was reported for GO towards PBS, which is among the highest nucleation efficiencies ever reported for this polymer. The nucleating efficiency for GO towards PLLA was, however, only ~15%, because a very small amount of GO nanoparticles were located in the PLLA.

2.6.4 Conductivity

The key factor determining whether the material can respond to electricity is the electrical conductivity of the nanocomposites. The pristine PBS/PCL copolymer belongs to a typical insulator due to its low electrical conductivity value of about 10^{-15} S cm^{-1}. The introduction of 1.0 wt% MWCNTs significantly improved the electrical conductivity of the PBS/PCL/MWCNTs nanocomposites to 6.25 x 10^{-4} S cm^{-1}, so that the nanocomposites with an electrical conductive network are achieved, and an insulator transforms into a conductor. For comparison, the conductivity of PBS/MWCNTs was evaluated as 9.79 x 10^{-5} S cm^{-1}, which is lower than that of PBS/PCL/MWCNTs. The authors suggested that this could be proof of the selective dispersion of MWCNTs in the PBS domain [92].

2.7 Conclusions

Carbon nanotubes have clearly demonstrated their capability as a filler in various polyester matrices such as PCL, PBS and PC. Nanocomposites prepared through solution mixing showed no apparent aggregation, giving rise to better interfacial interactions between the polymer and the carbon nanotubes. Furthermore, functionalization of

MWCNTs as well as the MWCNTs masterbatch gave rise to significant improvements in the thermal, electrical, and mechanical properties of the nanocomposites as compared to pristine MWCNTs. The masterbatch technology is also a suitable way to (i) obtain well dispersed MWCNTs nanocomposites with electrical conductivity at low amounts of nanotubes, and (ii) to limit inhalation exposure to MWCNTs in occupational settings because it operates in solvent-less environments. In all the nanocomposites, addition of a small amount of carbon nanotubes, e.g., 0.5 wt%, was sufficient to enhance the thermal and mechanical properties, and thermal and electrical conductivities, of the nanocomposites, because adding more carbon nanotubes resulted in agglomerates due to the strong van der Waals interaction between the nanotubes at higher loadings. There is currently no published information on PBS/PC blends.

2.8 References

[1] J. Hopewell, R. Dvorak, E. Kosior. Review: Plastics recycling: Challenges and opportunities. Philosophical Transactions of the Royal Society B 2009; 364:2115-2126.
DOI: 10.1098/rstb.2008.0311

[2] J.H. Song, R.J. Murphy, R. Narayan, G.B.H. Davies. Biodegradable and compostable alternatives to conventional plastics. Philosophical Transactions of the Royal Society B 2009; 364:2127-2139.
DOI: 10.1098/rstb.2008.0289

[3] T.S. Mdletshe, S.B. Mishra, A.K. Mishra. Studies on the effect of silicon carbide nanoparticles on the thermal, mechanical, and biodegradation properties of poly(caprolactone). Journal of Applied Polymer Science 2015; 132:42145.
DOI: 10.1002/app.42145

[4] A. Bhatia, R.K. Gupta, S.N. Bhattacharya, H.J. Choi. Compatibility of biodegradable poly(lactic acid) (PLA) and poly(butylene succinate) (PBS) blends for packaging application. Korea-Australia Rheology Journal 2007; 19:125-131.

[5] M. Gigli, A. Negroni, G. Zanaroli, N. Lotti, F. Fava, A. Munari. Environmentally friendly PBS-copolyesters containing PEG-like subunit: Effect of block length on solid-state properties and enzymatic degradation. Reactive & Functional Polymers 2013; 73:764-771.
DOI: 10.1016/j.reactfunctpolym.2013.03.007

[6] I. Vroman, L. Tighzert. Biodegradable polymers. Materials 2009; 2:307-344.
DOI: 10.3390/ma2020307

[7] R. Morent, N. De Geyter, T. Desmet, P. Dubruel, C. Leys. Plasma surface modification of biodegradable polymers: A Review. Plasma Processes and Polymers 2011; 8:171-190.
DOI: 10.1002/ppap.201000153

[8] M.M. Reddy, S. Vivekanandhan, M. Misra, S.K. Bhatia, A.K. Mohanty. Biobased plastics and bionanocomposites: Current status and future opportunities. Progress in Polymer Science 2013; 38:1653-1689.
DOI: 10.1016/j.progpolymsci.2013.05.006

[9] R.P. Babu, K.O. Connor, R. Seeram. Current progress on bio-based polymers and their future trends. Progress in Biomaterials 2013; 2:1-16.
DOI: 10.1186/2194-0517-2-8

[10] E. Fortunati, M. Gigli, F. Luzi, N. Lotti, A. Munari, M. Gazzano, I. Armentano, J. M. Kenny. Poly(butylene cyclohexanedicarboxylate/diglycolate) random copolymers reinforced with SWCNTs for multifunctional conductive biopolymer composites. eXPRESS Polymer Letters 2016; 10:111-124.
DOI: 10.3144/expresspolymlett.2016.12

[11] L.M. Robeson. Polymer blends. A comprehensive review. Carl Hanser Verlag: München (2007).

[12] K. Fukushima, J.L. Feijoo, M. Yang. Comparison of abiotic degradation of PDLLA, PCL and partially miscible PDLLA/PCL blend. European Polymer Journal 2013; 49:706-717.
DOI: 10.1016/j.eurpolymj.2012.12.011

[13] R.V. Castillo, A.J. Müller, J. Raquez, P. Dubois. Crystallization kinetics and morphology of biodegradable double crystalline PLLA-*b*-PCL diblock copolymers. Macromolecules 2010; 43:4149-4160.
DOI: 10.1021/ma100201g

[14] A.S. Luyt, S. Gasmi. Influence of blending and blend morphology on the thermal properties and crystallization behaviour of PLA and PCL in PLA/PCL blends. Journal of Materials Science 2016; 51:4670-4681.
DOI: 10.1007/s10853-016-9784-z

[15] S. Ravati, B.D. Favis. Tunable morphologies for ternary blends with poly(butylene succinate): Partial and complete wetting phenomena. Polymer 2013; 54:3271-3281.

DOI: 10.1016/j.polymer.2013.04.005

[16] M.M. Reddy, A.K. Mohanty, M. Misra. Biodegradable blends from plasticized soy meal, polycaprolactone, and poly(butylene succinate). Macromolecular Materials and Engineering 2012; 297:455-463.
DOI: 10.1002/mame.201100203

[17] P. Nugroho, H. Mitomo, F. Yoshii, T. Kume, K. Nishimura. Improvement of processability of PCL and PBS blend by irradiation and its biodegradability. Macromolecular Materials and Engineering 2001; 286:316-323.
DOI: 10.1002/1439-2054(20010501)286:5<316::AID-MAME316>3.0.CO;2-N

[18] S. Ravati, B.D. Favis. Interfacial coarsening of ternary polymer blends with partial and complete wetting structures. Polymer 2013; 54:6739-6751.
DOI: 10.1016/j.polymer.2013.10.009

[19] Z. Qiu, M. Komura, T. Ikehara, T. Nishi. Miscibility and crystallization behavior of biodegradable blends of two aliphatic polyesters. Poly(butylene succinate) and poly(ε-caprolactone). Polymer 2003; 44:7749-7756.
DOI: 10.1016/j.polymer.2003.10.013

[20] E. Can, S. Bucak, E. Kinaci, A.C. Çalikoğlu, G.T. Köse. Polybutylene succinate (PBS)-polycaprolactone (PCL) blends compatibilized with poly(ethylene oxide)-block poly(propylene oxide)-blockpoly(ethylene oxide) (PEO-PPO-PEO) copolymer for biomaterial applications. Polymer-Plastics Technology and Engineering 2014; 53:1178-1193.
DOI: 10.1080/03602559.2014.886119

[21] Q. Liu, X.M. Zhou. Preparation of poly(butylene succinate)/poly(ε-caprolactone) blends compatibilized with poly(butylene succinate-co-ε-caprolactone) copolymer. Journal of Macromolecular Science, Part A: Pure and Applied Chemistry 2015; 52:625-629.
DOI: 10.1080/10601325.2015.1050634

[22] I. Kelnar, J. Kratochvil, I. Fortelny, L. Kapralkova, A. Zhigunov, V. Khunova, M. Nevoralova. Effect of halloysite on structure and properties of melt-drawn PCL/PLA microfibrillar composites. eXPRESS Polymer Letters 2016; 10:381-393.
DOI: 10.3144/expresspolymlett.2016.36

[23] Y. Zhao, J. Qu, Y. Feng, Z. Wu, F. Chen, H. Tang. Mechanical and thermal properties of epoxidized soybean oil plasticized polybutylene succinate blends. Polymers for Advanced Technologies 2012; 23:632-638.
DOI: 10.1002/pat.1937

[24] D.F. Coutinho, M.E. Gomes, N.M. Neves, R.L. Reis. Development of micropatterned surfaces of poly(butylene succinate) by micromolding for guided tissue engineering. Acta Biomaterialia 2012; 8:1490-1497.
DOI: 10.1016/j.actbio.2011.12.035

[25] C.T. Brunner, E.T. Baran, E.D. Pinho, R.L. Reis, N.M. Neves. Performance of biodegradable microcapsules of poly(butylene succinate), poly(butylene succinate-co-adipate) and poly(butylene terephthalate-co-adipate) as drug encapsulation systems. Colloids and Surfaces B: Biointerfaces 2011; 84:498-507.
DOI: 10.1016/j.colsurfb.2011.02.005

[26] S. Mizuno, T. Maeda, C. Kanemura, A. Hotta. Biodegradability, reprocessability, and mechanical properties of polybutylene succinate (PBS) photografted by hydrophilic or hydrophobic membranes. Polymer Degradation and Stability 2015; 117:58-65.
DOI: 10.1016/j.polymdegradstab.2015.03.015

[27] J. John, R. Mani, M. Bhattacharya. Evaluation of compatibility and properties of biodegradable polyester blends. Journal of Polymer Science: Part A: Polymer Chemistry 2002; 40:2003-2014.
DOI: 10.1002/pola.10297

[28] E. Hassan, Y. Wei, H. Jiao, Y. Muhuo. Dynamic mechanical properties and thermal stability of poly(lactic acid) and poly(butylene succinate) blends composites. Journal of Fiber Bioengineering and Informatics 2013; 6:85-94.
DOI: 10.3993/jfbi03201308

[29] C.W. Lee, K. Masutani, Y. Kimura. Ring-opening polymerization of a macrocyclic lactone monomer isolated from oligomeric byproducts of poly(butylene succinate) (PBS): An efficient route to high-molecular-weight PBS and block copolymers of PBS. Polymer 2014; 55:5673-5679.
DOI: 10.1016/j.polymer.2014.08.028

[30] Q. Charlier, E. Girard, F. Freyermouth, M. Vandesteene, N. Jacquel, C. Ladavière, A. Rousseau, F. Fenouillot. Solution viscosity-molar mass relationships for

poly(butylene succinate) and discussion on molar mass analysis. eXPRESS Polymer Letters 2015; 9:424-434.
DOI: 10.3144/expresspolymlett.2015.41

[31] X. Huang, C. Li, W. Zhu, D. Zhanga, G. Guana, Y. Xiao. Ultraviolet-induced crosslinking of poly(butylene succinate) and its thermal property, dynamic mechanical property, and biodegradability. Polymers for Advanced Technologies 2011; 22:648-656.
DOI: 10.1002/pat.1560

[32] M. Zaverl, O. Valerio, M. Misra, A. Mohanty. Study of the effect of processing conditions on the co-injection of PBS/PBAT and PTT/PBT blends for parts with increased bio-content. Journal of Applied Polymer Science 2015; 132:41278.
DOI: 10.1002/app.41278

[33] C.S. Lin, Y.F. Shih, R.J. Jeng, S.A. Dai, J.J. Lin, C.C. Lee. Nanocomposites with enhanced electrical properties based on biodegradable poly(butylene succinate) and polyetheramine modified carbon nanotube. Journal of the Taiwan Institute of Chemical Engineers 2012; 43:322-328.
DOI: 10.1016/j.jtice.2011.10.009

[34] H.M. Ye, X.T. Chen, P. Liu, S.Y. Wu, Z. Jiang, B. Xiong, J. Xu. Preparation of poly(butylene succinate) crystals with exceptionally high melting point and crystallinity from its inclusion complex. Macromolecules 2017; 50:5425-5433.
DOI: 10.1021/acs.macromol.7b00656

[35] R.R. Fan, L.X. Zhou, W. Song, D.X. Li, D.M. Zhang, R. Ye, Y. Zheng, G. Guo. Preparation and properties of g-TTCP/PBS nanocomposites and its in vitro biocompatibility assay. International Journal of Biological Macromolecules 2013; 59:227-234.
DOI: 10.1016/j.ijbiomac.2013.04.051

[36] R.R. Fan, L.X. Zhou, D.X. Li, D.M. Zhang, M. Wu, G. Guo. Preparation and characterization of composites based on poly(butylene succinate) and poly(lactic acid) grafted tetracalcium phosphate. Journal of Macromolecular Science, Part B Physics 2014; 53:296-308.
DOI: 10.1080/00222348.2013.810104

[37] L. Wang, J. Qiu, E. Sakai, X. Wei. The relationship between microstructure and mechanical properties of carbon nanotubes/polylactic acid nanocomposites

prepared by twin-screw extrusion. Composites Part A: Applied Science and Manufacturing 2016; 89:18-25.
DOI: 10.1016/j.compositesa.2015.12.016

[38] J.J. George, S. Bhadra, A.K. Bhowmick. Influence of carbon-based nanofillers on the electrical and dielectric properties of ethylene vinyl acetate nanocomposites. Polymer Composites 2010; 31:218-225.
DOI: 10.1002/pc.20788

[39] M. Bhattacharya. Review: Polymer nanocomposites – A Comparison between carbon nanotubes, graphene, and clay as nanofillers. Materials 2016; 9:1-35.
DOI: 10.3390/ma9040262

[40] A. Wurm, D. Lellinger, A.A. Minakov, T. Skipa, P. Pötschke, R. Nicula, I. Alig, C. Schick. Crystallization of poly(ε-caprolactone)/MWCNT composites: A combined SAXS/WAXS, electrical and thermal conductivity study. Polymer 2014; 55:2220-2232.
DOI: 10.1016/j.polymer.2014.02.069

[41] S.J. Chin, S. Vempati, P. Dawson, M. Knite, A. Linarts, K. Ozols, T. McNally. Electrical conduction and rheological behaviour of composites of poly(ε-caprolactone) and MWCNTs. Polymer 2015; 58:209-221.
DOI: 10.1016/j.polymer.2014.12.034

[42] P. Pötschke, T. Villmow, B. Krause. Melt mixed PCL/MWCNT composites prepared at different rotation speeds: Characterization of rheological, thermal, and electrical properties, molecular weight, MWCNT macrodispersion, and MWCNT length distribution. Polymer 2013; 54:3071-3078.
DOI: 10.1016/j.polymer.2013.04.012

[43] P.C. Ma, N.A. Siddiqui, G. Marom, J.K. Kim. Dispersion and functionalization of carbon nanotubes for polymer-based nanocomposites: A review. Composites: Part A 2010; 41:1345-1367.
DOI: 1016/j.compositesa.2010.07.003

[44] K. Prashantha, J. Soulestin, M.F. Lacrampe, P. Krawczak, G. Dupin, M. Claes. Masterbatch-based multi-walled carbon nanotube filled polypropylene nanocomposites: Assessment of rheological and mechanical properties. Composites Science and Technology 2009; 69:1756-1763.
DOI: 10.1016/j.compscitech.2008.10.005

[45] T. Wu, E. Chen, Y. Lin, M. Chiang, G. Chang. Preparation and characterization of melt-processed polycarbonate/multiwalled carbon nanotube composites. Polymer Engineering and Science 2008; 48:1369-1375.
DOI: 10.1002/pen.21094

[46] R.A. Pérez, J.V. López, J.N. Hoskins, B. Zhang, S.M. Grayson, M.T. Casas, J. Puiggalí, A.J. Müller. Nucleation and antinucleation effects of functionalized carbon nanotubes on cyclic and linear poly(ε-caprolactones). Macromolecules 2014; 47:3553-3566.
DOI: 10.1021/ma5005869

[47] Y.F. Shih, L.S. Chen, R.J. Jeng. Preparation and properties of biodegradable PBS/multi-walled carbon nanotube nanocomposites. Polymer 2008; 49:4602-4611.
DOI: 10.1016/j.polymer.2008.08.015

[48] S. Shokoohi, A. Arefazar. A review on ternary immiscible polymer blends: Morphology and effective parameters. Polymers for Advanced Technologies 2009; 20:433-447.
DOI: 10.1002/pat.1310

[49] S. Maiti, S. Suin, N.K. Shrivastava, B.B. Khatua. Low percolation threshold and high electrical conductivity in melt-blended polycarbonate/multiwall carbon nanotube nanocomposites in the presence of poly(ε-caprolactone). Polymer Engineering and Science 2014; 54:646-659.
DOI: 10.1002/pen.23600

[50] T.P. Gumede, A.S. Luyt, M.K. Hassan, R.A. Pérez-Camargo, A. Tercjak, A.J. Müller. Morphology, nucleation, and isothermal crystallization kinetics of poly(ε-caprolactone) mixed with a polycarbonate/MWCNTs masterbatch. Polymers 2017; 9:709.
DOI: 10.3390/polym9120709

[51] A.A.J. Ketelaars, Y. Papantoniou, K. Nakayama. Analysis of the density and the enthalpy of poly(ε-caprolactone)-polycarbonate blends: Amorphous phase compatibility and the effect of secondary crystallization. Journal of Applied Polymer Science 1997; 66:921-927.
DOI: 10.1002/(SICI)1097-4628(19971031)66:5<921::AID-APP12>3.0.CO;2-Q

[52] Y.W. Cheung, R.S. Stein, B. Chu, G. Wu. Evolution of crystalline structures of poly(ε-caprolactone)/polycarbonate blends. 1. Isothermal crystallization kinetics as

probed by synchrotron small-angle X-ray scattering. Macromolecules 1994; 27:3589-3595.
DOI: 10.1021/ma00091a021

[53] V. Balsamo, N. Calzadilla, G. Mora, A.J. Müller. Thermal characterization of polycarbonate/polycaprolactone blends. Journal of Polymer Science: Part B: Polymer Physics 2001; 39:771-785.
DOI: 10.1002/1099-0488(20010401)39:7<771::AID-POLB1052>3.0.CO;2-I

[54] C.A. Cruz, D.R. Paul, J.W. Barlow. Polyester-polycarbonate blends. IV. Poly(ε-caprolactone). Journal of Applied Polymer Science 1979; 23:589-600.
DOI: 10.1002/app.1979.070230228

[55] Y.S. Chun, J. Park, J.B. Sun, W.N. Kim. Blends of polycarbonate and poly(ε-caprolactone) and the determination of the polymer-polymer interaction parameter of the two polymers. Journal of Polymer Science: Part B: Polymer Physics 2000; 38:2072-2076.
DOI: 10.1002/1099-0488(20000801)38:153.3.CO;2-W

[56] J.M. Jonza, R.S. Porter. Bisphenol A polycarbonate/poly(ε-caprolactone) blends: Melting point depression and reactivity. Macromolecules 1986; 19:1946-1951.
DOI: 10.1021/ma00161a028

[57] D. Herrera, J.C. Zamora, A. Bello, M. Grimau, E. Laredo, A.J. Müller, T.P. Lodge. Miscibility and crystallization in polycarbonate/poly(ε-caprolactone) blends: Application of the self-concentration model. Macromolecules 2005; 38:5109-5117.
DOI: 10.1021/ma050481c

[58] J.D. Menczel, R.B. Prime. Thermal Analysis of Polymers. Fundamentals and Applications. John Wiley & Sons: New Jersey (2009).

[59] L. Pan, X. Pei, R. He, Q. Wan, J. Wang. Multiwall carbon nanotubes/polycaprolactone composites for bone tissue engineering application. Colloids and Surfaces B: Biointerfaces 2012; 93:226-234.
DOI: 10.1016/j.colsurfb.2012.01.011

[60] J.T. Yeh, M.C. Yang, C.J. Wu, C.S. Wu. Preparation and characterization of biodegradable polycaprolactone/multiwalled carbon nanotubes nanocomposites. Journal of Applied Polymer Science 2009; 112:660-668.
DOI: 10.1002/app.29485

[61] Z.X. Meng, W. Zheng, L. Li, Y.F. Zheng. Fabrication and characterization of three dimensional nanofiber membrane of PCL-MWCNTs by electrospinning. Materials Science and Engineering 2010; 30:1014-1021.
DOI: 10.1016/j.msec.2010.05.003

[62] H.H. Lee, U.S. Shin, G.Z. Jin, H.W. Kim. Highly homogeneous carbon nanotube polycaprolactone composites with various and controllable concentrations of ionically-modified MWCNTs. Bulletin of the Korean Chemistry Society 2011; 32:157-161.
DOI: 10.5012/bkcs.2011.32.1.157

[63] M.S. Mohlala, S.S. Ray. Preparation and characterization of polymer/multi-walled carbon nanotube nanocomposites. Solid State Phenomena 2008; 140:97-102.
DOI: 10.4028/www.scientific.net/SSP.140.97

[64] K. Saeed, S.Y. Park. Preparation and properties of multiwalled carbon nanotube/ polycaprolactone nanocomposites. Journal of Applied Polymer Science 2007; 104:1957-1963.
DOI: 10.1002/app.25902

[65] K. Saeed, S.Y. Park, H.J. Lee, J.B. Baek, W.S. Huh. Preparation of electrospun nanofibers of carbon nanotube/polycaprolactone nanocomposite. Polymer 2006; 47:8019-8025.
DOI: 10.1016/j.polymer.2006.09Sa.012

[66] M. Trujillo, M.L. Arnal, A.J. Müller, P. Dubois. Supernucleation and crystallization regime change provoked by MWCNT addition to poly(ε-caprolactone). Polymer 2012; 53:832-841.
DOI: 10.1016/j.polymer.2011.12.028

[67] V.H. Antolín-Cerón, S. Gómez-Salazar, M. Rabelero, V. Soto, G. Luna-Bárcenas, I. Katime, S.M. Nuño-Donlucas. Comparative study of the thermal and mechanical properties of nanocomposites prepared by in situ polymerization of ε-caprolactone and functionalized carbon nanotubes. Polymer Composites 2012; 33:562-572.
DOI: 10.1002/pc.22175

[68] Z. Qiu, H. Wang, C. Xu. Crystallization, mechanical properties, and controlled enzymatic degradation of biodegradable poly(ε-caprolactone)/multi-walled carbon nanotubes nanocomposites. Journal of Nanoscience and Nanotechnology 2011; 11:7884-7893.
DOI: 10.1166/jnn.2011.4714

[69] J.F. Vega, J. Fernández-Alcázar, J.V. López, R.M. Michell, R.A. Pérez-Camargo, B. Ruelle, J. Martínez-Salazar, M.L. Arnal, P. Dubois, A.J. Müller. Competition between supernucleation and plasticization in the crystallization and rheological behavior of PCL/CNT-based nanocomposites and nanohybrids. Journal of Polymer Science, Part B: Polymer Physics 2017; 55:1310-1325.
DOI: 10.1002/polb.24385

[70] B. Fillon, J.C. Wittmann, B. Lotz, A. Thierry. Self-nucleation and recrystallization of isotactic polypropylene (α phase) investigated by differential scanning calorimetry. Journal of Polymer Science Part B: Polymer Physics 1993; 31:1383-1393.
DOI: 10.1002/polb.1993.090311013

[71] B. Fillon, B. Lotz, A. Thierry, J.C. Wittmann. Self-nucleation and enhanced nucleation of polymers. Definition of a convenient calorimetric "efficiency scale" and evaluation of nucleating additives in isotactic polypropylene (α phase). Journal of Polymer Science Part B: Polymer Physics 1993; 31:1395-1405.
DOI: 10.1002/polb.1993.090311014

[72] A.J. Müller, M.L. Arnal. Thermal fractionation of polymers. Progress in Polymer Science 2005; 30:559-603.
DOI: 10.1016/j.progpolymsci.2005.03.001

[73] M.D. Sanchez-Garcia, J.M. Lagaron, S.V. Hoa. Effect of addition of carbon nanofibers and carbon nanotubes on properties of thermoplastic biopolymers. Composites Science and Technology 2010; 70:1095-1105.
DOI: 10.1016/j.compscitech.2010.02.015

[74] T.M. Wu, E.C. Chen. Crystallization behavior of poly(ε-caprolactone)/multiwalled carbon nanotube composites. Journal of Polymer Science Part B: Polymer Physics 2006; 44:598-606.
DOI: 10.1002/polb.20722

[75] C.A. Mitchell, R. Krishnamoorti. Non-isothermal crystallization of in situ polymerized poly(ε-caprolactone) functionalized-SWNT nanocomposites. Polymer 2005; 46:8796–8804.
DOI: 10.1016/j.polymer.2005.05.101

[76] M. Avrami. Granulation, phase change, and microstructure kinetics of phase change III. Journal of Chemical Physics 1941; 9:177-184.
DOI: 10.1063/1.1750872

[77] A.T. Lorenzo, M.L. Arnal, J. Albuerne, A.J. Müller. DSC isothermal polymer crystallization kinetics measurements and the use of the Avrami equation to fit the data: Guidelines to avoid common problems. Polymer Testing 2007; 26:222-231. DOI: 10.1016/j.polymertesting.2006.10.005

[78] G. Reiter, G.R. Strobl. Progress in Understanding Polymer Crystallization, Lecture Notes Physics 714 (Springer, Berlin Heidelberg 2007). DOI: 10.1007/b11903420

[79] A.T. Lorenzo, A.J. Müller. Estimation of the nucleation and crystal growth contributions to the overall crystallization energy. Journal of Polymer Science: Part B: Polymer Physics 2008; 46:1478-1487. DOI: 10.1002/polb.21483

[80] A.T. Lorenzo, A.J. Müller, M.C. Lin, H.L. Chen, US Jeng, D. Priftis, M. Pitsikalis, N. Hadjichristidis. Influence of macromolecular architecture on the crystallization of (PCL2)-b-(PS2) 4-miktoarm star block copolymers in comparison to linear PCL-b-PS diblock copolymer analogues. Macromolecules 2009; 42:8353-8364. DOI: 10.1021/ma901289t

[81] A.J. Müller, M.L. Arnal, M. Trujillo, A.T. Lorenzo. Super-nucleation in nanocomposites and confinement effects on the crystallizable components within block copolymers, miktoarm star copolymers and nanocomposites. European Polymer Journal 2011; 47:614-629. DOI: 10.1016/j.eurpolymj.2010.09.027

[82] A. Bello, E. Laredo, J.R. Marval, M. Grimau, M.L. Arnal, A.J. Müller. Universality and percolation in biodegradable poly(ε-caprolactone)/multiwalled carbon nanotube nanocomposites from broad band alternating and direct current conductivity at various temperatures. Macromolecules 2011; 44:2819-2828. DOI: 10.1021/ma102598h

[83] J. Bandyopadhyay, S.A. Al-Thabaiti, S.S. Ray, M. Bousmina. Viscoelastic and electrical properties of carbon nanotubes filled poly(butylene succinate). International Polymer Processing 2014; 29:88-94. DOI: 10.3139/217.2812

[84] G. Wang, B. Guo, J. Xu, R. Li. Rheology, crystallization behaviors, and thermal stabilities of poly(butylene succinate)/pristine multiwalled carbon nanotube composites obtained by melt compounding. Journal of Applied Polymer Science 2011; 121:59-67.

DOI: 10.1002/app.33222

[85] L. Yuan, D. Wu, M. Zhang, W. Zhou, D. Lin. Rheological percolation behavior and isothermal crystallization of poly(butyene succinate)/carbon nanotube composites. Industrial and Engineering Chemistry Research 2011; 50:14186-14192.
DOI: 10.1021/ie202039v

[86] S.S. Ray, S. Vaudreuil, A. Maazouz, M. Bousmina. Dispersion of multi-walled carbon nanotubes in biodegradable poly(butylene succinate) matrix. Journal of Nanoscience and Nanotechnology 2006; 6:2191-2195.
DOI: 10.1166/jnn.2006.368

[87] S. Filizgok, M. Kodal, G. Ozkoc. Non-isothermal crystallization kinetics and dynamic mechanical properties of poly(butylene succinate) nanocomposites with different type of carbonaceous nanoparticles. Polymer Composites 2016. (Published online)
DOI: 10.1002/pc.24261

[88] R.T. Zeng, W. Hu, M. Wang, S.D. Zhang, J.B. Zeng. Morphology, rheological and crystallization behavior in non-covalently functionalized carbon nanotube reinforced poly(butylene succinate) nanocomposites with low percolation threshold. Polymer Testing 2016; 50:182-190.
DOI: 10.1016/j.polymertesting.2016.01.003

[89] F.B. Ali, R. Mohan. Thermal, mechanical, and rheological properties of biodegradable polybutylene succinate/carbon nanotubes nanocomposites. Polymer Composites 2010; 31:1309-1314.
DOI: 10.1002/pc.20913

[90] L. Tan, Y. Chen, W. Zhou, S. Ye, J. Wei. Novel approach toward poly(butylene succinate)/single-walled carbon nanotubes nanocomposites with interfacial-induced crystallization behaviors and mechanical strength. Polymer 2011; 52:3587-3596.
DOI: 10.1016/j.polymer.2011.06.006

[91] K.P. Pramoda, N.T.T. Linh, C. Zhang, T. Liu. Multiwalled carbon nanotube nucleated crystallization behavior of biodegradable poly(butylene succinate) nanocomposites. Journal of Applied Polymer Science 2009; 111:2938-3945.
DOI: 10.1002/app.29349

[92] M.J. He, W.X. Xiao, H. Xie, C.J. Fan, L. Du, X.Y. Deng, K.K. Yang, Y.Z. Wang. Facile fabrication of ternary nanocomposites with selective

dispersion of multi-walled carbon nanotubes to access multi-stimuli-responsive shape-memory effects. Materials Chemistry Frontiers 2017; 1:343-353.
DOI: 10.1039/c6qm00047a

[93] S.E. Fenni, O. Monticelli, L. Conzatti, R. Doufnoune, P. Stagnaro, N. Haddaoui, D. Cavallo. Correlating the morphology of poly(L-lactide)/poly(butylene succinate)/graphene oxide blends nanocomposites with their crystallization behavior. eXPRESS Polymer Letters 2018; 12:58-70.
DOI: 10.3144/expresspolymlett.2018.5

CHAPTER 3

Morphology, nucleation, and isothermal crystallization kinetics of poly(ε-caprolactone) mixed with a polycarbonate/MWCNTs masterbatch

---

This chapter has been published as:

Thandi P. Gumede, Adriaan S. Luyt, Mohammad K. Hassan, Ricardo A. Pérez-Camargo, Agnieszka Tercjak, Alejandro J. Müller*. Morphology, nucleation, and isothermal crystallization kinetics of poly(ε-caprolactone) mixed with a polycarbonate/MWCNTs masterbatch. Polymers 2017; 9:709.*

(DOI: 10.3390/polym9120709)

Author contributions: *A.S.L. and A.J.M. conceived and designed the experiments. T.P.G. performed most of the experiments under the supervision of her advisors A.S.L. and A.J.M. The X-ray diffraction experiments as well as the mechanical properties tests were performed and analyzed by R.A.P.-C. under the supervision of A.J.M. The dielectric measurements were performed and analyzed by M.K.H. under the supervision of A.S.L. and A.J.M., whereas the AFM measurements as well as their analysis were performed by A.T. The analysis of the results and the writing of the paper were done mostly by T.P.G. and her advisors A.S.L. and A.J.M., however, the rest of the authors also contributed by writing the parts related to the experiments they performed.*

Abstract

In this study, nanocomposites were prepared by melt blending poly (ε-caprolactone) (PCL) with a (polycarbonate (PC)/multi-wall carbon nanotubes (MWCNTs)) masterbatch in a twin-screw extruder. The nanocomposites contained 0.5, 1.0, 2.0, and 4.0 wt% MWCNTs. Even though PCL and PC have been reported to be miscible, our DSC (Differential Scanning Calorimetry), SAXS (Small Angle X-ray Scattering), and WAXS (Wide Angle X-ray Scattering) results showed partial miscibility, where two phases were formed (PC-rich and PCL-rich phases). In the PC-rich phase, the small amount of PCL chains included within this phase plasticized the PC component and the PC-rich phase was therefore able to crystallize. In contrast, in the PCL-rich phase the

amount of PC chains present generates changes in the glass transition temperature of the PCL phase that were much smaller than those predicted by the Fox equation. The presence of two phases was corroborated by SEM, TEM, and AFM observations where a fair number of MWCNTs diffused from the PC-rich phase to the PCL-rich phase, even though there were some MWCNTs agglomerates confined to PC-rich droplets. Standard DSC measurements demonstrated that the MWCNTs nucleation effects are saturated at a 1 wt% MWCNT concentration on the PCL-rich phase. This is consistent with the dielectric percolation threshold, which was found to be between 0.5 and 1 wt% MWCNTs. However, the nucleating efficiency was lower than literature reports for PCL/MWCNTs, due to limited phase mixing between the PC-rich and the PCL-rich phases. Isothermal crystallization experiments performed by DSC showed an increase in the overall crystallization kinetics of PCL with increases in MWCNTs as a result of their nucleating effect. Nevertheless, the crystallinity degree of the nanocomposite containing 4 wt% MWCNTs decreased by about 15% in comparison to neat PCL. This was attributed to the presence of the PC-rich phase, which was able to crystallize in view of the plasticization effect of the PCL component, since as the MWCNT content increases, the PC content in the blend also increases. The thermal conductivities (i.e., 4 wt% MWCNTs) were enhanced by 20% in comparison to the neat material. The nanocomposites prepared in this work could be employed in applications were electrical conductivity is required, as well as lightweight and tailored mechanical properties.

Keywords: PCL; PC/MWCNTs masterbatch; nanocomposites; morphology; nucleation; conductivity; isothermal crystallization

3.1 Introduction

Biodegradable polymers have received considerable attention due to their contribution to the reduction of environmental concerns and to the realization that global petroleum resources are finite. Different types of biodegradable polymers such as poly(ε-caprolactone) (PCL), poly(butylene succinate) (PBS), poly(lactic acid) (PLA), and poly(alkanoates) (PHA, PHB, PHBV) have been studied as potential biomaterials for a variety of applications such as biomedical devices, biodegradable packaging, adhesives, agricultural areas, auto-motion, and construction [1–4].

Amongst the biodegradable commercial polymers, PCL can be singled out due to its elasticity, biocompatibility, and good ductility caused by its low T_g of −60 °C. It is also easy to be melt-processed by extrusion, melt-spinning, film blowing, and injection molding. However, it has relatively low mechanical strength, which limit practical applications. In order to enhance the thermal and mechanical properties of the matrix, and to produce thermally and electrically conductive materials, much research has been geared towards the production of conductive carbon-based bionanocomposites.

Conductive carbon-based fillers include carbon nanotubes (CNTs), carbon black (CB), graphite and carbon nanofibers (CNF). These materials have been extensively investigated due to their low density, inertness and good compatibility with most polymers [5]. However, CNTs have shown to have greater potential than any of the other carbon-based nanofillers for industrial applications, because of their unique one-dimensional structure with good electrical and thermal conductivity, and their excellent mechanical and thermal properties [6–8]. CNTs are extremely strong and stiff nanostructures of carbon atoms arranged in a cylindrical hexagonal network, and are often categorized in two different groups: single-walled carbon nanotubes (SWCNTs) and multi-walled carbon nanotubes (MWCNTs). SWCNTs consist of a single graphene layer rolled up into a seamless cylinder, whereas MWCNTs consist of two or more concentric cylindrical shells of graphene sheets coaxially arranged around a central hollow core with van der Waals forces between adjacent layers. MWCNTs are the ideal choice for high-volume industrial applications due to their bulk availability and better dispersion compared to SWCNTs [9–12].

Despite the advantages of carbon nanotubes, they have a tendency to form agglomerates during mixing with polymers. This is due to the van der Waals attraction between the nanotubes, which makes it difficult for them to be dispersed into polymers. Several methods have been used to enhance the dispersion of MWCNTs into polymer matrices [9,13–15]. The methods commonly employed to improve dispersion include (i) treatment of CNTs with inorganic solvents such as nitric acid (HNO_3), sulfuric acid (H_2SO_4), and phosphoric acid (H_3PO_4), in order to attach hydroxyl and carboxyl acid functional groups to the nanotubes, and (ii) the masterbatch approach, which is a direct encapsulation of the MWCNTs into a polymer matrix, and the subsequent release of the carbon nanotubes into the matrix polymer during mixing in the melt. The masterbatch method has received great interest from an industrial point of view because it does not involve solvents that are harmful to the environment [13,14].

Nanocomposites of PCL with MWCNTs have potential applications in the biodegradable packaging market, biomedical field, and automotive industry, since the presence of the MWCNTs could overcome the limitations of PCL regarding thermal, mechanical, and electrical properties [16–20].

Several researchers investigated the nucleation and crystallization behavior of PCL/CNT nanocomposites with and without chemical modification [16,17,19]. Trujillo *et al*. [16] investigated the nucleation behavior of simple melt mixed, untreated PCL/MWCNT nanocomposites, and reported for the first time a supernucleation effect of approximately 200% in a well dispersed melt mixed system any chemical modification of the nanotubes (note that Trujillo *et al*. [16] obtained a very low dielectric percolation threshold of 0.3%). A similar or better supernucleation effect was also reported when PCL was blended with PCL-grafted MWCNTs (MWCNTs-*g*-PCL) [19]. In both studies, the supernucleation effect was attributed to the excellent dispersion of the MWCNTs in the polymer matrix, which was even better in the presence of functionalized MWCNTs. Pérez and co-workers [17] reported that MWCNTs, functionalized with 2-hydroxyethylbenzocyclobutene (BCB-EO) through a Diels–Alder cycloaddition reaction, nucleated linear PCL (L-PCL), but showed an antinucleation effect in cyclic PCL (C-PCL). This was due to a weak interaction between the MWCNT surfaces and the C-PCL because of the threading effect induced by the C-PCL molecules.

An evaluation of the mechanical performance of pristine and functionalized MWCNTs/PCL nanocomposites showed that functionalized MWCNT (*f*-MWCNT) nanocomposites gave much better mechanical properties than non-functionalized MWCNT nanocomposites. This was ascribed to a better dispersion of the functionalized MWCNTs in the PCL matrix as compared to non-functionalized MWCNTs. The better dispersion of the *f*-MWCNTs in the polymer matrix provided a more uniform stress distribution, minimizing the presence of stress-concentration centers, and increasing the interfacial area for stress transfer from the polymer matrix to the MWCNTs [12,18,21–23].

In this study, MWCNTs were dispersed into a PCL matrix through melt-mixing of the PCL with a PC/MWCNTs masterbatch. The structure and properties of the nanocomposites were correlated with the dispersion, morphology, and nucleating effect of the MWCNTs on the PCL matrix. Additionally, the efficiency of the nucleation and the overall crystallization kinetics of the PCL component were determined by self-nucleation and isothermal crystallization studies.

3.2 Experimental

3.2.1 Materials

A commercial PCL (CAPA 6500, Johannesburg, South Africa) was purchased from Southern Chemicals. It has a density of 1.1 g cm^{-3}, a melting temperature of 58–60 °C, and a degree of crystallinity of ~35%. Its weight-average molecular weight (M_w) and number-average molecular weight (M_n) were measured by GPC, resulting in 113,400 g mol^{-1} and 73,620 g mol^{-1}, respectively, with a polydispersity index (M_w/M_n) of 1.54.

A conductive masterbatch based on 85% low viscosity polycarbonate (Makrolon® 2205 grade, M_w of 20,100 g mol^{-1} [24]) loaded with 15 wt% MWCNTs (industrial grade NC7000) was obtained from Nanocyl (Sambreville, Belgium). It had a density of 1.175 g cm^{-3}. The average diameter and length of the MWCNTs were, respectively, 10 nm and 3–4 µm. The carbon nanotubes contained more than 90% carbon and less than 10% metal oxide impurities.

The nanocomposites were prepared by melt-mixing in a twin-screw extruder (Thermo Scientific HAAKE Mini Lab II at the University of Pretoria, South Africa) operated under compressed air (100 rpm, 160 °C, 10 min). After extrusion, the samples were compression molded at 160 °C for 5 min under 50 kPa using a hydraulic melt press. The calculated weight percentages of the different components in each of the investigated nanocomposites are given in Table 3.1.

Table 3.1 Weight percentages of the components in the nanocomposites.

PCL (wt%)	PC (wt%)	MWCNTs (wt%)
100	0	0
97	2.55	0.45
93	5.95	1.05
87	11.05	1.95
73	22.95	4.05

3.2.2 Sample characterization

Scanning electron microscopy (SEM) analyses were done in a JSM-7800F Extreme-Resolution Analytical Field Emission (JEOL, Tokyo, Japan) scanning electron microscope. The samples were mounted on aluminum pin stubs with steel epoxy glue and coated with gold to produce conductive coatings onto the samples.

For transmission electron microscopy (TEM) analysis, the samples were cryo-sectioned at −100 °C using a Leica UC-FC7 cryo-microtome. The 120-nm-thick sections were mounted on copper grids and viewed at room temperature using an FEI Tecnai 20 transmission electron microscope operating at 200 kV.

Atomic force microscopy (AFM) experiments were performed in selected samples at room temperature using a Bruker Multimode 8 scanning probe microscope equipped with a Nanoscope V controller. The micrographs, whose size was in a range of 0.6–5 μm, were obtained in tapping mode by using microfabricated silicon tips/cantilevers (cantilever spring constant, k = 42 N m^{-1}, and resonance frequency, f_0 = 320 kHz (Bruker, Santa Barbara, CA, USA). Height and phase AFM images of lamellae and MWCNT were collected simultaneously and subjected to a first-order plane-fitting procedure to compensate the tilt. Both height and phase AFM images were similar, and consequently in this work only the phase AFM images will be reported. To obtain cross-section AFM images, samples were cut using an ultramicrotome Leica Ultracut R with a diamond blade.

Simultaneous SAXS/WAXS experiments were performed at the beamline BL11-NCD, ALBA Synchrotron facility in Barcelona, Spain. The samples were placed in DSC pans, and the DSC pans were put on a Linkam THMS600 hot stage coupled to a liquid nitrogen system. The hot stage was programmed to perform the crystallization and subsequent heating and at the same time register the SAXS/WAXS patterns. The thermal protocol was as follows: heating from room temperature to 100 °C, followed by holding for 3 min at 100 °C. Once the thermal history was erased, the samples were cooled down at 50 °C min^{-1} to the selected isothermal temperature. Different isothermal times were used depending on the temperature. Finally, after the isothermal step, the samples were heated at a rate of 5 °C min^{-1}. The energy of the X-ray source was 12.4 keV (λ = 1.0 Å). In the SAXS configuration, the sample-detector (ADSC Q315r detector, Poway, CA, USA) with a resolution of 3070 × 3070 pixels, pixel size of 102 μm^2 distance was 6495.0 mm with a tilt angle of 0°, whereas in the WAXS configuration, the sample-detector

(Rayonix LX255-HS detector, Evanston, IL, USA) with resolution of 1920 × 5760 pixels, pixel size of 44 μm^2 distance was 132.6 mm with a tilt angle of 21.2°. The intensity profile showed the plot of the scattering intensity as a function of the scattering vector, $q = 4\pi sin\theta\lambda^{-1}$, where λ is the X-ray wavelength (λ = 1.0 Å) and 2θ is the scattering vector. The scattering vector was calibrated using silver behenate (SAXS) and chromium (III) oxide (WAXS).

Dielectric relaxation measurements were performed using a Novocontrol GmbH Concept 40 broadband dielectric spectrometer (Montabaur, Germany), and data were collected over the frequency range 0.1–3 MHz at room temperature. Sample discs of 2 cm diameter were sandwiched between two gold-coated copper electrodes of 2 cm diameter and then transferred to the instrument for data collection. The AC conductivity was calculated, from the Novocontrol WinDETA software, by using the measured values of dielectric permittivity storage (ε') and the dielectric loss factor (ε'').

Differential scanning calorimetry (DSC) analyses were performed under ultra high purity nitrogen gas flow in a power compensation Perkin Elmer Pyris-1 DSC, equipped with a refrigerated cooling system Intracooler 2P. The sample weight was ~5 mg in all cases.

For the non-isothermal DSC analyses, the samples were melted in the DSC for 3 min at 160 °C to erase any previous thermal history. The samples were then cooled at 20 °C min^{-1} from 160 to −20 °C, and then heated at the same rate from −20 to 160 °C. The self-nucleation (SN) tests were performed according to a procedure established by Fillon *et al*. [25], and further developed and studied by Müller *et al*. [26–28]. The complete procedure is as follows:

(a) The sample was heated from 25 to 160 °C at 20 °C min^{-1} and maintained at that temperature for 3 min to erase thermal history.

(b) It was then cooled from 160 to −20 °C at 20 °C min^{-1} to create the initial "standard" state and held at that temperature for 3 min.

(c) It was then heated from −20 °C to a selected thermal treatment temperature or self-seeding temperature (T_s), located in the final melting temperature range of the sample, and held at that temperature for 5 min.

(d) It was again cooled to −20 °C, where the effects of thermal treatment would be reflected in the crystallization behavior of the sample.

(e) Finally, it was heated to 160 °C, where the effects of thermal treatment would also be reflected in the melting behavior of the sample.

The most important parameters during SN are (1) the heating and cooling rates used, (2) the T_s temperature, and (3) the time spent at T_s.

The isothermal crystallization experiments were performed by following the procedure recommended by Lorenzo *et al*. [29] in which isothermal crystallization temperatures (T_c) are chosen where no crystallization occurred during the cooling step from the melt (performed at 60 °C min^{-1}). The samples were heated to 160 °C and kept at this temperature for 3 min to erase the thermal history. Then, a controlled cooling was applied, making sure that the cooling rate was 60 °C min^{-1}, down to the set isothermal T_c temperature. The sample was then kept at the set T_c for a crystallization time (t_c) until saturation was reached. Finally, the sample was heated from T_c to 160 °C at 20 °C min^{-1} to record the melting behavior of the isothermally crystallized sample.

To determine the equilibrium melting temperatures, T_m^o, of the samples, the final step in the isothermal crystallization procedure, whereby the sample was heated at 20 °C min^{-1} in order to record the melting behavior of the isothermally crystallized polymer, was used to record the melting of the crystals formed at different crystallization temperatures, T_c. The Hoffman–Weeks extrapolation [30] was then applied by plotting the observed melting temperature ($T_{m(obs)}$) against T_c to observe the intersection of this line with another line with a slope equal to 1 ($T_m = T_c$).

Dynamic mechanical analyses (DMA) were performed from −100 °C to the onset of melting of PCL, which is ~50 °C, in the bending (dual cantilever) mode at a heating rate of 3 °C min^{-1} and a frequency of 1 Hz.

The tensile analysis of the samples was carried out using an Instron 4301 universal testing machine at a cross-head speed of 10 mm min^{-1}. The dumbbell shaped samples had a Gauge length of 20 mm, a thickness of 1 mm, and a width of 5 mm. The samples were tested at a controlled ambient temperature of 23 °C and 50% relative humidity. Three samples of each composition were tested, and average values with standard deviations are presented.

Thermal conductivity measurements were performed using a Therm Test Inc. Hot Disk TPS 500 thermal constant analyzer. The instrument uses the transient plane source method. A 3.2 mm radius Kapton disk type sensor was selected for the analysis. The sample discs were 5 mm thick and 12 mm in diameter. The sensor was placed between

two sample discs of the same composition. The measurements were made for a period of 25 s in order to prevent the heat flow from reaching the boundary of the samples. Three measurements were performed for each composition. The thermal conductivities are reported as average values with standard deviations.

3.3 Results and discussion

3.3.1 Miscibility assessment

The interaction between the components of a polymer blend can be determined from the composition dependence of the glass transition temperature (T_g). If two polymers are completely miscible, only one T_g is observed with its position determined by the composition of the blend. For immiscible polymer blends, two distinct T_g-values are observed at the same temperatures as those of the parent homopolymers. However, when the two polymers are partially miscible, there are still two T_g-values that will be shifted towards each other, with the degree of shift being dependent on both blend composition and miscibility degree [31].

In the present case, the T_g of the PC component in the nanocomposites could not be observed through either DSC, DMA, or dielectric analysis (DEA) because PCL (the major component of the blends, i.e., the matrix) melted at a temperature well below the T_g of PC (DMA analyses could not be performed at temperatures above the T_m of PCL) and because PC crystallized in the nanocomposites (see crystallization and melting peaks indicated with arrows in Figure 3.1). PC does not normally crystallize, as it has a semi-rigid chemical structure and its crystallization is too slow. However, when plasticizers are added into the PC matrix, its free volume increases, which enhances the mobility of the PC polymer chains and its ability to crystallize can be enhanced [32–34]. In our case, the PCL obviously acted as a plasticizer for PC, a sign of miscibility (either full miscibility or partial miscibility). As PC crystallizes, its T_g is difficult to observe by DSC, as the amount of mobile amorphous fraction per unit mass is very small in the blends.

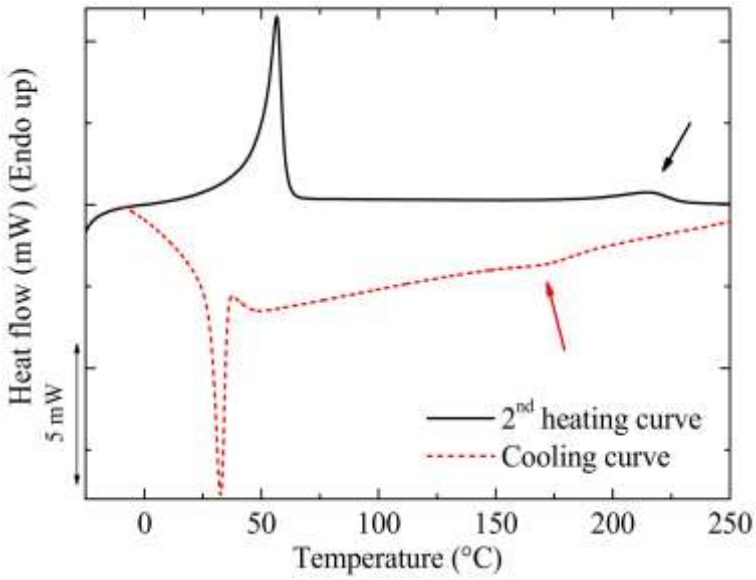

Figure 3.1 DSC (Differential Scanning Calorimetry) cooling and second heating curves for the selected 73/(23/4) *w*/*w* PCL/(PC/MWCNT) nanocomposite. The arrows indicate the crystallization and melting of the PC-rich phase in the blends.

The crystallization of the PC component was also confirmed by simultaneous SAXS/WAXS analyses of PCL and the 93/(6/1) *w*/*w* PCL/(PC/MWCNTs) and 73/(23/4) *w*/*w* PCL/(PC/MWCNT) nanocomposite samples. Figure 3.2 depicts the final X-ray patterns taken under the indicated isothermal crystallization temperatures. The main WAXS reflections shown by neat PCL are also present in the nanocomposites, since the MWCNTs in the masterbatch acted only as nucleating agents (see Section 3.3.5). The main reflection peaks of PCL are located at *q*-values of 15.2 and 16.8 nm^{-1}, and correspond to the (110) and (200) planes, respectively. It is worth noting that the characteristic shoulder in the PCL at 15.7 nm^{-1} appears in both neat PCL and the nanocomposites and corresponds to the (111) plane. All the reflections are consistent with the reported orthorhombic unit cell of PCL with unit cell parameters a = 7.48, b = 4.98, and c = 17.26 Å [35].

In addition to the PCL unit cell peaks, there is a peak at 12.4 nm^{-1} (equivalent to a 2θ of 17.4°), and this peak becomes pronounced as the PC content in the nanocomposites increases. This peak corresponds to the PC component that is able to crystallize due to the plasticization effect of the PCL, as will be shown in Figure 3.3. Figure 3.2(b) shows the SAXS patterns taken at the same condition used in the WAXS experiments. In these patterns, the PCL signal observed in the neat material and in the nanocomposites with

low PC content is dominant, since the single peak corresponds mainly to the long spacing of PCL lamellae. However, at a higher PC concentration (i.e., 23 wt%), the PC is able to crystallize due to the plasticization effect of the PCL. Therefore, the SAXS signal is not clear due to the overlap of the long spacings generated by the lamellae of PCL and PC. The signal observed is probably an average of these two long spacings.

For the sake of clarity, WAXS patterns were taken during heating after the isothermal step (see Figure 3.3) for the selected samples of 93/(6/1) and 73/(23/4) *w*/*w* PCL/(PC/MWCNT) nanocomposites (the heating patterns of the other samples are shown in Figure A.1). Figure 3.3 shows that the PC peak does not disappear when the PCL is already molten at $T > 60$ °C (see Figure 3.3). This behavior is clearly observed at higher PC concentrations in Figure 3.3(b). According to our results and the literature [33,34], PC is able to crystallize, as mentioned earlier in the discussion, due to the plasticization effect of PCL and shows a main reflection at a 2θ angle of 17.1°. The peak at 12.4 nm^{-1} can therefore be attributed to the PC component, which crystallizes as a result of the plasticization effect of the PCL.

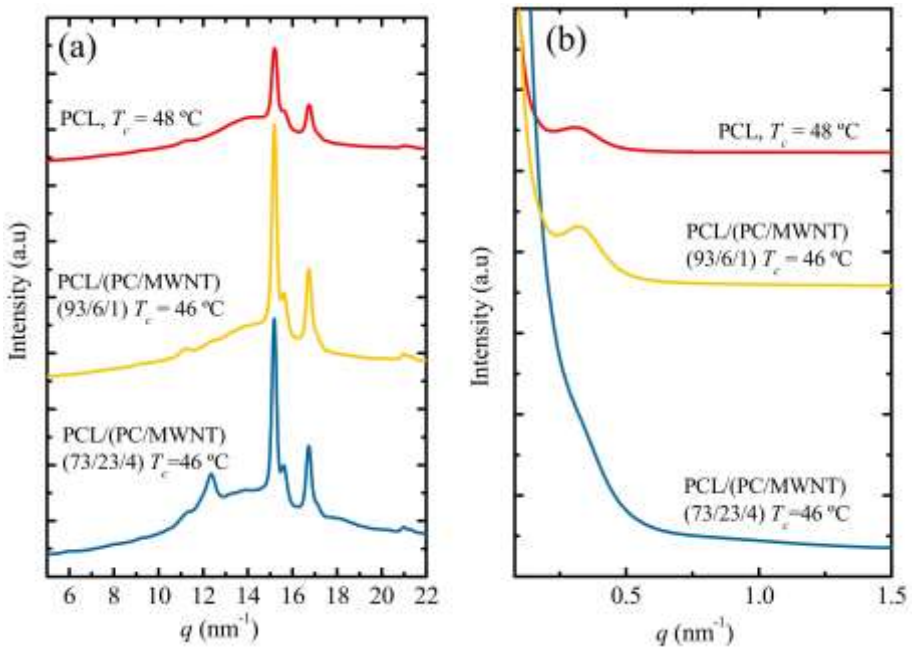

Figure 3.2 (a) WAXS (Wide Angle X-ray Scattering) diffractograms taken at selected isothermal temperatures; (b) SAXS (Small Angle X-ray Scattering) patterns taken at the same temperatures as in (a).

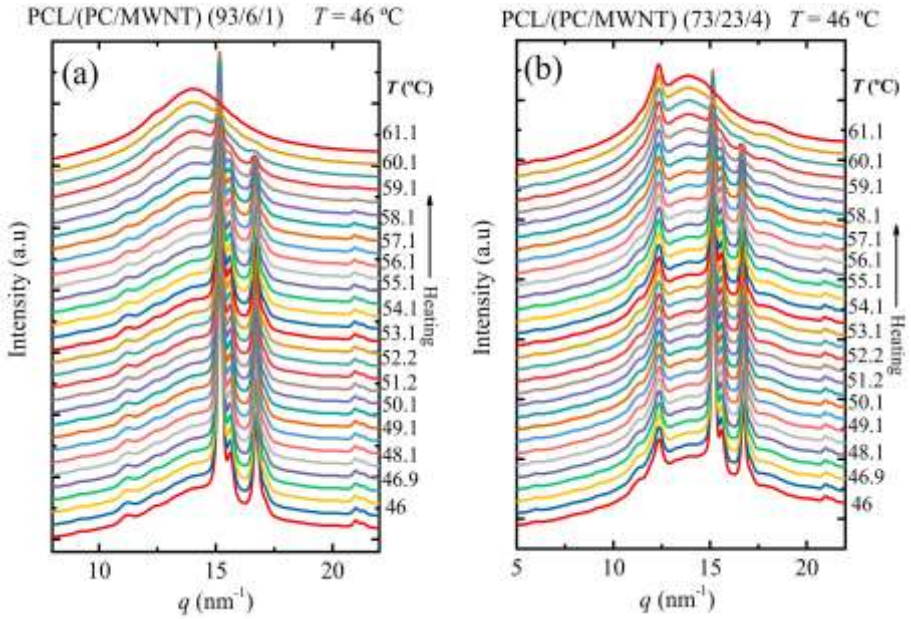

Figure 3.3 WAXS patterns taken during the heating at 5 °C min^{-1} after the isothermal step at 46 °C for (a) PCL/(PC/MWCNTs) (93/6/1) and (b) PCL/(PC/MWCNTs) (73/23/4).

The *d*-spacings for all the reflections shown in Figure 3.2(a) were calculated according to Equation (3.1), whereas the long periods were calculated from the main PCL peaks in the SAXS patterns in Figure 3.2(b). The relevant values are tabulated in Table 3.2.

$$d^* = \frac{2\pi}{q_{max}} \qquad (3.1)$$

The *d*-spacings and the *d**-values of neat PCL and the PCL in the nanocomposites are almost the same for neat PCL and low PC concentrations (i.e., 6 wt%). In the case of 73/(23/4) *w*/*w* PCL/(PC/MWCNT) nanocomposite, the peak related to the PC component is the same as the one reported in the literature (0.464 nm) [33]. In the SAXS patterns, an overlap between the long spacings of PC and PCL occurs, which explains the decrease in *d**-values in comparison with the other samples.

Table 3.2 Calculated values of *d*-spacing (from WAXS (Wide Angle X-ray Scattering) experiments) and long period (*d, obtained from SAXS (Small Angle X-ray Scattering) experiments) for the neat PCL and its nanocomposites.**

Sample	*d*-Spacing (nm)/(plane)	*d** (nm)
Neat PCL	0.378 (110) 0.343 (200) 0.400 (111)	19.8
93/(6/1) *w*/*w* PCL/(PC/MWCNTs)	0.378 (110) 0.344 (200) 0.400(111)	19.9
73/(23/4) *w*/*w* PCL/(PC/MWCNTs)	0.464 * 0.378 (110) 0.344 (200) 0.400 (111)	17.2 **

* PC signal; ** overlap of PC and PCL signals.

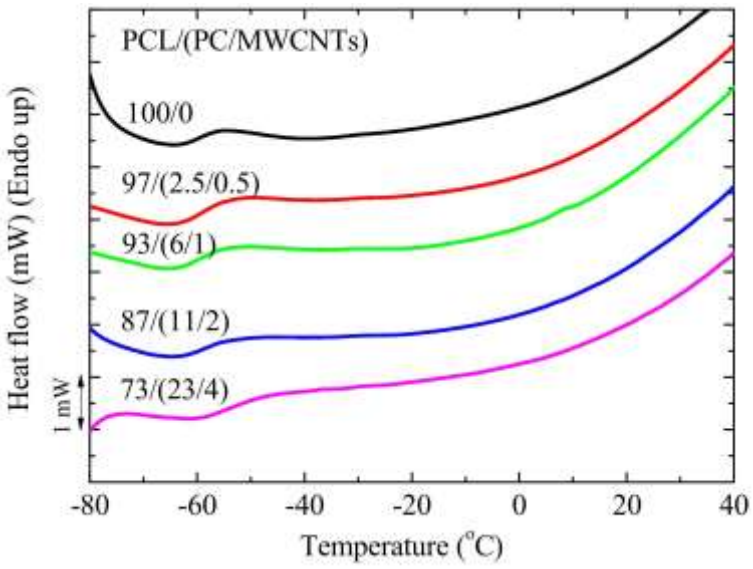

Figure 3.4 DSC heating curves for neat PCL and the PCL/(PC/MWCNT) nanocomposites, showing the glass transitions around −60 °C.

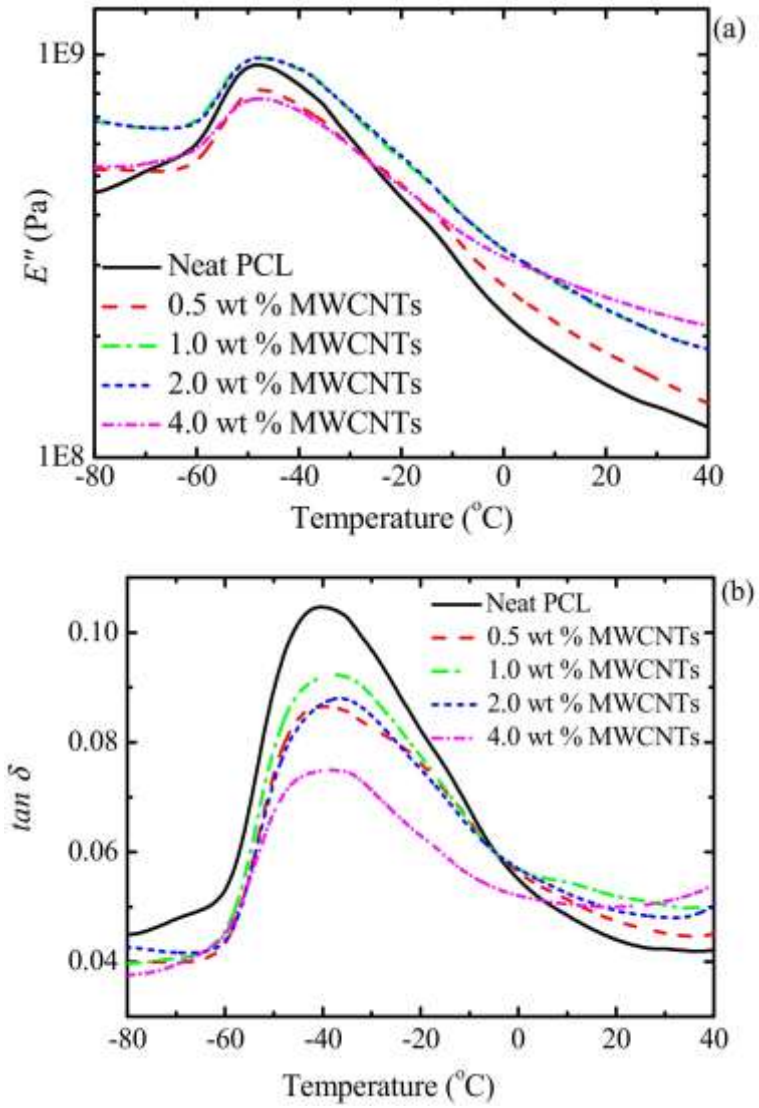

Figure 3.5 DMA (a) loss modulus (E'') and (b) tan δ curves for the investigated samples.

The DSC and DMA results in Figures 3.4 and 3.5 show little change between the T_g-values for neat PCL and PCL within the different nanocomposites. The T_g-values from the two techniques are different for the same sample, with $T_{g,DSC} < T_{g,E''} < T_{g,tan\delta}$ (Figure 3.6). This is well-known, as DMA applies not only a heating rate but also a mechanical deformation with a particular frequency, which, as a result, increases the rate at which T_g is being measured [36–38]. The trends from the different sets of results are, however, the same. The results show that the presence of the masterbatch had little effect on the T_g of PCL, which may be an indication of limited interfacial interaction between the PCL and the PC in the masterbatch. Theoretically, when two polymers are completely miscible,

the T_g of the PCL in the blend nanocomposites should have increased to approximate values calculated according to the Fox equation (Equation (3.2)).

$$\frac{1}{T_g} = \frac{w_1}{T_{g1}} + \frac{w_2}{T_{g2}} \qquad (3.2)$$

where T_g is the PCL/PC blend glass transition temperature, and T_{gi} and w_i are the respective glass transitions and weight fractions of PCL and PC. The glass transition temperatures of PCL obtained from both DSC and DMA did not change much across the composition range, and the values are lower than those predicted by the Fox equation (Figure 3.6), which could be an indication of immiscibility or partial miscibility between the PCL and PC.

However, a closer inspection of the DSC results (Figure 3.4) shows that the blend containing the highest amount of PC, i.e., 73/(23/4) PCL/(PC/MWCNTs) has a T_g-value of approximately 7 °C higher than neat PCL (see also Figure 3.5). DMA results also show an increase in T_g-values of this blend with respect to neat PCL (i.e., 3–4 °C). In fact, Figure 3.5 shows an increasing trend (much smaller than that predicted by the Fox equation but still significant) of T_g with increases in PC content in the blend.

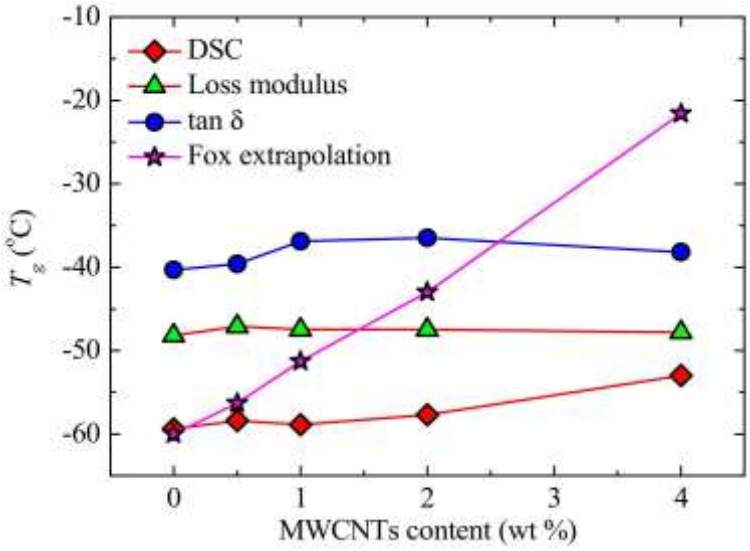

Figure 3.6 Glass transition temperatures of neat PCL and the PCL/(PC/MWCNT) nanocomposites as a function of MWCNT content.

If complete immiscibility would be present in the blends, no plasticization of PC would have been observed (as indicated by PC crystallization, demonstrated above). Taking into account the results presented so far, we can conclude that the blends are

partially miscible. Two phases are formed: (1) a PC-rich phase, where a small amount of PCL chains are present and can plasticize the PC component, such that it can crystallize, and (2) a PCL-rich phase, where the amount of PC chains present is very small, such that changes in the T_g of the PCL phase are much smaller than those predicted by the Fox equation.

3.3.2 Electron microscopy (SEM and TEM) and atomic force microscopy (AFM)

SEM and TEM images for the PCL/(PC/MWCNT) nanocomposites with different PC/MWCNT contents were obtained to confirm the presence of two phases (PCL-rich and PC-rich phases), and to see whether any of the MWCNTs diffused into the PCL phase.

The SEM and TEM images in Figures 3.7 and 3.8 show that there are no clear phase boundaries separating the PCL-rich and PC-rich phases, and that the MWCNTs were fairly well dispersed throughout the blend matrix, although there were areas where the MWCNTs were more concentrated that correspond to the PC-rich phase. The results corroborate the partial miscibility of the blends. If the blends were immiscible, all MWCNTs would be confined to the PC phase (as a PC-based masterbatch was employed). However, it is clear that, due to partial miscibility and the establishment of PC-rich and PCL-rich phases, a fair number of MWCNTs diffused from the PC-rich phase to the PCL-rich phase, even though areas were found where MWCNTs agglomerates were still confined to the PC-rich pockets.

Mixed reports about the miscibility of PC and PCL exists in the literature [20,34,39–44]. In our case, only partial miscibility was developed between the components.

Factors that determine whether the polymers are completely miscible or not include (i) molar-mass distribution, (ii) chemical structure, and (iii) molecular architecture of the components present [45,46]. The molecular weight of PC (20,100 g mol^{-1}) in the masterbatch was appreciably lower than that of PCL (113,400 g mol^{-1}). The PC crystallized in the presence of the PCL, which acted as a plasticizer and imparted enough mobility to the PC chains [32–34,43].

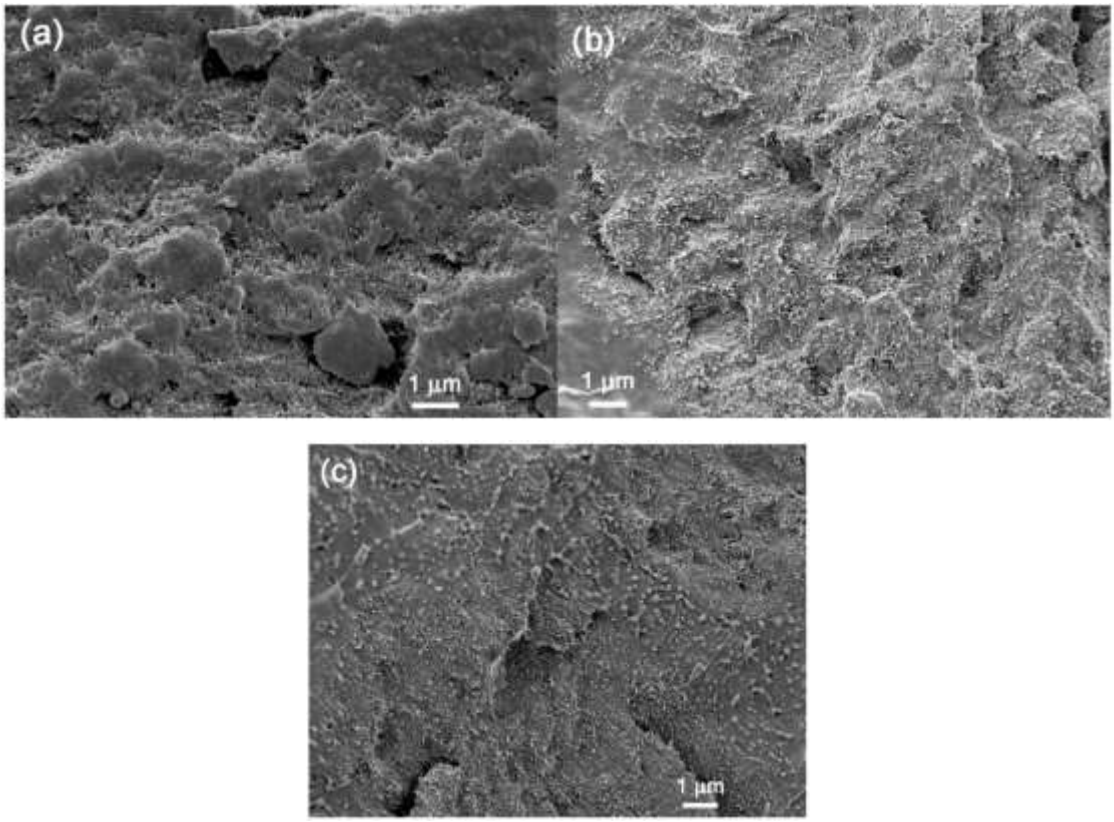

Figure 3.7 SEM micrographs for the PCL/(PC/MWCNT) nanocomposites, respectively, containing (a) 1.0 wt%, (b) 2.0 wt%, and (c) 4.0 wt% MWCNTs.

Shih *et al*. [47] studied the effect of molecular weight on the compatibility between blends of polycarbonate and poly(hexamethylene sebacate). They reported that, in all the blends prepared, the PC crystallized as a result of the plasticizing effect of the poly(hexamethylene sebacate). When a low molecular weight PC and a high molecular weight poly(hexamethylene sebacate) were used, the compatibility was enhanced because of the increased entropic contribution to the Gibbs free energy of mixing.

In our case, the PC crystallization probably reduced the miscibility between PC and PCL, making them only partially miscible. Another reason why we did not observe complete miscibility in our system, is that the MWCNTs probably had a strong interaction with the PC and with each other, which restricted the PC flow during the mixing process and resulted in a fair amount of the PC chains being unable to diffuse into the PCL-rich phase.

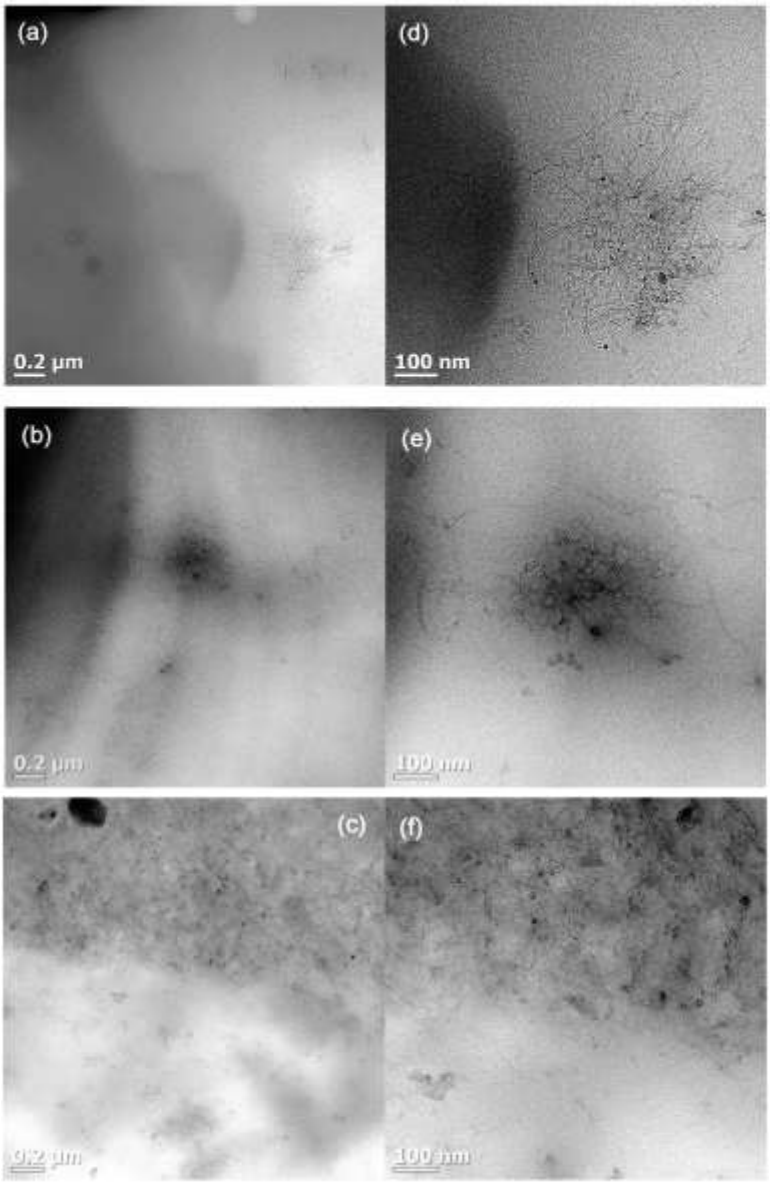

Figure 3.8 High and low magnification TEM micrographs for (a,d) 1.0 wt%, (b,e) 2.0 wt%, and (c,f) 4.0 wt% MWCNTs in the PCL/(PC/MWCNT) nanocomposites.

Figure 3.9 shows the atomic force microscopy (AFM) phase images for the 4 wt% MWCNT nanocomposite at different magnifications. It can be seen at low magnification (Figure 3.9(a)) that an interphase exists between the PCL matrix and the PC/MWCNT-rich phase. The interphase is clear but reveals a very intimate contact between the phases, which probably stems from partial miscibility. At higher magnification (Figure 3.9(b)), the MWCNTs can clearly be seen in the PC-rich phase (the one with the higher amount of nanotubes). However, in addition, some nanotubes can be observed crossing the interface from the PC-rich phase to the PCL-rich phase (see Figure 3.9(b)). Figure 3.9(c) shows that the MWCNTs are well dispersed within the PC-rich phase.

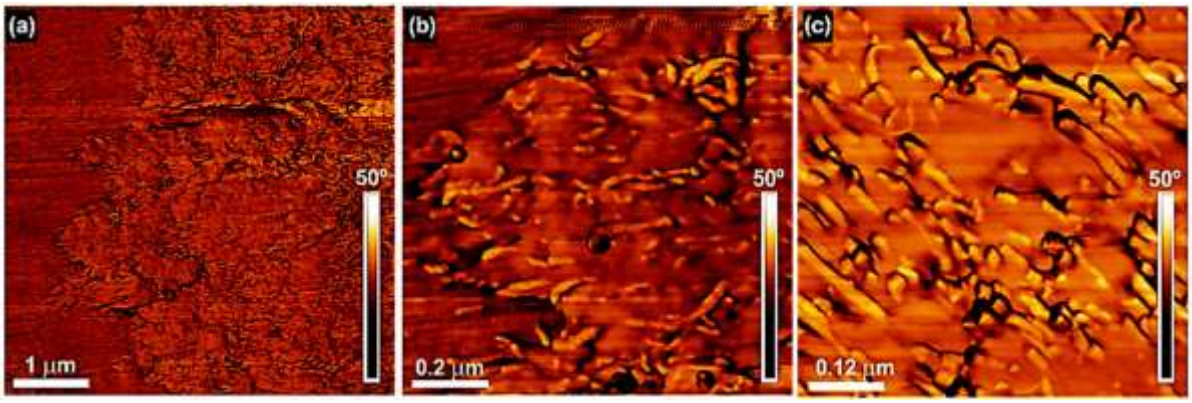

Figure 3.9 (a) Low and (b,c) high magnification AFM phase images for the 73/(23/4) *w*/*w* PCL/(PC/MWCNT) nanocomposite.

3.3.3 Dielectric measurements

AC conductivity vs. frequency (*f*) plots at 20 °C for all samples are demonstrated in Figure 3.10. For the sample with 0.5 wt% MWCNTs, the trend does not show any plateau regions, and the conductivity is gradually increasing with increasing frequency, which is primarily due to dipolar motions of the PCL chains [48–50]. At such a low concentration of MWCNTs, the nanotubes did not achieve a percolated network structure.

The DC conductivity increases and the plateau widens to include most of the measured frequency range for samples with an MWCNT concentration of 1.0 and 2.0 wt%. There could be two reasons for this kind of conductivity behavior: Firstly, increasing MWCNT content may have resulted in an increased charge carrier concentration and therefore better interparticle contact and an easier formation of a continuous pathway for electron hopping. Secondly, sharp differences in dielectric constant and conductivity of the MWCNTs in comparison to PCL or PC surrounding matrices may lead to the Maxwell–Wagner–Sillars (MWS) interfacial polarization effects, as mobile charges get accumulated at the interface between the MWCNTs and the two matrices [50,51]. Other important parameters including MWCNT dipole density and mobility, as well as the mobility of the surrounding polymer chains, are necessary for the MWS polarization phenomena to occur.

As the MWCNT content is increased to 4 wt%, the conductivity dropped sharply, almost by two orders of magnitude, which could reflect aggregation of the nanotubes within the PCL matrix, as well as the crystallization of the PC phase. This aggregation

could cause an accumulation of the mobile charges at the interfaces between the nanotubes and therefore act as barrier for long-range hopping events of the electrons, i.e., inter-nanotubes interfaces act as dead ends for the mobile charges [49].

From the obtained results the dielectric percolation threshold occurs between 0.5 and 1.0 wt% of MWCNTs or the critical concentration needed to form a connected conducting pathway for the electrons to hop between the nanotubes and throughout the surrounding polymer matrices. The formation of a percolation pathway also demonstrates that the MWCNTs were able to diffuse from the PC-rich phases to the PCL matrix. However, they did this more efficiently at lower PC concentrations. When the PC content was 23%, i.e., when the MWCNT content was increased to 4%, then aggregation of the nanotubes or less transfer of the nanotubes to the PCL matrix must have occurred. In fact, the AFM images shown in Figure 3.9 for the nanocomposite with 4% MWCNTs do show a much higher concentration of nanotubes in the PC-rich phase than in the PCL-rich phase.

Figure 3.11 depicts the conductivity as a function of the MWCNT content at room temperature and at the lowest measured frequency (0.1 Hz). The plot reveals a sharp increase in the conductivity as the MWCNTs' wt% increases from 0.5 to 1.0%, then a sharp drop after 2.0%. Trujillo *et al*. [16] reported a very low dielectric percolation threshold of 0.3 wt%, due to the excellent dispersion obtained in the PCL/MWCNT nanocomposites. Vega *et al*. [19] obtained a percolation threshold of 0.240 wt% for the same nanocomposites and 0.236 wt% for nanohybrids (PCL/MWCNT-*g*-PCL) determined by rheological measurements. It is worth noting that, in these systems [16,19] with such a low percolation threshold, a supernucleation effect (a nucleation efficiency of 200%) was reached. Higher percolation thresholds have been reported by Saeed *et al*. [52]. The authors obtained a percolation threshold of 2 wt%, for PCL/MWCNT nanocomposites prepared via in situ polymerization of the PCL on nitric acid-treated CNTs surfaces using rheological measurements. However, Pötschke *et al*. [53] reported values of 1 wt% of percolation thresholds for PC/MWCNT nanocomposites produced by melt-mixing using the masterbatch dilution method without any modification to the nanotubes. However, it is important to note the differences in the processing conditions used during the preparation of these nanocomposites, as the viscosity of the matrix greatly affects the dispersion of the nanotubes [49].

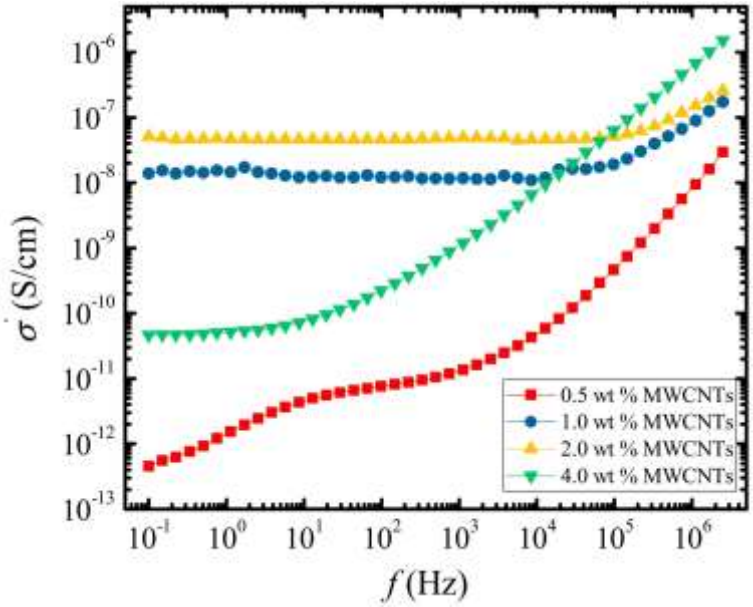

Figure 3.10 Conductivity vs. frequency at room temperature for the sample containing a different wt% of MWCNTs.

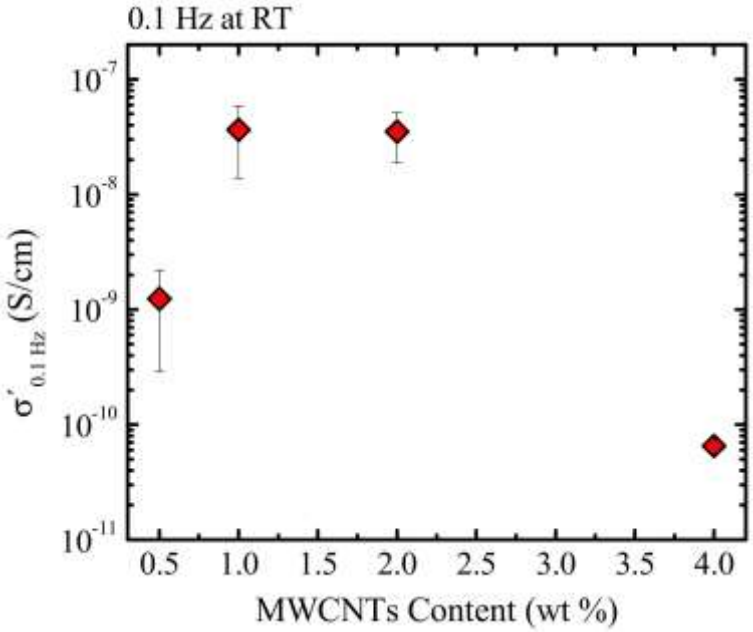

Figure 3.11 Conductivity vs. MWCNT content at room temperature and frequency of 0.1 Hz.

3.3.4 Non-isothermal DSC

Figure 3.12 shows the DSC (a) cooling scans after erasing the thermal history and (b) the subsequent heating scans performed at 20 °C min^{-1} for the different investigated samples. The crystallization peak temperatures (T_c) of PCL in the nanocomposites shifted to higher

temperatures as compared to that of neat PCL (Figure 3.12(a)). The DSC heating curves show little or no change in the melting temperature (T_m) of PCL in the nanocomposites compared to that of neat PCL (Figure 3.12(b)).

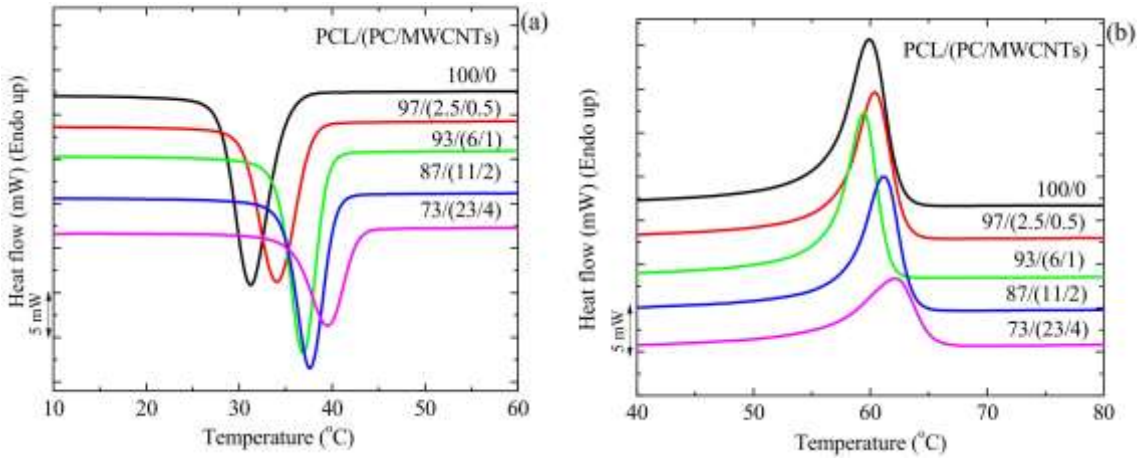

Figure 3.12 DSC (a) cooling and (b) second heating curves at 20 °C min^{-1} of neat PCL and the PCL/(PC/MWCNT) nanocomposites.

To examine the results presented in Figure 3.12, the T_c- and T_m-values were plotted in Figure 3.13 as a function of MWCNT content. The increase in T_c with increasing MWCNT content clearly indicates a nucleation effect of the MWCNTs that penetrated into the PCL-rich phase (as was demonstrated morphologically by SEM and AFM images). However, a saturation of this nucleation effect starts below 2 wt% MWCNTs, in line with the percolation threshold of 0.5–1 wt% found in the previous section. This saturation is related to the aggregation of MWCNTs and the limited diffusion of the MWCNTs with increasing PC content. The T_m remains almost constant with the increase in MWCNT content, as is expected when a nucleating agent is used. This is due to the metastable nature of polymer crystals that usually require large increases in T_c-values to give rise to T_m-values [16]. The nucleation action of the MWCNTs is further studied in the next section through self-nucleating experiments.

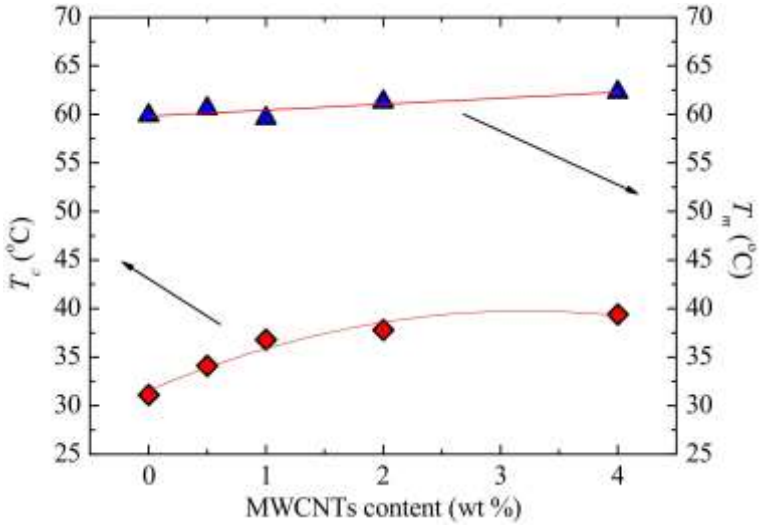

Figure 3.13 DSC crystallization and second heating melting temperatures as a function of MWCNT content for neat PCL and the PCL/(PC/MWCNT) nanocomposites. A linear fit and a polynomial fit for the experimental data of T_m and T_c, respectively, are used to guide the eye.

3.3.5 Self-nucleation (SN)

To evaluate the efficiency of MWCNTs as nucleating agents, it is necessary to compare their effect with that of PCL self-nuclei. Self-nucleation is a thermal protocol for the production of self-nuclei within a polymer melt, such that the nucleation density can be greatly increased. In theory, the best nucleating agent for any polymer is its own crystal fragments or chain segments with residual crystal memory [25–27]. Figure 3.14 shows the experimental data obtained during an SN experiment for neat PCL. The cooling scans after the isothermal step at T_s are presented in Figure 3.14(a), and the subsequent heating scans are shown in Figure 3.14(b). The dashed line indicates the PCL crystallization and melting temperatures under standard conditions. The three SN domains are described below as defined by Fillon *et al*. [25].

Domain I (The melting domain). The polymer is under *Domain I* when complete melting occurs and the crystalline history of the material is erased. All crystalline memory is erased and the melt is isotropic. For the PCL studied in Figure 3.14, *Domain I* is found at T_s larger or equal to 61 °C, since no change was detected in T_c when compared to the standard T_c. Both the crystallization and melting DSC scans are identical within *Domain I.*

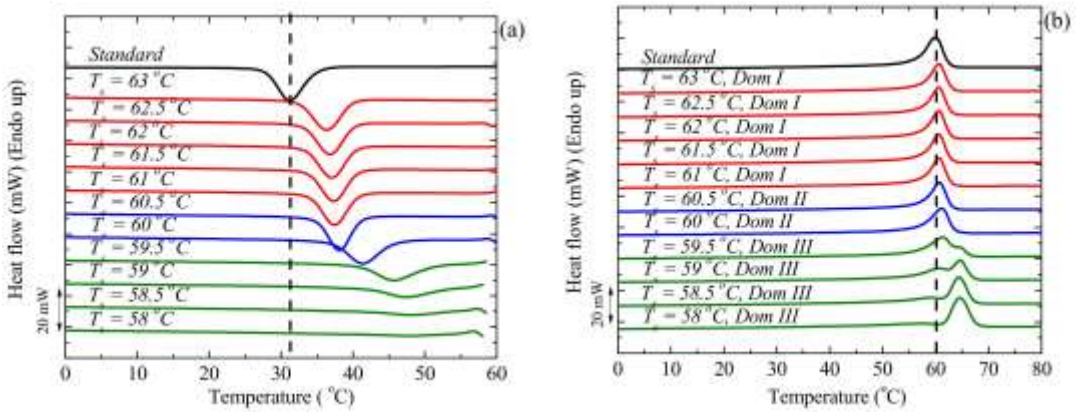

Figure 3.14 (a) DSC cooling scans for neat PCL after 5 min at the indicated T_s, and (b) subsequent heating scans after the cooling runs shown in (a).

Domain II (The self-nucleation domain). In this domain, the T_s range employed is low enough to produce self-nuclei, but high enough to avoid annealing. Therefore, *Domain II* is easily identified after 5 min at a given T_s, because the peak crystallization temperature of the sample increases compared the standard value. The start of *Domain II* for the PCL sample in Figure 3.14(a) occurred at a T_s = 60 °C, since the sample was self-nucleated without any annealing. The minimum T_s within *Domain II* is defined as the "ideal self-nucleation temperature" ($T_{s,ideal}$), a temperature that should be accurately determined. This is the temperature that causes maximum self-nucleation (maximum increase in T_c) without annealing. The subsequent melting curve in Figure 3.14(b) does not reveal any sign of annealing. In this domain, the nucleation density is enhanced, which makes the crystallization of PCL possible at higher temperatures.

Domain III (The self-Nucleation and annealing domain). When T_s is too low, partial melting occurs and the unmolten crystals anneal during the 5 min at T_s. Figure 3.14(b) shows that, when T_s < 60 °C, the melting endotherm exhibits a small high temperature peak that is a result of the melting of annealed crystals. At this T_s, the crystallization exotherm shows a high-temperature tail which reveals that the sample is in *Domain III*.

Figure 3.15 shows the location of the three self-nucleation domains for the PCL sample. The vertical dashed lines indicate the temperatures at which the material experiences a self-nucleation domain transition. The T_c-values are constant in *Domain I* and increase as the T_s-value crosses over to *Domain II*, as expected [25,26]. Since 60 °C is the lowest T_s-value in *Domain II*, it is called the ideal self-nucleation temperature, because it is the temperature at which there is maximum self-nucleation without any annealing. Employing the ideal T_s (60 °C), the T_c corresponding to the ideal T_s should be

used as the maximum crystallization temperature ($T_{c,max}$) when determining the nucleation efficiency of the nanofiller. For the PCL used in this study, $T_{c,max}$ is 42.8 °C.

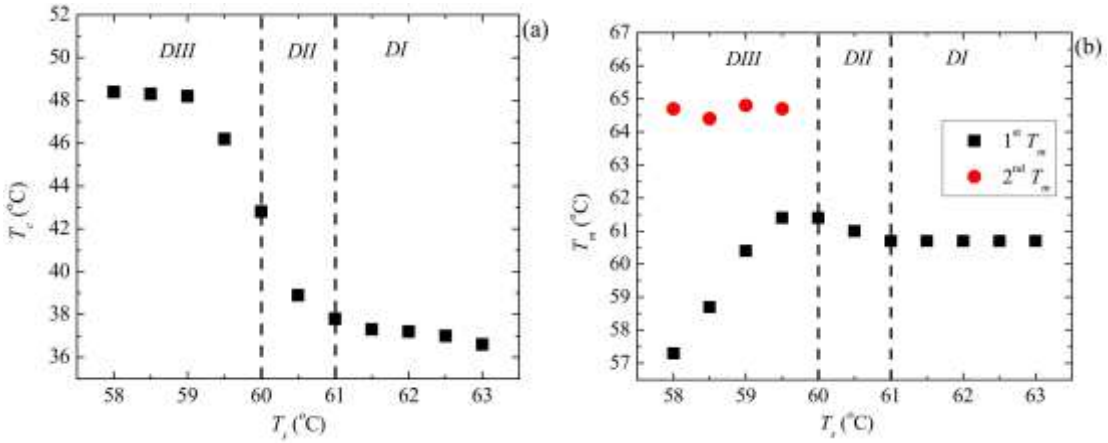

Figure 3.15 Dependence of (a) crystallization and (b) melting peak temperatures of neat PCL on T_s.

The efficiency of the MWCNTs as nucleating agents for the PCL matrix was calculated according to Equation (3.3), which was proposed by Fillon *et al*. [54].

$$NE = \frac{T_{c,NA} - T_{c,PCL}}{T_{c,max} - T_{c,PCL}} \times 100 \qquad (3.3)$$

where $T_{c,NA}$ is the peak T_c-value determined from non-isothermal DSC cooling run for a sample of the polymer with the nucleating agent (NA), $T_{c,PCL}$ is the peak T_c-value for neat PCL after its crystalline history has been erased (31.2 °C), (also determined from non-isothermal DSC cooling scan) and $T_{c,max}$ is the maximum peak crystallization temperature determined after neat PCL has been self-nucleated at the ideal T_s (42.8 °C) [27,54]. Figure 3.16 shows the percentage nucleation efficiency of MWCNTs in the PCL/(PC/MWCNT) nanocomposites.

The nucleating efficiency increases with increasing MWCNT content. Notice that, if the blends were totally immiscible, the MWCNTs would be trapped inside the PC phase and the increase in MWCNTs would probably cause no increase in nucleation efficiency. In this case, the nucleation efficiency clearly increases with MWCNTs, a result which is also consistent with the partial miscibility of the blends. The fast increase in the nucleation efficiency is observed until a concentration of 1 wt% is reached, which is in line with the percolation threshold obtained in the previous section as well as the DSC

results. At MWCNT concentrations above 1 wt%, the increase is slow, which corresponds to a saturation effect due to an agglomeration of MWCNTs and PC crystallization.

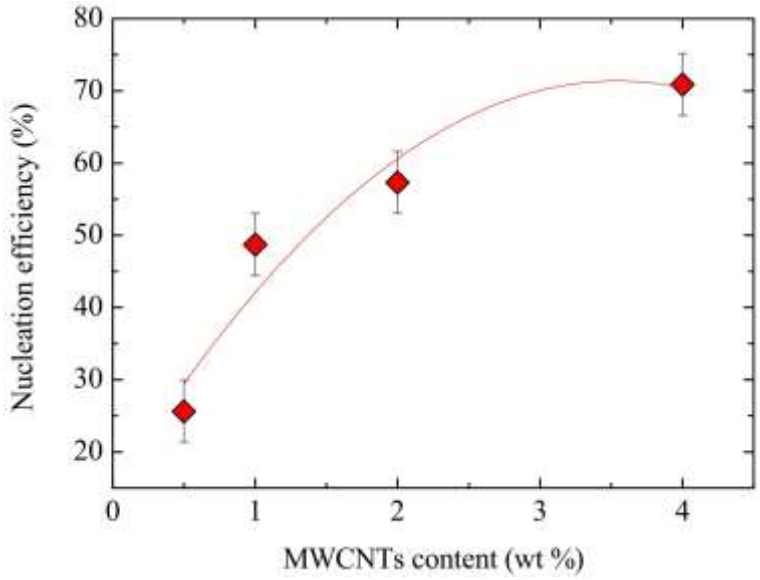

Figure 3.16 Nucleation efficiency as a function of MWCNT content. The experimental points are fitted with a polynomial fit to guide the eye.

The increase in nucleation efficiency (even if highly significant, up to 70%) is less than expected, as literature results indicate that MWCNTs can super nucleate PCL (i.e., can produce nucleation efficiencies larger than 100% with loading as low as 1% or less) [16,19]. In our case, the nucleating efficiency is lower due to limited phase mixing between the PC-rich and the PCL-rich phases. Only a limited quantity of MWCNTs can penetrate the PCL-rich phase and therefore contribute in nucleating PCL, while most of the MWCNTs agglomerated in the PC-rich phase.

3.3.6 Overall isothermal crystallization studied by DSC

The influence of the MWCNTs as well as PC (both components of the masterbatch employed) at different contents, over the isothermal crystallization kinetics of the PCL are studied. Figure 3.17 shows the inverse of the half crystallization time ($1/\tau_{50\%Exp}$), which is proportional to the overall crystallization rate as a function of isothermal crystallization temperatures (T_c) for neat PCL and the nanocomposites. The T_c range for neat PCL is lower than that for the nanocomposites. This indicates that a larger degree of supercooling is needed for neat PCL to crystallize, while the nanocomposites crystallize

more easily than does neat PCL, because of the nucleation effect that they have on the PCL-rich phase.

Another way to examine the results presented in Figure 3.17, is by taking the values of the crystallization temperature for which the blends reach a constant value of $1/\tau_{50\%}$ (i.e., 0.5 min^{-1}) (Figure 3.18(a)) and the $1/\tau_{50\%}$-values at a constant T_c (i.e., 47 °C) (Figure 3.18(b)), as a function of MWCNT content. Figure 3.18(a) shows the experimental and extrapolated data using the Lauritzen and Hoffman (L-H) theory, which is explained in detail in Section 3.3.6.2. It is clear that nucleation produces an interesting practical effect, as a higher T_c-value is needed to reach the same overall crystallization rate with increasing MWCNT content in the PCL-rich phase. This result is in agreement with previous works [16,17,19], where an increase in MWCNT content resulted in an increase in the peak crystallization temperature of PCL during non-isothermal crystallization.

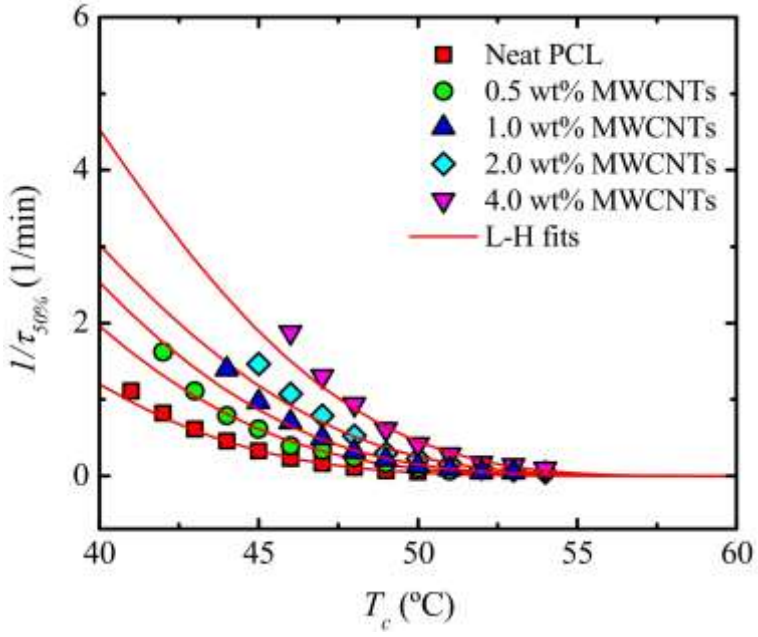

Figure 3.17 Overall crystallization rate ($1/\tau_{50\%}$) as a function of isothermal crystallization temperature (T_c) for neat PCL and for the PCL/(PC/MWCNT) nanocomposites. The red solid lines represent fits to the LH theory.

In Figure 3.18(b), the overall crystallization rate of the PCL-rich phase at a constant crystallization temperature increases with MWCNT loading, due to the nucleating effect of the MWCNTs. Despite the nucleating effect of MWCNTs, a reduction in the percentage crystallinity (X_c) of PCL is observed (see Figure 3.19), especially at high PC concentrations. It must be remembered (see Table 3.1) that, since the nanocomposites are prepared by mixing PCL and a masterbatch, as the MWCNT content increases, so does

the PC fraction in the blends. This decrease in X_c of the PCL matrix (Figure 3.19), during isothermal crystallization, is due to the presence of the PC-rich phase, which is able to crystallize because of the plasticization effect of the PCL component.

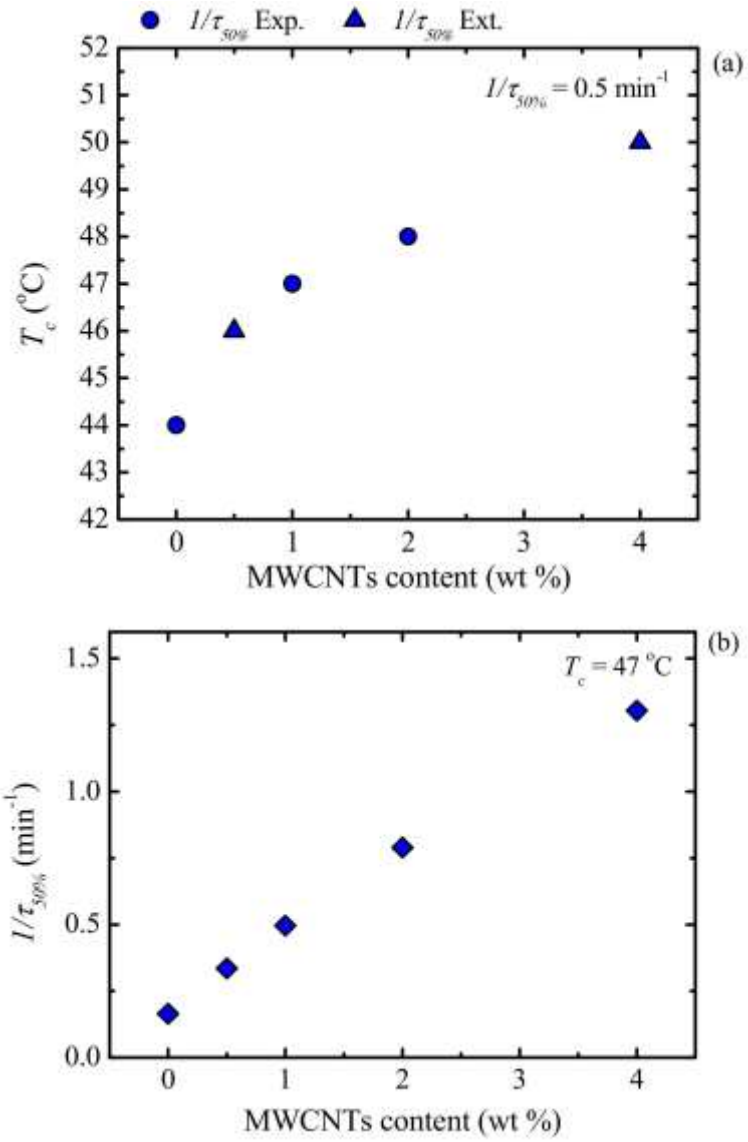

Figure 3.18 (a) Crystallization temperature as a function of MWCNT content at constant $1/\tau_{50\%} = 0.5$ min^{-1}; (b) overall crystallization rate as a function of MWCNT content at constant $T_c = 47$ °C.

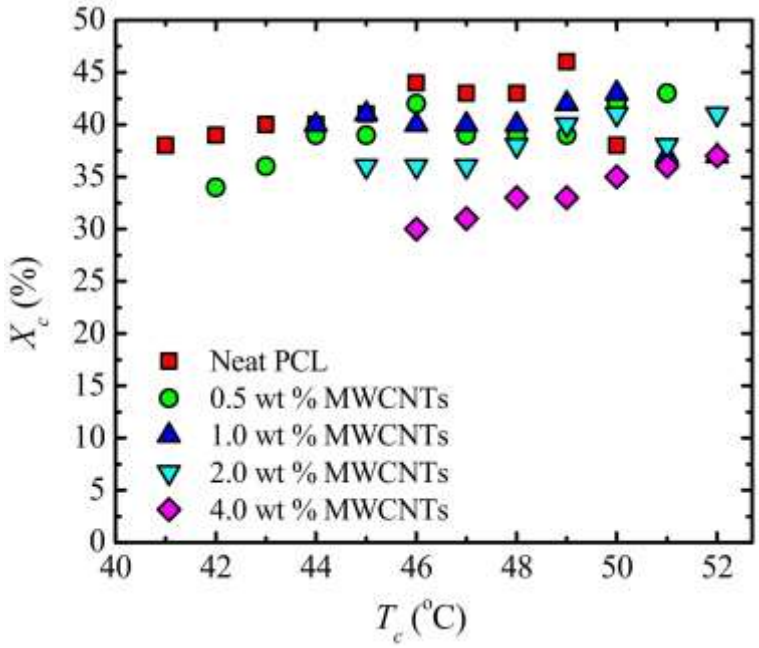

Figure 3.19 Relative crystallinity (X_c) as a function of isothermal crystallization temperature (T_c) for neat PCL and the PCL/(PC/MWCNT) nanocomposites.

3.3.6.1 Fitting DSC isothermal data to the Avrami model

The data obtained during the isothermal crystallization experiments were analyzed employing the Avrami equation, which can be expressed as follows [55]:

$$1 - V_c(t - t_0) = \exp(-K(t - t_0)^n) \tag{3.4}$$

where t is the experimental time, t_0 is the induction time, V_c is the relative volumetric transformed fraction, n is the Avrami index, and K is the overall crystallization rate constant. The procedure used to perform the fittings to the data was developed by Lorenzo *et al*. [29]. The kinetic parameters for all the investigated samples are plotted in Figure 3.20 and tabulated in Table A.1.

Figure 3.20(a) shows $1/\tau_{50\%}$-values as a function of T_c, whose trend was explained earlier in the discussion. The same trend is obtained with the $K^{1/n}$-values of the Avrami model (see Figure 3.20(b)), since this constant is related to the overall crystallization kinetics as well. Figure 3.20(c) shows the n-values for all the samples, which depend on the dimensionality of the crystalline superstructure and on their nucleation kinetics [29,55].

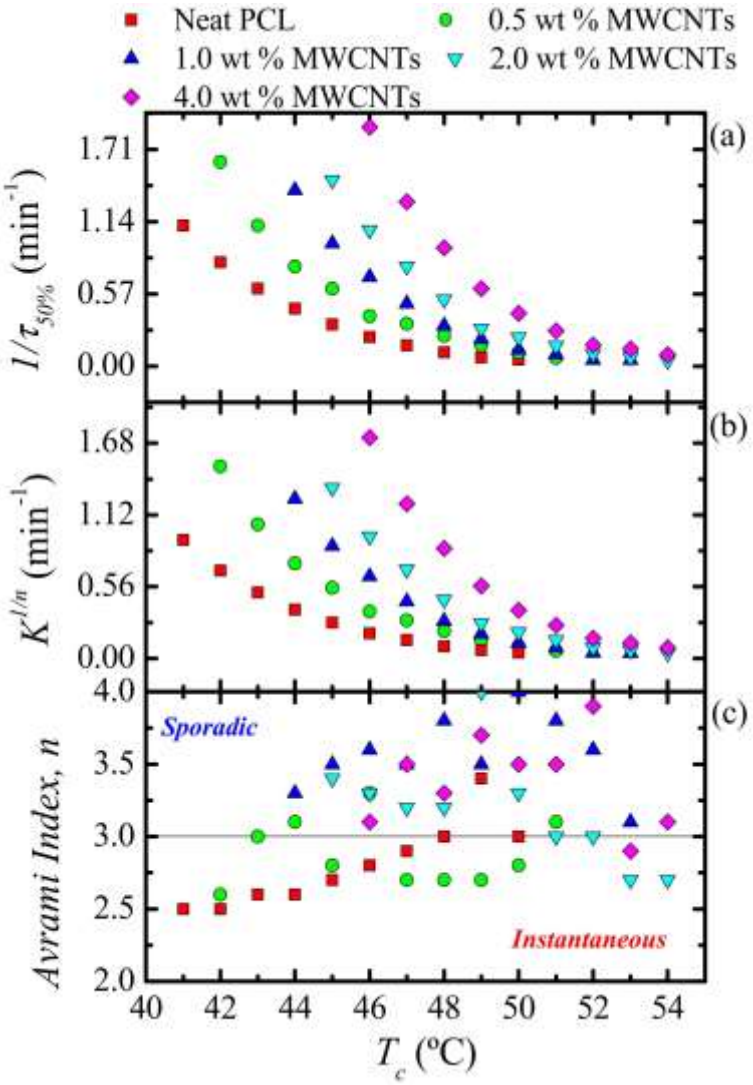

Figure 3.20 (a) Inverse of half crystallization times ($1/\tau_{50\%}$) (b) Normalized crystallization constant of the Avrami model ($K^{1/n}$) and (c) Avrami index (n) as a function of the isothermal crystallization temperature (T_c) for all the samples.

The values of n for neat PCL are approximately 3 in the investigated T_c range, which is an expected result for PCL [16,17]. A value of 3 indicates a spherulitic morphology with instantaneous nucleation, which is commonly observed in PCL homopolymers. Therefore, upon the addition of a nucleating agent, one would expect that the Avrami index would remain around 3 or would decrease (as the dimensionality of growth can switch from 3D to 2D when the nucleation density is greatly enhanced). Higher values than 3 for these PCL nanocomposites are not expected, especially when it has been demonstrated that MWCNTs are effective in nucleating PCL. Further studies are needed in order to understand the explanation of such unexpected results. Elsewhere in the

literature [16,17,19], the authors reported decreasing *n*-values for the nanocomposites as compared to neat PCL.

3.3.6.2 Overall isothermal crystallization data analyzed by the Lauritzen-Hoffman model

The overall crystallization kinetics is determined by contributions of primary nucleation and growth. The Lauritzen-Hoffman (LH) nucleation and growth theory can be applied to the isothermal crystallization kinetics data collected from DSC. Even though the LH theory has received much criticism lately [56], it is still one of a few models that provide easy to use analytical expressions capable of fitting the experimental data over a wide supercooling range [57]. Figure 3.17 shows solid lines that represent the mathematical fit of LH theory, which can be applied to the DSC overall crystallization data according to Equation (3.5).

$$\frac{1}{\tau_{50\%}}(T) = \frac{1}{\tau_0}\exp\left(\frac{-U^*}{R(T_c - T_\infty)}\right)\exp\left(\frac{-K_g^\tau}{T_c\Delta T_f}\right) \qquad (3.1)$$

where $1/\tau_{50\%}$ is the inverse of the experimental half-crystallization time, $1/\tau_0$ a pre-exponential factor that includes the nucleation and growth, U^* the activation energy for the transport of the chains to the growing front (a value of 1500 cal mol^{-1} is usually employed), R the gas constant, T_c the isothermal crystallization temperature (K), and $T\infty$ the temperature at which chain mobility ceases (usually taken as $T_g - 30$ K). ΔT = supercooling ($T_m^o - T_c$), and K_g^τ is a constant related to the energy barrier for crystallization and growth.

According to Figure 3.17, the lines can adequately fit the overall crystallization rate as a function of T_c for the explored range. The fittings were useful in constructing Figure 3.20, which was produced by extrapolating unavailable data in specific temperature ranges. Additionally, it was found, as expected and reported before in similar studies [16,17,19], that K_g^τ-values (proportional to the energy barrier for overall crystallization) decrease when the nanotube content increases as a result of their nucleating ability.

3.3.7 Thermal conductivity

The thermal conductivities of neat PCL and its PC/MWCNTs containing nanocomposites are shown in Figure 3.21. It is well known that phonon transport is the main mechanism for heat conduction in conductive polymer samples. Phonons transfer heat energy through interactions with each other and with subatomic particles [6–8]. The thermal conductivity values of the nanocomposites increased as MWCNT content increased. Since the thermal conductivity of carbon nanotubes ranges between 650 and 10,000 W m K^{-1}, and the thermal conductivity of a typical polymer ranges between 0.1 and 0.3 W m K^{-1} [10], the improvement in the thermal conductivity is most probably caused by the increasing numbers of high thermal conductivity MWCNTs in the blend composites. Since the MWCNTs were fairly well dispersed in the PCL/PC blend (although there were pockets where the MWCNTs are more concentrated, see already discussed SEM and TEM results), the MWCNTs were positioned closer to each other as the MWCNT content increased, which gave rise to more effective transport of the phonons through the nanocomposite, which improved the transportation of heat by high frequency phonon vibration, leading to higher thermal conductivities. In this case, the thermal conductivity does not seem to be affected by the aggregation of carbon nanotubes, which, as discussed previously, was detected when the filler level increased to 4%.

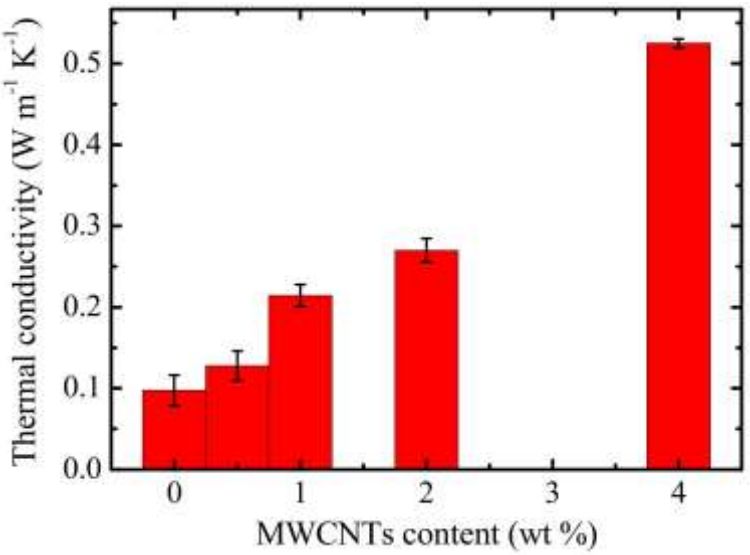

Figure 3.21 Influence of MWCNT content on the thermal conductivities of the nanocomposites.

3.3.8 Tensile properties

The mechanical properties of PCL and the nanocomposites were investigated employing tensile testing. These properties depend upon the interfacial interaction between the nanofiller and the different components in the polymer blend, chain stiffness, and the crystallinities of the individual components in the blend. This implies that, to utilize the reinforcing capability of carbon nanotubes and to maximize the mechanical properties of the nanocomposites, strong interfacial bonding is necessary. The extent of interaction depends on how well the filler is dispersed in the matrix [58].

Considering that the nanocomposites prepared here involve the increasing addition of both PC and MWCNTs to PCL, it is expected that the ductility of the PCL significantly decreases while the modulus increases. Table 3.3 presents the tensile tests results, which partially corroborate the expected trends. The strain at break significantly decreases as the masterbatch content increases (see Figure 3.22), a trend proportional to a reduction in ductility. Additionally, the elastic modulus is not significantly affected, until the maximum amount of masterbatch was used. In this last case, the value increased from 388 MPa for neat PCL to 592 MPa for the nanocomposite.

PC is a more rigid polymer than PCL. In the present blends, PC addition caused a small increase in the T_g of the PCL phase due to the partial miscibility. Additionally, the presence of PC-rich inclusions in a PCL matrix can act as stress concentrators that may trigger earlier fracture nucleation and propagation.

On the other hand, MWCNTs are known to increase overall rigidity of the polymer matrix to which they are added, when the dispersion is adequate and when there are strong interactions with the polymer matrix. In this case, the interactions may not be very strong with the PCL matrix, and the fact that the density of MWCNTs is higher in the PC-rich phase than in the PCL-rich phase probably has a stronger stress concentration effect and is less effective at enhancing the elastic modulus of the nanocomposites. This may be the reason why the positive effect on the elastic modulus can only be obtained at large masterbatch loadings. As both PC and MWCNT additions induce enhanced rigidity and stress concentrations in the PCL matrix, the stress at break is also seen to decrease with masterbatch additions.

Although increases in tensile strength, similar to that of the Young's modulus, have been reported in CNT-filled nanocomposites, the local nature of the shear yielding process, usually leads to constant or even decreasing values as CNT content increases

[59]. In this case, the yield stress of PCL first decreases slightly with masterbatch additions and then recovers at the maximum concentration of MWCNTs.

Table 3.3 Summary of tensile testing results for neat PCL and the nanocomposites.

w/*w* PCL/(PC/MWCNTs)	σ_b/MPa	ε_b/%	E/MPa	σ_y/MPa
100/0	34.3 ± 12.9	578 ± 151	388 ± 29	16.2 ± 1.9
97/(2.5/0.5)	15.9 ± 7.1	285 ± 152	354 ± 77	13.7 ± 3.3
93/(6/1)	10.3 ± 5.0	154 ± 198	352 ± 28	13.6 ± 1.0
87/(11/2)	6.9 ± 1.9	22.8 ± 2.0	336 ± 33	11.3 ± 4.1
73/(23/4)	15.6 ± 0.9	4.3 ± 0.7	592 ± 62	17.1 ± 1.4

σ_b —stress at break; ε_b—strain at break; E—Young's modulus; σ_y—yield strength.

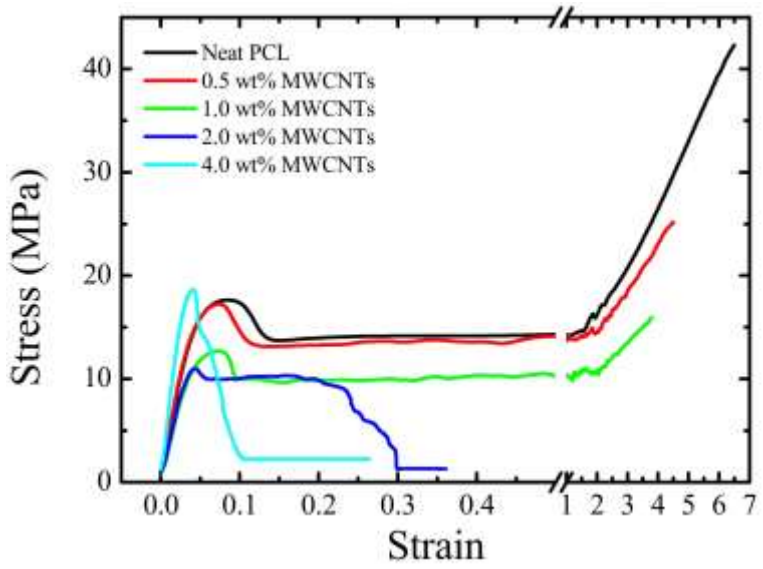

Figure 3.22 Stress–strain curves for neat PCL and the nanocomposites.

3.4 Conclusions

In light of an analysis of the DSC, SEM, DMA, TEM, and AFM results, it can be concluded that the PC and PCL blends prepared in this work are partially miscible. Two phases were formed: (1) A PC-rich phase, where a small amount of PCL chains are present and can plasticize the PC component, such that it can crystallize, and (2) a PCL-rich phase, where the amount of PC chains present is very small, such that changes in the T_g of the PCL phase are much smaller than those predicted by the Fox equation. Due to partial miscibility and the establishment of PC-rich and PCL-rich phases, a fair number

of MWCNTs diffused from the PC-rich phase to the PCL-rich phase as evidenced by the SEM and AFM images, but their diffusion depends on the PC (and MWCNT content) in the blend.

Standard DSC measurements demonstrated an increase in T_c with increasing MWCNT content due to the nucleation effect caused by the presence of MWCNTs that penetrated into the PCL-rich phase (as was demonstrated morphologically by SEM and AFM images). The nucleating efficiency is, however, low, due to limited phase mixing between the PC-rich and the PCL-rich phases. Only a limited quantity of MWCNTs can penetrate the PCL-rich phase and therefore contribute in nucleating PCL, while most of the MWCNTs agglomerated in the PC-rich phase at high MWCNT loadings (e.g., 4%). The nucleation effects saturated at a 1 wt% MWCNT concentration on the PCL-rich phase. This was corroborated by the determination of the dielectric percolation threshold, which ranged between 0.5 and 1.0 wt% MWCNTs.

Isothermal crystallization experiments performed by DSC showed an increase in the overall crystallization kinetics of PCL with increases in MWCNTs as a result of their nucleating effect. Despite the nucleating effect of MWCNTs, a reduction in the percentage crystallinity of PCL was observed especially at high PC concentrations. This was attributed to the presence of the PC-rich phase, which was able to crystallize in view of the plasticization effect of the PCL component.

The thermal conductivities and tensile properties of the nanocomposites were generally enhanced with the addition of MWCNTs.

3.5 References

[1] I. Vroman, L. Tighzert. Biodegradable polymers. Materials 2009; 2:307-344. DOI: 10.3390/ma2020307

[2] R. Morent, N. De Geyter, T. Desmet, P. Dubruel, C. Leys. Plasma surface modification of biodegradable polymers: A Review. Plasma Processes and Polymers 2011; 8:171-190. DOI: 10.1002/ppap.201000153

[3] M.M. Reddy, S. Vivekanandhan, M. Misra, S.K. Bhatia, A.K. Mohanty. Biobased plastics and bionanocomposites: Current status and future opportunities. Progress in Polymer Science 2013; 38:1653-1689. DOI: 10.1016/j.progpolymsci.2013.05.006

[4] R.P. Babu, K.O. Connor, R. Seeram. Current progress on bio-based polymers and their future trends. Progress in Biomaterials 2013; 2:1-16.
DOI: 10.1186/2194-0517-2-8

[5] J.J. George, S. Bhadra, A.K. Bhowmick. Influence of carbon-based nanofillers on the electrical and dielectric properties of ethylene vinyl acetate nanocomposites. Polymer Composites 2010; 31:218-225.
DOI: 10.1002/pc.20788

[6] A. Wurm, D. Lellinger, A.A. Minakov, T. Skipa, P. Pötschke, R. Nicula, I. Alig, C. Schick. Crystallization of poly(ε-caprolactone)/MWCNT composites: A combined SAXS/WAXS, electrical and thermal conductivity study. Polymer 2014; 55:2220-2232.
DOI: 10.1016/j.polymer.2014.02.069

[7] S.J. Chin, S. Vempati, P. Dawson, M. Knite, A. Linarts, K. Ozols, T. McNally. Electrical conduction and rheological behaviour of composites of poly(ε-caprolactone) and MWCNTs. Polymer 2015; 58:209-221.
DOI: 10.1016/j.polymer.2014.12.034

[8] P. Pötschke, T. Villmow, B. Krause. Melt mixed PCL/MWCNT composites prepared at different rotation speeds: Characterization of rheological, thermal, and electrical properties, molecular weight, MWCNT macrodispersion, and MWCNT length distribution. Polymer 2013; 54:3071-3078.
DOI: 10.1016/j.polymer.2013.04.012

[9] P.C. Ma, N.A. Siddiqui, G. Marom, J.K. Kim. Dispersion and functionalization of carbon nanotubes for polymer-based nanocomposites: A review. Composites: Part A 2010; 41:1345-1367.
DOI: 1016/j.compositesa.2010.07.003

[10] M. Bhattacharya. Review: Polymer nanocomposites – A Comparison between carbon nanotubes, graphene, and clay as nanofillers. Materials 2016; 9:1-35.
DOI: 10.3390/ma9040262

[11] K. Prashantha, J. Soulestin, M.F. Lacrampe, P. Krawczak, G. Dupin, M. Claes. Masterbatch-based multi-walled carbon nanotube filled polypropylene nanocomposites: Assessment of rheological and mechanical properties. Composites Science and Technology 2009; 69:1756-1763.
DOI: 10.1016/j.compscitech.2008.10.005

[12] K.C. Jajam, M.M. Rahman, M.V. Hosur, H.V. Tippur. Fracture behavior of epoxy nanocomposites modified with polyol diluent and amino-functionalized multi-walled carbon nanotubes: A loading rate study. Composites Part A: Applied Science and Manufacturing 2014; 59:57-69.
DOI: 10.1016/j.compositesa.2013.12.014

[13] M.M. Rahman, M. Hosur, S. Zainuddin, K.C. Jajam, H.V. Tippur, S. Jeelani. Mechanical characterization of epoxy composites modified with reactive polyol diluent and randomly-oriented amino-functionalized MWCNTs. Polymer Testing 2012; 31:1083-1093.
DOI: 10.1016/j.polymertesting.2012.08.010

[14] T. Wu, E. Chen, Y. Lin, M. Chiang, G. Chang. Preparation and characterization of melt-processed polycarbonate/multiwalled carbon nanotube composites. Polymer Engineering and Science 2008; 48:1369-1375.
DOI: 10.1002/pen.21094

[15] L.M. Robeson. Polymer blends. A comprehensive review. Carl Hanser Verlag: München (2007).

[16] M. Trujillo, M.L. Arnal, A.J. Müller, P. Dubois. Supernucleation and crystallization regime change provoked by MWCNT addition to poly(ε-caprolactone). Polymer 2012; 53:832-841.
DOI: 10.1016/j.polymer.2011.12.028

[17] R.A. Pérez, J.V. López, J.N. Hoskins, B. Zhang, S.M. Grayson, M.T. Casas, J. Puiggalí, A.J. Müller. Nucleation and antinucleation effects of functionalized carbon nanotubes on cyclic and linear poly(ε-caprolactones). Macromolecules 2014; 47:3553-3566.
DOI: 10.1021/ma5005869

[18] J.T. Yeh, M.C. Yang, C.J. Wu, C.S. Wu. Preparation and characterization of biodegradable polycaprolactone/multiwalled carbon nanotubes nanocomposites. Journal of Applied Polymer Science 2009; 112:660-668.
DOI: 10.1002/app.29485

[19] J.F. Vega, J. Fernández-Alcázar, J.V. López, R.M. Michell, R.A. Pérez-Camargo, B. Ruelle, J. Martínez-Salazar, M.L. Arnal, P. Dubois, Alejandro J. Müller. Competition between supernucleation and plasticization in the crystallization and rheological behavior of PCL/CNT-based nanocomposites and nanohybrids. Journal of Polymer Science, Part B: Polymer Physics 2017; 55:1310-1325.

DOI: 10.1002/polb.24385

[20] S. Maiti, S. Suin, N.K. Shrivastava, B.B. Khatua. Low percolation threshold and high electrical conductivity in melt-blended polycarbonate/multiwall carbon nanotube nanocomposites in the presence of poly(ε-caprolactone). Polymer Engineering and Science 2014; 54:646-659.
DOI: 10.1002/pen.23600

[21] Z. Qiu, H. Wang, C. Xu. Crystallization, mechanical properties, and controlled enzymatic degradation of biodegradable poly(ε-caprolactone)/multi-walled carbon nanotubes nanocomposites. Journal of Nanoscience and Nanotechnology 2011; 11:7884-7893.
DOI: 10.1166/jnn.2011.4714

[22] H.H. Lee, U.S. Shin, G.Z. Jin, H.W. Kim. Highly homogeneous carbon nanotube polycaprolactone composites with various and controllable concentrations of ionically-modified MWCNTs. Bulletin of the Korean Chemistry Society 2011; 32:157-161.
DOI: 10.5012/bkcs.2011.32.1.157

[23] L. Pan, X. Pei, R. He, Q. Wan, J. Wang. Multiwall carbon nanotubes/polycaprolactone composites for bone tissue engineering application. Colloids and Surfaces B: Biointerfaces 2012; 93:226-234.
DOI: 10.1016/j.colsurfb.2012.01.011

[24] G.R. Kasaliwal, A. Göldel, P. Pötschke, G. Heinrich. Influences of polymer matrix melt viscosity and molecular weight on MWCNT agglomerate dispersion. Polymer 2011; 52:1027-1036.
DOI: 10.1016/j.polymer.2011.01.007

[25] B. Fillon, J.C. Wittmann, B. Lotz, A. Thierry. Self-nucleation and recrystallization of isotactic polypropylene (α phase) investigated by differential scanning calorimetry. Journal of Polymer Science Part B: Polymer Physics 1993; 31:1383-1393.
DOI: 10.1002/polb.1993.090311013

[26] A.T. Lorenzo, M.L. Arnal, J.J. Sánchez, A.J. Müller. Effect of annealing time on the self-nucleation behaviour of semicrystalline polymers. Journal of Polymer Science Part B: Polymer Physics 2006; 44:1738-1750.
DOI: 10.1002/polb.20832.

[27] A.J. Müller, M.L. Arnal. Thermal fractionation of polymers. Progress in Polymer Science 2005; 30:559-603.
DOI: 10.1016/j.progpolymsci.2005.03.001

[28] R.M. Michell, A. Mugica, M. Zubitur, A.J. Müller. Self-nucleation of crystalline phases within homopolymers, polymer blends, copolymers, and nanocomposites. Advances in Polymer Science 2017; 276:215-256.

[29] A.T. Lorenzo, M.L. Arnal, J. Albuerne, A.J. Müller. DSC isothermal polymer crystallization kinetics measurements and the use of the Avrami equation to fit the data: Guidelines to avoid common problems. Polymer Testing 2007; 26:222-231.
DOI: 10.1016/j.polymertesting.2006.10.005

[30] J.D. Hoffman, J.J. Weeks. Melting process and the equilibrium melting temperature of polychlorotrifluoroethylene. Journal of Research of the National Bureau of Standards-A. Physics and Chemistry 1962; 66:13-28.

[31] J.D. Menczel, R.B. Prime. Thermal Analysis of Polymers. Fundamentals and Applications. John Wiley & Sons: New Jersey (2009).

[32] Y. Zhang, J.H. Han. Crystallization of high-amylose starch by the addition of plasticizers at low and intermediate concentrations. Journal of Food Science 2010; 75:N8-N16.
DOI: 10.1111/j.1750-3841.2009.01404.x

[33] A.J. Müller, E. Paredes. Melting behavior, mechanical properties and fracture of crystallized polycarbonates. Latin American Journal of Metallurgy and Materials 1985; 5:130-141.

[34] V. Balsamo, N. Calzadilla, G. Mora, A.J. Müller. Thermal characterization of polycarbonate/polycaprolactone blends. Journal of Polymer Science: Part B: Polymer Physics 2001; 39:771-785.
DOI: 10.1002/1099-0488(20010401)39:7<771::AID-POLB1052>3.0.CO;2-I

[35] H. Hu, D.L. Dorset. Crystal structure of poly(iε-caprolactone). Macromolecules 1990; 23:4604–4607.
DOI: 10.1021/ma00223a017

[36] P. Pötschke, A.R. Bhattacharyya, A. Janke, H. Goering. Melt mixing of polycarbonate/multi-wall carbon nanotube composites. Composite Interfaces 2003; 10:389-404.
DOI: 10.1163/156855403771953650

[37] J. Guo, Y. Liu, R. Prada-Silvy, Y. Tan, S. Azad, B. Krause, P. Pötschke, B.P. Grady. Aspect ratio effects of multi-walled carbon nanotubes on electrical, mechanical, and thermal properties of polycarbonate/MWCNT composites. Journal of Polymer Science, Part B: Polymer Physics 2014; 52:73-83.
DOI: 10.1002/polb.23402

[38] F.Y. Castillo, R. Socher, B. Krause, R. Headrick, B.P. Grady, R. Prada-Silvy, P. Pötschke. Electrical, mechanical, and glass transition behavior of polycarbonate-based nanocomposites with different multi-walled carbon nanotubes. Polymer 2011; 52:3835-3845.
DOI: 10.1016/j.polymer.2011.06.018

[39] C.A. Cruz, D.R. Paul, J.W. Barlow. Polyester-polycarbonate blends. IV. Poly(ε-caprolactone). Journal of Applied Polymer Science 1979; 23:589-600.
DOI: 10.1002/app.1979.070230228

[40] Y.S. Chun, J. Park, J.B. Sun, W.N. Kim. Blends of polycarbonate and poly(ε-caprolactone) and the determination of the polymer-polymer interaction parameter of the two polymers. Journal of Polymer Science: Part B: Polymer Physics 2000; 38:2072-2076.
DOI: 10.1002/1099-0488(20000801)38:153.3.CO;2-W

[41] A.A.J. Ketelaars, Y. Papantoniou, K. Nakayama. Analysis of the density and the enthalpy of poly(ε-caprolactone)-polycarbonate blends: Amorphous phase compatibility and the effect of secondary crystallization. Journal of Applied Polymer Science 1997; 66:921-927.
DOI: 10.1002/(SICI)1097-4628(19971031)66:5<921::AID-APP12>3.0.CO;2-Q

[42] J.M. Jonza, R.S. Porter. Bisphenol A polycarbonate/poly(ε-caprolactone) blends: Melting point depression and reactivity. Macromolecules 1986; 19:1946-1951.
DOI: 10.1021/ma00161a028

[43] D. Herrera, J.C. Zamora, A. Bello, M. Grimau, E. Laredo, A.J. Müller, T.P. Lodge. Miscibility and crystallization in polycarbonate/poly(ε-caprolactone) blends: Application of the self-concentration model. Macromolecules 2005; 38:5109-5117.
DOI: 10.1021/ma050481c

[44] Y.W. Cheung, R.S. Stein, B. Chu, G. Wu. Evolution of crystalline structures of poly(ε-caprolactone)/polycarbonate blends. 1. Isothermal crystallization kinetics as

probed by synchrotron small-angle X-ray scattering. Macromolecules 1994; 27:3589-3595.
DOI: 10.1021/ma00091a021

[45] R.J. Young, P.A. Lovell. Introduction to Polymers, 3rd Edition. CRC Press: New York (2011).

[46] B.D. Favis, D. Therrien. Factors influencing structure formation and phase size in an immiscible polymer blend of polycarbonate and polypropylene prepared by twin-screw extrusion. Polymer 1991; 32:1474-1481.
DOI: 10.1016/0032-3861(91)90429-M

[47] K.S. Shih, C.L. Beatty. Blends of polycarbonate and poly(hexamethylene sebacate): II. Effect of molecular weight on compatibility. Polymer Engineering and Science 1987; 27:1530-1541.
DOI: 10.1002/pen.760272008

[48] A. Oyarzabal, A. Cristiano-Tassi, E. Laredo, D. Newman, A. Bello, A. Etxeberría, J.I. Eguiazabal, M. Zubitur, A. Mugica, A.J. Müller. Dielectric, mechanical and transport properties of bisphenol A polycarbonate/graphene nanocomposites prepared by melt blending. Journal of Applied Polymer Science 2017; 134:44654-44667.
DOI: 10.1002/app.44654

[49] B. Greenhoe, M.K. Hassan, J.S. Wiggins, K.A. Mauritz. Universal power law behavior of the AC conductivity versus frequency of agglomerate morphologies in conductive carbon nanotube reinforced epoxy networks. Journal of Polymer Science Part B Polymer Physics 2016; 54:1918-1923.
DOI: 10.1002/polb.24121

[50] B. Belaabed, S. Lamouri, N. Naar, P. Bourson, S.O.S. Hamady. Polyaniline-doped benzene sulfonic acid/epoxy resin composites: Structural, morphological, thermal and dielectric behaviors. Polymer Journal 2010; 42:546-554.
DOI: 10.1038/pj.2010.41

[51] C. Arup. Polyaniline/silver nanocomposites: Dielectric properties and ethanol vapour sensitivity. Sensors and Actuators B: Chemical 2009; 138:318-325.
DOI: 10.1016/j.snb.2009.01.019

[52] K. Saeed, S.Y. Park. Preparation and properties of multiwalled carbon nanotube/ polycaprolactone nanocomposites. Journal of Applied Polymer Science 2007; 104:1957-1963.

DOI: 10.1002/app.25902

[53] P. Pötschke, M. Abdel-Goad, I. Alig, S. Dudkin, D. Lellinger. Rheological and dielectrical characterization of melt mixed polycarbonate-multiwalled carbon nanotube composites. Polymer 2004; 45:8863–8870.
DOI: 10.1016/j.polymer.2004.10.040

[54] B. Fillon, B. Lotz, A. Thierry, J.C. Wittmann. Self-nucleation and enhanced nucleation of polymers. Definition of a convenient calorimetric "efficiency scale" and evaluation of nucleating additives in isotactic polypropylene (α phase). Journal of Polymer Science Part B: Polymer Physics 1993; 31:1395-1405.
DOI: 10.1002/polb.1993.090311014

[55] M. Avrami. Granulation, phase change, and microstructure kinetics of phase change III. Journal of Chemical Physics 1941; 9:177-184.
DOI: 10.1063/1.1750872

[56] G. Reiter, G. R. Strobl. Progress in Understanding Polymer Crystallization, Lecture Notes Physics 714 (Springer, Berlin Heidelberg 2007).
DOI: 10.1007/b11903420

[57] A.T. Lorenzo, A.J. Müller. Estimation of the nucleation and crystal growth contributions to the overall crystallization energy. Journal of Polymer Science: Part B: Polymer Physics 2008; 46:1478-1487.
DOI: 10.1002/polb.21483

[58] R.L. Poveda, N. Gupta. Carbon Nanofiber Reinforced Polymer Composites; SpringerBriefs in Materials; Springer: Brooklyn, NY, USA (2016).

[59] H. Meng, G.X. Sui, P.F. Fang, R. Yang. Effects of acid- and diamine-modified MWNTs on the mechanical properties and crystallization behavior of polyamide 6. Polymer 2008; 49:610–620.
DOI: 10.1016/j.polymer.2007.12.001

CHAPTER 4

Morphology, nucleation, and isothermal crystallization kinetics of poly(butylene succinate) mixed with a polycarbonate/MWCNT masterbatch

---

This chapter has been published as:

Thandi P. Gumede, Adriaan S. Luyt, Ricardo A. Pérez-Camargo, Agnieszka Tercjak, Alejandro J. Müller*. Morphology, nucleation, and isothermal crystallization kinetics of poly(butylene succinate) mixed with a polycarbonate/MWCNTs masterbatch. Polymers 2018; 10:424.*

(DOI: 10.3390/polym10040424)

Author contributions: *Luyt and Müller conceived the project and guided the students, Gumede conceived and performed most of the experiments, Pérez-Camargo was responsible for the SAXS and WAXS analyses and the interpretation of these results, and Tercjak's expertise in AFM analysis helped the authors to correctly visualize the morphology of the investigated system.*

Abstract

In this study, nanocomposites were prepared by melt blending poly(butylene succinate) (PBS) with a polycarbonate (PC)/multi-wall carbon nanotubes (MWCNTs) masterbatch, in a twin-screw extruder. The nanocomposites contained 0.5, 1.0, 2.0, and 4.0 wt% MWCNTs. Differential scanning calorimetry (DSC), small angle X-ray scattering (SAXS) and wide angle X-ray scattering (WAXS) results indicate that the blends are partially miscible, hence they form two phases (i.e., PC-rich and PBS-rich phases). The PC-rich phase contained a small amount of PBS chains that acted as a plasticizer and enabled crystallization of the PC component. In the PBS-rich phase, the amount of the PC chains present gave rise to increases in the glass transition temperature of the PBS phase. The presence of two phases was supported by scanning electron microscopy (SEM) and atomic force microscopy (AFM) analysis, where most MWCNTs aggregated in the PC-rich phase (especially at the high MWCNTs content of 4 wt%) and a small amount of MWCNTs were able to diffuse to the PBS-rich phase. Standard DSC scans showed that the MWCNTs nucleation effects saturated at 0.5 wt% MWCNT content on

the PBS-rich phase, above this content a negative nucleation effect was observed. Isothermal crystallization results indicated that with 0.5% MWCNTs the crystallization rate was accelerated, but further increases in MWCNTs loading (and also in PC content) resulted in progressive decreases in crystallization rate. The results are explained by increased MWCNTs aggregation and reduced diffusion rates of PBS chains, as the masterbatch content in the blends increased.

Keywords: PBS; PC/MWCNTs masterbatch; nanocomposites; morphology; nucleation; conductivity; isothermal crystallization

4.1 Introduction

Recently, environmental pollution and resource crises related to fossil-based polymers have led to the development of biodegradable polymers with similar functionality as petrochemical polymers, but that are readily susceptible to microbial action [1–3]. Aliphatic polyesters are representatives of biodegradable polymers and they are considered to be high performance, environmentally friendly biodegradable plastics [4,5]. One of these aliphatic biodegradable polymers is poly(butylene succinate) (PBS), known under the trade name "Bionolle®". PBS is synthesized through the polycondensation reaction of glycols, such as ethylene glycol and 1,4-butanediol, and aliphatic dicarboxylic acids, such as succinic acid and adipic acid. This biodegradable polymer exhibits physical and mechanical properties closely comparable to those of the widely-used polyethylene (PE) and polypropylene (PP) [1,4,6]. PBS has many interesting properties such as biodegradability, melt processability, and thermal and chemical resistance. It can be processed in the field of textiles through melt blowing, multifilament, monofilament, nonwoven, flat, and split yarn, and also in the field of plastics through injection-molded products. However, other properties of PBS, such as softness, low melt viscosity and strength, as well as weak gas barrier properties, are often not sufficient for its further processing and end-use applications [3,5,7–10].

Incorporation of conductive carbon-based nanofillers, such as carbon nanotubes (CNTs), is an effective approach for improving the properties of PBS, provided that the CNTs are well dispersed in the polymer matrix. It is well known that the as-received CNTs tend to form agglomerates during mixing with polymers due to the strong van der Waals attraction between the carbon nanotubes [11]. In polymer/CNTs nanocomposites,

aggregation of CNTs may become a defect and cause the mechanical properties of the composite to deteriorate. This problem can be overcome by using functionalized carbon nanotubes [12,13], which can provide multiple bonding sites to the polymer matrix so that the load can be transferred to the CNTs and inhibit the separation between the surfaces of the polymer and the CNTs. Another approach is to use a masterbatch, which involves the direct encapsulation of the CNTs into a polymer matrix, and the release of the CNTs to the other component in the nanocomposites that takes place during heating [3,4,14–16].

Several chemical methods have been reported for the functionalization of CNTs, such as (i) the use of *N*,*N*'-dicyclohexylcarbodiimide (DCC) to introduce a long alkyl chain onto multi-walled CNTs (MWCNTs), and (ii) surface wrapping of poly(sodium 4-styrenesulfonate) (PSS) with the aid of ultrasound [3,4]. In these studies, the MWCNTs showed a very low percolation threshold between 0.1 and 0.3 wt% MWCNTs, indicating the formation of conductive pathways in the PBS matrix. This indicates that the MWCNTs were well dispersed in the PBS matrix and showed better interfacial adhesion with the PBS phase than with each other, due to π–π interactions between the benzene rings, and between the long alkyl chain groups and the graphite rings of the MWCNTs.

A commercially available polycarbonate (PC)/MWCNTs masterbatch has been used as a filler and added it to the PC matrix in the subsequent melting process [14,15]. In this case, the MWCNTs were well separated and uniformly distributed in the PC matrix, and the mechanical properties showed significant improvements in the storage modulus in comparison to that of the neat PC matrix. In our previous work [17], PCL was melt blended with a PC/MWCNTs masterbatch, and the results showed partial miscibility, where two phases were formed (PC-rich and PCL-rich phases). Only a small number of MWCNTs diffused from the PC-rich phase to the PCL-rich phase. There was a fair increase in the nucleation efficiency and overall crystallization rate of PCL, as well as the thermal conductivity of the nanocomposite, with increasing MWCNTs content, but the tensile properties reduced or showed little change. Amongst the different methods used for dispersing MWCNTs, the masterbatch approach is the most favoured method, because it involves a solvent-less procedure that is beneficial in preserving the environment. The masterbatch method using PC as the main component could be useful in the dispersion of multi-walled carbon nanotubes in a PBS matrix, although there is currently no published information on PBS/PC blends, as far as the authors are aware.

In spite of the lack of information related to PBS/PC blends, it is known that PBS has a biodegradable character and the use of CO_2 as one of the monomers in the preparation of polycarbonates would not only partially get rid of the dependence on petroleum but also provide a new approach in reducing the massive emission of CO_2, which contributes to the greenhouse effect [18]. Therefore, the PBS/PC blends represent an interesting approach, and it is expected that such blends in combination with MWCNTs might lead to the development of interesting materials.

In this paper, MWCNTs were dispersed into a PBS matrix by melt-mixing PBS with a PC/MWCNTs masterbatch. The structure and properties of the nanocomposites were correlated with the dispersion, morphology, and nucleating effect of the MWCNTs on the PBS matrix. Additionally, the efficiency of the nucleation and the crystallization kinetics of the PBS component were determined by self-nucleation and isothermal crystallization studies.

4.2 Experimental

4.2.1 Materials

A commercial poly(1,4-butylene succinate) (PBS), extended with 1,6-diisocyanatohexane, was purchased from Sigma-Aldrich (Johannesburg, South Africa). It has a density of 1.3 g cm^{-3} at 25 °C and a melting temperature of 120 °C. The weight-average molecular weight (M_w) of PBS was 63,000 g mol^{-1} [19].

A conductive masterbatch based on 85% low-viscosity polycarbonate (Makrolon® 2205 grade, M_w of 20,100 g·mol^{-1} [20]) loaded with 15 wt% of MWCNTs (industrial grade NC7000), was obtained from Nanocyl (Sambreville, Belgium). It has a density of 1.175 g cm^{-3}. The average diameter and length of the MWCNTs were respectively 10 nm and 3–4 µm. The MWCNTs contained more than 90% carbon and less than 10% metal oxide impurities.

The nanocomposites were prepared by melt-mixing in a twin-screw extruder (Thermo Scientific HAAKE Mini Lab II (Thermo Fischer Scientific, Waltham, MA, USA) at the University of Pretoria, South Africa) operated under compressed air (100 rpm, 160 °C, 10 min). After extrusion, the samples were compression-moulded at 160 °C for 5 min under 50 kPa using a hydraulic melt press. The calculated weight percentages

of the different components in each of the investigated nanocomposites are given in Table 4.1.

Table 4.1 Weight percentages of the components in the nanocomposites.

PBS (wt%)	PC (wt%)	MWCNTs (wt%)
100	0	0
97	2.55	0.45
93	5.95	1.05
87	11.05	1.95
73	22.95	4.05

4.2.2 Sample characterization

Scanning electron microscopy (SEM) analyses were performed using a TESCAN VEGA 3 (Brno, Czech Republic) scanning electron microscope. The samples were sputter-coated with gold for 60 s to produce conductive coatings onto the samples. The acceleration voltage used was 15 kV.

Atomic force microscopy (AFM) experiments were performed for the 93/(6/1) and 73/(23/4) *w*/*w* PBS/(PC/MWCNTs) samples at room temperature using a Bruker Multimode 8 scanning probe microscope equipped with a Nanoscope V controller. The micrographs, the sizes of which were in the range of 1.0–14.1 μm, were obtained in tapping mode by using microfabricated silicon tips/cantilevers (cantilever spring constant, k = 42 N m^{-1}, and resonance frequency, f_0 = 320 kHz, Bruker, Santa Barbara, CA, USA). Height and phase AFM images of lamellae and MWCNTs were collected simultaneously and subjected to a first-order plane-fitting procedure to compensate for the tilt. The height and phase AFM images were similar, and consequently in this work only the phase AFM images will be reported. To obtain cross-sectional AFM images, the samples were cut using an ultramicrotome Leica Ultracut R with a diamond blade.

Simultaneous small-angle X-ray scattering (SAXS) and wide-angle X-ray scattering (WAXS) experiments were performed at the beamline BL11-NCD, ALBA Synchrotron facility in Barcelona, Spain. Each sample was placed in a DSC pan, and was put on a Linkam THMS600 (Linkam Scientific Instruments, Tadworth, Surrey, UK) hot stage coupled to a liquid nitrogen cooling system. The hot stage was programmed to perform cooling and subsequent heating and at the same time measurements of the

SAXS/WAXS patterns were taken. The thermal protocol was as follows: heating from room temperature to 180 °C, followed by a holding step of 3 min. Once the thermal history was erased, the samples were cooled down at 50 °C min^{-1} to the selected isothermal temperature. Different isothermal times were used depending on the temperature. Finally, after the isothermal step, the samples were heated at a rate of 5 °C min^{-1}. The energy of the X-ray source was 12.4 keV (λ = 1.0 Å). In the SAXS configuration, the sample-detector used was an ADSC Q315r detector with a resolution of 3070 × 3070 pixels, a pixel size of 102 μm^2, and a distance of 6495.0 mm with a tilt angle of 0°, whereas in the WAXS configuration, the sample-detector was a Rayonix LX255-HS detector (Rayonix, Evanston, IL, USA) with a resolution of 1920 × 5760 pixels, a pixel size of 44 μm^2, and a distance of 132.6 mm with a tilt angle of 21.2°. The intensity profile showed the plot of the scattering intensity as a function of the scattering vector, $q = 4\pi\, sin\theta\, \lambda^{-1}$, where λ is the X-ray wavelength (λ = 1.0 Å) and 2θ is the scattering vector. The scattering vector was calibrated using silver behenate (SAXS) and chromium (III) oxide (WAXS).

Differential scanning calorimetry (DSC) analyses were performed using a heat flux Perkin Elmer DSC 6000 (Akron, OH, USA) under nitrogen flow (flow rate 20 mL min^{-1}) to minimize degradation of the samples, and the instrument was calibrated at a heating rate of 20 °C min^{-1} using the onset temperatures of melting of indium and zinc standards, and the melting enthalpy of indium. The sample weight was ~5 mg in all cases.

For the non-isothermal DSC analyses, the samples were melted in the DSC for 3 min at 270 °C to erase any previous thermal history. The samples were then cooled at 20 °C min^{-1} from 270 to −20 °C, and then heated at the same rate from −20 to 270 °C.

The self-nucleation (SN) tests were performed according to a procedure established by Fillon *et al*. [21], and further developed and studied by Müller *et al*. [22–24]. The complete procedure is as follows:

(a) The sample was heated from 25 to 270 °C at 20 °C min^{-1} and maintained at that temperature for 3 min to erase thermal history.
(b) It was then cooled from 270 to −20 °C at 20 °C min^{-1} to create the initial “standard” state, and held at that temperature for 3 min.
(c) It was then heated from −20 °C to a selected self-nucleation temperature (T_s), located in the final melting temperature range of the sample, and held at that temperature for 5 min.

(d) It was again cooled to −20 °C, where the effects of thermal treatment are reflected in the crystallization behaviour of the sample.
(e) Finally, it was heated to 270 °C, where the effects of thermal treatment are reflected in the melting behaviour of the sample.

The most important parameters during SN are: (1) the heating and cooling rates used, (2) the T_s temperature, and (3) the time spent at T_s.

The isothermal crystallization experiments were performed by following the procedure recommended by Lorenzo *et al*. [25], in which isothermal crystallization temperatures (T_c) are chosen where no crystallization occurred during the cooling step from the melt (performed at 60 °C min^{-1}). The samples were heated to 270 °C and kept at this temperature for 3 min to erase the thermal history. Then a controlled cooling at 60 °C min^{-1} was applied, down to the set isothermal T_c. The sample was then kept at the set T_c for a crystallization time (t_c) until saturation was reached. Finally, the sample was heated from T_c to 270 °C at 20 °C min^{-1}, to record the melting behaviour of the isothermally crystallized sample.

To determine the equilibrium melting temperatures, T_m^o, of the samples, the final step in the isothermal crystallization procedure (i.e., heating at 20 °C min^{-1}), was used to record the melting of the crystals formed at different crystallization temperatures, T_c. Hoffman–Weeks extrapolation [26] was then applied by plotting the observed melting temperature ($T_{m(obs)}$) against T_c to observe the intersection of this line with another line with a slope equal to 1 ($T_m = T_c$), which represents the thermodynamic equilibrium.

Dynamic mechanical analyses (DMA) were performed in a Perkin Elmer Diamond DMA (Akron, OH, USA) from −100 °C to the onset of melting of PBS, which is ~100 °C, in the bending (dual cantilever) mode at a heating rate of 3 °C min^{-1} and a frequency of 1 Hz.

The tensile analysis of the samples was carried out using an Instron 4301 universal testing machine (Instron, Norwood, MA, USA) at a cross-head speed of 10 mm min^{-1}. The dumbbell shaped samples had a Gauge length of 20 mm, a thickness of 1 mm and a width of 5 mm. The samples were tested at a controlled ambient temperature of 23 °C and 50% relative humidity. Three samples of each composition were tested and average values with standard deviations are presented.

Thermal conductivity measurements were performed using a Therm Test Inc. Hot Disk TPS 500 thermal constant analyser (Fredericton, NB, Canada). The instrument uses

the transient plane source method. A 3.2 mm radius Kapton disk type sensor was selected for the analysis. The sample discs were 5 mm thick and 12 mm in diameter. The sensor was placed between two sample discs of the same composition. The measurements were made for a period of 25 s in order to prevent the heat flow from reaching the boundary of the samples. Five measurements were performed for each composition. The thermal conductivities are reported as average values with standard deviations.

4.3 Results and discussion

4.3.1 Miscibility assessment

The glass transition temperature (T_g) is used to determine the interaction between the components of a polymer blend. The blend is considered completely miscible if only one T_g is observed with its position determined by the composition of the blend. Two distinct T_gs symbolize an immiscible blend with the T_gs corresponding to those of the two-parent homopolymers. However, when the two polymers are partially miscible, there are still two T_gs that will be shifted towards each other, with the degree of shift being dependent on both blend composition and degree of miscibility [27].

In the present study, the T_g of the PC component in the nanocomposites could not be detected through either DSC or DMA because (i) PBS, the major component in the blends, melted at a temperature below the T_g of PC (DMA analyses cannot be performed at temperatures above the T_m of PBS), and (ii) PC, the minor component in the blends, crystallized around 180 °C, as can be seen from the melting and crystallization peaks in Figure 4.1. Since the PC crystallized, its T_g was difficult to observe by DSC, as the amount of mobile amorphous fraction per unit mass was smaller in the blends.

The crystallization of the PC component was also confirmed by simultaneous SAXS/WAXS analyses for the 93/(6/1) and 73/(23/4) *w*/*w* PBS/(PC/MWCNTs) nanocomposites. Figure 4.2 shows the final X-ray patterns taken at a selected isothermal crystallization temperature of 90.5 °C. The main WAXS reflections shown by neat PBS are visible in the X-ray patterns of the nanocomposites. The main reflection peaks of PBS are located at q values of 13.9 and 16.0 nm^{-1}, and correspond to the (002) and (110) planes, respectively. The medium intense reflection at 15.5 nm^{-1}, which corresponds to the (012) plane, as well as the minor reflections at 18.4 and 20.4 nm^{-1}, which correspond to the (121) and (111) planes, also appear in all the samples. All the reflections are

consistent with the reported monoclinic unit cell of α-PBS with unit cell parameters a = 5.232, b = 9.057 and c = 10.900 Å and γ = 123.87°.

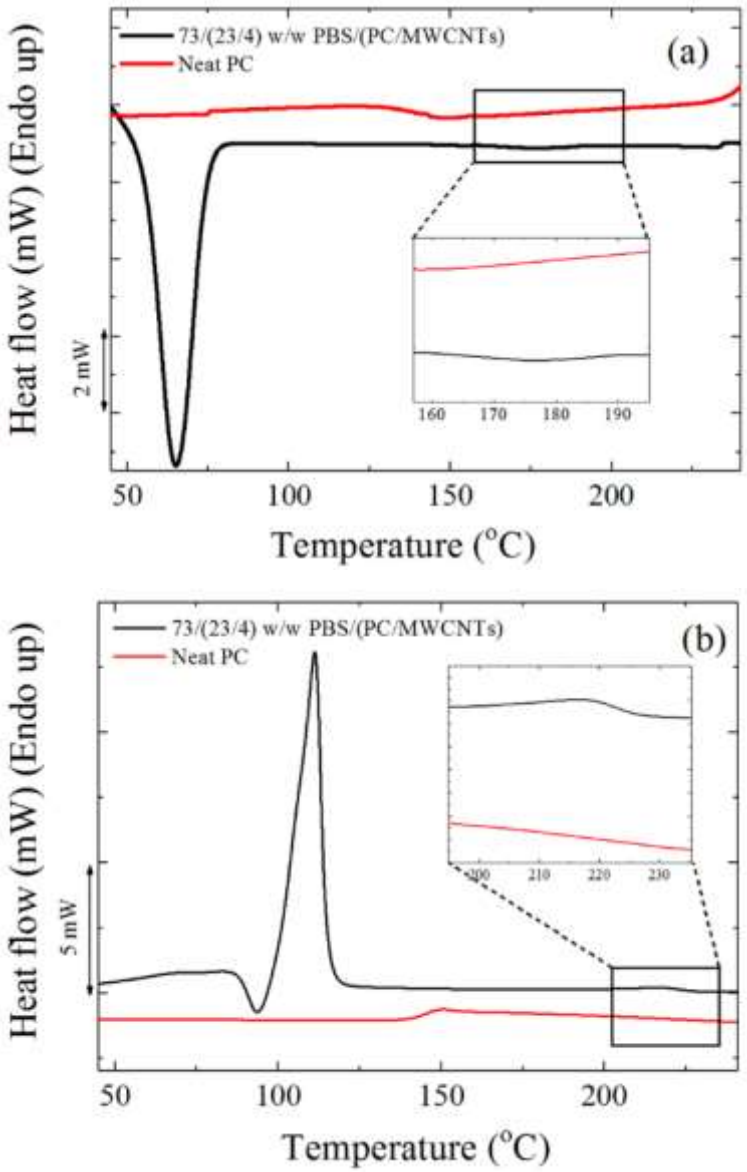

Figure 4.1 DSC (a) cooling and (b) second heating curves for neat polycarbonate (PC) and the 73/(23/4) *w*/*w* PBS/(PC/MWCNTs) nanocomposite. The zoomed regions correspond to the crystallization (see (a)) and melting (see (b)) of PC in the nanocomposites and its absence in the neat PC.

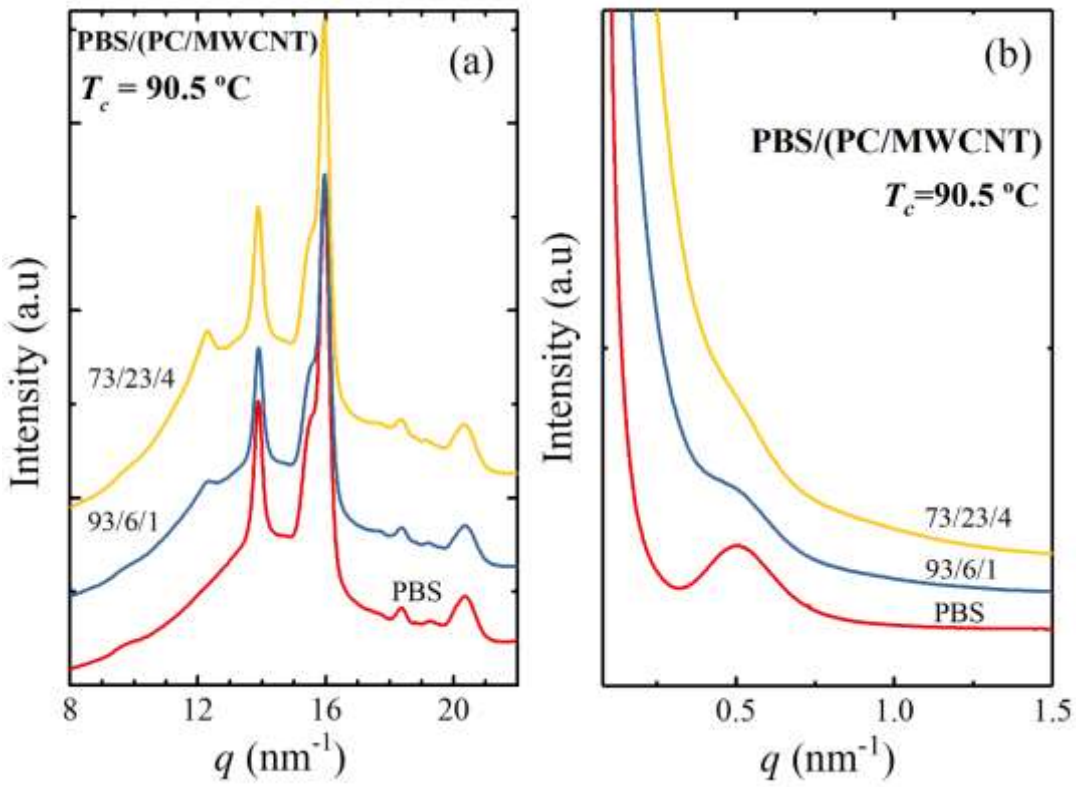

Figure 4.2 (a) WAXS diffractograms taken at a selected isothermal temperature of 90.5 °C; (b) SAXS patterns taken at the same temperature.

In addition to the PBS unit cell peaks, there is a peak at 12.3 nm^{-1} (equivalent to a 2θ of 17.4°), which appears in the nanocomposites and becomes more pronounced as the PC content in the nanocomposites increases. This peak corresponds to the PC component that is able to crystallize due to the plasticization effect of the PBS (see Figure 4.3). The same effect was observed in our previous work of PCL/(PC/MWCNT) nanocomposites at high PC contents [17]. Note that such a plasticization effect evidences the partial miscibility between the PBS and PC. Figure 4.2(b) shows the SAXS patterns taken at the same condition used in the WAXS experiments. In these patterns, the PBS signal observed for neat PBS decreased as the PC content increased, since the single peak corresponds mainly to the long spacing of PBS lamellae. However, at higher PC contents (i.e., 23 wt%), the PC is able to crystallize due to the plasticization effect of the PBS, and the SAXS signal is not clear due to the overlap of the long spacings generated by the lamellae of PBS and PC. The signal observed is probably an average of these two long spacings and is shifted to lower q values.

For the sake of clarity, the WAXS patterns were taken during heating after the isothermal step for some selected samples. Figure 4.3 shows that the PC peak does not disappear when the PBS is already molten at T > 116 °C. This behaviour is clearly observed at the higher PC content (Figure 4.3(c)). According to our results and the literature [28,29], PC is able to crystallize, as mentioned earlier in the discussion, due to the plasticization effect of PBS. As a result, it shows a main reflection at 2θ = 17.1° (12.34 nm^{-1}). This capability of plasticization is an evidence of partial miscibility. This PC peak is in line with the one reported in our previous work of the PCL/(PC/MWCNTs) nanocomposite, in which the PCL also acted as a plasticizer for PC [17].

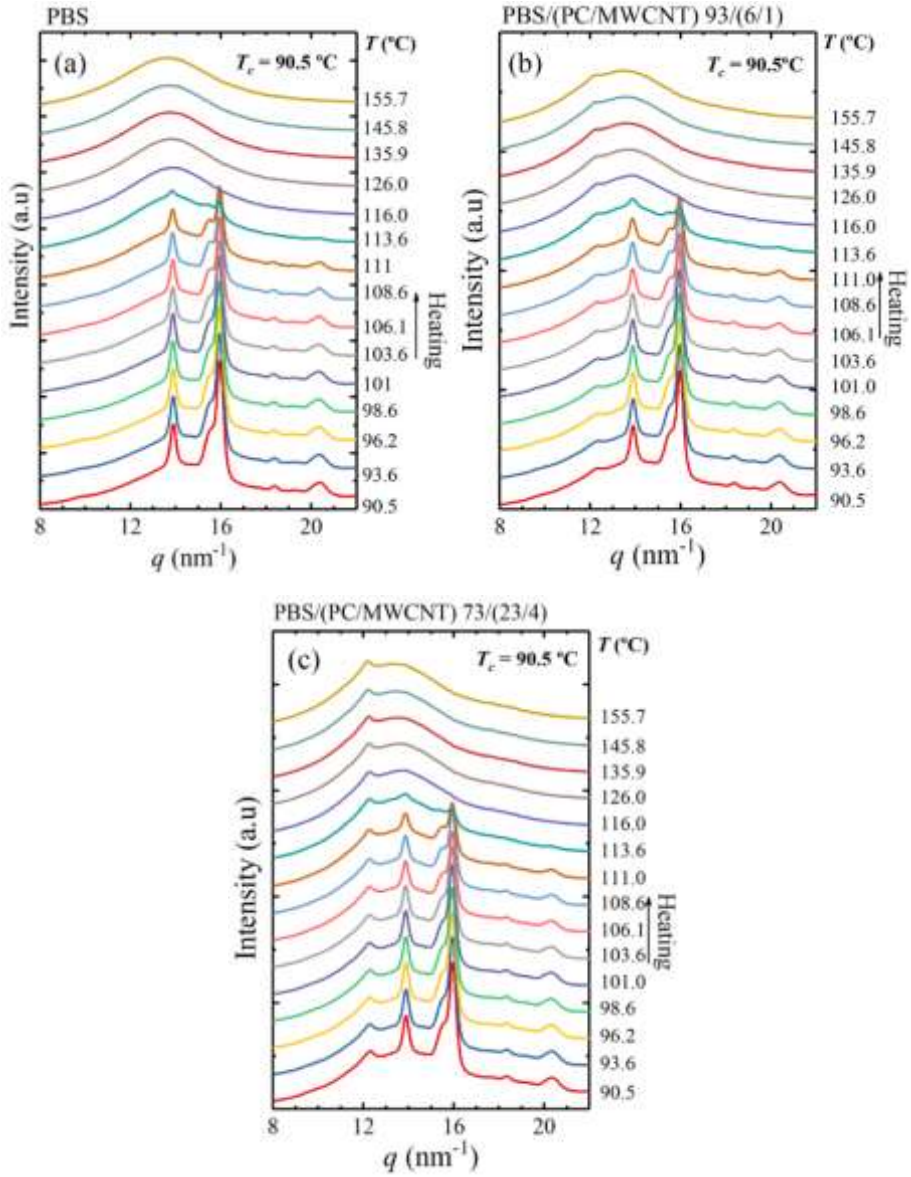

Figure 4.3 WAXS patterns taken during heating at 5 °C min^{-1} after the isothermal step at 90.5 °C for (a) neat PBS, (b) PBS/(PC/MWCNTs) (93/6/1), and (c) PB/(PC/MWCNTs) (73/23/4).

The *d*-spacings for all the reflections shown in Figure 4.2a were calculated from Equation (4.1). The long periods were calculated from the main PBS peaks in the SAXS patterns in Figure 4.2b. The relevant values are tabulated in Table 4.2.

$$d^* = \frac{2\pi}{q_{max}} \tag{4.2}$$

Table 4.2 Calculated values of *d*-spacing (from WAXS experiments) and long period (*d, obtained from SAXS experiments) for the neat PBS and its nanocomposites.**

Sample	q (nm^{-1})/*d*-spacing (nm)/(plane)	*d** (nm)
Neat PBS	13.88/0.426/(002) 15.54/0.381/(012) 15.96/0.371/(110) 18.38/0.322/(121) 20.36/0.291/(111)	12.3
93/(6/1) *w*/*w* PBS/(PC/MWCNTs)	13.90/0.426/(002) 15.52/0.381/(012) 15.97/0.371/(110) 18.35/0.323/(12-1) 20.42/0.291/(111) 12.34/0.479 *	11.9 **
73/(23/4) *w*/*w* PBS/(PC/MWCNTs)	13.88/0.426/(002) 15.55/0.381/(012) 15.95/0.371/(110) 18.34/0.323/(121) 20.36/0.291/(111) 12.30/0.481 *	8.3 **

* PC signal; ** overlap of PC and PBS signals.

The *d*-spacings and the *d** values of neat PBS and the PBS in the nanocomposites are almost the same at low PC contents (i.e., 6 wt%). In the case of the 73/(23/4) *w*/*w* PBS/(PC/MWCNTs) nanocomposite, the peak related to the PC component is the same as the one reported in the literature (0.464 nm) [28]. In the SAXS patterns, an overlap between the long spacings of PC and PBS occurs and this explains the decrease in *d** values compared to those for the other samples.

Figure 4.4 shows the loss modulus (*E"*) and tan δ curves for neat PBS and PBS in the different nanocomposites. The T_g values obtained from the loss modulus and tan δ curves are slightly different for the same sample, with $T_{g,E"} < T_{g,tan\ \delta}$ (Figure 4.5), as expected [15,30,31]. The trends from the different sets of results are, however, the same.

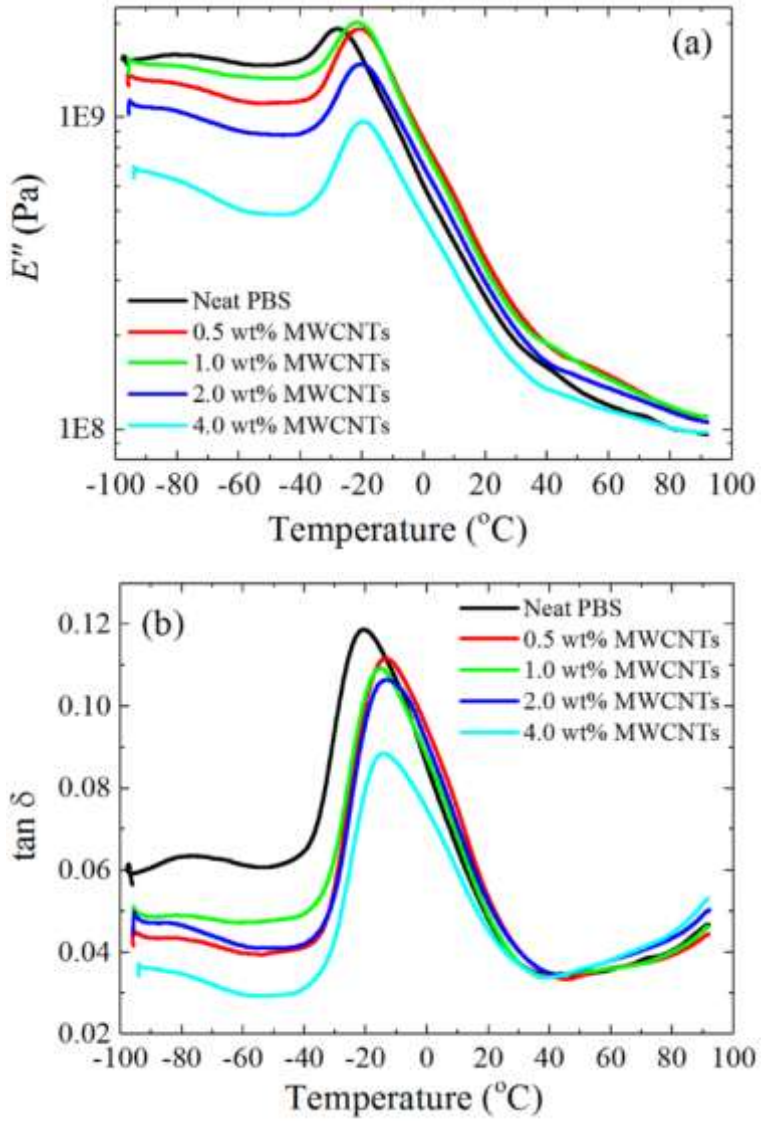

Figure 4.4 DMA (a) loss modulus (*E"*) and (b) tan δ curves for the investigated samples.

The results show that the T_g of PBS in the nanocomposites is higher than that of neat PBS. It is well known that when two polymers are completely miscible, the T_gs of the two polymers should change according to the trend predicted by the Fox equation (Equation (4.2)).

$$\frac{1}{T_g} = \frac{w_1}{T_{g1}} + \frac{w_2}{T_{g2}} \tag{4.3}$$

where T_g is the blend glass transition temperature, and T_{gi} and w_i are the respective glass transitions and weight fractions of the two blend components.

Figure 4.5 shows how the T_g values change with composition. The T_g increases (about 10 °C) upon addition of (6/1) *w*/*w* PC/CNTs, and then stays constant. The Fox equation only fits the change in T_g for the sample with the lowest content of PC (i.e., 6%). One possible explanation for the observed increase in T_g is that the MWCNTs imposed restrictions on the molecular mobility of PBS [32]. However, since the T_g does not change with increasing masterbatch content, this possibility can be ruled out.

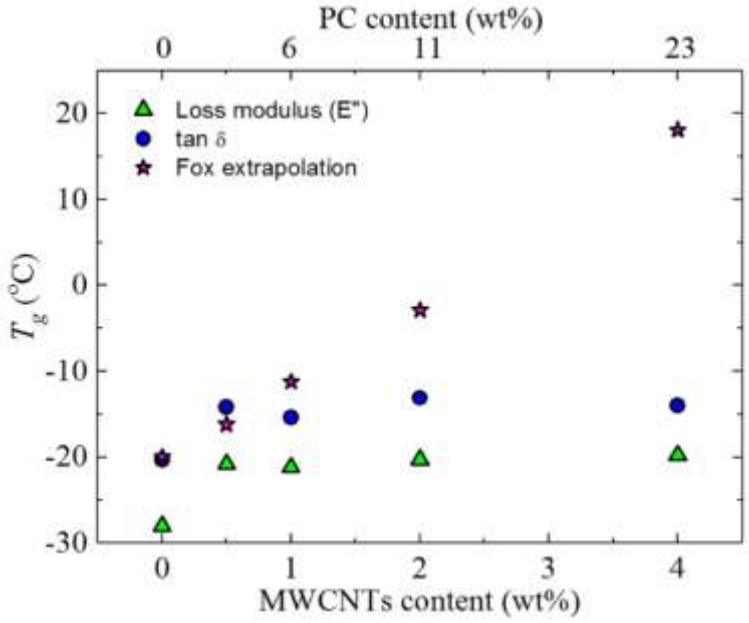

Figure 4.5 Glass transition temperatures of neat PBS and the PBS/(PC/MWCNTs) nanocomposites as a function of MWCNTs content (the corresponding PC content is indicated in the top x-axis). The Fox extrapolation T_g data was obtained using the *tan δ* values.

On the other hand, partial miscibility between PC and PBS can explain the T_g increase upon 6% PC addition, as a PBS-rich phase develops. The lack of variation of T_g with further increases in PC content may be related to a saturation effect of the amount of PC that can be dissolved in the PBS phase. Additionally, as in the PCL/(PC/MWCNTs) masterbatch case [17], the plasticization of PC by PBS led to PC crystallization. This, and the fact that the PBS melts at a temperature well below the T_g of PC, made it difficult to observe the PC glass transition. Based on the presented data, we conclude that the blends are partially miscible and contain both PC-rich and PBS-rich phases in the limited composition range explored in this work (from 6 to 23% PC content).

4.3.2 Morphology

SEM and AFM images for the 97/(2.5/0.5) and 73/(23/4) *w*/*w* PBS/(PC/MWCNTs) nanocomposites were obtained to confirm the presence of two phases (PBS-rich and PC-rich phases), and to observe whether MWCNTs diffused into the PBS phase.

It can be seen at low magnifications (Figure 4.6a,d) that there exists an interphase between the PBS-rich and the PC-rich phases, and that there are large ellipsoidal phases dispersed in the polymer matrix. The size of the dispersed phase (which corresponds to the PC-rich phase) is unexpectedly large considering the amount of the PC that has been added to the blends (i.e., 2.5 and 23 wt% for each blend examined in Figure 4.6), indicating a macro-phase segregation in the blends. In our previous work of PCL/(PC/MWCNTs) nanocomposites, the size of the dispersed phase was small, hence some of the MWCNTs were able to diffuse from the PC-rich phase to the PCL-rich phase [17]. In this case, the MWCNTs are mostly restricted within the ellipsoidal PC-rich phases. However, there are a certain number of nanotubes that can be observed in the PBS-rich phase (especially for the 0.5 wt% MWCNTs nanocomposite), when the micrographs are analysed in detail. Due to the limited miscibility between PC and PBS, only a small fraction of MWCNTs were able to migrate from the PC-rich phase to the PBS phase. The DSC results (to be presented below) also show nucleating effects of MWCNTs on the PBS-rich phase, which are present in the samples with low MWCNTs content. At higher contents, i.e., 4% MWCNTs, the nucleation effect disappears, most probably as a result of MWCNTs agglomeration.

Further evidence for partial miscibility that can be observed in Figure 4.6, is the nature of the interphase between the PBS-rich and the PC-rich phases. There are no voids

in between the phases (like in immiscible blends), but rather a smooth concentration gradient.

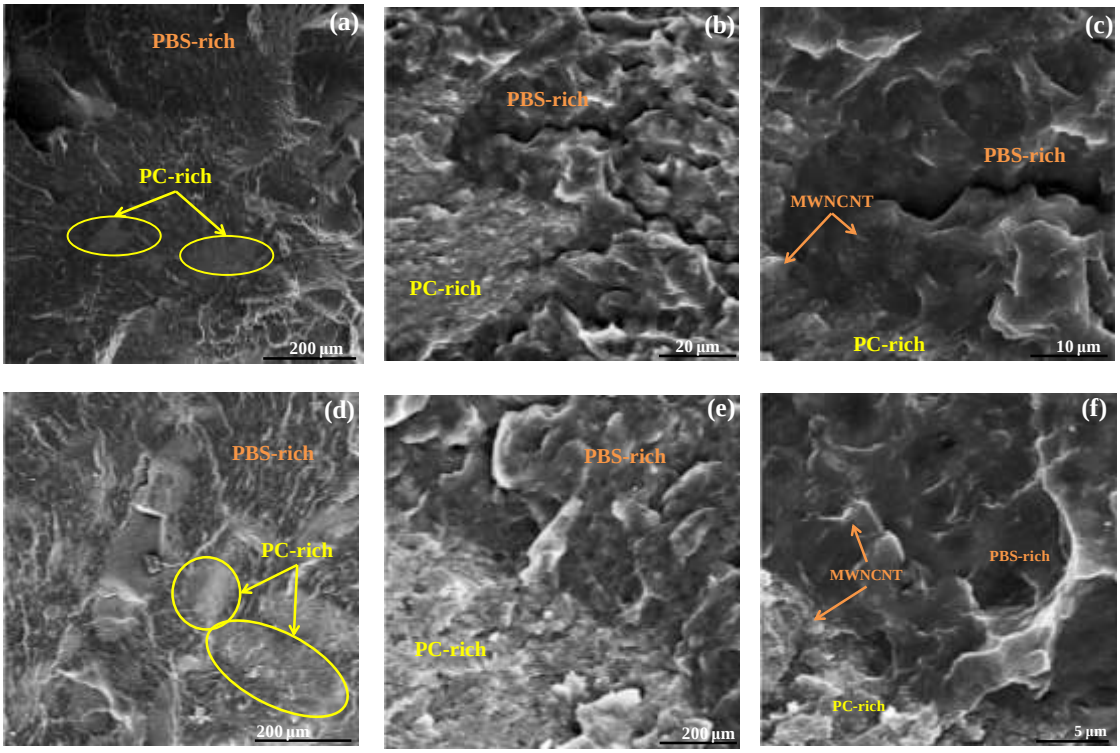

Figure 4.6 (a,d) Low and (b,c,e,f) high magnification SEM micrographs for the 97/(2.5/0.5) and 73/(23/4) *w/w* PBS/(PC/MWCNTs) nanocomposites. The yellow ellipses (see (a,d)) indicated the PC-rich phase. Figure 4.6b,e correspond to the interphase, whereas in c and f the PBS- and PC-rich phases as well as the position of MWCNTs in these phases are indicated.

Figure 4.7 shows AFM phase images for the 1 wt% MWCNT nanocomposite at different magnifications. Similar to the SEM results, the low-magnification AFM image allows one to distinguish both PBS-rich and PC-rich phases (Figure 4.7a). To facilitate the recognition of both phases, the PC-rich phase is marked with a yellow ellipse. Moreover, as can be clearly seen at higher magnifications (Figure 4.7b), there exists a clear interphase between the PBS-rich matrix and the PC/MWCNTs masterbatch. The interphase reveals an intimate contact between the two phases, which is probably a consequence of the partial miscibility between the two polymers in the blends. Higher magnification (Figure 4.7b) images also indicate the presence of MWCNT not only in the PC/MWCNTs masterbatch phase, but also in the PBS-rich matrix. At higher magnifications, single MWCNTs are clearly visible in the PBS-rich matrix in the AFM phase image of the PBS-rich phase (Figure 4.7c).

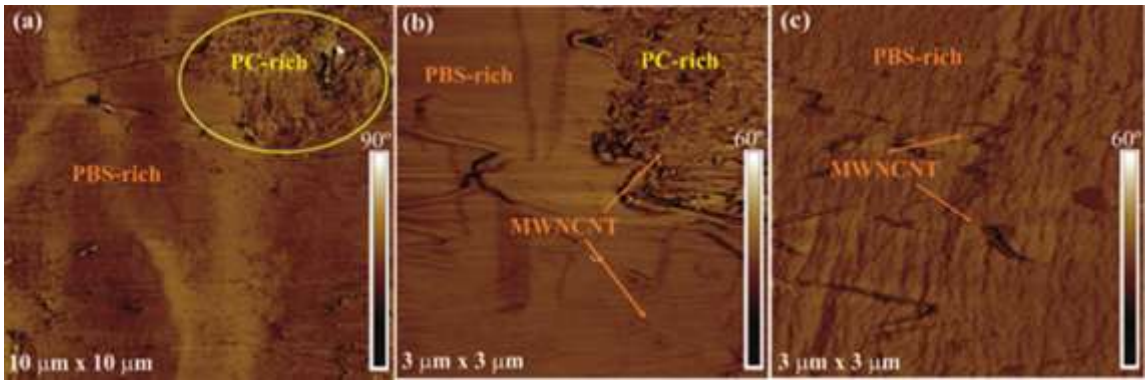

Figure 4.7 (a) Low and (b) high magnification AFM phase images for the 93/(6/1) *w*/*w* PBS/(PC/MWCNTs) nanocomposite, and high magnification AFM phase image of the PBS-rich matrix (c). The yellow ellipses (see (a)) indicate the PC-rich phase.

4.3.3 Non-isothermal DSC

Figure 4.8 shows the DSC (a) cooling scans after erasing the thermal history, and (b) the subsequent heating scans performed at 20 °C min^{-1} for the different investigated samples. All the investigated samples display a PBS-crystallization peak temperature (T_c) around 60–75 °C (Figure 4.8a). In the subsequent heating scans shown in Figure 4.8b, neat PBS and the nanocomposites display a melting peak (T_m) between 110 and 120 °C, and the melting peak is preceded by a cold crystallization peak at around 95 °C. This peak has been previously attributed to the recrystallization of partially melted thin lamellae of PBS [33].

To further examine the results presented in Figure 4.8, the T_c and T_m values were plotted as a function of MWCNTs as well as PC content in Figure 4.9. The T_c of the PBS in the nanocomposites is higher than that of neat PBS up to 2 wt% MWCNTs, and the nucleation effect of the MWCNTs is a maximum for the 0.5% MWCNTs composition. The MWCNTs diffusion to the PBS-rich phase should be most effective in this case because of the almost complete miscibility with the PC phase at this composition. At higher concentrations, there is a decrease in the nucleation effect as indicated by the decrease in T_c values. This is probably due to the MWCNTs aggregation in the PC-rich phase, which restricted the MWCNTs from diffusing into the PBS-rich phase and participating in nucleating PBS. At a concentration of 4% MWCNTs, an antinucleation effect appears, which can only be attributed to the migration of active nucleating heterogeneities from the PBS-rich phase to the PC-rich phase. At a composition of 4%

MWCNTs, the migration of MWCNTs to the PBS-rich phase did not occur, probably because of the higher amount of PC in the blend.

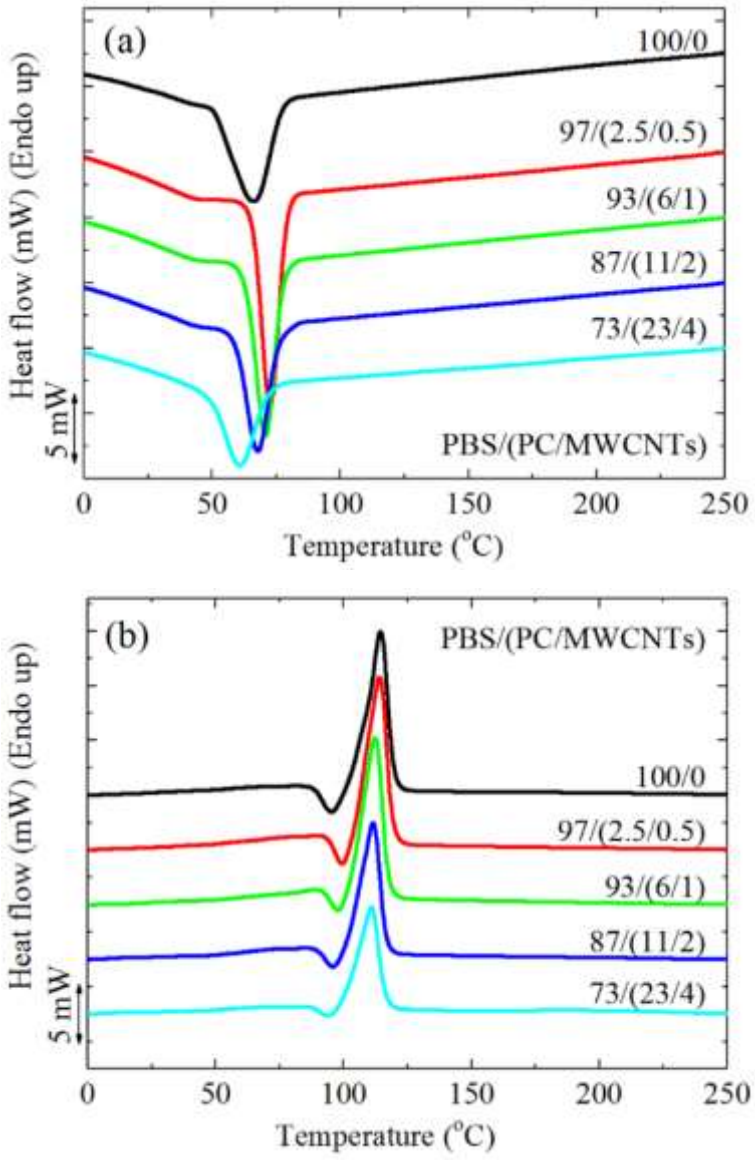

Figure 4.8 DSC (a) cooling and (b) second heating curves at 20 °C min^{-1} of neat PBS and the PBS/(PC/MWCNTs) nanocomposites.

A melting point depression is observed for the PBS component with an increase in the masterbatch content (Figure 4.9), which would have been caused by the partial miscibility with the PC chains in the blend, in combination with the drop in T_c values caused by the nucleation changes. The nucleating ability of the MWCNTs is quantified in the next section through self-nucleation experiments.

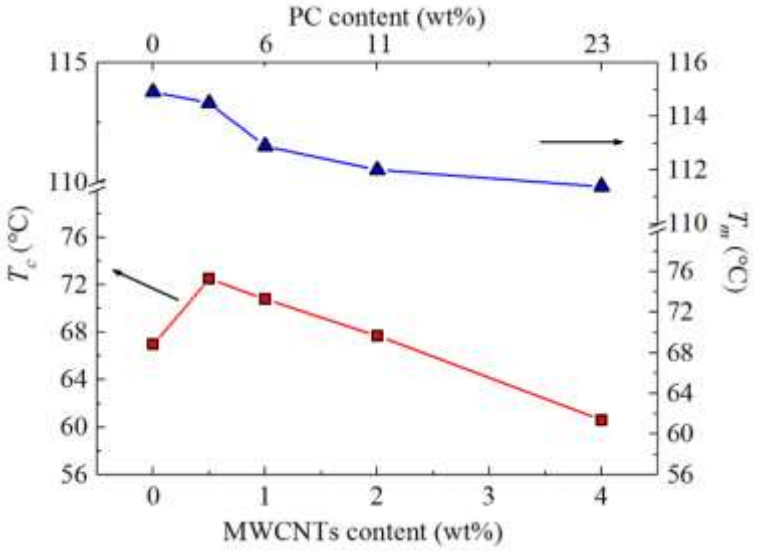

Figure 4.9 DSC crystallization and second heating melting temperatures as a function of MWCNTs content for neat PBS and the PBS/(PC/MWCNTs) nanocomposites (note that the PC content is indicated at the top x-axis).

4.3.4 Self-nucleation (SN)

Carbon nanotubes have been reported to act as nucleating agents for PBS [3,4,8,10,34,35], but their nucleating ability depends on the interaction between the polymer and the MWCNT surfaces. The maximum shift in T_c reported in previous works for functionalized CNTs acting as nucleating agents was around 5 °C [3,8].

To evaluate the efficiency of the MWCNTs as nucleating agents, it is necessary to compare their effect with that of the PBS self-nuclei. Self-nucleation is a thermal protocol for the production of self-nuclei within a polymer melt, so that the nucleation density can be greatly increased. In theory, the best nucleating agent for any polymer is its own crystal fragments or chain segments with residual crystal memories [21–24]. The self-nucleation of PBS has already been studied and reported in the literature but for a different sample [36]. In the present work, a commercial PBS was used, and the self-nucleation experiments and their results are reported in the Supplementary Information (Figures B.1 and B.2).

$$NE = \frac{T_{c,NA} - T_{c,PBS}}{T_{c,max} - T_{c,PBS}} \times 100 \quad (4.4)$$

The efficiency of the MWCNTs as nucleating agents for the PBS matrix was calculated according to Equation (4.3), which was proposed by Fillon *et al*. [37].
where $T_{c,NA}$ is the peak T_c value determined from the non-isothermal DSC cooling run for a sample of the polymer containing the nucleating agent (NA), $T_{c,PBS}$ is the peak T_c value for neat PBS after its crystalline history has been erased (67.0 °C) (also determined from the non-isothermal DSC cooling scan), and $T_{c,max}$ is the maximum peak crystallization temperature determined after neat PBS has been self-nucleated at the ideal T_s (89.3 °C, see the Supplementary Information for details on how to determine the ideal T_s value.) [23,37]. Figure 4.10 shows the percentage nucleation efficiency of MWCNTs in the PBS/(PC/MWCNTs) nanocomposites.

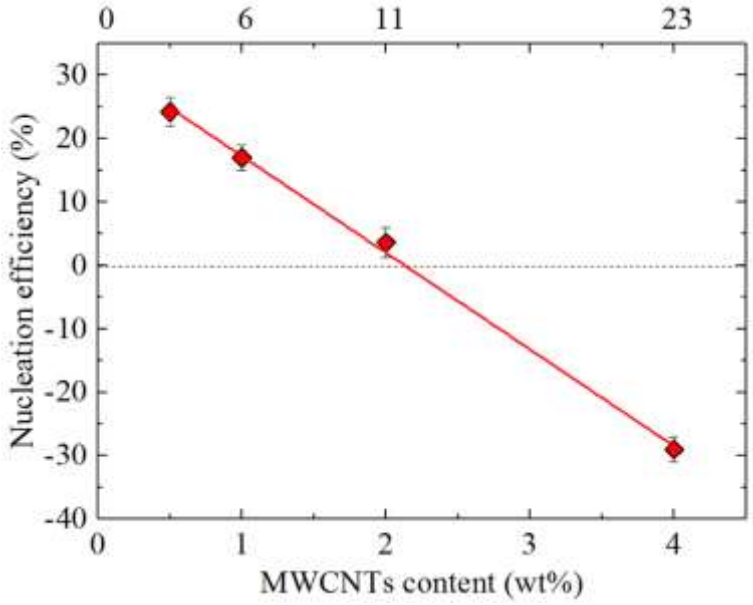

Figure 4.10 Nucleation efficiency as a function of MWCNTs content. The PC content is indicated in the top x-axis.

It is observed in Figure 4.10 that the nucleation efficiency decreases with increasing MWCNTs content. This is consistent with Figure 4.9. At the highest MWCNTs content (i.e., 4 wt%), the nucleation efficiency is below 0%. This behaviour is unexpected, since negative nucleation efficiencies (i.e., antinucleation effect) have been reported to be primarily due to interactions between the polymer matrix and the nucleating agent, e.g., C-PCL/MWCNT-*g*-L-PCL [38], polylactide grafted cellulose nanocrystals (CNC-*g*-

PLA) and poly(β-hydroxybutyrate) (PHB) [39], and PCL-*grafted*-lignin (with high lignin contents) system [40]. Generally, such interactions make the diffusion of the polymer matrix difficult. Some of these interactions are hydrogen bonding and threading effects, and it was also reported that the surface modified CNC particles retarded the heterogeneous nucleation of PHB crystals by restraining the relaxation of the neighbouring PHB chain segments.

In the work reported in this paper, there was no group in either the PBS matrix or the masterbatch that could cause similar interactions. Two possible reasons for this behaviour are therefore: (1) the MWCNT aggregation or (2) its encapsulation in the carrying polymer (i.e., the PC used in the masterbatch), which might lead to the saturation of the system, or to no or little contact between the MWCNTs and the PBS. In both cases, the expected behaviour is a nucleation efficiency equal to zero.

The significant decrease in the nucleation efficiency can only be explained by a complex behaviour in which a migration of heterogeneities from the PBS matrix to the PC in the masterbatch occurs, assisted by the previously reported plasticization effect (see Section 4.3.1). The MWCNTs are then confined to the PC, due to its crystallization, preventing the MWCNTs diffusion to the PBS matrix. Therefore, the PBS matrix has neither all the heterogeneities nor the MWCNTs, and as a result both its crystallization temperature as well as its crystallization kinetics decrease (see Section 4.3.5).

4.3.5 Overall isothermal crystallization studied by DSC

The combined effect of MWCNTs and PC at different contents on the isothermal crystallization kinetics of PBS is presented in this section. Figure 4.11 shows the inverse of the half crystallization time ($1/\tau_{50\%}$), which is an experimental measure of the overall crystallization rate, as a function of the isothermal crystallization temperature (T_c) for neat PBS and the nanocomposites. The results are a complex function of the nucleation efficiency of MWCNTs (which depends on the composition as demonstrated in Figures 4.9 and 4.10) and the partial miscibility with PC in the blends.

Figure 4.11 shows that the nucleation effect of the 0.5% MWCNTs can impact on the overall crystallization kinetics (which includes both nucleation and growth), accelerating it despite the higher T_g of the PBS-rich phase compared to that of neat PBS. For this composition, the nucleation effect can dominate the behaviour because of a possible depression in crystal growth which is a result of the reduced diffusion of the PBS

chains within the PBS-rich phase (the diffusion of which would be affected by the miscibility with the more rigid PC chains). Increasing the content of MWCNTs to 1% (and also the content of PC in the blend to 6 wt%) produces an equilibration effect between nucleation and growth that matches exactly the crystallization kinetics of neat PBS. Increasing the masterbatch content in the blends produces a decrease in the overall crystallization kinetics as the efficiency of nucleation decreases. The decrease in overall crystallization rate is particularly large for the blend with 4% MWCNT, a reflection of the antinucleation effect previously discussed.

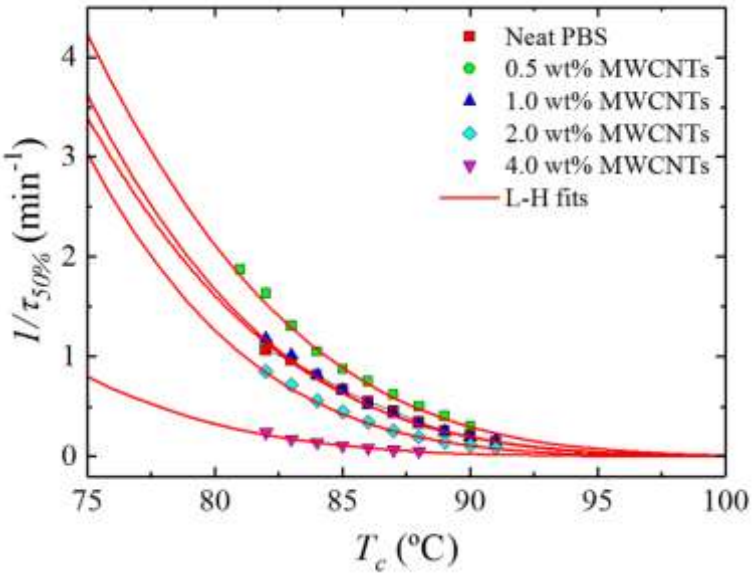

Figure 4.11 Overall crystallization rate ($1/\tau_{50\%}$) as a function of isothermal crystallization temperature (T_c) for neat PBS and for the PBS/(PC/MWCNTs) nanocomposites. The red solid lines represent fits to the LH theory.

Another way to examine the results presented in Figure 4.11 is by taking the values of the crystallization temperature for which the blends reach a constant value of $1/\tau_{50\%}$ (i.e., 0.43 min^{-1}) (Figure 4.12(a)) and the $1/\tau_{50\%}$ values at a constant T_c (i.e., 82 °C) (Figure 4.12b), as a function of MWCNTs content. Figure 4.12(a) shows the experimental and extrapolated data using the Lauritzen and Hoffman (LH) theory, which is explained in detail in Section 4.3.5.2. The results are fully consistent with the non-isothermal results presented in Figure 4.9 and with the self-nucleation results of Figure 4.10. Figure 4.12(a) shows that in order to obtain a predetermined (arbitrarily chosen) constant crystallization rate, the nanocomposite with only 0.5% MWCNTs needs a lower supercooling than neat PBS, but as the MWCNTs content increases (together with the PC content in the blends),

the supercooling applied to obtain the same rate needs to be substantially increased, even beyond that needed by neat PBS. Figure 4.12(b) shows a similar result. At a constant isothermal crystallization temperature, the overall crystallization rate goes through a maximum at 0.5% MWCNTs and then progressively decreases. Note that with 4% MWCNTs (and 23% PC) the overall crystallization rate is five times lower than that of neat PBS.

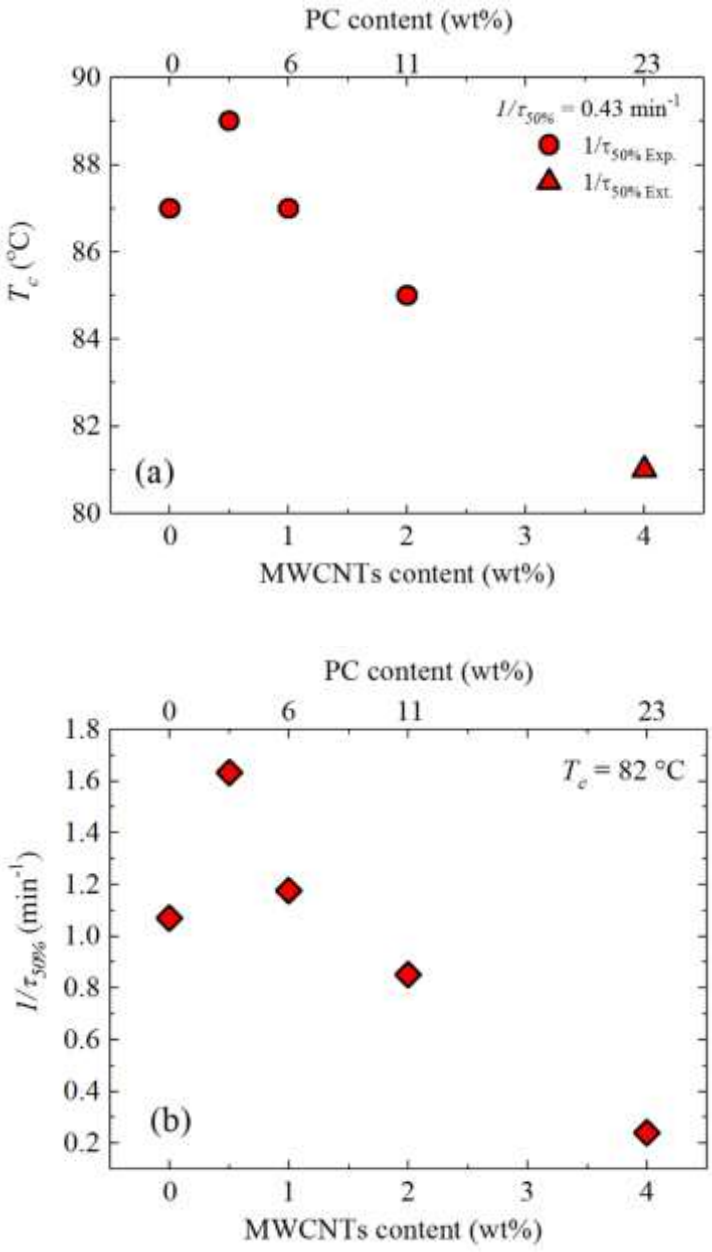

Figure 4.12 (a) Crystallization temperature as a function of MWCNTs content at constant $1/\tau_{50\%}$ = 0.43 min^{-1}; (b) overall crystallization rate as a function of MWCNTs content at constant T_c = 82 °C. The top x-axis indicates the PC content.

4.3.5.1 Fitting DSC isothermal data to the Avrami model

The data obtained during the isothermal crystallization experiments were analysed employing the Avrami equation, which can be expressed as Equation (4.4) according to ref. [25].

$$1 - V_c(t - t_0) = \exp(-k(t - t_0)^n) \qquad (4.5)$$

where t is the experimental time, t_0 is the induction time, V_c is the relative volumetric transformed fraction, n is the Avrami index, and k is the overall crystallization rate constant. The procedure used to perform the fittings to the data was developed by Lorenzo *et al*. [25]. The kinetic parameters for all the investigated samples are plotted in Figure 4.13 and tabulated in Table B.1 of the Supporting Information.

Figure 4.13(a) shows the experimental $1/\tau_{50\%}$ values as a function of T_c, and the observed trend was explained earlier in the discussion (Section 4.3.5). The same trend is obtained when the Avrami rate constant (k) is normalized by elevating it to the power n (i.e., $k^{1/n}$), and plotting it as a function of temperature (Figure 4.13(b)). This indicates that the fitting of the Avrami theory to the DSC data is consistent with the experimental results. In fact, the fitting was excellent in the primary crystallization range and examples of the comparison between experimental and fitted DSC isotherms can be found in the Supplementary Information (see Figure B.3). Figure 4.13(c) shows the n values for all the samples, which depend on the dimensionality of the crystalline superstructure and on their nucleation kinetics [25,41].

The Avrami index values (n) obtained are within the range of 2.5–3.0 for all the samples in the investigated T_c range, except for the 4 wt% MWCNTs containing nanocomposite. Avrami index values close to 3 indicate spherulitic morphology with instantaneous nucleation. For the 4 wt% MWCNTs nanocomposite, the value of n ranged between 2.0 and 2.3. Values lower than 3 are unexpected, especially when it has been demonstrated that MWCNTs are not effective in nucleating PBS at this content. It is well known that upon the addition of a nucleating agent, one would expect that the Avrami index would remain around 3 or would decrease (as the dimensionality of growth can switch from 3D to 2D when the nucleation density is greatly enhanced) [25,38,41]. In the present case, the nanocomposites with 4% MWCNTs exhibit a higher degree of aggregation and the dispersion in the matrix is rather poor. The PBS-rich phase contains

large aggregates of MWCNTs where the surrounding PBS chains may have a lower growth dimensionality (i.e., 2D or even 1D) as a result of being embedded within such large aggregates. The PBS chains away from the aggregates can still form spherulitic structures (3D) and since the overall kinetics takes into account all of the crystallizing PBS chains, it is possible that the resulting Avrami index falls below 2.5, as observed.

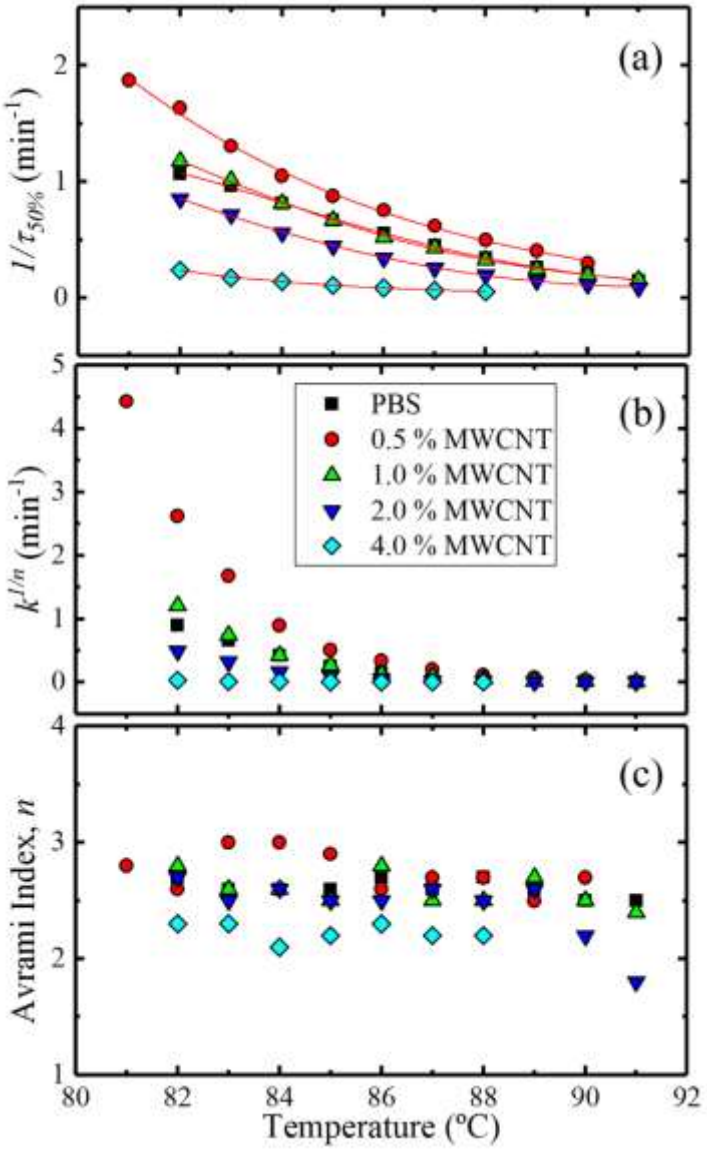

Figure 4.13 (a) Overall half-crystallization rate (the solid lines indicate the Lauritzen and Hoffman fitting); (b) Normalized crystallization constant of the Avrami model ($k^{1/n}$); (c) Avrami index (n) as a function of the isothermal crystallization temperature (T_c) for all the samples.

4.3.5.2 Overall isothermal crystallization data analysed by the Lauritzen–Hoffman model

The overall crystallization kinetics is determined by contributions of nucleation and growth. The Lauritzen–Hoffman (LH) nucleation and growth theory can be applied to the isothermal crystallization kinetics data collected from DSC. Even though the LH theory has received much criticism lately [42], it is still one of a few models that provides easy-to-use analytical expressions capable of fitting the experimental data over a wide supercooling range [43]. Figure 4.11 shows solid lines that represent the mathematical fit of the LH theory, which can be applied to the DSC overall crystallization data according to Equation (4.5).

$$\frac{1}{\tau_{50\%}}(T) = \frac{1}{\tau_0}\exp\left(\frac{-U^*}{R(T_c - T_\infty)}\right)\exp\left(\frac{-K_g^\tau}{T_c\Delta T_f}\right), \qquad (4.6)$$

where $1/\tau_{50\%}$ is the inverse of the experimental half-crystallization time, $1/\tau_0$ is a pre-exponential factor that includes nucleation and growth, U^* is the activation energy for the transport of the chains to the growth front (a value of 1500 cal.mol^{-1} is usually employed), R is the gas constant, T_c is the isothermal crystallization temperature (K), T_∞ is the temperature at which chain mobility ceases (usually taken as T_g–30 K), ΔT is the supercooling ($T_m^o - T_c$), T_m^o is the equilibrium melting temperature calculated for each blend (see Table 4.3), and K_g^τ is a constant related to the energy barrier for crystallization and growth. The value of K_g^τ is given by Equation (4.6) according to the LH theory.

$$K_g^\tau = \frac{jb_0\sigma\sigma_e T_m^0}{k\Delta h_f}, \qquad (4.7)$$

where b_0 is the width of the chain, σ is the lateral surface free energy, σ_e is the fold surface free energy, k is the Boltzmann constant and Δh_f is the heat of fusion of a perfect crystal. The parameter j is determined by the operating regime and was taken as 2 for regime II (note that j is equal to 4 for regime I and III). The product $\sigma\sigma_e$ is obtained from the values of K_g^τ, according to Equation (4.6). The following expressions allow the calculation of σ (and therefore σ_e) and q, the work done by the chain to form a fold.

$$\sigma = 0.1\Delta h_f\sqrt{a_0 b_0} \quad (4.8)$$

$$q = 2a_0 b_0 \sigma_e \quad (4.9)$$

where a_0b_0 is the cross-sectional area of the chain. To obtain the parameters of the LH theory, the following values were used: T_g = 213 K, T_g - 30 K, ΔH = 163 J g^{-1}, a_0 = 4.52 Å, b_0 = 4.12 Å, p_c = 1.1 g cm^{-3}, U^* = 1500 cal mol^{-1}.

Table 4.3 Parameters from the isothermal crystallization kinetics analyses for neat PBS and the PBS/(PC/MWCNTs) nanocomposites.

Sample	T_m^o (K)	$K_g^\tau \times 10^4$ (K^2)	σ (erg/cm^2)	σ_e (erg/cm^2)	$q \times 10^{-13}$ (erg)	R^2
100/0	394.0	8.16	8.08	81.13	2.99	0.995
97/(2.5/0.5)	393.0	8.01	8.08	79.83	2.95	0.998
93/(6/1)	392.1	7.91	8.08	79.04	2.92	0.999
87/(11/2)	391.1	6.99	8.08	70.01	2.58	0.987
73/(23/4)	389.1	6.79	8.08	68.32	2.52	0.997

The LH parameters for neat PBS and the nanocomposites are tabulated in Table 4.3. There is a slight variation of K_g^τ values with increasing masterbatch content. This is in line with the already discussed T_g values.

4.3.6 Thermal conductivity

Figure 4.14 shows the thermal conductivities of neat PBS and its PC/MWCNTs containing nanocomposites. Phonon transport is the main mechanism for heat conduction in conductive polymer samples. Phonons transfer heat energy through interactions with each other and with subatomic particles. In multi-phase systems, such as polymeric composites, scattering also occurs when phonons propagate through a boundary which separates one phase from another [44–46]. Generally, there is an improvement in the thermal conductivity of the blend nanocomposites in comparison to neat PBS. Possible explanations for the improvement in thermal conductivity of the nanocomposites include:

(1) the high thermal conductivity of the carbon nanotubes (650 to 10,000 $W \cdot m \cdot K^{-1}$) [43], and (2) the dispersion of the filler particles in the polymer blend.

For the lowest amount of nanotubes (0.5 wt%), there are too few nanotubes for phonons to move effectively, hence the low thermal conductivity value. As the amount of nanotubes increased, there was an increase in the effectiveness of the movement of the phonons through the nanocomposites up to 2 wt% MWCNTs. Above this content, there was a decrease in the thermal conductivity. This is because above this content, the MWCNTs aggregated in the PC-rich phase and became ineffective parts of the PBS matrix. The phonons could move well in the PC-rich phase, but the fairly large PBS-rich phase areas that separated the PC-rich phase areas considerably slowed down the phonon movement, giving rise to reduced thermal conductivity.

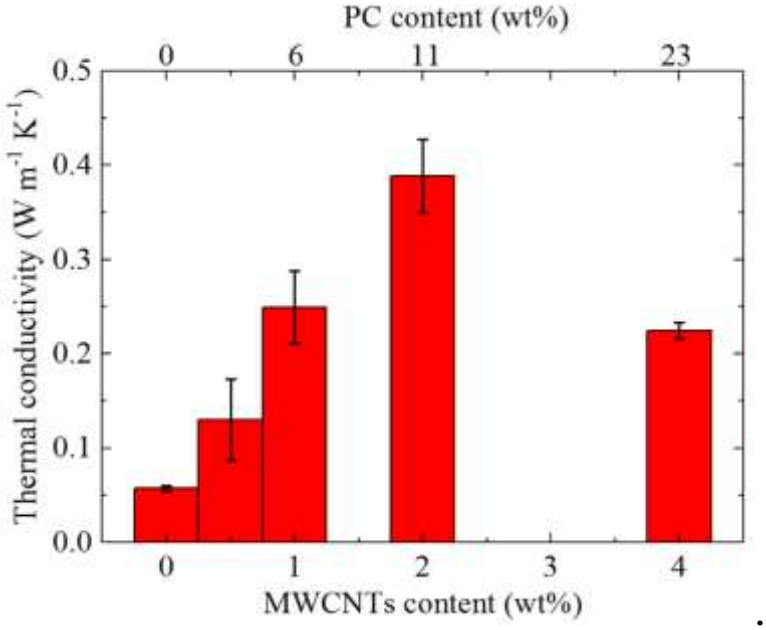

Figure 4.14 Influence of MWCNTs content on the thermal conductivities of the nanocomposites. The PC content is indicated in the top X-axis.

4.3.7 Tensile properties

The mechanical properties of neat PBS and the nanocomposites were investigated through tensile testing. Figure 4.15 shows typical stress-strain curves obtained for the samples, whereas Table 4.4 summarizes the tensile test results. PBS is a ductile material which becomes fragile with the incorporation of the MWCNTs masterbatch.

The stress at break shows a decrease with the incorporation of the masterbatch (Figure 4.15). However, the nanocomposites containing 0.5, 1.0, 2.0 wt% MWCNTs gave almost the same value. The initial drop in tensile stress with the inclusion of the masterbatch in the PBS matrix is the result of the formation of the sea island morphology, with the very large dispersed PC-rich phase acting as a stress concentration region. PBS loses its localized shear deformation ability to form a neck and instead becomes a fragile material, as cracks nucleate at the dispersed phase and grow to produce earlier fracture. As a consequence, the strain at break dramatically drops when the masterbatch is added.

The tensile stress, however, remains fairly high for the samples containing up to 2 wt% MWCNTs, which could be related to the partial miscibility of the blends, where in spite of the large size of the dispersed PC-rich phase, there is adhesion between the PC-rich and the PBS-rich phases, as manifested in the lack of void formation at the interphase between the phases, as documented by SEM and AFM. For the 4 wt% MWCNTs nanocomposite, there was a very large drop in the tensile stress. This is probably due to the MWCNTs aggregates within the PC-rich phase (in addition to the PC-phase crystallization) that result in an increasing chance that the polymer will fracture at a much lower stress.

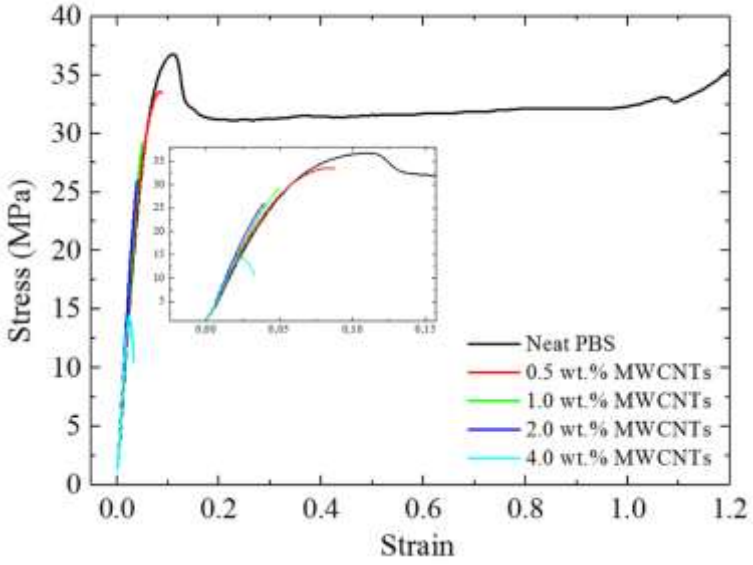

Figure 4.15 Stress-strain curves for neat PBS and the nanocomposites.

Table 4.4 shows little change in the Young's modulus with increasing masterbatch content, taking into account the experimental error indicated by the standard deviation values. PBS had a modulus value of 579 ± 139 MPa, and this value remained virtually constant with increasing masterbatch content, despite the fact that the masterbatch had a

Young's modulus value of approximately 2800 MPa. There are two possible reasons why the modulus of the blend nanocomposites did not increase as expected: (1) The poor dispersion of the MWCNTs in the PBS-rich phase, and (2) the high level of nanoparticle aggregation in the PC-rich matrix [47].

Table 4.4 Summary of tensile testing results for neat PBS and the nanocomposites.

***w/w* PBS/(PC/MWCNTs)**	**σ_b (MPa)**	**ε_b (%)**	***E* (MPa)**
100/0	38.1 ± 2.1	210 ± 110	579 ± 139
97/(2.5/0.5)	28.3 ± 6.1	7.0 ± 2.9	641 ± 50
93/(6/1)	29.4 ± 0.5	5.0 ± 0.1	672 ± 44
87/(11/2)	26.0 ± 6.6	5.0 ± 1.0	715 ± 84
73/(23/4)	10.9 ± 0.6	4.0 ± 0.8	638 ± 79

σ_b— stress at break; ε_b—strain at break; E—Young's modulus.

4.4 Conclusions

The results reported in this paper showed that the PBS/masterbatch blends were partially miscible and formed PC-rich and PBS-rich phases, while the majority of the MWCNTs were inside the PC-rich phase. PBS plasticization caused some PC crystallization. The MWCNTs were able to nucleate the PBS-rich phase at low loading contents (below 4%), indicating that some of the MWCNTs were able to transfer from the PC-rich to the PBS-rich phase, as visualized by AFM. However, when the content of MWCNTs reached 4%, the PBS-rich phase was antinucleated. This was explained by the agglomeration of MWCNTs, which remained encapsulated inside the PC-rich phase, and the decreased ability of the PBS chains to nucleate. Such lower nucleation density may have arisen by a combination of reasons: impurities transfer from the PBS-rich to PC-rich phase and increased T_g value of the PBS-rich phase in comparison to neat PBS. The isothermal crystallization rate also increased with low contents of MWCNTs, went through a maximum and then decreased in a consistent way with the non-isothermal results.

The thermal conductivities and tensile properties of the nanocomposites varied but could generally be explained in terms of the observed morphology of the nanocomposites. For example, a significant decrease in thermal conductivity was observed for the 4 wt% MWCNTs content, which probably was the result of a high level of nanoparticle

aggregation in the PC-rich matrix. This was probably also the reason for the low stress-at-break value for this particular sample, which resulted in enhanced stress concentrations leading to early fracture.

The last part of this study will focus on PCL-PBS blends that we plan to mix with the PC-MWCNT masterbatch. This study will be conducted along the same lines as the work done in the present paper, but it will be interesting to see the influence of the presence of low-melting PCL on the morphology and crystallization behaviour of respectively PCL and PBS. This will obviously be determined by the extent to which the MWCNTs disperse into this tri-polymer system.

4.5 References

[1] C.S. Lin, Y.F. Shih, R.J. Jeng, S.A. Dai, J.J. Lin, C.C. Lee. Nanocomposites with enhanced electrical properties based on biodegradable poly(butylene succinate) and polyetheramine modified carbon nanotube. Journal of the Taiwan Institute of Chemical Engineers 2012; 43:322-328.
DOI: 10.1016/j.jtice.2011.10.009

[2] M. Gigli, A. Negroni, G. Zanaroli, N. Lotti, F. Fava, A. Munari. Environmentally friendly PBS-copolyesters containing PEG-like subunit: Effect of block length on solid-state properties and enzymatic degradation. Reactive & Functional Polymers 2013; 73:764-771.
DOI: 10.1016/j.reactfunctpolym.2013.03.007

[3] R.T. Zeng, W. Hu, M. Wang, S.D. Zhang, J.B. Zeng. Morphology, rheological and crystallization behavior in non-covalently functionalized carbon nanotube reinforced poly(butylene succinate) nanocomposites with low percolation threshold. Polymer Testing 2016; 50:182-190.
DOI: 10.1016/j.polymertesting.2016.01.003

[4] Y.F. Shih, L.S. Chen, R.J. Jeng. Preparation and properties of biodegradable PBS/multi-walled carbon nanotube nanocomposites. Polymer 2008; 49:4602-4611.
DOI: 10.1016/j.polymer.2008.08.015

[5] A.G. Potapov, I.K. Shundrina. The influence of different fillers on mechanical and physical properties of high-molecular-weight biodegradable aliphatic polyesters. Polymer Science Series A 2016; 58:585–592.
DOI: 10.1134/S0965545X1604012X

[6] T. Fujimaki. Processability and properties of aliphatic polyesters, 'BIONOLLE', synthesized by polycondensation reaction. Polymer Degradation and Stability 1998; 59:209-214.
DOI: 10.1016/S0141-3910(97)00220-6

[7] K.P. Pramoda, N.T.T. Linh, C. Zhang, T. Liu. Multiwalled carbon nanotube nucleated crystallization behavior of biodegradable poly(butylene succinate) nanocomposites. Journal of Applied Polymer Science 2009; 111:2938-3945.
DOI: 10.1002/app.29349

[8] L. Tan, Y. Chen, W. Zhou, S. Ye, J. Wei. Novel approach toward poly(butylene succinate)/single-walled carbon nanotubes nanocomposites with interfacial-induced crystallization behaviors and mechanical strength. Polymer 2011; 52:3587-3596.
DOI: 10.1016/j.polymer.2011.06.006

[9] L. Yuan, D. Wu, M. Zhang, W. Zhou, D. Lin. Rheological percolation behavior and isothermal crystallization of poly(butyene succinate)/carbon nanotube composites. Industrial and Engineering Chemistry Research 2011; 50:14186-14192.
DOI: 10.1021/ie202039v

[10] G. Wang, B. Guo, J. Xu, R. Li. Rheology, crystallization behaviors, and thermal stabilities of poly(butylene succinate)/pristine multiwalled carbon nanotube composites obtained by melt compounding. Journal of Applied Polymer Science 2011; 121:59-67.
DOI: 10.1002/app.33222

[11] M. Bhattacharya. Review: Polymer nanocomposites – A comparison between carbon nanotubes, graphene, and clay as nanofillers. Materials 2016; 9:1-35.
DOI: 10.3390/ma9040262

[12] K.C. Jajam, M.M. Rahman, M.V. Hosur, H.V. Tippur. Fracture behavior of epoxy nanocomposites modified with polyol diluent and amino-functionalized multi-walled carbon nanotubes: A loading rate study. Composites Part A: Applied Science and Manufacturing 2014; 59,:57-69.
DOI: 10.1016/j.compositesa.2013.12.014

[13] M.M Rahman, M. Hosur, S. Zainuddin, K.C. Jajam, H.V. Tippur, S. Jeelani. Mechanical characterization of epoxy composites modified with reactivepolyol diluent and randomly-oriented amino-functionalized MWCNTs. Polymer Testing 2012; 31:1083-1093.

DOI: 10.1016/j.polymertesting.2012.08.010

[14] T. Wu, E. Chen, Y. Lin, M. Chiang, G. Chang. Preparation and characterization of melt-processed polycarbonate/multiwalled carbon nanotube composites. Polymer Engineering and Science 2008; 48:1369-1375.
DOI: 10.1002/pen.21094

[15] P. Pötschke, A.R. Bhattacharyya, A. Janke, H. Goering. Melt mixing of polycarbonate/multi-wall carbon nanotube composites. Composite Interfaces 2003; 10:389-404.
DOI: 10.1163/156855403771953650

[16] K. Prashantha, J. Soulestin, M.F. Lacrampe, P. Krawczak, G. Dupin, M. Claes. Masterbatch-based multi-walled carbon nanotube filled polypropylene nanocomposites: Assessment of rheological and mechanical properties. Composites Science and Technology 2009; 69:1756-1763.
DOI: 10.1016/j.compscitech.2008.10.005

[17] T.P. Gumede, A.S. Luyt, M.K. Hassan, R.A. Pérez-Camargo, A. Tercjak, A.J. Müller. Morphology, nucleation, and isothermal crystallization kinetics of poly(ε-caprolactone) mixed with a polycarbonate/MWCNTs masterbatch. Polymers 2017; 9:709.
DOI: 10.3390/polym9120709

[18] M.Z. Pang, J.J. Qiao, J. Jiao, S.J. Wang, M. Xiao, Y.Z. Meng. Miscibility and properties of completely biodegradable blends of poly(propylene carbonate) and poly(butylene succinate). Journal of Applied Polymer Science 2008; 107:2854-2860.
DOI: 10.1002/app.27252

[19] T. Wang, H. Wang, H. Li, Z. Gan, S. Yan. Banded spherulitic structures of poly(ethlylene adipate), poly(butylene succinate) and in their blends. Physical Chemistry Chemical Physics 2009; 11:1619-1627.
DOI: 10.1039/b817597g

[20] G.R. Kasaliwal, A. Göldel, P. Pötschke, G. Heinrich. Influences of polymer matrix melt viscosity and molecular weight on MWCNT agglomerate dispersion. Polymer 2011; 52:1027-1036.
DOI: 10.1016/j.polymer.2011.01.007

[21] B. Fillon, J.C. Wittmann, B. Lotz, A. Thierry. Self-nucleation and recrystallization of isotactic polypropylene (α phase) investigated by differential scanning

calorimetry. Journal of Polymer Science Part B: Polymer Physics 1993; 31:1383-1393.
DOI: 10.1002/polb.1993.090311013

[22] A.T. Lorenzo, M.A. Arnal, J.J. Sánchez, A.J. Müller. Effect of annealing time on the self-nucleation behaviour of semicrystalline polymers. Journal of Polymer Science Part B: Polymer Physics 2006; 44:1738-1750.
DOI: 10.1002/*polb*.20832

[23] A.J. Müller, M.L. Arnal. Thermal fractionation of polymers. Progress in Polymer Science 2005; 30:559-603.
DOI: 10.1016/j.progpolymsci.2005.03.001

[24] R.M. Michell, A. Mugica, M. Zubitur, A.J. Müller. Self-nucleation of crystalline phases within homopolymers, polymer blends, copolymers, and nanocomposites. Advances in Polymer Science 2015; 276:215-256.
DOI: 10.1007/12_2015_327

[25] A.T. Lorenzo, M.L. Arnal, J. Albuerne, A.J. Müller. DSC isothermal polymer crystallization kinetics measurements and the use of the Avrami equation to fit the data: Guidelines to avoid common problems. Polymer Testing 2007; 26:222-231.
DOI: 10.1016/j.polymertesting.2006.10.005

[26] J.D. Hoffman, J.J. Weeks. Melting process and the equilibrium melting temperature of polychlorotrifluoroethylene. Journal of Research of the National Bureau of Standards - A. Physics and Chemistry 1962; 66:13-28.
DOI: 10.6028/jres.066A.003

[27] J.D. Menczel, R.B. Prime. Thermal Analysis of Polymers. Fundamentals and Applications. John Wiley & Sons, New Jersey (2009).

[28] A.J. Müller, E. Paredes. Melting behavior, mechanical properties and fracture of crystallized polycarbonates. Latin American Journal of Metallurgy and Materials 1985; 5:130-141.

[29] V. Balsamo, N. Calzadilla, G. Mora, A.J. Müller. Thermal characterization of polycarbonate/polycaprolactone blends. Journal of Polymer Science: Part B: Polymer Physics 2001; 39:771-785.
DOI: 10.1002/1099-0488(20010401)39:7<771::AID-POLB1052>3.0.CO;2-I

[30] J. Guo, Y. Liu, R. Prada-Silvy, Y. Tan, S. Azad, B. Krause, P. Pötschke, B.P. Grady. Aspect ratio effects of multi-walled carbon nanotubes on electrical, mechanical, and

thermal properties of polycarbonate/MWCNT composites. Journal of Polymer Science, Part B: Polymer Physics 2014; 52:73-83.
DOI: 10.1002/polb.23402

[31] F.Y. Castillo, R. Socher, B. Krause, R. Headrick, B.P. Grady, R. Prada-Silvy, P. Pötschke. Electrical, mechanical, and glass transition behavior of polycarbonate-based nanocomposites with different multi-walled carbon nanotubes. Polymer 2011; 52:3835-3845.
DOI: 10.1016/j.polymer.2011.06.018

[32] M. Mukherjee, T. Das, R. Rajasekar, S. Bose, S. Kumar, C.K. Das. Improvement of the properties of PC/LCP blends in the presence of carbon nanotubes. Composites Part A: Applied Science and Manufacturing 2009; 40:1291-1298.
DOI: 10.1016/j.compositesa.2009.05.024

[33] G. Liu, L. Zheng, X. Zhang, C. Li, S. Jiang, D. Wang. Reversible lamellar thickening induced by crystal transition in poly(butylene succinate). Macromolecules 2012; 45:5487-5493.
DOI: 10.1021/ma300530a

[34] S.S. Ray, S. Vaudreuil, A. Maazouz, M. Bousmina. Dispersion of multi-walled carbon nanotubes in biodegradable poly(butylene succinate) matrix. Journal of Nanoscience and Nanotechnology 2006; 6:2191-2195.
DOI: 10.1166/jnn.2006.368

[35] F.B. Ali, R. Mohan. Thermal, mechanical, and rheological properties of biodegradable polybutylene succinate/carbon nanotubes nanocomposites. Polymer Composites 2010; 31:1309-1314.
DOI: 10.1002/pc.20913

[36] I. Arandia, A. Mugica, M. Zubitur, A. Arbe, G. Liu, D. Wang, R. Mincheva, P. Dubois, A.J. Müller. How composition determines the properties of isodimorphic poly(butylene succinate-*ran*-butylene azelate) random biobased copolymers: From single tp double crystalline random copolymers. Macromolecules 2015; 48: 43-57.
DOI: 10.1021/ma5023567

[37] B. Fillon, B. Lotz, A. Thierry, J.C. Wittmann. Self-nucleation and enhanced nucleation of polymers. Definition of a convenient calorimetric “efficiency scale” and evaluation of nucleating additives in isotactic polypropylene (α phase). Journal of Polymer Science Part B: Polymer Physics 1993; 31:1395-1405.
DOI: 10.1002/polb.1993.090311014

[38] R.A. Pérez, J.V. López, J.N. Hoskins, B. Zhang, S.M. Grayson, M.T. Casas, J. Puiggalí, A.J. Müller. Nucleation and antinucleation effects of functionalized carbon nanotubes on cyclic and linear poly(ε-caprolactones). Macromolecules 2014; 47:3553-3566.
DOI: 10.1021/ma5005869

[39] J. Chen, D. Wu, K.C. Tam, K. Pan, Z. Zheng. Effect of surface modification of cellulose nanocrystal on nonisothermal crystallization of poly(β-hydroxybutyrate) composites. Carbohydrate Polymers 2017; 157:1821-1829.
DOI: 10.1016/j.carbpol.2016.11.071

[40] R.A. Pérez-Camargo, G. Saenz, S. Laurichesse, M.T. Casas, J. Puiggalí, L. Avérous, A.J. Müller. Nucleation, crystallization, and thermal fractionation of poly (ε-caprolactone)-grafted-lignin: Effects of grafted chains length and lignin content. Journal of Polymer Science Part B: Polymer Physics 2015; 53:1736-1750.
DOI: 10.1002/polb.23897

[41] M. Avrami. Granulation, phase change, and microstructure kinetics of phase change III. Journal of Chemical Physics 1941; 9:177-184.
DOI: 10.1063/1.1750872

[42] G. Reiter, G. R. Strobl. Progress in Understanding Polymer Crystallization, Lecture Notes Physics 714 (Springer, Berlin Heidelberg 2007).
DOI: 10.1007/b11903420

[43] A.T. Lorenzo, A.J. Müller. Estimation of the nucleation and crystal growth contributions to the overall crystallization energy. Journal of Polymer Science: Part B: Polymer Physics 2008; 46:1478-1487.
DOI: 10.1002/polb.21483

[44] A. Wurm, D. Lellinger, A.A. Minakov, T. Skipa, P. Pötschke, R. Nicula, I. Alig, C. Schick. Crystallization of poly(ε-caprolactone)/MWCNT composites: A combined SAXS/WAXS, electrical and thermal conductivity study. Polymer 2014; 55:2220-2232.
DOI: 10.1016/j.polymer.2014.02.069

[45] S.J. Chin, S. Vempati, P. Dawson, M. Knite, A. Linarts, K. Ozols, T. McNally. Electrical conduction and rheological behaviour of composites of poly(ε-caprolactone) and MWCNTs. Polymer 2015; 58:209-221.
DOI: 10.1016/j.polymer.2014.12.034

[46] P. Pötschke, T. Villmow, B. Krause. Melt mixed PCL/MWCNT composites prepared at different rotation speeds: Characterization of rheological, thermal, and electrical properties, molecular weight, MWCNT macrodispersion, and MWCNT length distribution. Polymer 2013; 54:3071-3078.
DOI: 10.1016/j.polymer.2013.04.012

[47] X. Ma, Y. Zare, K.Y. Rhee. A two-step methodology to study the influence of aggregation/agglomeration of nanoparticles on Young's modulus of polymer nanocomposites. Nanoscale Research Letters 2017; 12:621.
DOI: 10.1186/s11671-017-2386-0

CHAPTER 5

Isothermal crystallization kinetics and morphology of double crystalline PCL/PBS blends and the polycarbonate/MWCNTs masterbatch

---

This chapter will be submitted for publication as:

Thandi P. Gumede, Adriaan S. Luyt, Ricardo A. Pérez-Camargo, Agnieszka Tercjak, Alejandro J. Müller*. The influence of polycarbonate/MWCNTs masterbatch on the morphology and isothermal crystallization kinetics of PCL/PBS blends.*

Author contributions: *Luyt and Müller conceived the project and guided the students, Gumede conceived and performed most of the experiments, Pérez-Camargo was responsible for the tensile testing analyses, and Tercjak's expertise in AFM analysis helped the authors to correctly visualize the morphology of the investigated system.*

Abstract

In this work, 70/30 and 30/70 w/w PCL/PBS blends and their filled PCL/PBS/(PC/MWCNTs) nanocomposites were melt blended in a twin-screw extruder. The nanocomposites contained 1.0 and 4.0 wt% MWCNTs. Scanning electron microscopy (SEM) results for the blends showed a sea-island morphology with discrete droplets of the minor phases within the matrix of the major phase, typical of immiscible polymer blends. In the case of the nanocomposites, three phases were formed: (i) the matrix (either PCL or PBS rich phase depending on the composition), (ii) dispersed polymer droplets of small size (either PCL or PBS rich phase depending on the composition), and (iii) the dispersed aggregates of tens of micron sizes that were clearly the PC/MWCNTs masterbatch. Atomic force microscopy (AFM) results indicated that although most MWCNTs were located in the PC dispersed phase, some of the MWCNTs migrated from the dispersed phase to the polymer matrix. This is due to partial miscibility and intimate contact at the interfaces between the PC-rich and PCL-rich phases, or the PC-rich and the PBS-rich phases. The polar component surface energy and interfacial tension values suggested that the MWCNTs would preferably disperse better in the PBS-rich phase because of the closeness of the polar surface values of PBS and the

PC/MWCNTs masterbatch and the small interfacial tension value. Standard DSC scans for the PCL/PBS blends showed an increase in T_c values indicating a nucleation effect. For the nanocomposites there was a decrease in the T_c values. This was attributed to the competition between two effects: (1) the partial miscibility of the PC-rich and the PCL-rich and PBS-rich phases, and (2) the nucleation effect of the MWCNTs. The decrease in the T_c values indicated that miscibility is the dominating effect. Isothermal crystallization results indicated that the nanocomposites crystallized slower than the neat blends and the homopolymers. Miscible PC chains within PCL-rich and PBS-rich phases can decrease their crystallization rate. The difference between the crystallization rate of neat PBS and the PBS-rich nanocomposite and the PCL and PCL-rich nanocomposite was very large. This confirmed that the PBS-rich phase is more miscible than the PCL-rich phase with the PC-rich phase. The introduction of the masterbatch generally increased the thermal conductivity of the blend nanocomposites and showed little change in the Young's modulus of the nanocomposites. This was due to the miscibility effect.

Keywords: PC/MWCNTs masterbatch; PCL/PBS blends; nanocomposites; morphology; conductivity; isothermal crystallization

5.1 Introduction

Global environmental issues have attracted considerable attention due to environmental concerns and the realization that petroleum resources are finite. Biodegradable polymers offer a potential solution to the environmental hazard posed by conventional plastics [1-3]. Different types of biodegradable polymers such as poly(ε-caprolactone) (PCL), poly(butylene succinate) (PBS), poly(lactic acid) (PLA), and poly(alkanoates) (PHA, PHB, PHBV) have been studied as potential biomaterials for a variety of applications. Amongst the mentioned biodegradable polymers, poly(butylene succinate) (PBS) has been favoured in most applications because of its relatively good melt processability, biodegradability, acceptable strength and modulus which is closely comparable to those of the widely-used polyethylene (PE) and polypropylene (PP) [2,3]. Despite some advantages, the PBS biopolymer suffers from some disadvantages such as brittleness, which results in a low elongation at break.

It is well known that blending of two or more polymers is essential for achieving a desirable combination of properties which are often absent in pure polymers. Blending

offers advantages such as cost effectiveness and less time-consumption compared to the development of new monomers as a basis for new polymeric materials [4]. In order to improve the toughness of PBS, several authors blended it with PCL [5-7]. Generally, the authors reported that the tensile strength decreased as the PCL content increased in the blends, while the elongation at break and impact strength increased with increasing PCL content. The decreased tensile strength indicated poor interfacial interaction between the blend phases. The higher elongation values showed improved ductility and toughness in the blends, due to the plasticization by PCL, which led to improved chain mobility and energy absorbed by the material before fracturing.

PBS/PCL blends are, however, immiscible as evidenced by the composition independent glass transition temperatures and the biphasic melt, which leads to poor interfacial adhesion and macrophase separation [7]. A number of studies investigated the effect of adding copolymers (poly(ethylene oxide)-block-poly(propylene oxide)-block-poly(ethylene oxide) (PEO-PPO-PEO) and poly(butylene succinate-*co*-ε-caprolactone) (P(BS-*co*-CL)) and thermoplastic soy meal (TSM) in order to improve miscibility, interfacial adhesion and the resultant mechanical properties of PCL/PBS blends [8-10]. In these studies, copolymers (PEO-PPO-PEO and P(BS-*co*-CL)) and thermoplastic soy meal (TSM) were used as compatibilizers. The compatibilizer was generally found to encapsulate itself between the polymer phases, reducing the spherical particle sizes and increasing the surface contact area between the blend components. In some cases, the addition of the compatibilizer resulted in the disappearance of the spherical domains, exhibiting a rougher fracture surface than the blend without the compatibilizer. This apparently confirmed the effective reduction of interfacial tension and a significant improvement in compatibility and interfacial adhesion. Liu *et al*. [10] studied the effect of adding a P(BS-*co*-CL) compatibilizer in amounts up to 5 wt% in a 80/20 w/w PBS/PCL blend system. The modulus of elasticity, yield stress and fracture strain dramatically increased with increasing compatibilizer content. This behaviour was attributed to the improved interfacial compatibility in the presence of the compatibilizer. However, the properties declined significantly with further increases in the compatibilizer content. Can *et al*. [9] used PEO-PPO-PEO as a compatibilizer for PCL/PBS blends with different ratios. The E" value for PBS shifted to lower temperatures with increasing PCL content, while the E" value for PCL slightly increased compared to that of neat PCL. This indicated interaction and compatibility between the two polymers in the presence of the compatibilizer.

Recent reports [11-13] revealed that adding conductive carbon-based nano-fillers such as carbon nanotubes (CNTs) into PCL and PBS matrices can enhance some of the matrix properties to better levels than those of the copolymers or polymers filled with metal powders, as well as produce electrically conductive materials with better mechanical properties. This is due to their low density, inertness and better compatibility than metal powders with most polymers. CNTs have shown to have greater potential than any other carbon-based nano-fillers (i.e., carbon black (CB), carbon nanofibres (CNF), and graphite) because of their unique one-dimensional structure with good electrical conductivity, as well as excellent mechanical and thermal properties [14-16]. Furthermore, it was shown that the localization of carbon nanotubes in the PCL/PBS blends affected the material properties. He *et al*. [11] introduced MWCNTs into double-crystalline PBS/PCL blends using solution mixing and solvent casting processes. The MWCNTs exhibited a much finer dispersion morphology in the PBS/MWCNTs nanocomposite than in the PCL/MWCNTs nanocomposite. This was attributed to the wetting coefficient data for the MWCNTs introduced into the binary copolymer which was calculated as 1.74 (harmonic-mean equation) or -3.43 (geometric-mean equation). According to the authors, this meant that the MWCNTs were selectively distributed in the PBS phase. The selective dispersion of MWCNTs in the PBS hard segment improved the strength of the material without deteriorating its ductility.

In this paper, MWCNTs were dispersed into PCL/PBS blends through melt-mixing of the blend with a PC/MWCNTs masterbatch. The structure and properties of the blend nanocomposites were correlated with the morphology of the PCL/PBS blends, and the dispersion of PC and MWCNTs in these blends. We also kinetically followed the crystallization of the PCL and PBS components in the blends.

5.2 Experimental

5.2.1 Materials

A commercial PCL (CAPA 6500, Johannesburg, South Africa) was purchased from Southern Chemicals. It has a density of 1.1 g cm^{-3}, a melting temperature of 58–60 °C, and a degree of crystallinity of ~35%. It has a weight-average molecular weight (M_w) and number-average molecular weight (M_n) of respectively 113,400 g mol^{-1} and 73,620 g

mol^{-1}, and a polydispersity index of 1.54. It has a melt flow index (MFI) of 11.5 g/10 min (2.16 kg / 190 °C).

A commercial poly(1,4-butylene succinate) (PBS), extended with 1,6-diisocyanatohexane, was purchased from Sigma-Aldrich (Johannesburg, South Africa). It has a density of 1.3 g cm^{-3} at 25 °C and a melting temperature of 120 °C. The weight-average molecular weight (M_w) of PBS is 63,000 g mol^{-1} [17]. It has melt flow index (MFI) of 20.9 g/10 min (2.16 kg / 190 °C).

A conductive masterbatch based on 85% low viscosity polycarbonate (Makrolon® 2205 grade, M_w of 20,100 g mol^{-1} [18]) loaded with 15 wt.% of MWCNTs (industrial grade NC7000), was obtained from Nanocyl (Sambreville, Belgium). It has a density of 1.175 g cm^{-3} and an MFI of 5.6 g/10 min, according to the specifications provided by the suppliers. The average diameter and length of the MWCNTs were respectively 10 nm and 3-4 µm. The MWCNTs contained more than 90% carbon and less than 10% metal oxide impurities.

The nanocomposites were prepared by melt-mixing in a twin-screw extruder (Thermo Scientific HAAKE Mini Lab II at the University of Pretoria, South Africa) operated under compressed air (100 rpm, 160 °C, 10 min). After extrusion, the samples were compression moulded at 160 °C for 5 min under 50 kPa using a hydraulic melt press. The calculated weight percentages of the different components in each of the investigated nanocomposites are given in Table 5.1.

Table 5.1 Weight percentages of the components in the nanocomposites.

PCL (%)	PBS (%)	PC (%)	MWCNTs (%)
100	0	0	0
70	30	0	0
65	28	6	1
51	22	23	4
22	51	23	4
28	65	6	1
30	70	0	0
0	100	0	0

5.2.2 Sample characterization

Scanning electron microscopy (SEM) analyses were done in a TESCAN VEGA 3 scanning electron microscope. The samples were sputter coated with gold for 60 seconds to produce conductive coatings onto the samples. The acceleration voltage used was 15 kV.

Atomic force microscopy (AFM) experiments were performed on selected samples at room temperature using a Bruker Multimode 8 scanning probe microscope equipped with a Nanoscope V controller. The micrographs, with sizes in the range of 0.6-5 μm, were obtained in tapping mode by using microfabricated silicon tips/cantilevers (cantilever spring constant, k = 42 N m^{-1}, and resonance frequency, f_0 = 320 kHz, Bruker). Height and phase AFM images of lamellae and MWCNTs were collected simultaneously and subjected to a first-order plane-fitting procedure to compensate for the tilt. The height and phase AFM images were similar, and therefore only the phase AFM images will be reported in this paper. To obtain cross-sectional AFM images, the samples were cut using an ultramicrotome Leica Ultracut R with a diamond blade.

The contact angle measurements of the samples were conducted at room temperature on a surface energy evaluation system, based on the sessile drop method. Five replicates for each sample were analyzed to ensure reproducibility of the results. Distilled water (H_2O), and diiodomethane (CH_2I_2) were used as polar and non-polar solvents, respectively. The literature values of their surface energies are: H_2O: γ^p = 50.7 mJ m^{-2} and γ^d = 22.1 mJ m^{-2}; CH_2I_2: γ^p = 6.7 mJ m^{-2} and γ^d = 44.1 mJ m^{-2}.

Differential scanning calorimetry (DSC) analyses were performed using a heat flux Perkin Elmer DSC 6000 under nitrogen flow (flow rate 20 mL min^{-1}) to minimize degradation of the samples, and the instrument was calibrated at a heating rate of 10 °C min^{-1} using the onset temperatures of melting of indium and zinc standards, and the melting enthalpy of indium. The sample weight was almost exactly 5 mg in all cases.

For the non-isothermal DSC analyses, the samples were melted in the DSC for 3 min at 270 °C to erase any previous thermal history. The samples were then cooled at 20 °C min^{-1} from 270 to -60 °C, and then heated at the same rate from -60 to 270 °C.

The isothermal crystallization experiments were performed by following the procedure recommended by Lorenzo *et al*. [19], in which isothermal crystallization temperatures (T_c) are chosen where no crystallization occurred during the cooling step

from the melt (performed at 60 °C min^{-1}). The samples were heated to 270 °C and kept at this temperature for 3 min to erase the thermal history. The samples were then cooled at 60 °C min^{-1} to the set isothermal T_c. The sample was then kept at the set T_c for a crystallization time (t_c) until saturation was reached. Finally, the sample was heated from T_c to 270 °C at 20 °C min^{-1}, to record the melting behaviour of the isothermally crystallized sample.

To determine the equilibrium melting temperatures, T_m^o, of the samples, the final step in the isothermal crystallization procedure, whereby the sample was heated at 20 °C min^{-1} in order to record the melting behaviour of the isothermally crystallized polymer, was used to record the melting of the crystals formed at different crystallization temperatures, T_c. The Hoffman–Weeks extrapolation [20] was then applied by plotting the observed melting temperature ($T_{m(obs)}$) against T_c to observe the intersection of this line with another line with a slope equal to 1 ($T_m = T_c$).

Thermal conductivity measurements were performed using a Therm Test Inc. Hot Disk TPS 500 thermal constant analyser. The instrument uses the transient plane source method. A 3.2 mm radius Kapton disk type sensor was selected for the analysis. The sample discs were 5 mm thick and 12 mm in diameter. The sensor was placed between two sample discs of the same composition. The measurements were done for 25 s in order to prevent the heat flow from reaching the boundary of the samples. Ten measurements were performed for each composition. The thermal conductivities are reported as average values with standard deviations.

The tensile analysis of the samples was carried out using an Instron 4301 universal testing machine at a cross-head speed of 10 mm min^{-1}. The dumbbell shaped samples had a Gauge length of 20 mm, a thickness of 1 mm and a width of 5 mm. The samples were tested at a controlled ambient temperature of 23 °C and 50% relative humidity. Three samples of each composition were tested and average values with standard deviations are presented.

5.3 Results and discussion

5.3.1 Phase morphology of PCL/PBS blends and PCL/PBS/(PC/MWCNTs) blend nanocomposites

Phase morphology plays an important role in the mechanical behaviour of polymer blends. The type of morphology and the sizes of dispersed phases in the polymer blends are important factors that determine the physical properties of these blends. In order to evaluate the morphology of the PCL/PBS blends and its filled nanocomposites, scanning electron microscopic (SEM) and atomic force microscopic (AFM) analysis were conducted. Figure 5.1 shows SEM micrographs of the PCL/PBS blends and the PCL/PBS/(PC/MWCNTs) blend nanocomposites at different blend and masterbatch ratios.

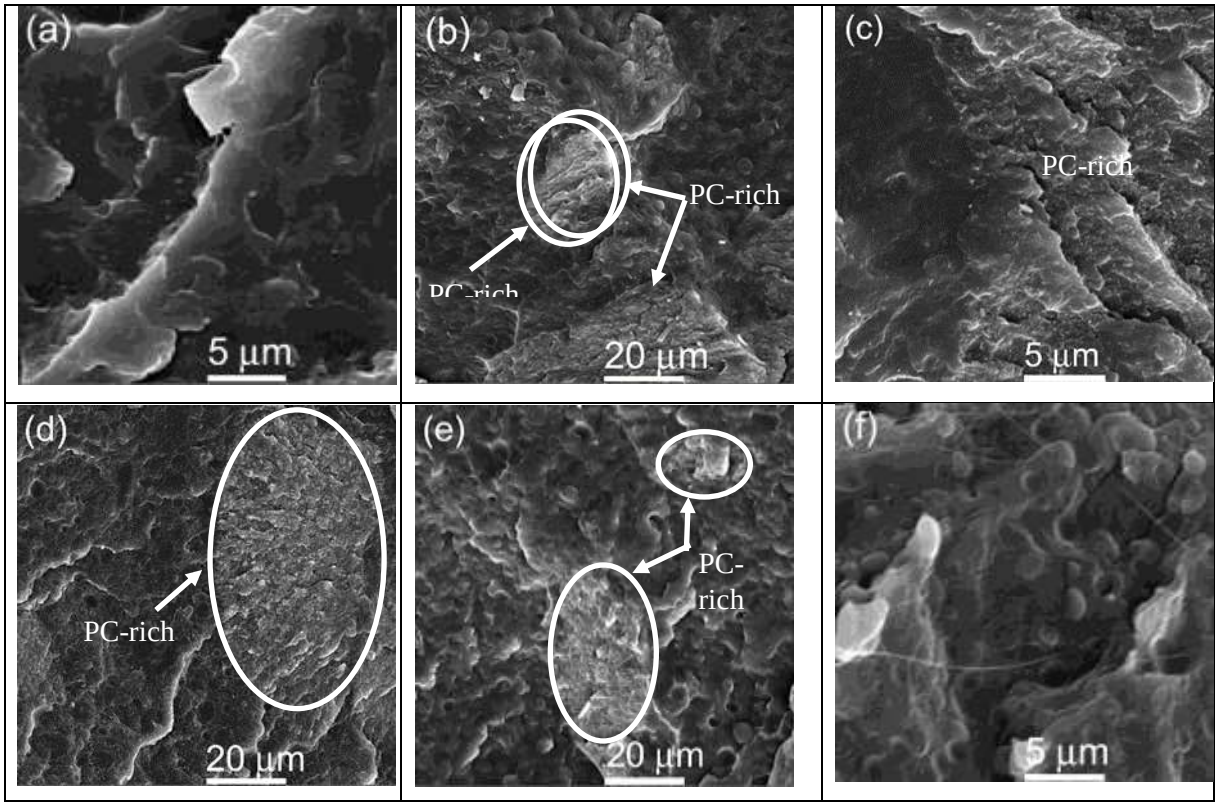

Figure 5.1 SEM images for (a) 30/70/0, (b) 28/65/(6/1), (c) 22/51/(23/4), (d) 51/22/(23/4), (e) 65/28/(6/1) and (f) 70/30/0 w/w PCL/PBS/(PC/MWCNTs) blend nanocomposites.

The SEM images in Figures 5.1(a) and 1(f) show a sea-island morphology with discrete droplets of the minor phase within the matrix of the major phase, typical of immiscible polymer blends. The approximate diameters of the dispersed minor phases are shown in Table 5.2. It can be seen that the size of the minor phase for the 30/70 PCL/PBS blend (Figure 5.1(a)) is smaller than that of the 70/30 PCL/PBS blend (Figure 5.1(f)). There are several factors that determine the final particle size of the dispersed phases in polymer blends, such as surface energy, interfacial tension, polar character, blend

composition, molar mass, viscosity ratio, and differences between the degree of crystallinity of the components in the blend, as well as time, shear stress, and temperature of mixing [21]. Amongst the mentioned factors, it seems as if viscosity ratio plays a major role in the sizes of the dispersed phases. This is because a high-viscosity fluid inhibits motion due to the way its molecules are structured and creates a lot of internal friction giving rise to larger particle sizes [22].

Table 5.2 Particle sizes of the dispersed polymer phases in the PCL/PBS blends.

w/w PCL/PBS/(PC/MWCNTs)	**Dispersed polymer droplets (d_n (μm) / d_v (μm) / D)**
30/70/0	0.4 / 0.6 / 1.4
28/65/(6/1)	3.1 / 3.8 / 1.2
22/51/(23/4)	0.5 / 0.6 / 1.2
51/22/(23/4)	2.9 / 4.3 / 1.5
65/28/(6/1)	2.0 / 3.4 / 1.7
70/30/0	1.3 / 1.5 / 1.2

d_n – number average diameter; d_v – volume average diameter; D – particle size polydispersity; (PC/MWCNTs) is the masterbatch

In the case of the blends filled with the (PC/MWCNTs) masterbatch (Figure 5.1(b), 1(c), 1(d) and 1(e)), the SEM images show three phases: (i) the matrix (either PCL or PBS rich phase depending on the composition), (ii) dispersed polymer droplets of small size (either PCL or PBS rich phase depending on the composition), typically 3 μm or less and (iii) dispersed phases of tens of micron sizes containing large concentrations of MWCNTs, which clearly is the (PC/MWCNTs) masterbatch, and which are indicated in Figure 5.1 with white circles or ellipsoids. However, although most MWCNTs are located in the PC dispersed phases (Figures 5.1(d) and 1(e)), some of the MWCNTs (indicated with a black circle in the AFM images in Figure 5.2) migrated from the dispersed PC phase to the polymer matrix outside the dispersed phase. This is due to the partial miscibility and intimate contact at the interfaces between the PC-rich and PCL-rich phases, or the PC-rich and PBS-rich phases, as previously reported by us [23,24].

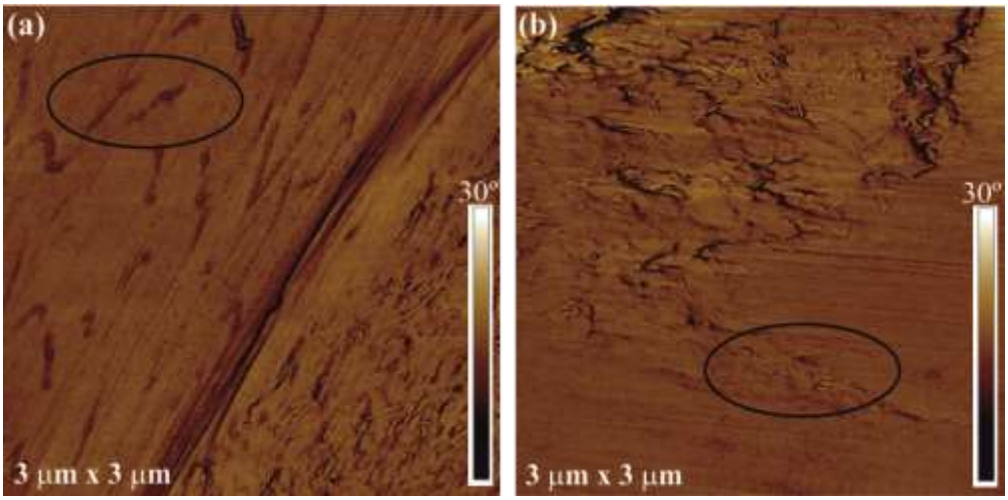

Figure 5.2 AFM images for the (a) 65/28/(6/1) and (b) 51/22/(23/4) w/w PCL/PBS/(PC/MWCNTs) blend nanocomposites.

It is worth noting that when the PCL/PBS blends were loaded with 1 wt% MWCNTs, the sizes of the dispersed polymer droplets for the 65/28/(6/1) w/w PCL/PBS/(PC/MWCNTs) nanocomposite were smaller than those of the 28/65/(6/1) w/w PCL/PBS/(PC/MWCNTs) nanocomposite. When the PCL/PBS blends were loaded with 4 wt% MWCNTs, the sizes of the dispersed polymer droplets were smaller in the 22/51/(23/4) w/w PCL/PBS/(PC/MWCNTs) nanocomposite than those in the 51/22/(23/4) w/w PCL/PBS/(PC/MWCNTs) blend nanocomposite (Table 5.2). The smaller droplets indicate that there is compatibilization between the component phases. However, amongst the nanocomposites investigated in this chapter, the 22/51/(23/4) PCL/PBS/(PC/MWCNTs) nanocomposite is the one giving the smallest particle sizes of the dispersed phase. This is due to the lower interfacial tension values between PBS and the PC/MWCNTs masterbatch compared to those between PCL and the PC/MWCNTs masterbatch (see Table 5.3). At equilibrium the particles will likely disperse in the phase where the affinity between the polymer and the nanoparticles is high.

The contact angles, total surface energies, as well as their dispersive and polar surface components, were calculated using the Owens-Wendt method [12,25,26] through Equations 5.1 and 5.2.

$$\gamma_s = \gamma_s^d + \gamma_s^p \tag{5.1}$$

$$\gamma_1(1 + cos\theta) = 2\sqrt{\gamma_s^d . \gamma_l^d + \gamma_s^p . \gamma_l^p} \tag{5.2}$$

where θ is the contact angle, γ is the surface energy, the subscripts 's' and 'l' respectively indicate solid and liquid, while 'd' and 'p' respectively indicate the dispersive and polar components. If the contact angle of at least two liquids, usually polar and nonpolar liquids with known γ_l^d and γ_l^p values, are measured on a solid surface, the γ_s^d and γ_s^p and the total surface energy (γ_s) of the solid can be calculated by combining Equations 5.2 and 5.3 [27]. The interfacial tensions between the components in a blend were calculated from the surface energy measurement results using the geometric mean equation (Equation 5.3) [12], and the wetting coefficient (Equation 5.4) from the interfacial tensions.

$$\gamma_{12} = \gamma_{1+\gamma_2} - 2\sqrt{\gamma_1^d.\gamma_2^d + \gamma_1^p.\gamma_2^p} \tag{5.3}$$

where γ_{12} = interfacial tension between components 1 and 2 in the blend, γ_1 and γ_2 are the total surface energies of components 1 and 2, γ_1^d and γ_2^d are the dispersive surface energies of components 1 and 2, and γ_1^p and γ_2^p are the polar surface energies of the components in the nanocomposites. The wetting coefficient, w_α, is calculated by using Equation 5.4.

$$w_\alpha = \frac{\gamma_{polymer\ B-Filler} - \gamma_{polymer\ A-Filler}}{\gamma_{polymerA-polymerB}} \tag{5.4}$$

where $\gamma_{polymerB\text{-}Filler}$ is the interfacial tension between polymer B and the filler, $\gamma_{polymerA\text{-}Filler}$ the interfacial tension between polymer A and the filler, and $\gamma_{polymerA\text{-}polymerB}$ the interfacial tension between polymers A and B. The value of the wetting coefficient is normally used to determine where the filler is likely expected to disperse. If $\omega_\alpha < -1$, the particles are predicted to be localised in polymer B, if $\omega_\alpha > 1$, they are dispersed in polymer A, and if the value of ω_α is between -1 and 1, the nanoparticles are likely dispersed on the interface between the two polymers in the blend. In rare cases where the particles are dispersed in both the interface and one of the phases, the third condition does not apply, so that a negative ω_α indicates dispersion of the particles in polymer B as well as the interface, and a positive ω_α indicates dispersion of the particles in polymer A and on the interface [28,29]. The results are summarised in Tables 5.3 and 5.4.

Table 5.3 shows that the polar component of surface energy, γ^p, for the masterbatch is closer to that of PBS. In terms of the interfacial tension values reported in Table 5.4, it can be seen that the interfacial tension between PCL and (PC/MWCNTs) (0.97 mN m^{-1}) is larger than that between PBS and (PC/MWCNTs) (0.36 mN m^{-1}). These results and the -0.26 mN m^{-1} wetting coefficient value suggest that the nanotubes would preferably disperse better in the PBS-rich phase.

Similar results were reported by He *et al*. [11], who introduced MWCNTs to a double crystalline PBS/PCL blends using solution mixing and solvent casting processes. The MWCNTs exhibited a much finer dispersion morphology in the PBS/MWCNT nanocomposite than in the PCL/MWCNT nanocomposite. This was attributed to the wetting coefficient data for MWCNTs introduced into the binary copolymer which was calculated as 1.73 (harmonic-mean equation) or -3.43 (geometric-mean equation). According to the authors, this meant that the MWCNTs were selectively distributed in the PBS phase.

Table 5.3 Summary of surface properties for neat PCL, neat PBS and the (PC/MWCNTs) masterbatch.

Sample	Contact angle/ degree		Surface energy / mN m^{-1}			MFI (g/10 min)
	H_2O	CH_2I_2	γ	γ^d	γ^p	
Neat PCL	59.7 ± 1.3	16.1 ± 0.2	58.4	48.8	9.6	11.5
Neat PBS	35.9 ± 0.7	14.8 ± 0.3	70.7	49.1	21.6	20.9
PC/MWCNTs masterbatch	47.6 ± 1.1	23.7 ± 1.0	63.2	46.6	16.6	5.6

γ = surface energy, γ^d = dispersive component of surface energy, γ^p = polar component of surface energy

Table 5.4 Interfacial tensions and wetting coefficient of the investigated materials.

Component pair	Interfacial tension / mN m^{-1}
PCL/PBS	2.38
PCL/(PC/MWCNTs)	0.97
PBS/(PC/MWCNTs)	0.36
Wetting coefficient (w_α)	-0.26

Taking into account the results presented so far, we can conclude that a fair number of MWCNTs diffused from the PC-rich phase into the PCL-rich and PBS-rich phases, although one would expect, from the interfacial tension results, to find more MWCNTs in the PBS-rich phase. The majority of the MWCNTs were, however, still confined to the PC-rich droplets, despite the partial miscibility of the blends, and the intimate phase boundaries between the different components in the blends.

The ternary morphology obtained for the blends with PC/MWCNT masterbatch, and especially the large sizes of the PC/MWCNTs phases, is obviously not the best as stress transfer may not be ideal, even when the phase boundaries obtained are small. Tuning of the morphology to obtain better mixing would have to be studied by varying extrusion conditions, screw configurations and processing variables in general. However, this study would be outside the scope of the present work.

5.3.2 Non-isothermal DSC

Figure 5.3(a) shows the DSC cooling scans after erasing the thermal history, and Figure 5.3(b) the subsequent heating scans performed at 20 °C min^{-1} for the different investigated samples. Since PBS crystallizes first, its crystallization peak appears at about 60 °C, followed by the crystallization peak of the PCL component at 30 °C. When 30 wt% PCL is added to 70 wt% PBS, there is a shift in the crystallization temperature (T_c) of PBS to higher temperatures. This indicates a nucleation effect in the blend. There are two possible explanations for this observation: (1) transference of the impurities from the PCL phase to the PBS phase, and (2) since the PBS crystallizes first, the PCL droplets may have crystallized by surface induced nucleation on the interphase with the PBS crystallized matrix with nucleation at the interface. However, when 30 wt% PBS was added to 70 wt% PCL, there was fractionated crystallization of the PBS component, and the T_c value of the PCL component shifted to higher temperatures, indicating nucleation with respect to the homopolymer. It is well known that fractionated crystallization occurs when the number of droplets is at least of the same order of magnitude as the number of heterogeneities present in the bulk polymer. Hence, the smaller the droplet size, the higher the probability of fractionated crystallization [30-33]. In this case it is interesting to observe fractionated crystallization in the 70/30 PCL/PBS (d_n=1.3 microns) and not in

the 30/70 PCL/PBS (d_n=0.4 microns). The fractionated crystallization in the 70/30 blend could be due to the interaction between the phases in terms of nucleation.

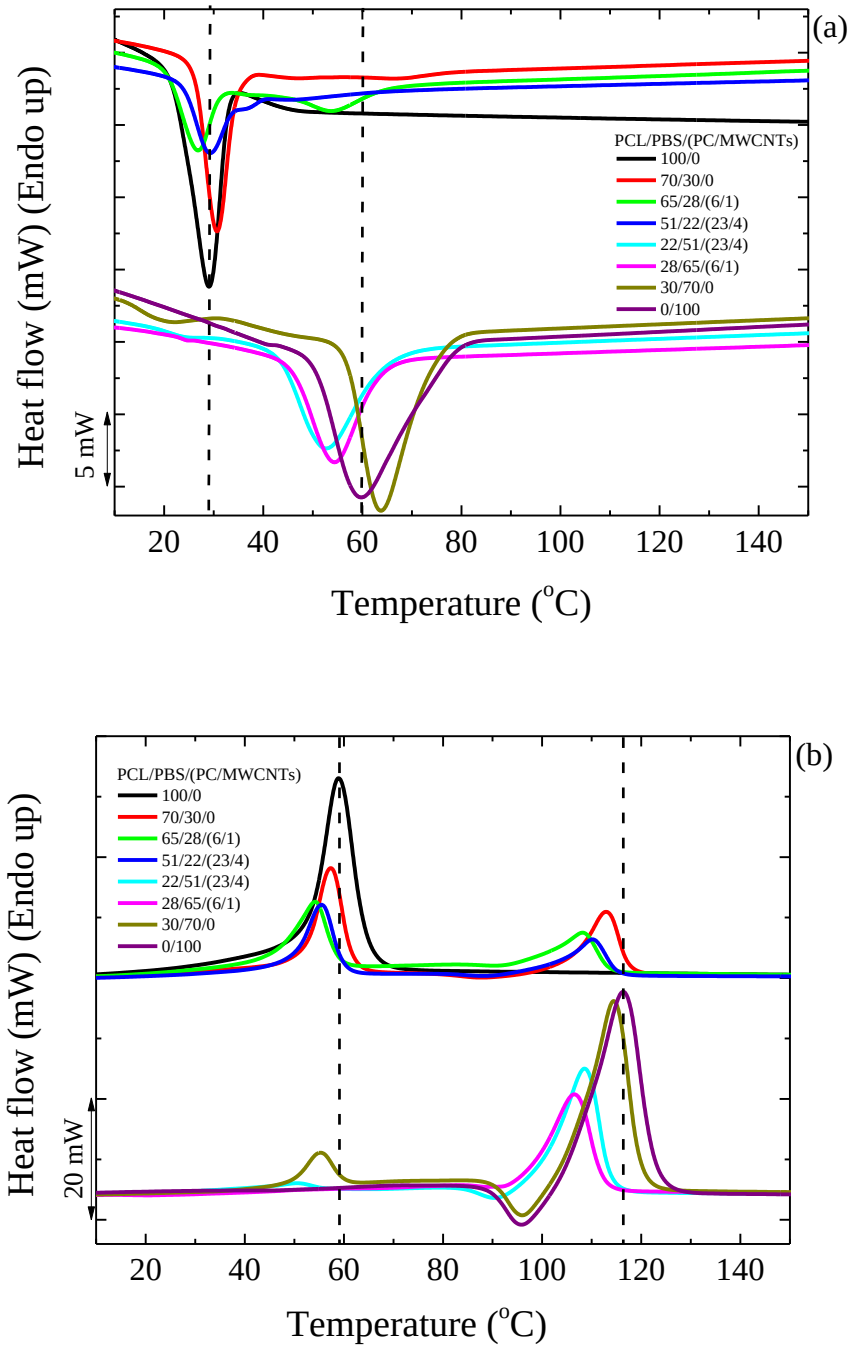

Figure 5.3 DSC (a) cooling and (b) second heating curves for the PCL/PBS blends and their nanocomposites.

When the PCL/PBS blends were loaded with different amounts of PC/MWCNTs masterbatch, the T_c of the PBS-rich nanocomposites shifted to lower temperatures than

those of the neat PBS and the blend with PBS as the major phase. The same is true for the PCL-rich nanocomposites, although the change was less significant. This is due to the competition between two effects: (1) the partial miscibility of the PC-rich, the PCL-rich, and the PBS-rich phases, and (2) the nucleation effect of the MWCNTs. Miscibility between the different components in the blend tends to decrease the values of T_c, while the nucleation effect tends to increase the T_c values. In this case, since the MWCNTs and PC are simultaneously added, the miscibility effect dominates because of the decrease in the T_c values of the nanocomposites.

In the subsequent heating scans shown in Figure 5.3(b), the melting temperature (T_m) of the PCL/PBS blends and its filled nanocomposites decreased (more especially in the nanocomposites) compared to the neat materials. Normally, when the blends are immiscible, the T_m is not affected. In this case, the decrease in the melting temperature values is due to miscibility effects. The PCL melting peak in the 28/65/(6/1) PCL/PBS/(PC/MWCNTs) nanocomposite is almost invisible. This is probably due to the PCL dissolving in the rigid PC chains, making it difficult for PCL to crystallize, therefore forming fewer crystals.

To further examine the results presented in Figure 5.3, the T_c and T_m values were plotted as a function of sample composition in Figure 5.4. Figure 5.4(a) shows that the 30/70 PCL/PBS blend seems to be slightly more nucleated than the 70/30 PCL/PBS blend. This is because of the smaller particle size observed in the 30/70 blend (d_n = 0.4 microns) compared to that of the 70/30 blend (d_n = 1.3 microns), giving rise to a better dispersion and enhanced nucleation. The decrease in the T_c values for the nanocomposites is attributed to the competition between partial miscibility with the PC-rich phase and the nucleation effect of the MWCNTs. It is clear that miscibility is the dominating factor.

In Figure 5.4(b), the changes in T_m are most significant when the masterbatch is added, because of the partial miscibility between the PCL-rich and PC-rich phases, as well as the PBS-rich and PC-rich phases. In the PBS-rich phase nanocomposites, the decrease in T_m is more significant than in the PCL-rich nanocomposites. This is an indication that the PBS-rich phase is more compatible with the PC-rich phase than the PCL-rich phase, as indicated by the interfacial tension values in Table 5.4.

Figure 5.5 shows the normalized crystallization and melting enthalpy values for all the samples. The normalized enthalpies for the PCL/PBS blends are almost the same as those of the homopolymers. This indicates that the total crystallinities of each of the two polymers are not significantly influenced by the presence of the other polymer in the

blend. However, in the presence of the masterbatch, the normalized crystallization and melting enthalpy values for both polymers are lower than those of the neat polymers. This is due to the PC that immobilized the PCL and PBS chains at the interface and reduces the non-isothermal crystallization rate.

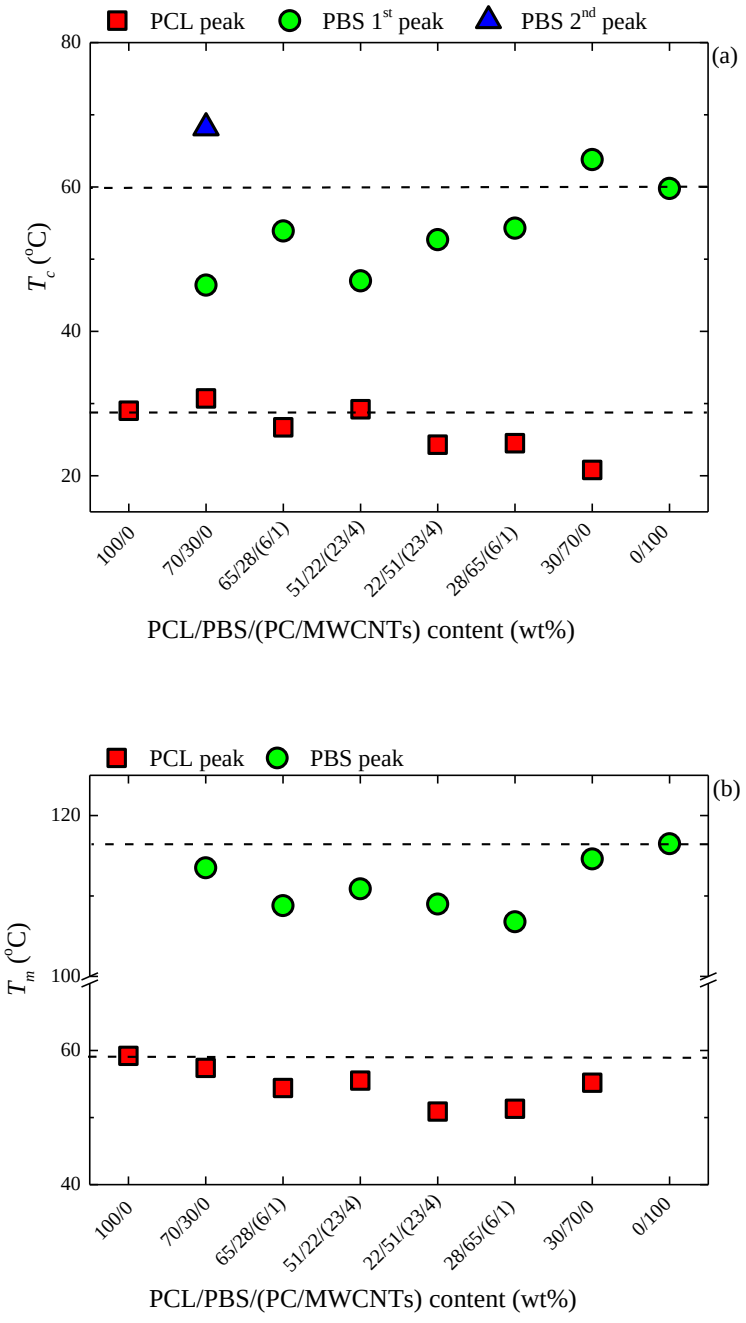

Figure 5.4 DSC (a) crystallization and (b) second heating melting temperatures for the PCL/PBS blends and the PCL/PBS/(PC/MWCNTs) nanocomposites.

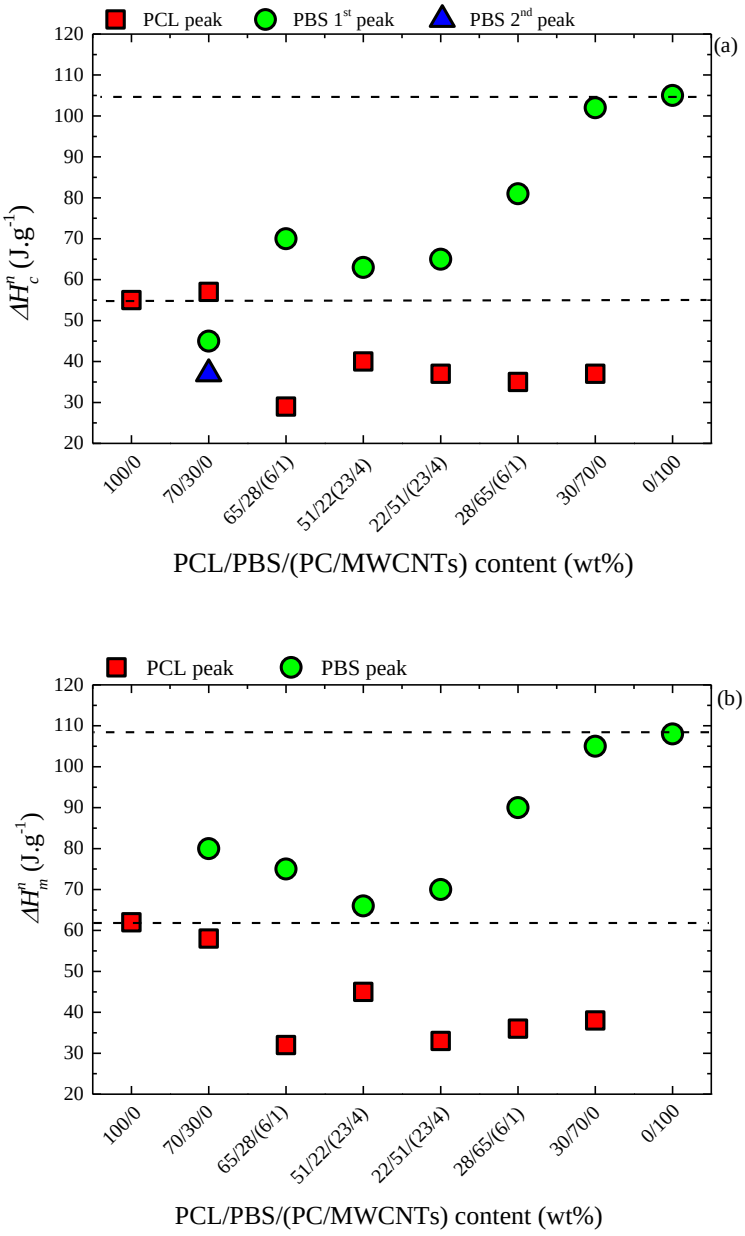

Figure 5.5 Normalized (a) crystallization and (b) melting enthalpies for the PCL/PBS blends and the PCL/PBS/(PC/MWCNTs) nanocomposites.

5.3.3 Overall isothermal crystallization studied by DSC

The influence of the PC/MWCNTs masterbatch on the isothermal crystallization kinetics of the PCL/PBS blends is presented in this section. The blend consists of two crystallisable components, i.e. PCL and PBS. The inverse of the half crystallization time ($1/t_{50\%}$) as a function of the isothermal crystallization temperature (T_c) for some of the investigated samples is shown in Figure 5.6. PBS clearly crystallizes at a higher

temperature than PCL. The experimental and extrapolated data was obtained using the Lauritzen and Hoffman (LH) theory, which is explained in detail in Section 5.3.3.2.

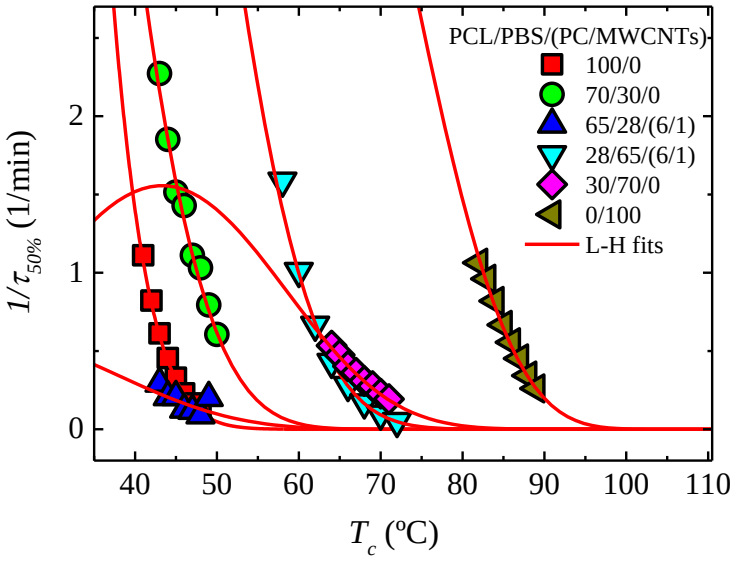

Figure 5.6 Inverse of half crystallization time ($1/t_{50\%}$) as a function of isothermal crystallization temperature (T_c) for neat PCL, neat PBS, the PCL/PBS blends and the nanocomposites. The red solid lines represent fits to the LH theory.

Neat PBS crystallizes faster than the 30/70 PCL/PBS blend. If the 30/70 PCL/PBS blend is immiscible, one would not expect a change in the kinetics unless there is a change in nucleation. Since the 30/70 blend shows nucleation effects, an increase in the crystallization rate is expected, and not a decrease as observed in Figure 5.6. We cannot currently explain this contradiction, but further experiments will be performed to clarify this issue. When the PC/MWCNTs masterbatch is added to the 30/70 PCL/PBS blend, the crystallization rate is lower than that of neat PBS and the blend. This is because of the partial miscibility between the PC-rich and PCL-rich phases as well as the PC-rich and PBS-rich phases. Miscible PC chains (which are more rigid than either PCL or PBS chains) within PCL-rich and PBS-rich phases can decrease the rate of crystallization.

Contrary to what was observed for PBS, the 70/30 PCL/PBS blend crystallizes faster than neat PCL. This is attributed to nucleation, because PBS crystallizes first and PCL probably nucleates on the already crystallized PBS at the interface between the two polymers. The blend with the masterbatch shows a slightly lower crystallization rate. This is due to the competition between the nucleation of the MWCNTs and the partial

miscibility with PC. However, the miscibility effect obviously dominated, giving rise to a lower crystallization rate.

It is worth noting that the difference between the crystallization rate of neat PBS and the PBS-rich nanocomposite is much larger than that between the neat PCL with the PCL-rich nanocomposite. This suggests that the PBS-rich phase is more miscible with the PC than the PCL-rich phase.

5.3.3.1 Fitting DSC isothermal data to the Avrami model

The data obtained during the isothermal crystallization experiments were analysed using the Avrami equation (Equation 5.5) [34].

$$1 - V_c(t - t_0) = \exp(-K(t - t_0)^n) \qquad (5.5)$$

where t is the experimental time, t_0 is the induction time, V_c is the relative volumetric transformed fraction, n is the Avrami index, and K is the overall crystallization rate constant. The procedure used to perform the fittings to the data was developed by Lorenzo *et al*. [19]. The kinetic parameters for all the investigated samples are plotted in Figure 5.7 and tabulated in Table C.1.

Figure 5.7(a) shows $1/t_{50\%}$-values as a function of T_c, the trend of which was explained earlier in the discussion (Section 5.3.3). A similar trend was obtained with the $K^{1/n}$-values of the Avrami model (see Figure 5.7(b)), since this constant is also related to the overall crystallization rate. Figure 5.7(c) shows the Avrami index values, n, for all the samples. In the case of the PCL-rich samples, neat PCL and the 70/30 blend have n-values between 2.5 and 3.0. This is probably due to the development of a spherulitic morphology with instantaneous nucleation. However, for its filled nanocomposite (65/28/(6/1) PCL/PBS/(PC/MWCNTs)), the value of n is between 1.5 and 2.0, which is approximately 2.0, indicating instantaneous axialites. It is known that the addition of a nucleating agent can cause the Avrami index values to change from 3.0 to 2.0 (as the dimensionality of growth can switch from 3D to 2D when the nucleation density is enhanced) [19,34,35]. It was demonstrated in our previous study that the MWCNTs nucleate the PCL-rich phase [23]. The carbon nanotubes therefore affect the nucleation and the resultant morphology, while the crystallization rate is determined by the miscibility between the components.

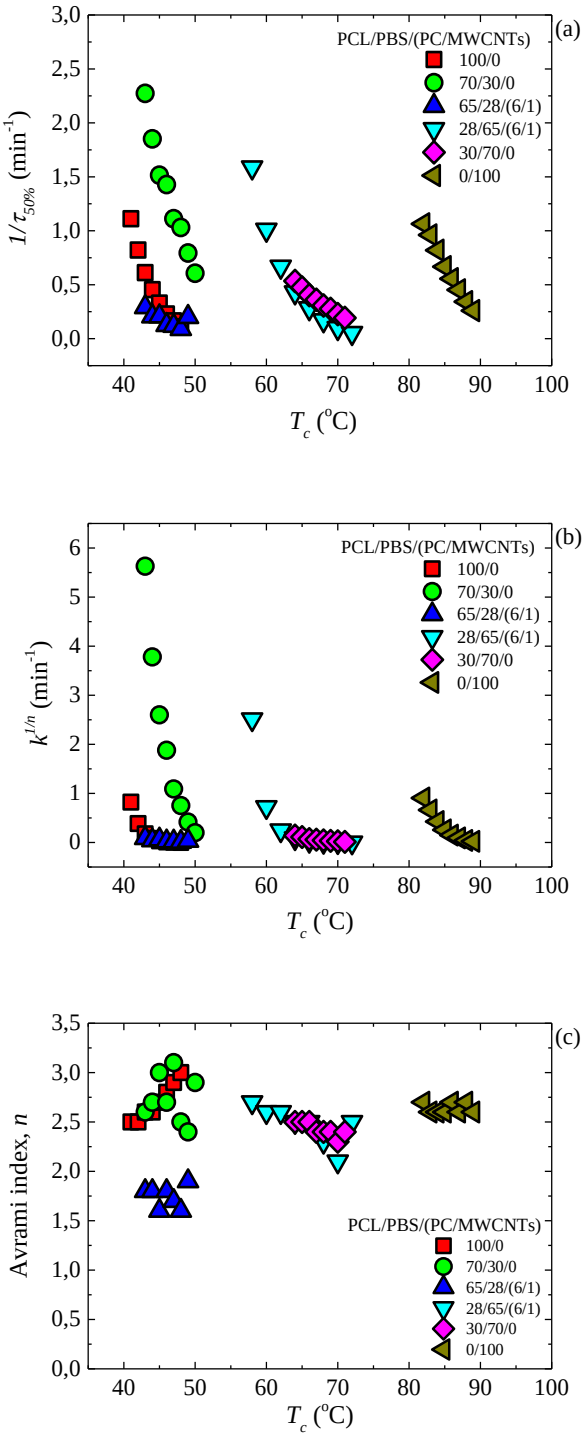

Figure 5.7 (a) Inverse of half crystallization times ($1/t_{50\%}$), (b) normalized crystallization constant of the Avrami model ($K^{1/n}$), and (c) Avrami index (n) as a function of the isothermal crystallization temperature (T_c) for all the samples.

The Avrami index values for neat PBS are within the range of 2.5-2.7, which is close to 3.0 indicating spherulitic morphology with instantaneous nucleation. For the

blend and its nanocomposite, the *n*-values can be averaged to 2.3. This is because of a larger number of nucleation sites, which caused the formation of more crystals with an accompanying decrease in crystal growth. A larger number of 2D axialites probably formed in this case.

5.3.3.2 Overall isothermal crystallization data analysed by the Lauritzen–Hoffman model

The overall crystallization kinetics is determined by contributions of nucleation and growth. The Lauritzen–Hoffman (LH) nucleation and growth theory can be applied to the isothermal crystallization kinetics data collected from DSC. Figure 5.6 shows solid lines that represent the mathematical fit of the LH theory, which can be applied to the DSC overall crystallization data according to Equation (5.6).

$$\frac{1}{\tau_{50\%}}(T) = \frac{1}{\tau_0}\exp\left(\frac{-U^*}{R(T_c - T_\infty)}\right)\exp\left(\frac{-K_g^\tau}{T_c\Delta T_f}\right), \qquad (5.6)$$

where $1/\tau_{50\%}$ is the inverse of the experimental half-crystallization time, $1/\tau_0$ is a pre-exponential factor that includes nucleation and growth, U^* is the activation energy for the transport of the chains to the growth front (a value of 1500 cal mol^{-1} is usually employed), R is the gas constant, T_c is the isothermal crystallization temperature (K), T_∞ is the temperature at which chain mobility ceases (usually taken as T_g – 30 K), ΔT is the supercooling ($T_m^o - T_c$), T_m^o is the equilibrium melting temperature calculated for each blend (see Table 5.5), and K_g^τ is a constant related to the energy barrier for crystallization and growth. The value of K_g^τ is given by Equation (5.7) according to the LH theory.

$$K_g^\tau = \frac{jb_0\sigma\sigma_e T_m^0}{k\Delta h_f}, \qquad (5.7)$$

where b_0 is the width of the chain, σ is the lateral surface free energy, σ_e is the fold surface free energy, k is the Boltzmann constant and Δh_f is the heat of fusion of a perfect crystal. The parameter j is determined by the operating regime and was taken as 2 for regime II (note that j is equal to 4 for regime I and III). The product $\sigma\sigma_e$ is obtained from the values

of K_g^{τ}, according to Equation (5.7). Equations 5.8 and 5.9 allow the calculation of σ (and therefore σ_e) and q, the work done by the chain to form a fold.

$$\sigma = 0.1\Delta h_f\sqrt{a_0 b_0} \tag{5.8}$$

$$q = 2a_0 b_0 \sigma_e \tag{5.9}$$

where a_0b_0 is the cross-sectional area of the chain. To obtain the parameters of the LH theory, the following values were used: T_g = 213 K, T_g – 30 K, ΔH = 163 J g^{-1}, a_0 = 4.52 Å, b_0 = 4.12 Å, p_c = 1.1 g cm^{-3}, U^* = 1500 cal mol^{-1}. The LH parameters for all the samples are tabulated in Table 5.5. It can be seen that there is a general reduction in the K_g^t values of the PCL-rich samples. The same however, is not observed for the PBS-rich samples. In this case the K_g^t values are of the same order of magnitude. This is because K_g^t is a factor proportional to the energy barrier for both nucleation and growth. The trend in the other LH parameters (i.e., σ_e and q) is the same as that shown by K_g^t.

Table 5.5 Parameters from the isothermal crystallization kinetics analyses for the PCL/PBS blends and the PCL/PBS/(PC/MWCNTs) nanocomposites.

w/w PCL/PBS/(PC/MWCNTs)	T^o_m (K)	K^t_g x 10^5	σ	σ_e	q x 10^{-12}	R^2
100/0	373.0	4.52	8.08	474.90	1.75	0.9999
70/30/0	371.4	1.43	8.08	154.74	0.571	0.9916
65/28/(6/1)	369.8	0.96	8.08	104.24	0.385	0.9041
28/65/(6/1)	375.3	1.53	8.08	159.82	0.590	0.9957
30/70/0	379.8	1.19	8.08	123.07	0.454	0.9985
0/100	394.0	1.24	8.08	123.45	0.456	0.9974

5.3.4 Thermal conductivity

Figure 5.8 shows the thermal conductivity values for all the investigated samples. The homopolymers and the neat blends are typical insulators, hence their low thermal conductivity values (between 0.07 and 0.2 W m K^{-1}).

The introduction of the masterbatch increased the thermal conductivity of the blend nanocomposites. This is because the carbon nanotubes have high thermal conductivities

(in the range between 650 and 10,000 W m K^{-1}) [36]. However, the thermal conductivity value of the 28/65/(6/1) sample is significantly lower than those of the other nanocomposites. The reason for this is probably the large number average particle diameter (d_n = 3.1 microns) of the dispersed phase that gives rise to a weaker interaction. This increased the acoustic impendance, which resulted in a large thermal contact resistance at the interface and a reduction in the thermal conductivity value of this nanocomposite.

In the case of the 4 wt% MWCNTs containing nanocomposites, the 22/51/(23/4) nanocomposite has a slightly higher thermal conductivity than the 51/22/(23/4) nanocomposite. The reason for this is probably the smaller and better dispersed MWCNTs particles in the nanocomposite. The smaller dispersed particles introduced more phonon scattering interfaces at the boundaries and facilitated better phonon transport due to the larger thermal contact areas.

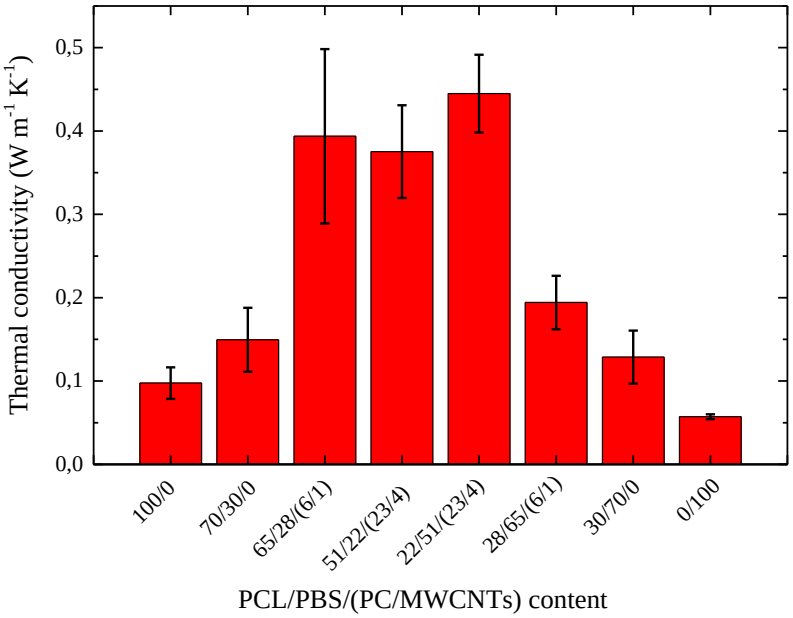

Figure 5.8 Influence of PC/MWCNTs masterbatch content on the thermal conductivities of the nanocomposites.

5.3.5 Tensile properties

Figure 5.9 shows typical stress-strain curves obtained for all the samples, and Table 5.6 summarizes the tensile testing results. The Young's modulus of the PCL/PBS blends is lower than that of the homopolymers for both PCL and PBS. This is associated with the

weak interaction between the two polymers. The addition of the PC/MWCNTs masterbatch to the PCL/PBS blends generally showed little change in the Young's modulus of the nanocomposites, taking into account the experimental error indicated by the standard deviation values. This may be due to the miscibility effect.

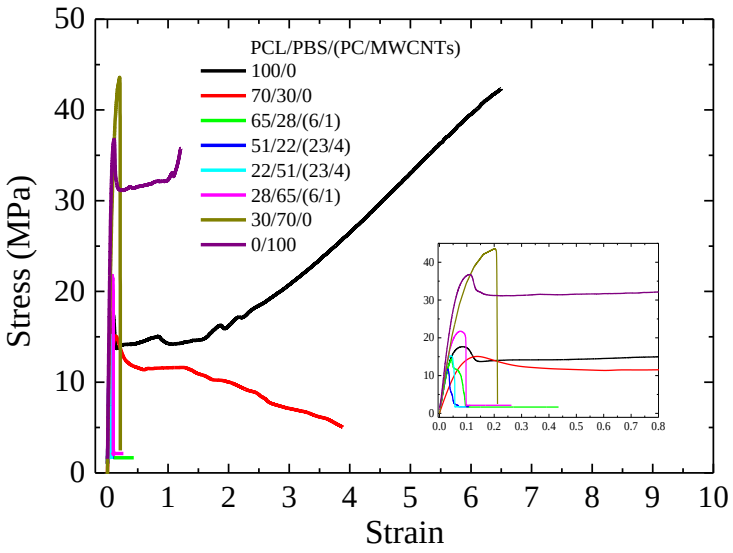

Figure 5.9 Stress-strain curves for neat PCL, neat PBS, PCL/PBS blends and its filled nanocomposites.

Table 5.6 Summary of tensile testing results for all the samples.

w/w PCL/PBS/ (PC/MWCNTs)	σ_y / MPa	ε_y / %	σ_b / MPa	ε_b / %	E / MPa
100/0	16.2 ± 1.9	14.2 ± 8.0	34.3 ± 12.9	578 ± 151	388 ± 29
70/30/0	15.3 ± 1.6	12.4 ± 13.0	12.1 ± 4.2	520 ± 142	274 ± 2
65/28/(6/1)	15.7 ± 1.3	4.4 ± 0.2	7.9 ± 1.4	7.7 ± 0.3	457 ± 39
51/22/(23/4)	-	-	10.6 ± 1.8	4.0 ± 0.8	432 ± 43
22/51/(23/4)	-	-	8.6 ± 2.7	5.8 ± 0.4	484 ± 35
28/65/(6/1)	-	-	19.7 ± 0.3	8.7 ± 0.8	448 ± 22
30/70/0	-	-	28.4 ± 7.5	49.5 ±0.9	438 ± 11
0/100	-	-	38.1± 2.1	210 ± 110	579 ± 139

σ_y – stress at yield; ε_y – strain at yield; σ_b – stress at break; ε_b – strain at break; E – Young's modulus

The stress and strain at break of the samples show a decrease after blending and after the incorporation of the masterbatch (Table 5.6). This is the result of the formation of the sea island morphology, and a very large PC-rich dispersed phase acting as a stress concentration region. Cracks nucleate at the dispersed phases and grow to produce earlier fracture. Yield stress and strain was only observed for the PCL-rich samples (due to the much higher ductility of PCL), and its values are decreasing with the addition of PBS and the incorporation of the masterbatch. This is attributed to the miscibility effect. Both PBS and PC restrict the polymer chain mobility and form defect centres.

5.4 Conclusions

Based on the SEM, AFM and surface property results, it can be concluded that the PCL/PBS blends are immiscible with discrete droplets of the minor phase within the matrix of the major phase. The nanocomposites prepared in this work are partially miscible. Three phases were formed: (i) the matrix (either PCL or PBS rich phase depending on the composition), (ii) dispersed polymer droplets of small size (either PCL or PBS rich phase depending on the composition), and (iii) the dispersed aggregates of tens of micron sizes which were clearly the PC/MWCNTs masterbatch. Due to the partial miscibility and the establishment of PC-rich, PCL-rich and PBS-rich phases, some of the MWCNTs migrated from the dispersed phase to the polymer matrix as evidenced by the AFM images.

Standard DSC measurements demonstrated an increase in T_c for the PCL/PBS blends due to a nucleation effect. There are two possible explanations for this observation: (1) transference of the impurities from the PCL phase to the PBS phase, and (2) since the PBS crystallizes first, the PCL droplets may have crystallized by surface induced nucleation on the interface with the PBS crystallized matrix and nucleated at the interphase. The nanocomposites showed a decrease in T_c values. This was attributed to a competition between two effects: (1) the partial miscibility of the PC-rich with the PCL-rich and PBS-rich phases, and (2) the nucleation effect of the MWCNTs. The miscibility effect dominated because of the decrease in the T_c values of the nanocomposites.

Isothermal crystallization experiments performed by DSC showed a decrease in the overall crystallization rates of the nanocomposites as a result of the competition between nucleating effect and miscibility. Since the PC-rich phase is partially miscible with the PCL-rich and PBS-rich phases, the miscible PC chains within PCL-rich and PBS-rich

phases can decrease their rate of crystallization. The difference between the crystallization rate of neat PBS and the PBS-rich nanocomposite was much larger than that of the neat PCL and the PCL-rich nanocomposite. This confirmed that the PBS-rich phase is more miscible than the PCL-rich phase with the PC-rich phase.

The thermal conductivities of the nanocomposites were generally enhanced with the addition of the masterbatch, while the tensile properties of the nanocomposites varied, which was ascribed to the competition between the nucleation and miscibility effects.

5.5 References

[1] J.H. Song, R. J. Murphy, R. Narayan, G.B.H. Davies. Biodegradable and compostable alternatives to conventional plastics. Philosophical Transactions of the Royal Society B 2009; 364:2127-2139.
DOI: 10.1098/rstb.2008.0289

[2] A. Bhatia, R.K. Gupta, S.N. Bhattacharya, H.J. Choi. Compatibility of biodegradable poly(lactic acid) (PLA) and poly(butylene succinate) (PBS) blends for packaging application. Korea-Australia Rheology Journal 2007; 19:125-131.

[3] M. Gigli, A. Negroni, G. Zanaroli, N. Lotti, F. Fava, A. Munari. Environmentally friendly PBS-copolyesters containing PEG-like subunit: Effect of block length on solid-state properties and enzymatic degradation. Reactive & Functional Polymers 2013; 73:764-771.
DOI: 10.1016/j.reactfunctpolym.2013.03.007

[4] L.M. Robeson. Polymer blends. A comprehensive review. Carl Hanser Verlag: München (2007).

[5] P. Nugroho, H. Mitomo, F. Yoshii, T. Kume, K. Nishimura. Improvement of processability of PCL and PBS blend by irradiation and its biodegradability. Macromolecular Materials and Engineering 2001; 286:316-323.
DOI: 10.1002/1439-2054(20010501)286:5<316::AID-MAME316>3.0.CO;2-N

[6] J. John, R. Mani, M. Bhattacharya. Evaluation of compatibility and properties of biodegradable polyester blends. Journal of Polymer Science: Part A: Polymer Chemistry 2002; 40:2003-2014.
DOI: 10.1002/pola.10297

[7] Z. Qiu, M. Komura, T. Ikehara, T. Nishi. Miscibility and crystallization behavior of biodegradable blends of two aliphatic polyesters. Poly(butylene succinate) and poly(ε-caprolactone). Polymer 2003; 44:7749-7756.
DOI: 10.1016/j.polymer.2003.10.013

[8] M.M. Reddy, A.K. Mohanty, M. Misra. Biodegradable blends from plasticized soy meal, polycaprolactone, and poly(butylene succinate). Macromolecular Materials and Engineering 2012; 297:455-463.
DOI: 10.1002/mame.201100203

[9] E. Can, S. Bucak, E. Kınacı , A.C. Çalıkoğlu, G.T. Köse. Polybutylene succinate (PBS)-polycaprolactone (PCL) blends compatibilized with poly(ethylene oxide)-block poly(propylene oxide)-blockpoly(ethylene oxide) (PEO-PPO-PEO) copolymer for biomaterial applications. Polymer-Plastics Technology and Engineering 2014; 53:1178-1193.
DOI: 10.1080/03602559.2014.886119

[10] Q. Liu, X.M. Zhou. Preparation of poly(butylene succinate)/poly(ε-caprolactone) blends compatibilized with poly(butylene succinate-co-ε-caprolactone) copolymer. Journal of Macromolecular Science, Part A: Pure and Applied Chemistry 2015; 52:625-629.
DOI: 10.1080/10601325.2015.1050634

[11] M.J. He, W.X. Xiao, H. Xie, C.J. Fan, L. Du, X.Y. Deng, K.K. Yang, Y.Z. Wang. Facile fabrication of ternary nanocomposites with selective dispersion of multi-walled carbon nanotubes to access multi-stimuli-responsive shape-memory effects. Materials Chemistry Frontiers 2017; 1:343-353.
DOI: 10.1039/c6qm00047a

[12] D. Wu, D. Lin, J. Zhang, W. Zhou, M. Zhang, Y. Zhang, D. Wang, B. Lin. Selective localization of nanofillers: Effect on morphology and crystallization of PLA/PCL blends. Macromolecular Chemistry and Physics 2011; 212:613 626.
DOI: 10.1002/macp.20100057

[13] L. Li, W.H. Ruan, M.Q. Zhang, M.Z. Rong. Studies on the selective localization of multi-walled carbon nanotubes in blends of poly(vinylidene fluoride) and polycaprolactone. eXPRESS Polymer Letters 2015; 9:77-83.
DOI: 10.3144/expresspolymlett.2015.8

[14] A. Wurm, D. Lellinger, A.A. Minakov, T. Skipa, P. Pötschke, R. Nicula, I. Alig, C. Schick. Crystallization of poly(ε-caprolactone)/MWCNT composites: A combined

SAXS/WAXS, electrical and thermal conductivity study. Polymer 2014; 55:2220-2232.
DOI: 10.1016/j.polymer.2014.02.069

[15] S.J. Chin, S. Vempati, P. Dawson, M. Knite, A. Linarts, K. Ozols, T. McNally. Electrical conduction and rheological behaviour of composites of poly(ε-caprolactone) and MWCNTs. Polymer 2015; 58:209-221.
DOI: 10.1016/j.polymer.2014.12.034

[16] P. Pötschke, T. Villmow, B. Krause. Melt mixed PCL/MWCNT composites prepared at different rotation speeds: Characterization of rheological, thermal, and electrical properties, molecular weight, MWCNT macrodispersion, and MWCNT length distribution. Polymer 2013; 54:3071-3078.
DOI: 10.1016/j.polymer.2013.04.012

[17] T. Wang, H. Wang, H. Li, Z. Gan, S. Yan. Banded spherulitic structures of poly(ethylene adipate), poly(butylene succinate) and in their blends. Physical Chemistry Chemical Physics 2009; 11:1619-1627.
DOI: 10.1039/b817597g

[18] G.R. Kasaliwal, A. Göldel, P. Pötschke, G. Heinrich. Influences of polymer matrix melt viscosity and molecular weight on MWCNT agglomerate dispersion. Polymer 2011; 52:1027-1036.
DOI: 10.1016/j.polymer.2011.01.007

[19] A.T. Lorenzo, M.L. Arnal, J. Albuerne, A.J. Müller. DSC isothermal polymer crystallization kinetics measurements and the use of the Avrami equation to fit the data: Guidelines to avoid common problems. Polymer Testing 2007; 26:222-231.
DOI: 10.1016/j.polymertesting.2006.10.005

[20] J.D. Hoffman, J.J. Weeks. Melting process and the equilibrium melting temperature of polychlorotrifluoroethylene. Journal of Research of the National Bureau of Standards - A. Physics and Chemistry 1962; 66:13-28.
DOI: 10.6028/jres.066A.003

[21] L.A. Utracki, C. Wilkie. Polymer Blends Handbook, 2nd Edition. Springer, Netherlands (2014).

[22] M.A. Huneault, F. Mighri, G.H. Ko, F. Watanabe. Dispersion in high viscosity ratio polyolefin blends. Polymer Engineering and Science 2004; 41:672-683.
DOI: 10.1002/pen.10762

[23] T.P. Gumede, A.S. Luyt, M.K. Hassan, R.A. Pérez-Camargo, A. Tercjak, A.J. Müller. Morphology, nucleation, and isothermal crystallization kinetics of poly(ε-caprolactone) mixed with a polycarbonate/MWCNTs masterbatch. Polymers 2017; 9:709.
DOI: 10.3390/polym9120709

[24] T.P. Gumede, A.S. Luyt, R.A. Pérez-Camargo, A. Tercjak, A.J. Müller. Morphology, nucleation, and isothermal crystallization kinetics of poly(butylene succinate) mixed with a polycarbonate/MWCNT masterbatch. Polymers 2018; 10:424.
DOI: 10.3390/polym10040424

[25] H. Xiu, H.W. Bai, C.M. Huang, C.L. Xu, X.Y. Li, Q. Fu. Selective localization of titanium dioxide nanoparticles at the interface and its effect on the impact toughness of poly(Llactide)/poly(ether)urethane blends. eXPRESS Polymer Letters 2013; 7:261-271.
DOI: 10.3144/expresspolymlett.2013.24

[26] H. Yang, X. Zhang, C. Qu, B. Li, L. Zhang, Q. Zhang, Q. Fu. Largely improved toughness of PP/EPDM blends by adding nano-SiO2 particles. Polymer 2007; 48:860-869.
DOI: 10.1016/j.polymer.2006.12.022

[27] D.K Owens, R.C. Wendt. Estimation of the surface free energy of polymers. Journal of Applied Polymer Science 1969; 13:1741-1747.
DOI: 10.1002/app.1969.070130815

[28] X. Wang, K.-J. Xu, X.-B.Xu, S.-J. Park, S. Kim. Selective particle distribution and mechanical properties of nano-CaCO3/ethylene-propylene-diene terpolymer/polypropylene composites with high content of nano-$CaCO_3$. Journal of Applied Polymer Science 2009; 113:2485-2491.
DOI: 10.1002/app.30078

[29] F. Fenouillot, P. Cassagnau, J.C. Majeste. Uneven distribution of nanoparticles in immiscible fluids: Morphology development in polymer blends. Polymer 2009; 50:1333-1350.
DOI: 10.1016/j.polymer.2008.12.029

[30] M.L. Arnal, V. Balsamo, F. López-Carrasquero, J. Contreras, M. Carrillo, H. Schmalz, V. Abetz, E. Laredo, A.J. Müller. Synthesis and characterization of

polystyrene-*b*-poly(ethylene oxide)-*b*-poly(ε-caprolactone) block copolymers. Macromolecules 2001; 34:7973-7982.
DOI: 10.1021/ma011058g

[31] M.L. Arnal, M.E. Matos, R.A. Morales, O.O. Santana, A.J. Müller. Evaluation of the fractionated crystallization of dispersed polyolefins in a polystyrene matrix. Macromolecular Chemistry and Physics 1998; 199:2275-2288.
DOI:10.1002/(SICI)1521-3935(19981001)199:10<2275::AID-MACP2275>3.0.CO;2-#

[32] V. Balsamo, L.M. Gouvena. Interplay of fractionated crystallization and morphology in polypropylene/poly(ε-caprolactone) blends. Journal of Polymer Science Part B: Polymer Physics 2007; 45:1365-1379.
DOI: 10.1002/polb.21137

[33] R.V. Castillo, A.J. Müller, J. Raquez, P. Dubois. Crystallization kinetics and morphology of biodegradable double crystalline PLLA-*b*-PCL diblock copolymers. Macromolecules 2010; 43:4149-4160.
DOI: 10.1021/ma100201g

[34] M. Avrami. Granulation, phase change, and microstructure kinetics of phase change III. Journal of Chemical Physics 1941; 9:177-184.
DOI: 10.1063/1.1750872

[35] R.A. Pérez, J.V. López, J.N. Hoskins, B. Zhang, S.M. Grayson, M.T. Casas, J. Puiggalí, A.J. Müller. Nucleation and antinucleation effects of functionalized carbon nanotubes on cyclic and linear poly(ε-caprolactones). Macromolecules 2014; 47:3553-3566.
DOI: 10.1021/ma5005869

[36] M. Bhattacharya. Review: Polymer nanocomposites – A Comparison between carbon nanotubes, graphene, and clay as nanofillers. Materials 2016; 9:1-35.
DOI: 10.3390/ma904026234

CHAPTER 6

General conclusions

According to the results presented in this thesis, it can be concluded that PCL and PBS blends are immiscible, with discrete droplets of the minor phase within the matrix of the major phase. The nanocomposites prepared in this work were partially miscible, where PC-rich, PCL-rich and PBS-rich phases were formed. Due to the partial miscibility and the establishment of PC-rich, PCL-rich and PBS-rich phases, a fair number of MWCNTs diffused from the PC-rich phase to the PCL-rich and PBS-rich phases. However, the extent of miscibility was different for each system. The polar component surface energy, interfacial tension and isothermal crystallization results suggested that the MWCNTs would preferably disperse better into the PBS-rich phase than the PCL-rich phase.

Standard DSC results for PCL/PBS blends, PCL/(PC/MWCNTs) and PBS/(PC/MWCNTs) nanocomposites showed an increase in T_c due to a nucleation effect. The nucleation effect in the blends was attributed to: (1) transference of the impurities from the PCL phase to the PBS phase, and (2) since the PBS crystallized first, the PCL droplets may have crystallized by surface induced nucleation on the interface with the PBS crystallized matrix and nucleate at the interphase. In the case of PCL/(PC/MWCNTs) and PBS/(PC/MWCNTs) nanocomposites the nucleation effect was due to the MWCNTs that penetrated the PCL-rich and PBS-rich phases. For the PCL/PBS/(PC/MWCNTs) nanocomposites, there was a decrease in the T_c values. This was due to a competition between two effects: (1) the partial miscibility of the PC-rich phase with the PCL-rich and PBS-rich phases, and (2) the nucleation effect of the MWCNTs. The decrease in the T_c values indicated that miscibility was the dominating effect determining the crystallization of PCL and PBS in these nanocomposites.

Isothermal crystallization experiments performed by DSC showed an increase in the overall crystallization rates of PCL with increases in MWCNT contents as a result of their nucleating effect. For the PBS/(PC/MWCNTs) nanocomposites, the isothermal crystallization rate also increased with low contents of MWCNTs (0.5 wt%), went through a maximum and then showed a decrease, probably because of MWCNTs aggregation in the PC-rich phase and reduced diffusion rates of the PBS chains. In the case of the ternary blend nanocomposites, the overall crystallization rates decreased as a result of a competition between nucleation and miscibility. Since the PC-rich phase is

partially miscible with the PCL-rich and PBS-rich phases, the PC probably immobilized the PCL and PBS chains and inhibited the rate of crystallization.

The thermal conductivities of the nanocomposites were generally enhanced with the addition of MWCNTs, while the tensile properties of the nanocomposites varied. This was explained in terms of the competition between MWCNTs nucleation and polymer miscibility between the different polymers used in this study.

ACKNOWLEDGEMENTS

First and foremost, I would like to thank **God** for His never-ending grace, mercy, and will to plan and complete this thesis despite all challenges.

I would like to express my sincere gratitude to my supervisors, **Prof. Adriaan Stephanus Luyt and Prof. Alejandro Jesus Müller** for their compassionate, excellent supervision and immense knowledge. Their guidance really helped me. I could not have imagined having better supervisors than them.

I also want to thank my collaborators from Spain and Qatar: Ricardo A. Pérez-Camargo, Agnieszka Tercjak and Mohammad K. Hassan for providing insight and expertise that greatly assisted the research.

I also express my gratitude to Dr. Jonas Mochane for enlightening me the first glance of research. I am really thankful for his aspiring guidance, invaluably constructive critism and friendly advice during this research work.

I thank all my fellow labmates from the Polymer Research Group: Ms. Nomvula Kokozela, Ms. Tholwana Motloung, Mr. Tibello Tsotetsi, Mrs. Mothepane Radebe, Ms. Lesley Mukwada, Mr. Tokelo Selemakoro, Mr. Tsietsi Tsotetsi, Mr. Tyson Mosoabisane for the stimulative discussions, and for all the fun we had in the last three years. In particular, I am grateful to Dr. Puseletso Mofokeng for sharing with me the truthful and illuminating views on a number of issues related to this project, and Mrs. Cheryl-Ann for her patience in repeating many of my SEM analysis ☺.

Special thanks to **Mr. Alfred Maduba** for having such immense support with everything that I do. Having him as my number one cheerleader is such a blessing, because I know I will always have someone rooting for me. He has helped me to grow so much and I know he will help me to improve for the better even more in the future. Thank you for all that you are to me ☺.

Lastly, I am very grateful for the financial support I received from the National Research Foundation (NRF) and Sasol Inzalo Foundation (SaIF), South Africa.

APPENDIX A

Simultaneous SAXS/WAXS experiments

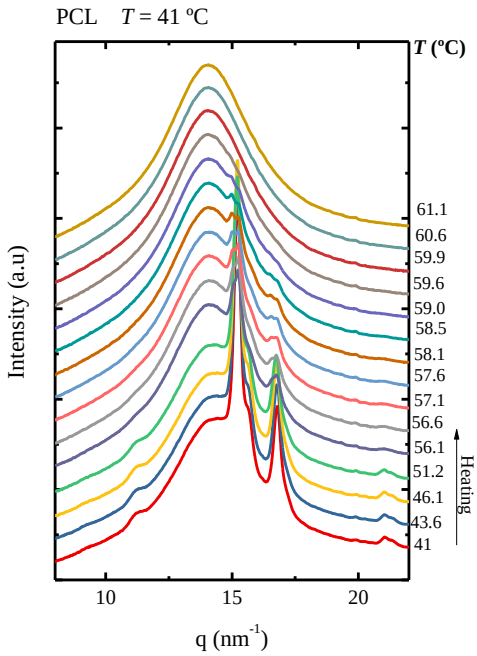

Figure A.1 Heating of PCL after isothermal crystallization at 41 ºC.

Fitting of DSC isothermal data to the Avrami model

The kinetic parameters for all the investigated samples are shown in Table A.1. It is worth noting that a conversion range of approximately 3–20% was used and this corresponds to the primary crystallization range where the Avrami analysis is most adequate. In such a range the correlation coefficients of the fit are mostly in excess of 0.999 (Table A.1). For all the samples studied, the half crystallization times for the experimental data ($\tau_{50\%\ Exp}$) and the Avrami fittings ($\tau_{50\%\ Theo}$) are almost the same, which indicates that the Avrami model predicts very well the crystallinity up to 50% relative crystallinity.

Table A.1 Kinetic parameters for all the investigated samples during isothermal crystallization.

PCL/(PC/MWCNTs) Sample	T_c [°C]	$t_{o\,[}$min]	ΔH [J.g^{-1}]	V_c range [%]	n	K [min^{-n}]	R^2	$\tau_{50\%\ Theo}$ [min]	$\tau_{50\%\ Exp}$ [min]	$(\tau_{50\%\ Exp})^{-1}$ [min^{-1}]	X_c [%]
100/0 ***w/w***	41.0	0.35	52	3-20	2.5	8.21E-01	0.9998	0.93	0.90	1.1111	38
	42.0	0.52	53	3-20	2.5	3.86E-01	0.9999	1.26	1.22	0.8217	39
	43.0	0.50	54	3-20	2.6	1.77E-01	0.9999	1.68	1.63	0.6124	40
	44.0	0.67	55	3-20	2.6	8.13E-02	0.9999	2.25	2.20	0.4545	40
	45.0	1.03	56	3-20	2.7	3.20E-02	1.0000	3.09	3.03	0.3297	41
	46.0	1.13	60	3-20	2.8	1.03E-02	1.0000	4.40	4.37	0.2290	44
	47.0	1.63	59	3-20	2.9	3.64E-03	1.0000	6.16	6.07	0.1648	43
	48.0	1.82	59	3-20	3.0	8.24E-04	0.9999	9.15	9.03	0.1107	43
	49.0	1.02	63	3-20	3.4	8.36E-05	0.9995	14.76	14.43	0.0693	46
	50.0	2.27	51	3-20	3.0	7.94E-05	0.9976	20.21	18.87	0.0530	38
97/(2.5/05) ***w/w***	42.0	0.35	45	3-20	2.6	2.86E+00	1.0000	0.58	0.62	1.6207	34
	43.0	0.47	48	3-20	3.0	1.14E+00	0.9998	0.85	0.90	1.1111	36
	44.0	0.43	52	3-20	3.1	3.95E-01	1.0000	1.20	1.27	0.7893	39
	45.0	0.67	52	3-20	2.8	1.89E-01	1.0000	1.59	1.63	0.6124	39
	46.0	0.67	55	3-20	3.3	3.62E-02	1.0000	2.44	2.53	0.3948	42
	47.0	1.46	51	3-20	2.7	3.79E-02	1.0000	2.97	2.98	0.3352	39
	48.0	2.25	51	3-20	2.7	1.50E-02	0.9999	4.22	4.18	0.2391	39
	49.0	3.10	52	3-20	2.7	5.04E-03	1.0000	6.15	6.10	0.1639	39
	50.0	4.63	56	3-20	2.8	1.39E-03	1.0000	9.35	9.40	0.1064	42
	51.0	5.67	57	3-20	3.1	1.54E-04	1.0000	15.45	15.58	0.0642	43
93/(6/1) ***w/w***	44.0	0.32	50	3-20	3.3	2.07E+00	0.9998	0.72	0.72	1.3947	40
	45.0	0.50	52	3-20	3.5	6.30E-01	0.9998	1.03	1.03	0.9681	41
	46.0	0.53	50	3-20	3.6	2.02E-01	0.9999	1.42	1.42	0.7057	40
	47.0	0.77	50	3-20	3.5	5.81E-02	0.9999	2.01	2.02	0.4958	40

	48.0	0.95	51	3-20	3.8	9.17E-03	0.9999	3.11	3.13	0.3192	40
	49.0	1.48	53	3-20	3.5	3.20E-03	0.9995	4.71	4.65	0.2151	42
	50.0	1.92	55	3-20	4.0	2.19E-04	0.9999	7.65	7.72	0.1296	43
	51.0	3.68	47	3-20	3.8	7.89E-05	1.0000	10.77	10.85	0.0922	37
	52.0	2.53	47	3-20	3.6	1.23E-05	0.9959	21.82	20.35	0.0491	37
	53.0	14.85	30	3-20	3.1	5.35E-05	0.9997	20.34	19.70	0.0508	24
87/(11/2) ***w/w***	45.0	0.33	43	3-20	3.4	2.63E+00	0.9999	0.68	0.68	1.4641	36
	46.0	0.57	43	3-20	3.3	8.52E-01	0.9999	0.94	0.93	1.0718	36
	47.0	0.67	43	3-20	3.2	3.10E-01	0.9998	1.29	1.27	0.7893	36
	48.0	0.90	45	3-20	3.2	8.34E-02	0.9998	1.92	1.90	0.5263	38
	49.0	0.80	47	3-20	4.1	4.93E-03	1.0000	3.30	3.35	0.2985	40
	50.0	1.98	48	3-20	3.3	5.26E-03	0.9999	4.39	4.40	0.2273	41
	51.0	3.75	45	3-20	3.0	2.87E-03	0.9999	6.26	6.20	0.1613	38
	52.0	5.35	49	3-20	3.0	6.52E-04	0.9999	10.34	10.22	0.0979	41
	53.0	11.22	46	3-20	2.7	5.95E-04	1.0000	14.13	14.08	0.0710	39
	54.0	20.92	44	3-20	2.7	1.96E-04	0.9996	20.38	21.63	0.0462	37
73/(23/4) ***w/w***	46.0	0.28	30	3-20%	3.1	5.40E+00	1.0000	0.52	0.53	1.8762	30
	47.0	0.43	31	3-20%	3.5	1.93E+00	1.0000	0.75	0.77	1.3038	31
	48.0	0.47	33	3-20%	3.3	6.03E-01	0.9999	1.04	1.07	0.9372	33
	49.0	0.55	33	3-20%	3.7	1.21E-01	0.9999	1.61	1.63	0.6124	33
	50.0	0.85	35	3-20%	3.5	3.27E-02	0.9996	2.42	2.40	0.4167	35
	51.0	1.52	36	3-20%	3.5	8.79E-03	1.0000	3.54	3.58	0.2791	36
	52.0	2.20	37	3-20%	3.9	7.41E-04	1.0000	5.81	5.97	0.1676	37
	53.0	5.25	29	3-20%	2.9	2.22E-03	0.9996	7.50	7.23	0.1383	29
	54.0	9.62	24	3-20%	3.1	4.73E-04	1.0000	10.86	10.77	0.0929	24

APPENDIX B

Self-nucleation (SN) experiments

Figure B.1 shows the experimental data obtained during an SN experiment for neat PBS. The cooling scans after the isothermal step at T_s are presented in Figure B.1(a), and the subsequent heating scans are shown in Figure B.1(b). The dashed line indicates the PBS crystallization and melting temperatures under standard conditions. The three SN domains are described below as defined by Fillon *et al.* [1,2].

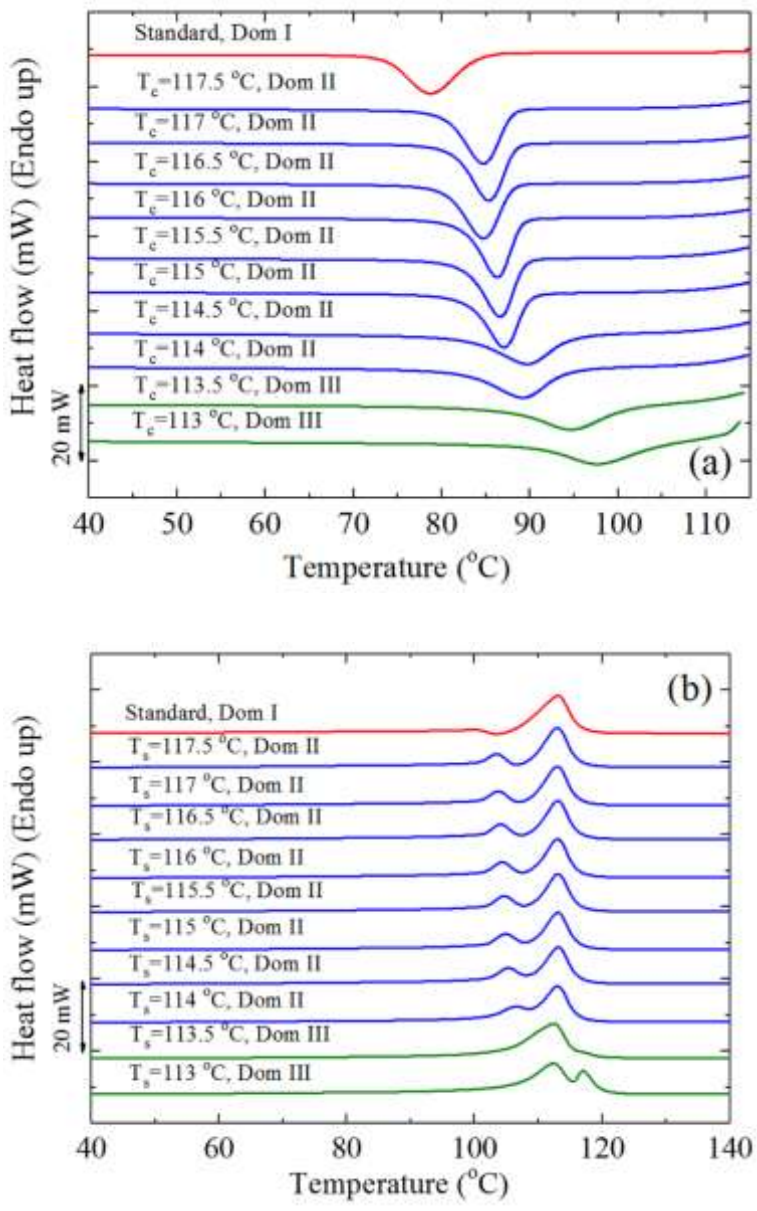

Figure B.1 (a) DSC cooling scans for neat PBS after 5 min at the indicated T_s, and (b) subsequent heating scans after the cooling runs shown in (a).

Domain I or melting domain. The polymer is under *Domain I* when complete melting occurs and the crystalline history of the material is erased. For the PBS, *Domain I* is found at T_s equal to 120 °C, since no change was detected in the T_c when compared to the standard T_c. Both the crystallization and melting DSC scans are identical within *Domain I*.

Domain II or self-nucleation domain. In this domain, the T_s range employed is low enough to produce self-nuclei, but high enough to avoid annealing. Therefore, *Domain II* is easily identified after 5 min at a given T_s, because the peak crystallization temperature of the sample increases compared to the standard value. The start of *Domain II* for the PBS sample occurred at a T_s = 114 °C (Figure B.1(a)), since the sample was self-nucleated without any annealing. The minimum T_s within *Domain II* is defined as the 'ideal self-nucleation temperature ($T_{s,ideal}$)', a temperature which should be accurately determined. This is the temperature that causes maximum self-nucleation (maximum increase in T_c) without annealing. The subsequent melting curve in Figure B.1(b) does not reveal any sign of annealing. In this domain the nucleation density is greatly enhanced.

Domain III or self-nucleation and annealing domain. When T_s is too low, partial melting occurs and the unmolten crystals anneal during the 5 min at T_s. Figure B.1(b) shows that at T_s < 114 °C the melting endotherm exhibits a small high temperature peak that is the result of the melting of the annealed crystals. At this T_s, the crystallization exotherm shows a high temperature tail which reveals that the sample is in *Domain III*.

Figure B.2 shows the location of the three self-nucleation domains for the PBS sample. The vertical dashed lines indicate the temperatures at which the material experiences a self-nucleation domain transition [1,3]. Since 114 °C is the lowest T_s value in *Domain II*, it is called the ideal self-nucleation temperature, because it is the temperature at which there is maximum self-nucleation without any annealing. Employing the ideal T_s (114 °C), the T_c corresponding to the ideal T_s should be used as the maximum crystallization temperature ($T_{c,max}$) when determining the nucleation efficiency of the nanofiller. For the PBS used in this study, $T_{c,max}$ is 89.3 °C.

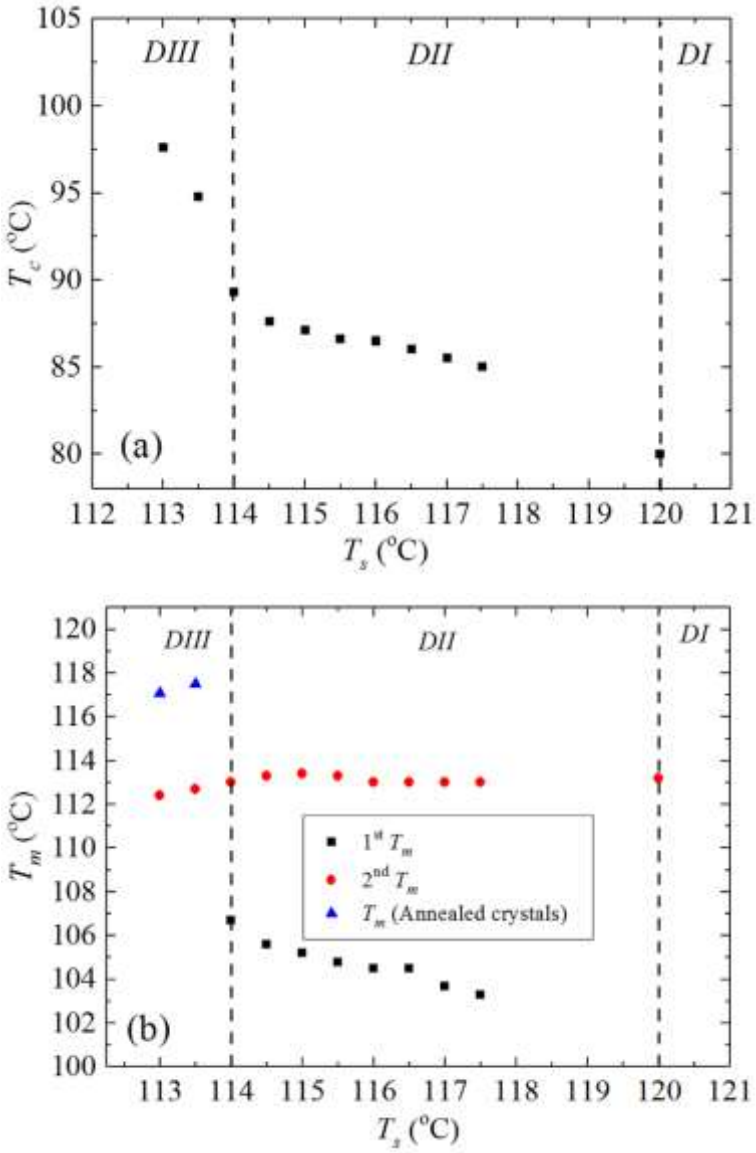

Figure B.2 Dependence of (a) crystallization- and (b) melting peak temperatures of neat PBS on T_s.

Fitting of DSC isothermal data to the Avrami model

The data obtained by isothermal DSC tests were used to perform the Avrami fits and the graphical comparisons between the experimental data and the predictions of the theory.

An example of such a comparison is shown in Figure B.3 for the 73/(23/4) w/w PBS/(PC/MWCNTs) isothermally crystallized at 83.0 °C, in which the experimental results and the corresponding Avrami prediction for the isothermally crystallized samples is shown. Figure B.3(a) shows the data obtained from integration of the DSC isotherm and the vertical purple dashed lines indicate the integration range used. The vertical green dashed lines indicate the half crystallization time found experimentally. Figure B.3(b) shows a plot of 1 - V_c or the relative amorphous fraction as a function of crystallization time derived from an

integration of the data in Figure B.3(a). A typical sigmoidal shape describes the kinetics of transformation to the semicrystalline state. In this case the data is well described by the Avrami equation up to a conversion fraction of 0.8 (or 80%). Figure B.3(c) shows the experimental data (circles) obtained from the isothermal crystallization and the solid line represents the Avrami fit. The normalised crystallization enthalpies as function of the crystallization time from the experimental results correlates well with the Avrami fit (Figure B.3(d)). This indicates that the Avrami model predicts very well the isothermal crystallization.

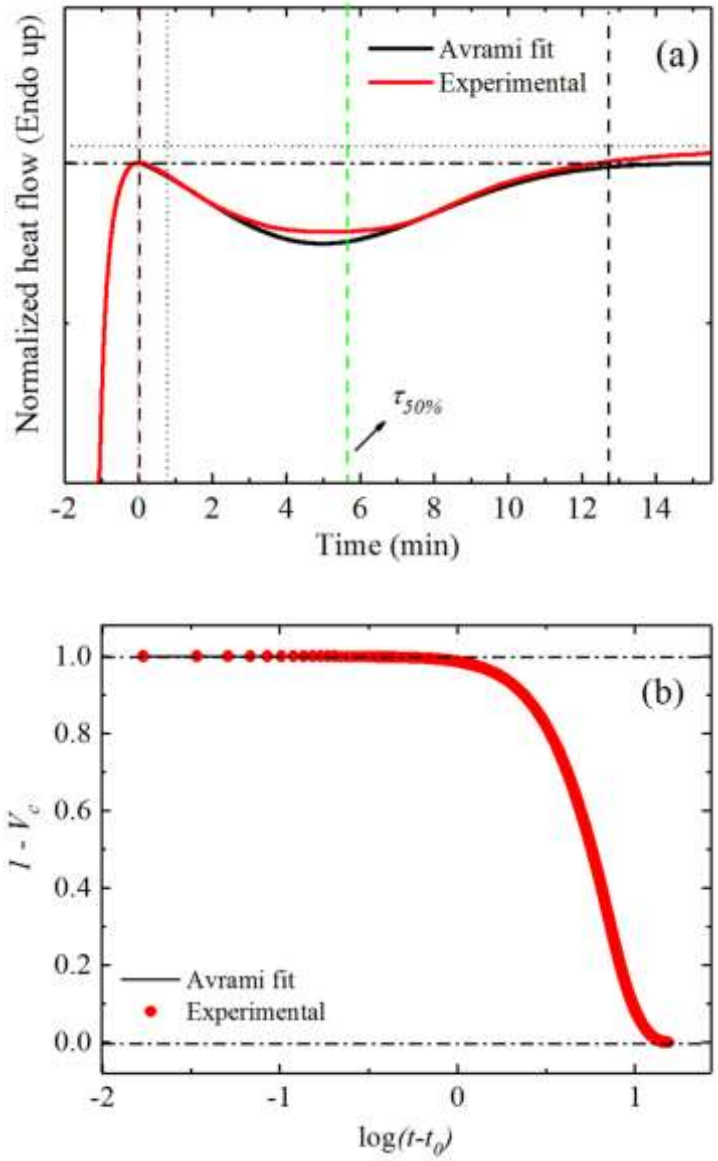

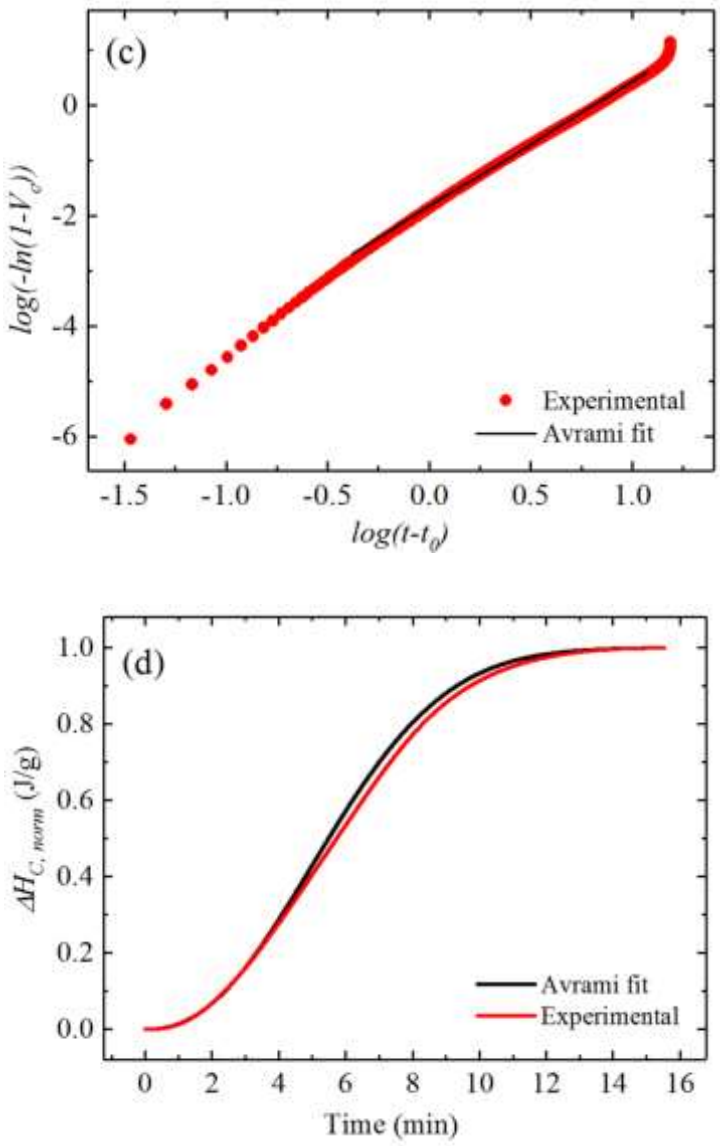

Figure B.3 Comparison between experimental results and the corresponding Avrami prediction for a 73/(23/4) *w/w* PBS/(PC/MWCNTs) nanocomposite isothermally crystallized at 83.0 °C: (a) isothermal heat flow; (b) unconverted relative fraction; (c) Avrami plot; (d) normalized ΔH_c as a function of time.

The kinetic parameters for all the investigated samples are shown in Table B.1. It is worth noting that a conversion range of approximately 3–20% was used and this corresponds to the primary crystallization range where the Avrami analysis is most adequate. In such a range the correlation coefficients of the fit are mostly in excess of 0.999 (Table B.1). For all the samples studied, the half crystallization times for the experimental data ($\tau_{50\%\ Exp}$) and the Avrami fittings ($\tau_{50\%\ Theo}$) are almost the same, which indicates that the Avrami model predicts very well the crystallinity up to 50% relative crystallinity.

Table B.1 Kinetic parameters for all the investigated samples during isothermal crystallization.

PBS/(PC/MWCNTs) Sample	T_c (°C)	t_0 (min)	ΔH (J.g^{-1})	V_c range (%)	n	k (min^{-n})	R^2	$\tau_{50\% \text{ Theo}}$ (min)	$\tau_{50\% \text{ Exp}}$ (min)	$(\tau_{50\% \text{ Exp}})^{-1}$ (min^{-1})
Neat PBS	82.0	1.46	30	3-20	2.7	9.05E-01	0.9999	0.91	0.94	1.0638
	83.0	1.58	33	3-20	2.6	6.62E-01	1.0000	1.02	1.04	0.9615
	84.0	1.62	37	3-20	2.6	4.27E-01	1.0000	1.20	1.22	0.8197
	85.0	1.68	40	3-20	2.6	2.57E-01	1.0000	1.46	1.50	0.6667
	86.0	1.72	41	3-20	2.7	1.49E-01	0.9999	1.76	1.80	0.5556
	87.0	1.84	49	3-20	2.6	9.19E-02	0.9999	2.16	2.21	0.4525
	88.0	1.89	53	3-20	2.7	4.17E-02	0.9998	2.81	2.92	0.3425
	89.0	1.99	57	3-20	2.6	2.23E-02	0.9999	3.76	3.84	0.2604
	90.0	2.13	61	3-20	2.5	1.24E-02	1.0000	4.97	5.00	0.2000
	91.0	2.18	64	3-20	2.5	6.19E-03	1.0000	6.58	6.63	0.1508
97/(2.5/0.5) *w/w* PBS/(PC/MWCNTs)	81.0	1.33	25	3-20	2.8	4.43E+00	1.0000	0.52	0.53	1.8868
	82.0	1.48	28	3-20	2.6	2.62E+00	1.0000	0.60	0.61	1.6393
	83.0	1.50	28	3-20	3.0	1.68E+00	0.9998	0.74	0.77	1.2987
	84.0	1.53	30	3-20	3.0	8.99E-01	0.9998	0.92	0.95	1.0526
	85.0	1.58	31	3-20	2.9	5.08E-01	0.9999	1.11	1.14	0.8772
	86.0	1.70	31	3-20	2.6	3.43E-01	1.0000	1.31	1.33	0.7519
	87.0	1.75	32	3-20	2.7	2.01E-01	1.0000	1.59	1.62	0.6173
	88.0	1.84	34	3-20	2.7	1.12E-01	0.9998	1.96	2.01	0.4975
	89.0	2.01	37	3-20	2.5	7.48E-02	1.0000	2.45	2.47	0.4049
	90.0	2.01	44	3-20	2.7	3.04E-02	0.9999	3.24	3.33	0.3003
93/(6/1) *w/w* PBS/(PC/MWCNTs)	82.0	1.51	19	3-20	2.8	1.21E+00	0.9999	0.82	0.85	1.1765
	83.0	1.70	19	3-20	2.6	7.40E-01	1.0000	0.98	0.99	1.0101
	84.0	1.79	21	3-20	2.6	4.23E-01	1.0000	1.21	1.22	0.8197
	85.0	1.92	22	3-20	2.5	2.63E-01	1.0000	1.47	1.50	0.6667
	86.0	1.94	22	3-20	2.8	1.24E-01	0.9996	1.84	1.92	0.5208
	87.0	2.11	24	3-20	2.5	8.65E-02	0.9999	2.28	2.33	0.4292

	88.0	2.21	27	3-20	2.5	4.35E-02	0.9999	2.97	3.04	0.3289
	89.0	2.28	17	3-20	2.7	1.81E-02	0.9997	3.86	4.01	0.2494
	90.0	2.60	30	3-20	2.5	1.25E-02	0.9999	4.93	5.05	0.1980
	91.0	2.98	31	3-20	2.4	7.87E-03	0.9999	6.27	6.40	0.1563
87/(11/2) *w/w* PBS/(PC/MWCNTs)	82.0	1.67	14	3-20	2.7	4.88E-01	0.9999	1.14	1.17	0.8547
	83.0	1.87	14	3-20	2.5	3.23E-01	0.9999	1.35	1.39	0.7194
	84.0	1.94	16	3-20	2.6	1.69E-01	0.9997	1.71	1.79	0.5587
	85.0	2.06	17	3-20	2.5	1.02E-01	0.9999	2.19	2.24	0.4464
	86.0	2.18	19	3-20	2.5	5.43E-02	0.9999	2.83	2.91	0.3436
	87.0	2.21	21	3-20	2.6	2.22E-02	0.9994	3.68	3.91	0.2558
	88.0	2.36	24	3-20	2.5	1.29E-02	0.9997	4.84	5.07	0.1972
	89.0	2.33	27	3-20	2.6	5.88E-03	0.9998	6.50	6.77	0.1477
	90.0	2.18	31	3-20	2.2	5.57E-03	0.9997	8.89	8.72	0.1147
	91.0	2.16	40	3-20	1.8	7.43E-03	0.9990	12.83	11.46	0.0873
73/(23/4) *w/w* PBS/(PC/MWCNTs)	82.0	2.30	30	3-20	2.3	2.99E-02	0.9998	4.00	4.18	0.2392
	83.0	2.43	36	3-20	2.3	1.47E-02	0.9998	5.48	5.73	0.1745
	84.0	2.77	36	3-20	2.1	1.09E-02	1.0000	6.95	7.07	0.1414
	85.0	2.94	36	3-20	2.2	5.57E-03	1.0000	8.92	9.04	0.1106
	86.0	2.94	34	3-20	2.3	2.73E-03	1.0000	11.64	11.71	0.0854
	87.0	3.32	33	3-20	2.2	1.64E-03	1.0000	14.96	14.84	0.0674
	88.0	3.59	27	3-20	2.2	1.05E-03	0.9999	19.84	18.48	0.0541

References

[1] B. Fillon, J.C. Wittmann, B. Lotz, A. Thierry. Self-nucleation and recrystallization of isotactic polypropylene (α phase) investigated by differential scanning calorimetry. Journal of Polymer Science Part B: Polymer Physics 1993; 31:1383-1393.
DOI: 10.1002/polb.1993.090311013

[2] R.M. Michell, A. Mugica, M. Zubitur, A.J. Müller. Self-nucleation of crystalline phases within homopolymers, polymer blends, copolymers, and nanocomposites. Advances in Polymer Science 2015; 276:215-256.
DOI: 10.1007/12_2015_327

[3] A.T. Lorenzo, M.A. Arnal, J.J. Sánchez, A.J. Müller. Effect of annealing time on the self-nucleation behaviour of semicrystalline polymers. Journal of Polymer Science Part B: Polymer Physics 2006; 44:1738-1750.
DOI: 10.1002/*polb*.20832

APPENDIX C

Table C.1 Kinetic parameters for all the investigated samples during isothermal crystallization.

PCL/PBS/(PC/MWCNTs) Sample	T_c [°C]	$t_{0\,[}$ [min]	V_c range [%]	n	K [min^{-n}]	R^2	$\tau_{50\%\ Theo}$ [min]	$\tau_{50\%\ Exp}$ [min]	$(\tau_{50\%\ Exp})^{-1}$ [min^{-1}]
100/0 ***w/w***	41.0	0.35	3-20	2.5	8.21E-01	0.9998	0.93	0.90	1.1111
	42.0	0.52	3-20	2.5	3.86E-01	0.9999	1.26	1.22	0.8217
	43.0	0.50	3-20	2.6	1.77E-01	0.9999	1.68	1.63	0.6124
	44.0	0.67	3-20	2.6	8.13E-02	0.9999	2.25	2.20	0.4545
	45.0	1.03	3-20	2.7	3.20E-02	1.0000	3.09	3.03	0.3297
	46.0	1.13	3-20	2.8	1.03E-02	1.0000	4.40	4.37	0.2290
	47.0	1.63	3-20	2.9	3.64E-03	1.0000	6.16	6.07	0.1648
	48.0	1.82	3-20	3.0	8.24E-04	0.9999	9.15	9.03	0.1107
70/30/0 ***w/w***	43.0	2.79	3-20	2.6	5.63E+00	1.0000	0.44	0.44	2.2727
	44.0	2.84	3-20	2.7	3.78E+00	0.9998	0.54	0.54	1.8519
	45.0	2.82	3-20	3.0	2.60E+00	0.9996	0.64	0.66	1.5152
	46.0	2.86	3-20	2.7	1.88E+00	1.0000	0.69	0.70	1.4286
	47.0	2.83	3-20	3.1	1.09E+00	0.9994	0.87	0.9	1.1111
	48.0	2.96	3-20	2.5	7.53E-01	1.0000	0.97	0.97	1.0309
	49.0	2.96	3-20	2.4	4.16E-01	1.0000	1.24	1.26	0.7938
	50.0	2.86	3-20	2.9	1.98E-01	0.9993	1.54	1.65	0.6061
65/28/(6/1) ***w/w***	43.0	6.12	3-20	1.8	8.72E-02	0.9998	3.26	3.42	0.2924
	44.0	7.48	3-20	1.8	4.36E-02	0.9896	4.85	4.85	0.2062
	45.0	9.40	3-20	1.6	6.13E-02	0.9981	4.81	4.83	0.2070
	46.0	11.41	3-20	1.8	2.29E-02	0.9973	6.79	7.91	0.1264
	47.0	14.18	3-20	1.7	2.02E-02	0.9996	8.39	8.38	0.1193
	48.0	23.97	3-20	1.6	1.32E-02	0.9929	12.30	11.14	0.0898

	49.0	17.53	3-20	1.9	3.21E-02	0.9977	5.08	4..98	0.2008
28/65/(6/1) ***w/w***	58.0	1.99	3-20	2.7	2.51E+00	1.0000	0.62	0.63	1.5873
	60.0	2.11	3-20	2.6	7.21E-01	1.0000	0.99	0.99	1.0101
	62.0	2.26	3-20	2.6	2.48E-01	1.0000	1.48	1.50	0.6667
	64.0	2.41	3-20	2.5	8.60E-02	0.9998	2.27	2.33	0.4292
	66.0	2.58	3-20	2.5	3.34E-02	0.9997	3.45	3.55	0.2817
	68.0	3.03	3-20	2.3	1.29E-02	0.9998	5.71	5.85	0.1709
	70.0	4.05	3-20	2.1	5.20E-03	1.0000	10.07	10.17	0.0983
	72.0	4.61	3-20	2.5	5.05E-04	0.9991	18.11	19.21	0.0521
30/70/0 ***w/w***	64.0	2.02	3-20	2.5	1.42E-01	1.0000	1.87	1.87	0.5348
	65.0	2.16	3-20	2.5	1.11E-01	1.0000	2.11	2.11	0.4739
	66.0	2.16	3-20	2.5	7.02E-02	0.9998	2.47	2.48	0.4032
	67.0	2.23	3-20	2.4	5.83E-02	0.9999	2.76	2.77	0.3610
	68.0	2.28	3-20	2.4	4.27E-02	0.9999	3.27	3.25	0.3077
	69.0	2.33	3-20	2.4	3.26E-02	1.0000	3.67	3.62	0.2762
	70.0	2.43	3-20	2.3	2.40E-02	1.0000 0	4.41	4.40	0.2273
	71.0	2.31	3-20	2.4	1.25E-02	0.9999	5.26	5.20	0.1923
0/100 ***w/w***	82.0	1.46	3-20	2.7	9.05E-01	0.9999	0.91	0.94	1.0638
	83.0	1.58	3-20	2.6	6.62E-01	1.0000	1.02	1.04	0.9615
	84.0	1.62	3-20	2.6	4.27E-01	1.0000	1.20	1.22	0.8197
	85.0	1.68	3-20	2.6	2.57E-01	1.0000	1.46	1.50	0.6667
	86.0	1.72	3-20	2.7	1.49E-01	0.9999	1.76	1.80	0.5556
	87.0	1.84	3-20	2.6	9.19E-02	0.9999	2.16	2.21	0.4525
	88.0	1.89	3-20	2.7	4.17E-02	0.9998	2.81	2.92	0.3425
	89.0	1.99	3-20	2.6	2.23E-02	0.9999	3.76	3.84	0.2604